DISPERSION IMAGING AND SUBSURFACE PROFILING USING PASSIVE ROADSIDE MASW SURVEY

A Thesis

Submitted in Partial Fulfilment of the Requirements

for the Degree of

DOCTOR OF PHILOSOPHY

by

Dipjyoti Baglari

Department of Civil Engineering

Indian Institute of Technology Guwahati

Guwahati - 781039, India

September 2019

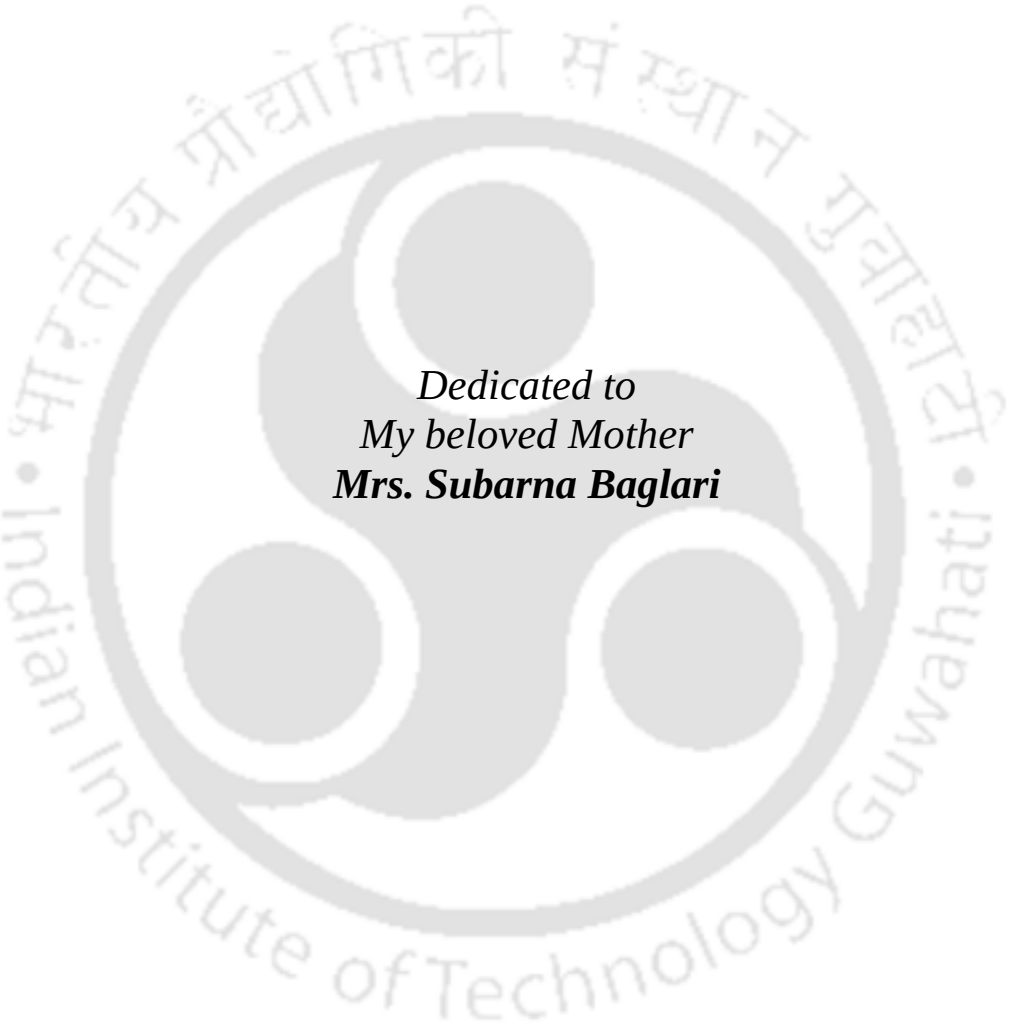

Dedicated to
My beloved Mother
Mrs. Subarna Baglari

STATEMENT

I do hereby declare that the matter embodied in this thesis is the result of investigations carried out by me in and with the aid of the Department of Civil Engineering, Indian Institute of Technology Guwahati, Assam, India.

In keeping with the general practice of reporting scientific observations, due acknowledgements have been made wherever the work described is based on the findings of other investigators.

Date: **(Dipjyoti Baglari)**

Place: IIT Guwahati

CERTIFICATE

This is to certify that the thesis entitled **"Dispersion Imaging and Subsurface Profiling using Passive Roadside MASW Survey"** submitted by **Dipjyoti Baglari** Roll No. 136104024, to the Indian Institute of Technology Guwahati, for the award of the degree of Doctor of Philosophy in Civil Engineering is a record of bonafide research work carried out by him under my supervision and guidance. The thesis work, in my opinion, has reached the requisite standard fulfilling the requirements for the degree of Doctor of Philosophy.

The results contained in this thesis have not been submitted in part or full to any other University or Institute for award of any degree or diploma.

Dr. Arindam Dey
Associate Professor
Department of Civil Engineering
Indian Institute of Technology, Guwahati
Guwahati-781039, India

Place: Guwahati

Date:

ACKNOWLEDGEMENTS

I express my deep sense of gratitude and indebtedness to my thesis supervisor and research guide Dr. Arindam Dey for his inspiring guidance and constant encouragement throughout the course of this research work. I am grateful to him for sparing his precious time and efforts throughout the entire work. I am highly obliged to him for all the insightful discussions, affection and kind suggestions, which helped me to complete the work successfully. I consider myself extremely fortunate to have him as my research guide, whose able guidance and valuable advice have helped me in every way throughout this work.

My gratitude is extended to doctoral committee members Prof. Sreedeep S., Dr. Sandip Das and Dr. Prithwijit Guha for reviewing my work and providing their valuable inputs that helped in improving my thesis. I would also like to thank the other faculty members of Geotechnical engineering of Civil Engineering Department specially Dr. A. Murali Krishna, Dr. Ajay Dashora and Dr. Abhishek Kumar for their valuable suggestions and support during my PhD. I owe great thanks to the staff of Geotechnical Engineering, particularly Junior Technical Superintendent Mr. Hari Ram Upadhyaya and Technical Officer Mr. Samarjyoti Kalita for their helps in conducting the field experiments. I thank all office staffs of Civil Engineering Department for their help and cooperation in pursuing my work.

I thank Jumrik and Shibayan, the two of my laboratory companions, with whom I have started my PhD work for their help, support and companionship. I specially thank Devdeep Basu and Dipankar Das who helped me many a times in the tough field tests spending their selfless time and efforts. I thank Mustafizur Rahman, my M.Tech student with whom I have conducted many field

tests. I thank my friends Ashish, Shiv Shankar, Vinay, Mriganabh, Niranjan, Sudheer, Rana, Yagom, Chandrabhanu, Janarul and many others for their support, encouragement and companionship.

My mother has always been a constant source of inspiration for me. Her support, encouragement and prayers have always been my energy. I cannot thank enough my brothers Robijit and Pranjal for their love and sacrifices for me throughout my academic life. I am grateful to my wife Swapnali for her support and understanding in the last couple of years, which was really crucial for me. I am grateful to my other family members, friends and well-wishers who have supported me along the way.

Finally, I wholeheartedly thank the Institute for providing me all the facilities for successful completion of this work.

Dipjyoti Baglari

ABSTRACT

Passive methods of Multichannel Analysis of Surface wave (MASW) utilizes surface waves generated from natural (microtremors) or cultural sources (tidal or traffic) to determine the subsoil profile in terms of Shear wave velocity (V_s). Passive Roadside survey aims to record the surface waves generated from traffic-originated sources by employing 1-D linear array and, hence, is a more suitable method in congested urban areas. In roadside survey, the road surface irregularities such as the potholes or speed inhibitors serve as sources of surface wave as the vehicles pass over them. However, the field data acquisition and corresponding processing for dispersion imaging is complicated in passive roadside survey owing to the unknown numbers and locations of sources. The objective of the present research is to critically examine various parameters controlling the resolution and quality of dispersion imaging of passive roadside data, so that robust and confident V_s profile can be obtained, irrespective of site and test conditions.

An extensive experimentation programme of passive roadside survey was conducted at three sites inside and around IIT Guwahati campus. Site 1 was selected inside IIT Guwahati campus beside the cricket field, Site 2 is a road stretch from IIT Guwahati to Amingaon market, and Site 3 is a road stretch of the National Highway NH 31. The roads at each of these sites comprise different volumes of traffic comprising light, medium and heavy traffic, respectively. The raw field records from all the three sites have been critically analyzed for wavefield propagation and arrival, frequency-amplitude spectra, wavefield contamination and their respective effect on the resolution of dispersion imaging. The quality of raw field records in a passive roadside survey is not controllable by the investigator. It is found that even without existence of major surface sources on the road, traction of heavyweight vehicles produces significant energy, much greater than

conventionally used sources in active survey. At sites with medium to heavy traffic volume, wavefield contamination is a major problem in obtaining a cleaner record. At such sites, it is necessary to cautiously record field data with smaller recording time, in the range of 1-5 s, to avoid wavefield contamination.

Receiver array length and acquisition time significantly affect the resolution of dispersion image. Thicker energy band and poor resolution in lower frequency band of dispersion image is found to be the outcome of utilizing shorter arrays. Irrespective of the site conditions, a short receiver array of length 23 m is found to be insufficient to produce dispersion image with sufficient resolution. With longer arrays of 46-92 m, the resolutions of dispersion images is found to be enhanced. At site with heavy traffic volume, raw field records from longer receiver array suffers severe contamination that resulted in poor resolution dispersion image. The ratio between longest measurable wavelength to the receiver array length is found to be approximately in the range of 0.6-1. Further, the highest ratio between the depths of investigation to longest wavelength has been found to be 0.4. The acquisition or recording time is largely influenced by the volume of the traffic and numbers of existing sources on the road surface. For site with light to medium traffic volume, acquisition time between 2.8-21.8 s have been found to be sufficient. Smaller recording time is effective during raw data acquisition at site with heavier traffic volume.

Implementing optimum processing parameters during dispersion analysis is critical in obtaining high-resolution dispersion image. Setting optimum frequency and velocity range during dispersion analysis, by discarding contaminating energy bands, helps in enhancing dispersion image resolution. An appropriate selection of azimuthal quadrants allow identifying directions of major

wavefield sources, making energy computation along azimuth axis accurate and resulting in a dispersion image with superior resolution. Offline distance of receiver array controls the dispersion imaging process and adoption of appropriate processing scheme. An inline processing (IP) scheme for a closely situated source results in a broader energy band in the dispersion image and overestimated phase velocity in the extracted dispersion curve. Offline cylindrical (OC) or Offline plane (OP) scheme is found suitable for the cases of intra-line sources, which automatically incorporates the planar or cylindrical wave propagation through the receiver array depending on the offline distance between the array and the centreline of the road. Vertical stacking is an advantageous method for enhancement of dispersion image resolution especially in passive MASW survey. In most of the field situations, minimum 10 numbers of vertical stacking is required for high-resolution dispersion image. A new approach to vertical stacking is proposed to obtain a superior quality dispersion image when there are only a few numbers of good quality field records available.

The lowest frequency point on a dispersion curve controls the maximum achievable investigation depth. However, upon extending the selection of dispersion curve in lower frequency part, the corresponding Root-Mean-Square (RMS) value increases, which is a sign of deviations of the soil profile from its true scenario. Therefore, it is found that depending on the requirement of depth of investigation, the selection of dispersion curve should be limited in its lower frequency part to avoid deviation between measured and actual soil profile. The density of dispersion points, for representing the dispersion curve within a selected frequency range, affects the stability of inversion and the reliability of obtained V_s profile. It is found that to obtain a reliable V_s profile, the frequency interval of dispersion points for the extraction of dispersion curve should be 0.5 Hz

or lesser. Adoption of higher number of earth layers in the initial earth model is observed to give more stable and reliable V_s profile. For a depth range of 18-30 m, the number of layers in the initial earth model to be used should be 7 or more.

Passive roadside surveys involve complex source characteristics with multiple source existence having varying azimuthal characteristics. In the study, the influence of source location in terms of intra-line and outer-line positioning of sources, existence of multiple numbers of strong sources of wavefields, and the effect of offline distance of receiver arrays on the resolution of dispersion image is highlighted. The intra-line source produces a dispersion image with better resolution, particularly in lower frequency band, attributed to the ability of recording stronger low frequency components of surface waves. Multiple sources shows marginal effect on the resolution of dispersion imaging until there is no contamination on the raw records by mutual interferences. Usability of roadside survey vastly depends on the accommodated offline distance. Based on the present study, to have recognizable dispersion image, the highest offline distance that can be adopted has been found to be 15 m. Based on the close comparison of results of Passive Roadside MASW survey with those of conventional surveys, the efficacy and applicability of the adopted Passive Roadside MASW technique in identifying subsurface characteristics utilizing the vehicular movement on the roads is suitably established. Finally, from the present research, a robust set of guidelines have been provided which would aid in a good field and analysis practice to conduct Passive Roadside MASW survey to obtain meaning subsurface V_s profiles.

Keywords*: Passive Roadside MASW survey, Data acquisition, Resolution of dispersion image, Vertical stacking, Shear wave velocity profile*

TABLE OF CONTENTS

LIST OF FIGURES

LIST OF TABLES

CHAPTER 1

INTRODUCTION

1.1 Background

Rayleigh wave is a type of surface wave that travels along a solid surface, such as earth-air or earth-water interface, with low velocity, low frequency and high amplitude. These waves are formed because of the interference of Primary (P-wave) and vertically polarised shear wave (S-wave). In a homogenous matter, it travels with a velocity of $0.9194V_s$, where V_s is the shear wave velocity (Xia *et al.*, 1999, 2004b). Such inherent relationship between Rayleigh wave and shear wave velocity is useful for determining the shear wave velocity profile of subsoil. This property have been utilised in many recent surface wave techniques of subsurface exploration. Shear wave velocity is considered as a critical engineering parameter for evaluating the dynamic characteristics of soil as it is directly related to its stiffness ($G= \rho V_s^2$, where G is shear modulus and ρ is the density of the material). Along with its conventional use in soil classification, it has a number of crucial geotechnical applications, namely in the area of seismic risk studies, seismic hazard zonation, evaluation of liquefaction potential, landslide potential, slope stability, load bearing capacity, stiffness and the settlement of foundation and soil (Lin *et al*., 2004; Liu *et al*., 2005; Akin *et al.*, 2011; Coccia *et al*., 2011; Eker *et al.*, 2012; Kanli *et al.*, 2006; Keceli, 2012; Trupti *et al.*, 2012).

Currently, building codes of many countries such as National Building Code of Canada (NBC), Uniform Building Code (UBS) and Eurocode-8 are based on V_{s30} (i.e., average shear wave velocity

of top 30 m layer of subsoil) for soil classifications and corresponding seismic design (Kanli *et al.*, 2006; Molnar *et al.*, 2007; Savvaidis *et al.,* 2014). The National Earthquake Hazard Reduction Program (NEHRP), established in 1977 by the U.S. Congress, proposed a site classification based on average V_{s30} as listed in Table 1.1. The International Building Code (IBC) also adopted the same guidelines and classification system as per NEHRP (Park, 2013).

Table 1.1 Site classification based on NEHRP site classification (NEHRP BSSC, 2003)

Site class	S-wave velocity (m/s)
A (Hard Rock)	> 1500
B (Rock)	760-1500
C (Very dense soil and soft rock)	360-760
D (Stiff soil)	180-360
E (Soft clay soil)	< 180
F (Soils requiring additional response)	< 180 and meeting some additional conditions

1.2 Various Methods of Determination of Shear Wave Velocity

There are various invasive and non-invasive techniques available for determination of the shear-wave velocity profile of subsurface soil. Some popular examples from both the categories are as follows (Foti *et al*., 2014):

Invasive methods:

a) Standard penetration test
b) Cross hole test
c) Down hole test
d) Up-hole test
e) P-S suspension logging

Non- Invasive methods:

a) Seismic Refraction survey
b) Seismic Reflection survey
c) Ground Penetrating Radar (GPR)
d) Spectral analysis of surface waves (SASW)
e) Multichannel analysis of surface wave (MASW)

In the determination of V_s profile, the invasive techniques are still being conventionally used in many parts of the world, attributed to their established guidelines and process of direct measurement. Standard penetration tests are the simplest and oldest method for subsurface characterisation. Though the method does not directly yield information about the shear wave velocity, a number of established empirical correlations are available between SPT-N value and V_s (Akin *et al*., 2011). In the cross-hole test, the source and receivers are placed at the same depth in two adjacent boreholes, and the wave propagation velocity is estimated based on the travel time and distance between them. In the down-hole test, an active source, placed at the surface, is utilised to produce the seismic wavefield, which is recorded in the borehole by a set of receivers at different depths. In the up-hole test, seismic waves are generated at various depths in a borehole and receivers are located along the ground surface for the recording. In P-S suspension logging, a single cable wired instrument containing a seismic source with a number of receivers is inserted in the borehole to record local measurement of seismic wave propagation. The primary drawbacks of invasive methods include high cost due to the requirement of boreholes and information of only a smaller volume of substrata.

Non-invasive techniques allow the exploration of deeper and more representative volume of soil, while they are usually more cost effective. Seismic refraction method is based on the recording of

the arrival time of refracted primary (P) waves from the interfaces between layers possessing different stiffness. The objective of seismic reflection surveys lies in detecting and imaging interfaces among different layers of substrata using reflected P-waves. Ground penetrating radar addresses the imaging of the subsurface based on the arrival time of the transmitted signal and the difference in the dielectric characteristics of the medium. The SASW test utilises a single impulsive source and two receiver arrangements. The technique is based on the estimation of arrival time of surface waves comprising different frequency components at the two receiver locations. The technique has the disadvantage of being a time consuming one and its inability to detect the multimodal dispersion features of the subsurface. The major limitations of the two receiver approach is mostly overcome with the aid of multiple receiver arrangement, brief details of which are furnished in the following subsection.

1.3 Introduction to Multichannel Analysis of Surface Waves

In seismic surveys, where a compressional or vertical source is utilised for surface wave generation, a large part of the wavefield (> 2/3rd part) comprises Rayleigh waves. Such waves, while propagating through heterogeneous soil medium, exhibits dispersive characteristics attributed to which different frequency component of the wave propagates with different phase velocities. Velocities of the dispersive Rayleigh waves are primarily governed by the shear wave velocities of the medium (Park, 2013). Therefore, by analysing the propagation characteristics of dispersive Rayleigh waves, shear wave velocities of soil substrata can be estimated. The MASW method utilises the dispersive property of Rayleigh waves for evaluation of V_s profile of soil substrata. The method, thus, fruitfully utilises surface waves that are considered as “noise” in other seismic wave based methods.

The MASW technique is based on similar working principle to that of SASW, except that it uses multiple receivers for recording surface wave signals that increases its efficiency and accuracy. It is a less expensive technique and provides the benefit of precision and swiftness to estimate the subsurface shear-wave velocity profile. The method is effective in identifying multimodal nature of surface waves, which was not possible through SASW method. It yields 1-D shear-wave velocity profile at the centre of the deployed receiver array from a single layout. Moreover, it can be performed in a roll along mode, to cover a large range of area within a very short duration of time, and construct results of ground stiffness in 2-D or 3-D formats through an appropriate interpolation scheme. This is achieved by placing each 1-D V_s profile at a surface location corresponding to the middle of the receiver line, as shown in Fig. 1.1.

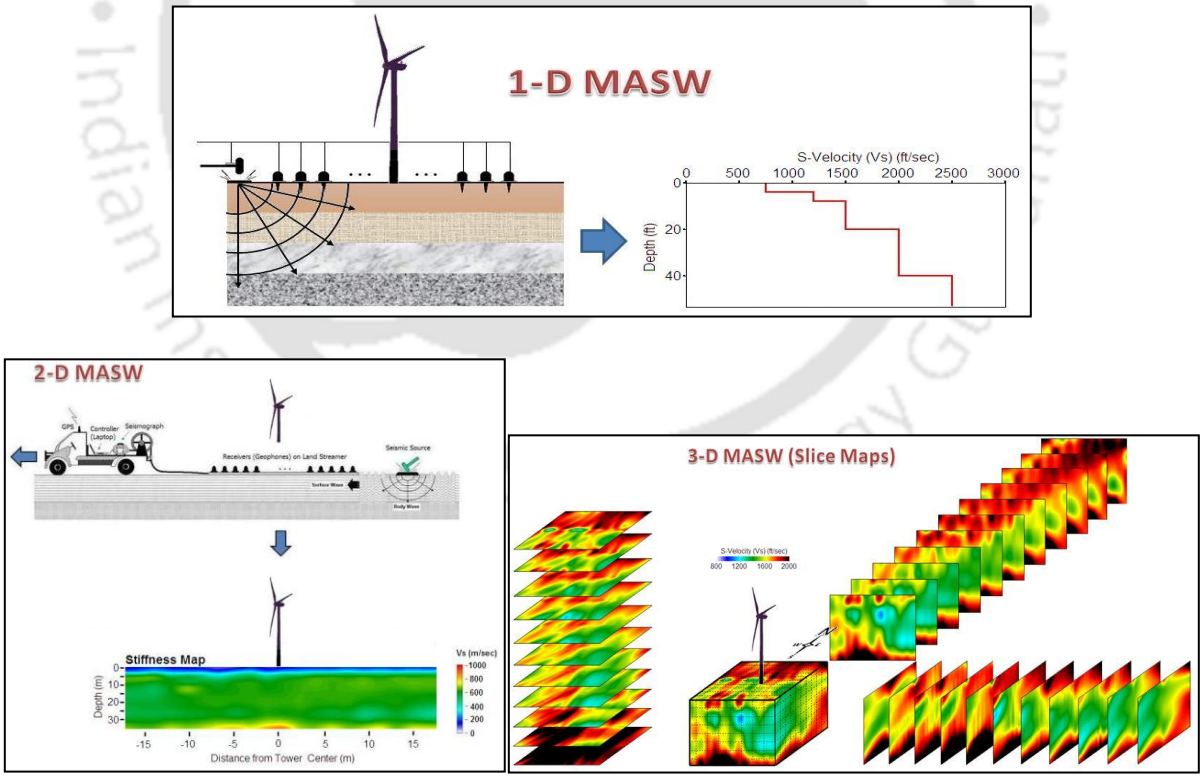

Fig. 1.1 MASW survey in 1-D, 2-D and 3-D format (Park *et al*., 2007)

A typical MASW survey consist of three primary steps. Firstly, acquisition of raw field data of Rayleigh wave propagation; secondly, dispersion analysis to produce a map of phase velocity variations with frequency (known as dispersion image), and, finally, inversion analysis to obtain the V_s profile of the surveyed area. The systematic procedure of the method is shown in Fig. 1.2.

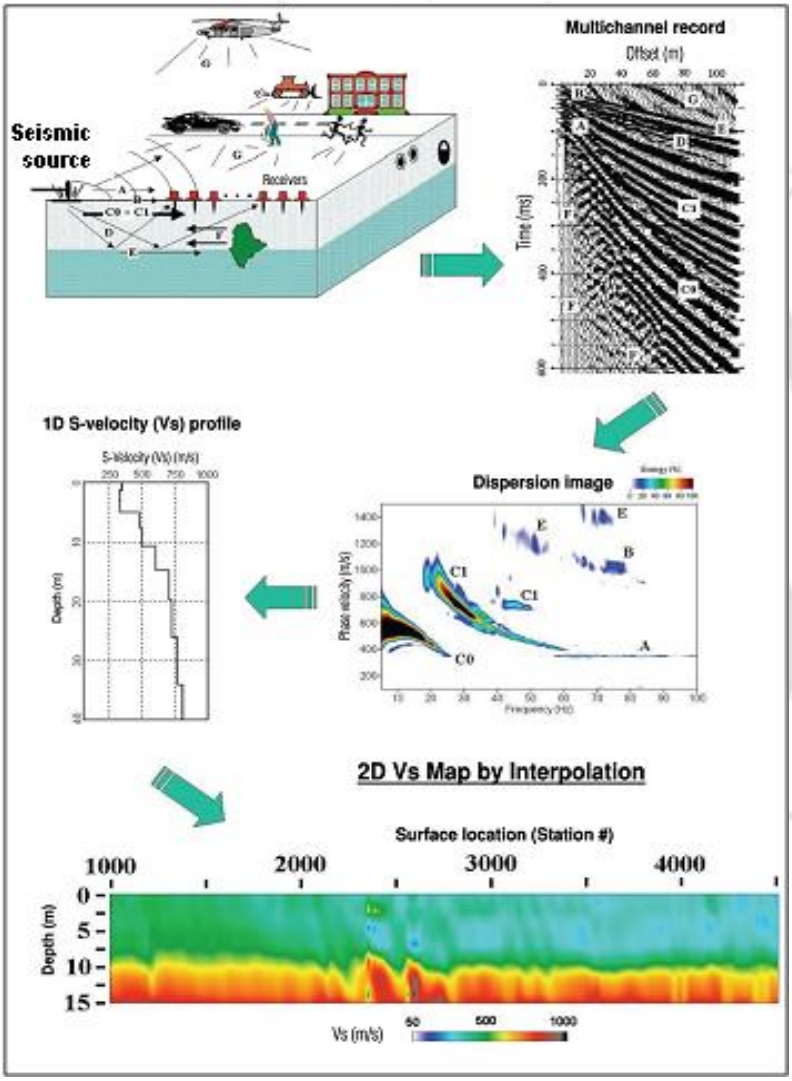

Fig. 1.2 Detailed procedure of MASW survey (Park *et al.*, 2007)

The most crucial part in MASW is to extract an accurate dispersion curve (normally corresponding to the fundamental mode) from the dispersion analysis, since the accuracy of the final V_s profile primarily depends upon the accuracy of the selected dispersion curve (called as measured dispersion curve). Therefore, it becomes imperative to obtain a dispersion image with high resolution, where the fundamental mode dispersion curve is identified as the points of spectral maxima. The dispersion imaging process is significantly affected by the properties of the input source (e.g., weight of the source, distance and azimuth from the recording channel) and the parameters related to the receivers such as its natural frequency, spacing, numbers, orientation and layout (Park *et al.*, 1999, 2001).

1.4 Types of MASW Survey

1.4.1 Active MASW Survey

It is the conventionally used mode of MASW survey with an active source of wavefield generation. An active source can be either an impulsive source such as a sledgehammer or weight drop, or a swept source like Vibroseis, and is purposely used to generate surface wavefield for the survey. The impact by the source is received by a 1-D linear geophone array, placed at desired offset. The survey can be conducted using 24 or more numbers of geophones for data acquisition. A schematic view of active MASW is shown in Fig. 1.3

Active MASW utilizes surface waves propagating horizontally along the surface of measurement directly from impact point to receivers. A linear array can be quickly deployed in the ground resulting fast acquisition of raw wavefield data. The survey can be continued in a roll along mode (exchanging the first receiver position to the last, after each data acquisition) to cover a large area

of survey in a short time. Thus, the method provides the V_s information of the subsurface in 1-D (depth) or 2-D (depth and surface location) format and in a cost effective and time efficient manner. The processing techniques of active MASW is comparatively simpler than other similar techniques. The maximum depth of investigation is usually in the range of 10-30 m, although this depends upon the site characteristics and type of active source used (Park *et al.*, 2007).

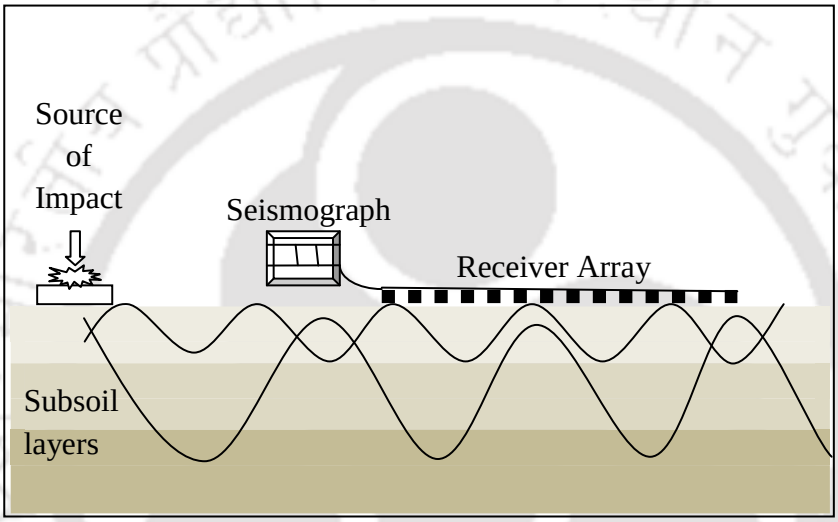

Fig. 1.3 Schematic representation of an Active MASW survey

1.4.2 Passive MASW survey

One of the major limitations of active MASW method is its limitation in the achievable depth of investigation. As the surface-wave based methods are gaining popularity, demand for increasing depth of investigation is also on the rise. An active source, such as a sledgehammer, weighing 5-10 kg, is capable producing wavefield in the frequency band of 15-50 Hz. However, to investigate deeper subsoil layer, frequencies of generated wavefield is required to be much lower in the range of <10 Hz. To produce wavefield of lower frequencies, a much larger impact is required which eventually needs much heavier active source. On the other hand, passive surface waves, generated

from natural (e.g., tidal motion) or cultural (e.g., traffic) sources, are usually of low frequency (1-30 Hz), with wavelengths ranging from a few metres (cultural sources) to several kilometres (natural sources). Thus, such sources provide a wide range of penetration depths and, therefore, a strong motivation develops about their successful utilization (Park *et al.*, 2007). The passive MASW method utilises these surface waves originating from passive sources with multichannel recording. Based on field logistics, Passive MASW is divided into two different types, namely Passive Remote and Passive Roadside MASW surveys, which are described in the following sub-sections.

1.4.2.1 Passive Remote Survey

The Passive Remote Survey, as shown in Fig. 1.4, uses different shapes of 2-D receiver array layouts to record passive surface waves originating from natural or cultural sources. The method can yield accurate evaluation of 1-D shear-wave velocity up to a great depth (even up to hundreds of meters). It has an intensive field operation and requires a wide-open space for the large 2-D array layout. This method can be a good choice if relatively regional 1-D V_s profiling is needed with sufficient accuracy. Any type of 2-D receiver array, of fairly symmetric shape, can be used for this mode of survey. An array of significant asymmetric shape (such as an elliptical or an elongated rectangular shape) is not recommended due to the bias towards a specific direction of incoming surface waves that may not represent the actual direction of major surface wave energy. The common array types include the criss-cross, circular, square, triangular, and symmetric random orientations (Fig. 1.5). Intensive modelling tests by Park *et al*. (2007) indicated an insignificant difference between the influences by different array types, as far as the symmetry of the array is maintained. Therefore, the choice of the specific array type to be used depends upon

the convenience of field operation. Some of the field experiments with circular and cross arrays indicate the circular array may result in dispersion images with a slightly higher resolution and better definition (Park *et al.*, 2007).

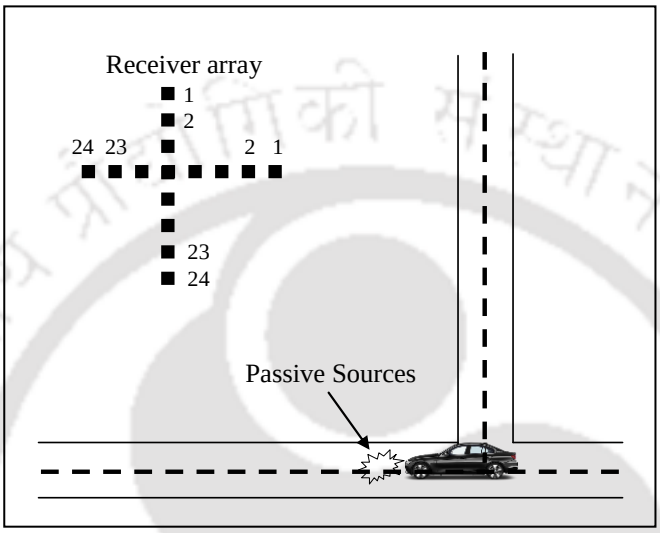

Fig. 1.4 Schematic of Passive Remote MASW survey with a receiver array of criss-cross layout

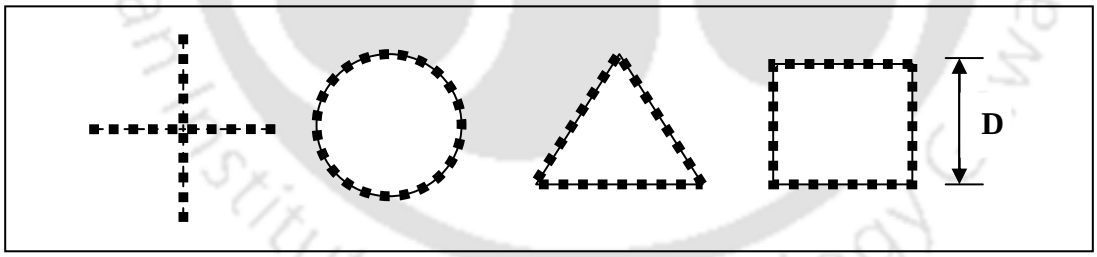

Fig. 1.5 Different types of 2-D receiver arrays commonly employed in Passive Remote tests

1.4.2.2 Passive Roadside Survey

The Passive Roadside Survey, as shown in Fig. 1.6, adopts the conventional mode of survey with linear receiver array and attempts to record the surface waves originating only from traffic sources. This method can also provide a large investigation depth, in the range of 20-100 m, with the aid

of a comparatively easier fieldwork than passive remote survey. The receiver array is normally placed on the shoulder, sidewalk or the median of a road, in a direction parallel to the alignment of the road. Raw wavefield records are collected during the passage of vehicles through the nearby road. Further, an active test can also be performed from one end of the array in the same field set up, resulting in a simultaneous active and passive survey at the same time. Thus, both the surveys can be conducted in a roll along mode, resulting in a 2-D V_s profile providing both shallow and deeper layer information. The method alleviates many limitations of the passive remote method, such as the difficulty in securing a spacious area and inconvenience in field operations. However, this mode of survey little bit compromises the accuracy (usually less than 10%) in the final V_s evaluation, attributed to the surface wave data collection by 1-D receiver array (Park *et al*., 2007). Several earlier researchers have successfully applied the Passive Roadside MASW survey for characterizing the shear-wave velocity profile of the subsurface, which yielded meaningful and reliable estimates (Park and Miller, 2008; Park, 2010; Banab and Motazedian, 2010; Brandes *et al*., 2011; Gonsiewski, 2011; Khalil and Hafeiz, 2012; Ezersky *et al*, 2013; Saez *et al*., 2014; Anbazhagan *et al*., 2018; Cheng *et al*., 2018; Park *et al*., 2019).

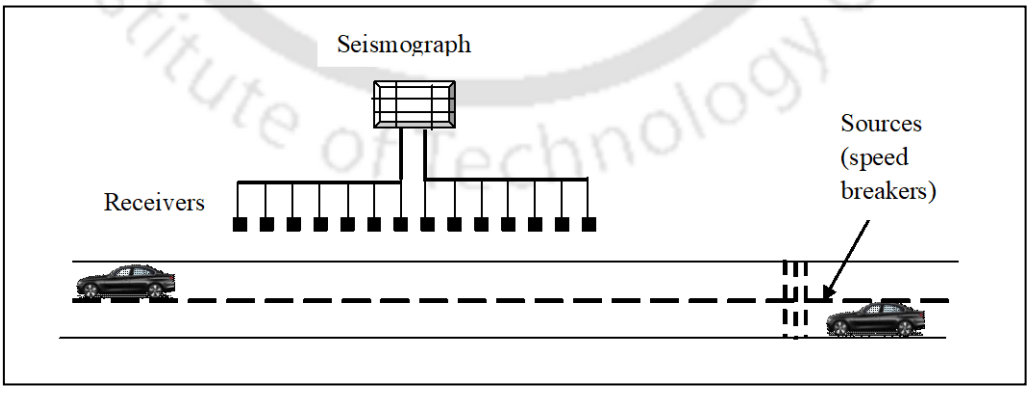

Fig. 1.6 Schematic of Passive Roadside MASW survey with a linear receiver array

.

1.4.3 Combined Active and Passive MASW Survey

It is often useful or necessary to conduct simultaneous active and passive survey at a site and to combine the resultant dispersion images processed from both active and passive data sets for the following reasons:

I. To enlarge the analysable frequency band of dispersion image and attain deeper investigation depth.

II. To identify the multi modal nature of dispersion trends in a better manner, especially in the dominant modal nature of the traffic generated surface waves.

III. To attain more confidence in the resultant V_s profile.

1.5 Motivation of the Present Study

Overall, passive roadside method is advantageous over the remote method attributed to its simple 1-D linear array, which consumes much less space, and, hence, a more practical method that can be adopted especially in congested urban areas. In urban areas, the space for securing large area for field experimentation is very difficult to obtain, which restricts the use of Remote MASW Survey. In such areas, it is also often difficult to acquire good quality active field records because of prevailing high-energy ambient noise. Under such circumstances, the passive roadside method, utilizing the surrounding traffic sources and prevailing vehicular movements in an urban area, offers a good alternative approach for subsurface profiling. Usually, in the urban areas, the linear patches of the sidewalks and shoulders of the road sections would be available which are conducive for the passive roadside test employing linear 1-D receiver array. In addition, attributed to the linear array configuration, a combined active-passive survey can be conducted at the same test setup, wherever possible, which could give information of both shallower and deeper layers.

However, very little research has been conducted on the true effectiveness and real field complicacies of roadside survey until date. Moreover, as already mentioned, the efficacy of the method relies on attaining better level dispersion images. Literature survey shows that such studies aimed to elucidate the influence of different factors in producing a good quality dispersion image from a passive roadside method is very scanty. Owing to these deficits, the method is yet to become a self-sufficient method for subsurface profiling, and yet depends on large-scale validations with active, passive remote or borehole methods. Further, the passive roadside method is based on the utilisation of surface waves originated from traffic sources, which generally caries wavefields of long wavelengths, which may help in identifying deeper soil layers. Thus, the lacunae present in this direction of research, associated with this particular non-destructive method of subsurface profiling, provides the motivation of the study. The present research work comprises the detailed investigations conducted on various aspects of passive roadside MASW survey, with special emphasize on the factors influencing its resolution of dispersion imaging.

1.6 Organisation of the Dissertation

The present research is presented in the form of a dissertation having the following chapters:

- **Chapter 1** provides the importance of shear-wave velocity as a dynamic property of soil, along with a brief overview of the MASW survey and its different types. The motivation of conducting the present research is also elucidated.
- **Chapter 2** presents a detailed literature survey on various aspects related particularly to the enhancement of dispersion imaging of passive MASW survey. Subsequently, the objective and scope of the present work has been highlighted.

- **Chapter 3** comprises the theoretical background of dispersion imaging and inversion techniques used in the analysis of the results from passive roadside MASW survey.
- **Chapter 4** presents the details of the test sites adopted in this study for the field experimentation. It also contains the details of instrumentation and software utilized in this study.
- **Chapter 5** reports the detailed study of the quality of raw field records from different traffic source origin in terms of its frequency and energy content, and its impact on dispersion imaging.
- **Chapter 6** describes the influence of acquisition parameters, mainly length of receiver array and acquisition time, at sites with different traffic volume on the resolution of dispersion imaging.
- **Chapter 7** presents the influence of various processing parameters, such as scanning range of frequency and phase velocity, searching quadrants, processing scheme and vertical stacking, on the resolution of dispersion image.
- **Chapter 8** presents the effect of dispersion curve selection, in terms of range of selection and density of points, on the accuracy and reliability of resultant V_s profile.
- **Chapter 9** describes the significance of source location and offline distance of receiver array on the resolution of dispersion imaging.
- **Chapter 10** presents the summary and conclusions drawn from the present study. A set of recommendations and guidelines are provided in relation to adopting a good practice of conducting a passive roadside MASW survey, in terms of generating better resolution dispersion images and reliable V_s profiles of the subsurface. Based on the limitations of the present study, a list of future scopes is also provided.

CHAPTER 2

LITERATURE REVIEW AND SCOPE OF PRESENT STUDY

2.1 General

This chapter reviews the basics of the MASW and its evolution from different surface wave techniques with special emphasize on Passive MASW survey. It highlights the earlier research works and developments in various data acquisition and processing parameters affecting the resolution of dispersion imaging, especially in the case of passive MASW survey.

2.2 Review of Multichannel Analysis of Surface Waves

With the advent of surface wave techniques in characterizing subsurface profile, geophysical exploration has taken a long leap. As many surface wave techniques being still evolving, the technique known as Multichannel Analysis of Surface Waves, or, shortly, MASW, has recently been the most critically acclaimed one (Park *et al.,* 1996, 1999, 2007). It yields subsurface information in terms of shear wave velocity (V_s) profile of the surveyed area. V_s is a very useful dynamic property of soil and has established correlations with many soil parameters such as shear modulus, bulk modulus, fundamental frequency of vibration, seismic amplification and Poisson's ratio etc. (Dikmen *et al.,* 2010). It also has a number of established correlation with popular field parameter obtained from the Standard Penetration Test, SPT-N value (Imai and Tonouchi, 1982; Dikmen, 2009; Uma Maheswari *et al.,* 2010; Anbazhagan *et al.,* 2012; Fauzi *et al.,* 2014). Having such vital connections with important soil properties, V_s has been successfully utilized in many significant areas of geotechnical and earthquake engineering, namely seismic site effect

evaluation, determination of soil liquefaction potential, seismic site characterization, and seismic microzonation studies (Kanli *et al.,* 2006; Lin *et al.,* 2004; Picozi *et al.,* 2009; Eker *et al.,* 2012; Trupti *et al.,* 2012; Uyanik *et al.,* 2013).

MASW is primarily popular for its swiftness in data recording and analysis, deeper subsoil investigation and cheaper operational cost. Researchers have obtained good agreement between V_s profile obtained from MASW method and conventional borehole techniques (Anbazhagan and Sitharam, 2006; Uma Maheswari *et al.,* 2010). It utilizes propagation of surface wave, mainly Rayleigh wave, also known as ground roll, for subsurface characterization. Rayleigh wave based geophysical methods have two major advantages – firstly, in any vertical surface event, Rayleigh wave constitutes almost 2/3rd part of the total wavefield, and thus bears a high signal to noise ratio (SNR). Secondly, it possess the ability of distinguishing soft layers of soil sandwiched between stiffer layers, which was difficult in earlier methods (Tokimatsu *et al.,* 1991; Xia *et al.,* 2000b; Park *et al.,* 2007; Park, 2013). Rayleigh waves are produced from the interference of P-waves and vertically polarized S-waves. They travel along or near the ground surface with low velocity, high frequency (> 2 Hz) and high energy or amplitude. Particle motion in Rayleigh wave follows retrograde motion (anti-clockwise motion) in an elliptical shape along the surface, where the major axis is oriented in the vertical direction. At depth, the particle motion turns prograde (clockwise motion) with similar elliptical shape (Beaty *et al.,* 2002; Xia *et al.,* 2002; Xia *et al.,* 2004a; Gosar *et al.,* 2008). MASW is based on the principle of Rayleigh wave dispersion. This implies that Rayleigh wave travels with different propagation velocities (both phase and group velocity) at different frequencies while propagating through a heterogeneous soil medium. This property of Rayleigh wave is utilized for obtaining a dispersion curve that is a plot between phase velocity and

frequency. Finally, the dispersion curve is inverted with an efficient algorithm to obtain the V_s profile of the surveyed area (Tokimatsu *et al.,* 1992; Park *et al.,* 1998b; Miller *et al.,* 1999; Park *et al.*, 1999; Xia *et al.*, 1999; Moura *et al.*, 2012).

For a layered earth model, Rayleigh wave phase velocity is a function of frequency and four earth parameters and those are compressional wave velocity (V_p), shear wave velocity (V_s), density and thickness of layers. However, for the fundamental mode Rayleigh waves, and in the high frequency range of 5-40 Hz, shear wave velocity is found to be the most influencing parameter to the sensitivity of dispersion curve (Xia *et al.,* 1999, 2000b). Thus, the inversion of dispersion curve becomes a logical tool to obtain a V_s profile of the surveyed area. Inversion of dispersion curves to estimate V_s profile of the earth was first attempted by Dorman and Ewing (1962).

MASW was first developed by Park *et al.* (1998a). The method has two basic modes of field surveying, primarily based on utilization of source of wavefield generation, and they are termed as (a) Active MASW survey and (b) Passive MASW survey. An active MASW survey utilizes a user-controlled source of wavefield generation such as a sledgehammer, automated or manual weight drops, harmonic shaker, accompanied with a linear receiver array spread in line with the source. The depth of investigation achievable via active test is normally in the range of 20-30 m, which is primarily dependent upon the wavelength of waves generated by the impact. Longer the wavelength, greater will be the depth of penetration, and hence larger is the depth of the investigation. To increase the wavelength of signals, larger impact is required with heavier weight that becomes impractical in regular field experimentations. Some researchers have used large weight with enhanced height of fall to generate high energy and longer wavelengths. Comina *et*

al. (2011) used a weight of 130 kg falling from a height of 3 m and a weight of 750 kg falling from a height of 1.6 m for an active MASW survey.

Passive mode of survey utilizes ambient vibrations originating from various natural (e.g., tidal) or cultural (e.g., traffic) sources. This mode of survey is useful in urban noisy environments where a conventional active source created wavefields bear contamination from ambient stronger energy. Further, such passively originated wavefields carries waves of much longer wavelength, and thus capable of yielding information of deeper layers of soil. Hence, such passive ambient vibration is an effective tool to delineate subsurface material to a greater depth (Aki, 1957; Horike, 1985; Tokimatsu *et al.*, 1992a; Okada, 2003; Kühn *et al.*, 2011).

2.3 History of Surface Wave Methods

As per the author's knowledge, surface wave testing was first attempted in Germany in 1938 (Jones, 1958). The Germans used mechanical vibrators to produce ground vibrations in the frequency range of 10-60 c/s (cycles per second) and observed that with increase in frequency, the velocity of propagating waves decrease. It was understood that the variation was attributed to the change in properties of soil with depth. However, the type of wave produced by the vibration was not recognized, which restrict a provision of sufficient explanation. Jones (1958, 1962) presented a technique, popularly known as Steady State Rayleigh Method, and started new possibilities in surface wave testing. The method is based on single station and single source mechanism. The source utilized is an electromagnetic vibrator producing frequency range in between 35-400 c/s. The author established the fact that a vertically impacting surface event mostly produces Rayleigh waves. The objective of the method is to locate ground positions that remain in phase with source

vibration. The distance between two such successive positions is considered the wavelength and is used in phase velocity determination.

A very effective and popular surface wave method finds its inception in the form of Microtremor Survey Method (MSM) in Japan, and, still being used for many applications. This method is a passive survey method and uses 2-D arrays with different shapes and with limited number of receivers to record ambient vibrations i.e., microtremors (Aki, 1965; Okada, 2013). Microtremor can be defined as the naturally occurring seismic waves from non-seismic sources. Precisely, these are short period vibrations originating from natural sources such as sea waves, atmospheric loading, wind forces on structures, and plants, and cultural sources such as traffic, trains, construction machineries (Asten and Henstridge, 1984; Asten *et al.,* 2004; Molnar *et al.,* 2007; Rosas *et al.,* 2011). Primary complications in MSM method are reported to be the cases when wavefield is strongly directional and contains multiple modes.

Microtremor based studies can be broadly divided into two groups – (a) single station spectral methods, and (b) array studies with multiple stations or receivers. In the first method, the microtremors are recorded with the help of single-station three-component seismometer, which are then analyzed in a frequency domain platform. Fundamental frequency of soft sediments overlying hard bedrock can be obtained from spectral ratio between the records of horizontal and vertical components. The method is popularly known as Horizontal-to-Vertical Spectral Ratio (HVSR) method. The primary disadvantage of the HVSR method is the unavailability of standard guidelines for data acquisition and processing (Gosar *et al.,* 2008). In the second group of studies, array methods are used to measure phase velocities of microtremor data. Most widely used

processing schemes in array methods are Spatial Autocorrelation (SPAC) and frequency wavenumber (*f-k*) analysis (Okada, 2003; Foti *et al.*, 2007). Microtremor method with SPAC tool has been found to be better choice in site characterization than HVSR technique, particularly where the shear wave velocity contrasts are low (Asten *et al.*, 2004).

In urban areas, using MSM method with large 2-D receiver arrays to record ambient surface waves is impractical. A comparatively simple method known as Refraction Microtremor, or ReMi, which uses a simple linear receiver array (Louie, 2001; Cox and Beekman, 2011) to record passive surveys waves was introduced in the early 2000s. One critical assumption in this method is that the surface waves originating from strong sources, situated out of line with receiver array, manifest itself on the higher side of the phase velocities. Therefore, on a dispersion energy image obtained from existence of such sources, dispersion curve is extracted by selecting points of lowest phase velocities (Cheng *et al.*, 2016). Though the method is not as accurate as other 2-D passive surveys, attributed to its easier field works and simple processing, it has been used in various applications in recent times. Coccia (2011) utilized the method in studying a landslide area in the Caramanico Terme, Italy. Panzera and Lombardo (2013) used combined application of ReMi and MASW to evaluate various features of the local seismic response and to determine dynamic properties of soil.

In early 1980's, an active method named Spectral Analysis of Surface Waves (SASW) has been developed at the University of Texas at Austin (Heisey *et al.*, 1982; Nazarian *et al*., 1983). The method is a two-receiver technique and uses an active source for the generation of required wavefield that can be either an impulsive or a harmonic one. Phase velocity is evaluated by estimating time required for the arrival of the wavefield at the two receiver locations at every

frequency component, which allows the direct construction of dispersion curve. However, the dispersion curve has to be estimated by using several receiver spacing configurations, owing to the limitations on the frequency range due to the two-receiver approach. Finally, individual dispersion curves obtained from different receiver spacing configurations are combined to form a single composite dispersion curve. The method has become popular attributed to its easier data acquisition over the others. It has been utilized in many applications such as determination of stiffness of Portland cement concrete, road pavement stiffness, and rock mass characterization (Rix *et al.*, 1990; Ismail *et al.*, 2012; Goh *et al.*, 2011). A primary limitation of the method is that only one phase velocity can be estimated at a particular frequency and hence multimodal characteristics of dispersion image may not be retrieved (Ryden *et al.*, 2004).

In pursuit of the solutions of various limitations of two-receiver approach of SASW, use of multi-station recording of data has been carried out in early 1990's (McMechan and Yedlin, 1981; Gabriels *et al.*, 1987). Later, Park *et al.* (1996, 1998a) has further developed and introduced the method as Multichannel Analysis of Surface Waves, i.e., MASW. The method, and corresponding analytical tools, had been initially started for only active surveys, but later developed for passive surveys as well (Park *et al.*, 2004; Park and Miller, 2005).

2.4 Passive MASW Survey

Depending on geometrical layout of receiver array and utilization of source of wavefield generation, Passive MASW survey can be divided into two modes, namely (a) Passive Remote survey, and (b) Passive Roadside survey. In passive remote survey, 2-D symmetrical arrays such as circular array, cross array, square and rectangular arrays are utilized to record the ambient

vibrations of natural or cultural origin. Natural origin refers to tidal waves and microseisms, whereas cultural sources refer to surface waves from traffic, vibrations from construction or other machineries. Long wavelengths generated from natural and cultural sources penetrates deeper into the subsurface and hence can give information of deeper layers of soil in the range of 200-250 m, which cannot be achieved by active MASW survey (Park *et al.*, 2007). Passive remote method requires large 2-D arrays to be deployed for recording waves of longer wavelength. However, passive roadside survey is much easier to conduct as it merely uses a linear receiver array along the sidewalk or shoulder of a road and records traffic originated waves. Such survey can also yield information up to significant depth of 100-150 m depending upon weight and speed of vehicles. It is important to note here that, with existence of heterogeneous and layered subsurface profile with low V_s values or intermediate soil layers with decreasing V_s values, the recorded wavelength may not necessarily give theoretical depth of investigation. In this regard, Noorlandt *et al.* (2017) reported recording of surface waves with maximum wavelength of nearly 200 m, which on inversion could result penetration depth of only in the range of 10-50 m. It was reported that 2-D arrays in remote survey have better control in accounting omni-directional nature of wavefields originating from multi-azimuthal locations and hence can result more accurate phase velocity information (Comina *et al.*, 2011). Because of the 1-D nature of array, roadside method mildly compromises the accuracy in phase velocity estimation. Overall, roadside method offers great flexibility and a more practical methodology than the passive remote survey due to its easier field operation. It also possesses the ability to conduct combined active and passive survey with the same linear array, giving higher frequency band of analysis and resulting in a robust and complete survey of the site. It can be understood here that passive remote method has evolved from microtremor survey method (MSM), and both are based on similar methodology with only

difference of lesser numbers of receivers in the latter. Similarly, passive roadside and ReMi techniques are based on similar principle of linear array and collecting signals from cultural sources. However, in roadside survey, receiver array is conventionally placed parallel to the road alignment, while no such conditions exist for ReMi method (Roma and Moura, 2009; Roma *et al.*, 2011).

Park *et al*. (2007) introduced the term Passive Roadside MASW method and its basic working principle that has been used in the thesis. The various advantages of Passive Roadside MASW survey employing linear array over the 2-D Passive Remote MASW survey or other similar methods (e.g., MSM) were also highlighted. It was specifically reported that the Passive Roadside MASW method records signal originated only from the local traffic. Park and Miller (2008) developed the schemes for processing field records obtained from Passive Roadside MASW survey. In the context of recording of field data, the researchers considered various combinations of source location with respect to the recording geophone array. Depending upon the varying nature of wavefield arrival in the receiver array, Inline Plane (IP), Offline Plane (OP) and Offline Cylindrical (OC) processing schemes were proposed for each of the conditions. These processing schemes are also incorporated in the SurfSeis software that has been used in the thesis. Park (2010) further researched on the Passive roadside method for the enhancement of the resolution of dispersion imaging and for the detection of source location in a typical urban roadside MASW survey. Banab and Motazedian (2010) utilized moving trucks and heavy vehicles to conduct Passive roadside MASW survey for the characterization of subsoil layers with high velocity contrast. The maximum exploration depth achieved through this study ranged from 55-95 m beneath the ground surface. Brandes *et al*. (2011) have successfully used passive roadside method,

to a site at Hawaii, to identify the soil and rock characteristics up to a depth of 25-30 m. Saez *et al*. (2014) conducted geophysical surveys of two piers affected by liquefaction induced lateral spreading due to the 2010 Maule earthquake. In the reported study, both active and passive roadside measurements, employing linear receiver arrays, were carried out simultaneously. Cheng *et al*. (2018) have used passive roadside method in the search of effectiveness of imposing active source events during high frequency passive surface wave measurement. Anbazhagan *et al*. (2018) extensively studied the characterization of Indo-Gangetic Basin at 275 sites utilizing combined active, passive roadside and passive remote MASW methods. As per the NEHRP recommendations (BSSC, 2003), the entire basin was classified in terms of the achieved shear wave velocity.

Irrespective of the mode of MASW survey, the primary steps for V_s profiling are (a) raw field data acquisition, (b) dispersion analysis, and (c) inversion analysis. Raw data are acquired by a seismograph and is normally recorded in offset v/s time format. Dispersion analysis involves conversion of raw time domain data to frequency domain with the help of wavefield transformation processes that are mainly based on Fourier transformation. The objective of the process is to utilize the dispersive property of surface waves in heterogeneous media and to construct a plot of phase velocity v/s frequency for each surface wave component. Such a curve is known as dispersion curve, and the accuracy of final V_s profile entirely depends upon the accuracy of the identified dispersion curve. Finally, inversion of dispersion curve is done using an appropriate inversion algorithm to obtain the subsurface shear wave velocity profile.

2.5 Dispersion Imaging in MASW

Dispersion imaging of raw wavefield data is the most important stage of MASW as the accuracy of final V_s profile entirely depends on the accuracy of the experimental dispersion curve. Most of the existing processing techniques rely on Fourier Transformation (FT) of the signal that separates the frequency components of the signal. The separated frequency components are subsequently processed by means of various techniques to obtain phase velocity v/s frequency relationship i.e., the dispersion curve. Foti *et al.* (2014) categorized dispersion imaging techniques in the following divisions:

- Direct assessments of propagation parameters, e.g., Steady State Rayleigh Method (SSRM) and Spectral Analysis of Surface Waves (SASW).
- Regression methods, e.g., Multi-Offset Phase Analysis (MOPA) and Spatial Autocorrelation (SPAC).
- Transform based methods, e.g., Frequency-Wavenumber analysis (*f*-*k*), Frequency-Slowness analysis (ω-*p*), and Frequency-Phase velocity analysis (*f*-ϕ_v).

Steady State Rayleigh Method (SSRM) was proposed by Jones (1958). It is a one source and one receiver technique and uses both Rayleigh and Love wave for subsoil characterization (Foti *et al.*, 2014). Here, the lone receiver is continuously moved away from the source until both arrive in phase and such locations of the receiver on the field are marked. The distance between two adjacent in-phase locations from the fixed source is considered as the wavelength of the wave at the measured frequency. Then, utilizing fundamental relationship between frequency, wavelength and phase velocity i.e., $\lambda = c/f$, the latter is evaluated. This procedure is repeated with different operating frequencies to produce the dispersion curve. The SASW technique developed by Nazarian *et al.*

(1983) is based on phase delay that is also a direct assessment technique of Rayleigh wave propagation. Here, the phase velocity of a single sinusoidal wave is determined by dividing the distance travelled by the required time or, simply, the time delay. Strobbia and Foti (2006) improved the SASW technique with multichannel approach that is known as Multi-Offset Phase Analysis or MOPA. In this method, the phase velocity is estimated by processing phase and offset of the particle motion. Aki (1957, 1965) developed the Spatial Autocorrelation (SPAC) method to determine the dispersion curve from microtremor data.

Lately, wavefield transformation methods are becoming popular for dispersion analysis, mainly for their ability to differentiate different seismic events and for the identification of multiple modes of Rayleigh wave propagation. The common principle in these techniques is to transform the experimental time domain data into a different domain where the propagation characteristics of surface waves are identified as spectral maxima. Most of these methods make use of Fourier transformation that separates different frequency component of a signal and thus transforming it into frequency domain. Subsequently, phase velocities at different frequencies are estimated using suitable processing technique (Foti *et al.*, 2011a). Normally, time domain data are transformed to frequency wavenumber domain, i.e., *f-k* domain, and frequency slowness domain, i.e., ω-*p* domain, by applying numerical transformation methods. To obtain energy spectrum in the *f-k* domain, Fourier transformation is applied in both time and space on the field data, and thus the field data is transformed into an image of energy space as a function of frequency and wavenumber. The ω-*p* transform is based on slant stack (τ-*p*) or linear Radon transforms (Cox and Beekman, 2011; Foti *et al.*, 2014), where τ is the time delay at zero offset and *p* is the slowness or velocity inverse. The τ-*p* transform decomposes a wavefield into linear plane wave components. The transform can be

determined by first transforming the wavefield $u(x,t)$ into the *f-k* domain and then calculating the one dimensional (1-D) inverse Fourier transform along a straight line $k=fp$ for each p value. This transform is faster than *f-k* transform and result in a dispersion image with higher resolution.

Both *f-k* and ω-p method requires a large number of traces to yield better results. Park *et al.* (1998a) proposed a faster method known as phase-shift method that requires a limited number of traces and is capable of generating dispersion image with much better resolution and higher accuracy. Here, Fourier transformation is applied to time axis of a shot gather $u(x,t)$ to convert it into a frequency domain function $U(x,\omega)$. Subsequently, an integral transformation is applied on $U(x,\omega)$ to obtain the frequency domain characteristics as $V(\omega,\phi)$. Dispersion curves are finally obtained by transforming $V(\omega,\phi)$ with changes in its variables such that the phase velocity is obtained as $C=\omega/\phi$.

2.5.1 Dispersion Imaging in Passive MASW

Dispersion imaging method for Passive MASW has to take account of unknown positioning of sources, their strength and multiple numbers of sources. The primary unknown field parameters in passive survey are the azimuth and distance of a source from receiver array. In preliminary dispersion imaging processes of MASW, azimuth is considered as the dominant parameter that influences the dispersion imaging process. Park *et al.* (2004) modified the conventional phase-shift method of active survey to utilize for passive remote survey as well. The modified method transforms wavefields of propagating horizontal plane waves into two orthogonal axes. For the development of the scheme, a cross layout of receivers has been utilized. It is a composite scheme of the slant stack and the conventional frequency wavenumber (*f-k*) methods. For a 2-D passive survey, the scheme has three scanning parameters, i.e., frequency, phase velocity and azimuth. For

each frequency (ω), the energy for a phase velocity is calculated for an azimuth. This calculation of energy is carried over a scanning range of phase velocity and repeated over a scanning range of azimuth. Attributed to the two orthogonal receiver spread, the calculation is carried over both the axes. Thus, for every value of ω, one c-θ space is formed where multiple energy peaks occurring at different phase velocities and azimuths represents different modes and sources respectively. To produce an energy space with only phase velocity axis, the energy in c-θ space is stacked at different azimuths along the azimuth axis. Peaks in the space indicate phase velocities for different modes for the analyzed frequency. All these steps are repeated for different frequencies to finally result energy distribution in terms of c-ω space, where dispersion trends are recognized through the energy accumulation patterns. Major complications of passive survey such as phase velocities due to multiple sources, modes and spatial aliasing can be effectively alleviated by this transformation (Park and Miller, 2005). This method, thus, ignores the distance of the source and considers only azimuth in the imaging process. However, Park and Miller (2008) reported significant overestimation of phase velocities of Rayleigh waves in lower frequency band, due to the waves of long wavelength arrived from closely situated sources whose distance were not considered in the scheme.

Park and Miller (2008) have proposed a dispersion analysis scheme for passive roadside surveys that is based on the same principle as that of remote surveys. Despite having a linear array mode of recording surface waves, a 2-D mode of dispersion analysis is needed to account for offline and cylindrical nature of surface waves. The authors considered three possibilities of wave arrival while formulating the scheme for passive roadside: inline plane (IP), offline plane (OP) and offline cylindrical (OC). When a road is fairly straight for a long stretch and waves are generated from

sources situated at a great distance, the wavefield arrival will be mostly of IP type. When the wavefield is produced from a distant source not situated in line with the surveyed road, then the wavefield arrival will be OP type. When the sources are situated too close to the deployed receiver array, the wavefield recorded will be mostly OC type. The author compared three schemes made for each of the above case and found out that the OC scheme to be most accurate that takes account of both azimuth and distance parameter of a source, and thereby considers both offline and cylindrical nature of wavefield respectively. The authors also reported that the OC scheme should yield high resolution dispersion image in the presence of strong sources situated within the receiver array length also known as intra-line sources, though there is no experimental validation of the same.

2.5.2 Challenges and Uncertainties in Dispersion Imaging

Dispersion image contains information of Rayleigh wave dispersion characteristics at varying frequencies. Xia *et al*. (1999) reported that for a layered earth model, S-wave velocity has the most dominant influence on fundamental mode Rayleigh wave phase velocity and hence inversion of the same is an effective tool to obtain V_s information. Even during early studies, one of the primary assumptions in surface wave method has been that Rayleigh wave propagation belongs mainly to the most energetic fundamental mode (Weaver *et al.*, 1982; Karray and Lefebvre, 2008). It was reported that in case of normally dispersive profile, where stiffness increases with depth, fundamental mode Rayleigh wave propagation dominates in a field record. However, in case of inversely dispersive soil profile, e.g., a stiff layer overlying a loose layer, there is a high possibility of higher mode dominance (Gucunski and Woods, 1992; Tokimatsu *et al.*, 1992b). Further, a

dispersion image obtained from a field record can be of multimodal characteristics along with interference from body wave, back or side scattered surface waves, airwaves etc. In such a dispersion image, it is normally difficult to differentiate the fundamental mode dispersion curve from the other modes, and there is a high possibility of mode misidentification leading to V_s results substantially deviated from actual subsoil profile (Boaga *et al.*, 2014). Particularly, in case of passive surveys, higher mode dispersion curve is often misinterpreted as the fundamental mode that may lead to erroneous V_s result (Park *et al.*, 2005; 2007).

The efficiency of dispersion imaging techniques can be defined in terms of resolution, noise content (SNR), and computation times (Dal Moro *et al.*, 2003; Luo *et al.*, 2008). A high resolution of dispersion image, with thinner energy band, and with proper distinction from higher modes and other contaminations, is of critical importance for the inversion process to obtain an accurate V_s profile. A very crucial issue in dispersion curve estimation in a dispersion image is the selection and extraction of the peak points of energy spectra which is the true representation of the dispersion curve. With the increase in the thickness of the energy band, extraction of points of spectral maxima becomes difficult. Normally, the true peak points on an energy band are the points of greatest SNR value. It is difficult to ascertain the points of largest SNR by visual inspection, and often found to have a non-unique solution to the problem. However, a quantitative or a mathematical analysis capable of accurately extracting the dispersion points on mathematical support, rather than visual inspection, has not been reported yet.

In surface wave methods, resolution can be defined as its capacity to accurately determine the vertical and horizontal characteristics of subsurface earth. Hence, efficiency of a method is

evaluated based on its horizontal as well as vertical resolution capacity. In general, horizontal resolution can be defined as the ability to distinguish anomalous objects that are laterally displaced from each other (Yilmaz, 1987; Yin *et al.*, 2016; Mi *et al.*, 2017). In terms of MASW, horizontal resolution is the pseudo 2-D profile obtained through stacking of 1-D V_s profiles calculated at the centre of receiver array at each successive roll (Xia *et al.*, 2005). On the other hand, vertical resolution is the capacity as to how accurately the final V_s profile, with respect to depth, can be obtained from a MASW survey. Both horizontal and vertical resolution of MASW is affected by a number of field and processing parameters. Receiver array length, acquisition interval are some of the important parameters influencing horizontal resolution (Park, 2005; Xia *et al.*, 2005). On the other hand, vertical resolution largely depends upon receiver array length, inter receiver spacing, and natural frequency of geophone. However, both horizontal and vertical resolution entirely depends upon the quality of the dispersion image, and, hence, is considered the most critical in the analysis of MASW survey records.

2.6 Parameters Influencing Resolution of Dispersion Imaging in Passive MASW Survey

2.6.1 Geometrical Parameters - Source Offset and Receiver Array

In passive MASW survey, the ambient noises are recorded by exercising various geometrical array shapes depending upon the requirement, site conditions and limitations. The method requires special geometrical requirements to fully exploit the effective recording of low frequency ambient noise. The following section describes two primary geometrical field parameters i.e., source offset and receiver array, controlling the quality of recorded raw field data and the subsequent dispersion imaging process.

Source offset, i.e., the ground distance between the source of impact and the 1st receiver of the array, is a very important parameter in MASW survey. Surface waves require a minimum distance of propagation from the point of generation before turning into horizontally propagating plane wave. The undesirable effect due to smaller source offset in a multichannel record is called near-field effect. The effect causes recording of wavefield of high frequency and weak energy lacking coherency. To avoid this effect, source offset has to be greater than half the maximum desired wavelength. Further, if the far offset is too large, attributed to larger receiver spacing or large number of receivers, the raw record at the far receivers will contain wavefields resulting from interference from dominant high frequency body waves. This effect is called far-field effect that compels to limit the far offset distance and the highest frequency at which phase velocity can be measured. To avoid far field effects, the far offset distance should be within twice the desired investigation depth (Stokoe *et al.,* 1994; Park *et al.,* 1999; Xia *et al.,* 2004b; Mohamed *et al.,* 2013). However, in passive method, as the sources of wavefield generation are not known prior to data processing, the two effects are not addressed much in the literature. Further, the low frequency wavefield from passive sources suffers lesser attenuation and contamination from body waves. To record these low frequency waves, larger arrays of specific shapes are needed. However, rapid attenuation property of higher frequency components of passive surface waves limits the receiver spacing and array length (Foti *et al.,* 2007).

Xia *et al.* (2004b) reported that longer the geophone spread, higher is the resolution of the dispersion image. To avoid spatial aliasing, the receiver spacing should be less than half the shortest measured wavelength. Depending on site requirement and existing conditions, different

array shapes can be used in recording passive surface waves. Normally symmetrical shapes such as cross, circular, and square arrays are recommended for passive remote MASW. The use of unsymmetrical arrays such as rectangular and acute triangular arrays are not recommended due the possibility of bias in recording waves coming from a pseudo-direction rather than actual direction of surface wave.

Asten *et al.* (2004), with the aid of Microtremor method (MTM) method, compared the influence of triangular, hexagonal and semicircular arrays. The author reported that uses of semicircular arrays are advantageous particularly when there is strong directional wavefield. However, for identification of multiple modes, both hexagonal and semicircular arrays were reported to be equally suitable. Banab and Motazedian (2010), in the study for evaluating efficiency of MASW technique for determination of sharp velocity contrast between subsurface layers, conducted extensive active and passive tests. Linear arrays of length 34.5–80.5 m have been used for roadside survey and triangular array of side 40 m were used for remote survey in the study. Comina *et al*. (2011) used circular arrays of diameter ranging from 50-75 m with 8-24 numbers of low frequency receiver. The receivers were evenly spaced along the circumference of the circular array with inter receiver spacing ranging from 10.35-19.41 m. Ariffin *et al*. (2015) used L-shaped arrays in the combined study of active and passive MASW survey. The authors used 9 receivers to place on a 30 m array in both leg of the L-shaped array with constant inter-receiver spacing of 5 m.

2.6.2 Data Acquisition Parameters

During data acquisition in MASW survey, there are various recording parameters which directly influences the quality of raw field data and, thereby, the resolution of dispersion image. Data

acquisition in passive survey is different from an active survey from many aspects. Most important parameters are the natural frequency of geophone, acquisition time, sampling frequency and stacking of raw records or dispersion images.

2.6.2.1 Natural Frequency of Geophone

The geophones, or receivers, are the first component of a surface wave recording system. Geophones convert the ground motion into an electrical or electromagnetic signal that is transmitted and recorded by the acquisition device. The geophone casing comprises a magnet that is surrounded by a small wire coil suspended by a spring. The acoustic waves propagating through the soil vibrates the soil particles. These vibrations are picked up by the geophone spike that remain pierced inside the ground. The vibration is further transmitted to the magnet, which generates a magnetic field, resulting in the displacement of the wire coil. Owing to its inertia, the relative movement of the coil produces electromagnetic voltages proportional to the relative velocity of the coil. These voltages are collected in the form of seismic data by the seismograph (Foti *et al.*, 2014).

Natural frequency of geophones largely affects the frequency bandwidth of the recorded signal. It controls the minimum usable frequency below which the amplitude of waves is severely attenuated. For example, if a 40 Hz geophone is used for collecting surface wave data, it will severely attenuate wavefields of frequencies lower than 40 Hz. Thus, in order to investigate deeper layers of soil, it is necessary to collect low frequency or longer wavelength component of surface wave. Therefore, in surface wave testing, geophones with a low natural frequency are normally used in order to obtain the maximum possible investigation depth. In preliminary MASW studies,

Park *et al*. (1998b) utilised 10 Hz geophones to obtain active-source surface wave data in an investigation of anomaly detection at 2 m beneath the earth surface. Xia *et al*. (2000b) suggested use of low frequency geophone of less than 8 Hz to acquire active surface data. Currently, geophones with low natural frequency up to 2-4.5 Hz are widely used for both active and passive survey (Park *et al.,* 1999; Xia *et al.,* 2004b; Kanli *et al.,* 2008; Foti *et al.,* 2014). However, compared to an active survey, passive survey attempts to collect longer wavelength signals, leading to the requirement of lower frequency geophones (0.1 Hz, 1 Hz, 2 Hz, and 2.5 Hz). Comina *et al*. (2011) used very low frequency geophone of 2 Hz for a study with passive microtremor signals.

From the literatures, it is observed that 4.5 Hz geophones are quite common and is widely considered in their applicability for both active and passive MASW surveys. Park *et al*. (2004) utilized 4.5 Hz frequency geophones in recording field data while formulating the dispersion-imaging scheme for passive surface waves generated from nearby heavy traffic. The receivers were placed at a spacing of 5 m in a cross-layout, thus making 115 m each arm of the array. The dispersion curve extracted from the passive survey was obtained in a frequency range of 8-20 Hz and investigation depth was obtained to be approximately 80 m. Park *et al*. (2005) utilized 4.5 Hz frequency geophones for combined Active and Passive MASW dispersion imaging. The study highlighted the fundamental mode dispersion trends from the passive data are prominent in the range of 7-18 Hz. Several other researchers also reported the utilization of traffic-originated surface waves with frequencies higher than 5 Hz, resulting in wavelengths of several tens of meters (Zywicki, 1999; Asten *et al.*, 2004; Yoon and Rix, 2004; Suzuki and Hayashi, 2003; Okada, 2003). Park (2010) utilized 4.5 Hz frequency geophones in passive roadside MASW survey for dynamic detection of source location in the nearby road. The retrieved frequency range from a combined

application of active and passive roadside MASW survey was found, approximately, in the range of 10-50 Hz. Mahajan *et al*. (2011) used 4.5 Hz frequency geophones for conducting both active and passive (remote) MASW test for characterization of the sedimentary cover in the Himalayan Region, India. Using 4.5 Hz geophones, the researchers could record passive surface wave energy in as low as 2-3 Hz frequencies. It was specifically reported that lowest recognizable frequency in a dispersion image is not limited by the natural frequency of the geophone. Similar outcomes were also observed by other researchers (Park *et al*., 2002; Long and Donohue, 2007) while the effectiveness of 4.5 Hz, 10 Hz and 40 Hz geophones were compared in recording surface waves of lower frequencies. It was stated that the 10 Hz geophones could detect signals as low as 5 Hz; while, the 4.5 Hz geophone could recognize signals to the extent of 2-3 Hz. Mendecki *et al*. (2014) used MASW and Refraction Microtremor (ReMi) method for characterization of subsoil profile in the urban areas. For both sets of test, the researchers used 4.5 Hz geophones with a 115 m array length to identify the subsurface profile up to the depth of 40 m. Ariffin *et al*. (2015) used active and passive MASW tests with 4.5 Hz geophones for the site characterization comprising marine clay deposit in Penang, Malaysia. The authors used L-shaped arrays for passive surveys with an inter-receiver spacing of 5 m. The frequency range obtained from passive surveys was in the range of 3-14 Hz, which resulted in an exploration depth of approximately 40 m. Cheng *et al*. (2018) studied the effectiveness of imposing active source events during continuous passive surface wave recording. The authors used both 2.5 Hz and 4.5 Hz geophones for the collection of passive surface waves generated by roadside traffic along with the conventional portable active sources.

2.6.2.2 Acquisition (Recording) Time

Data recording or acquisition time is the time limit to be set in the digital acquisition system during which the surface waves are recorded. Setting an optimum acquisition time depends upon source offset, receiver spread length and stiffness of the propagating medium. In almost all cases of active MASW survey, a short acquisition time in the range of 1-2 sec is normally sufficient to record the surface wave event attributed to the short source offset, and the concentration lies only on the single surface event. On the other hand, in passive MASW survey, source locations, as well as their times of occurrences, of the passive events are nearly unknown, and hence a longer acquisition time is normally set. Park *et al.* (2004), in the study for imaging dispersion curves of passive surface waves, recorded field data for 20 s with 48 numbers of geophones arranged in a cross layout with 5 m inter-receiver spacing. Park *et al*. (2007) adopted a 30 s recording time while conducting a combined active-passive survey, keeping first 2 s for active and rest 28 s for passive surface wave recording. Park (2008), while studying for imaging dispersion of passive surface wave via active scheme, utilized passive field records collected over a time frame of 12 s. In the work, the author reported that in passive surveys, major portion of dominant surface wave energy originate and are recorded mainly from one surface location. Hence, an approximate determination of the location of such major source point will make the passive method more acceptable, and similar processing schemes as used in active survey can be utilized for the processing of passive data.

Gosar *et al*. (2008) utilized a recording time of 32 s at every location for passive surveys, while only 2 s has been devoted for the active surveys. Park (2010) utilized a long recording time of 120 s for recording both active source generated surface waves and passive surface waves generated

from traffic origin. The record was then divided into a number of sub-records of 1 s each. Dispersion images obtained from each of these sub-records were finally stacked to form an enhanced dispersion image. The inter-receiver spacing of the array was 1.2 m with 30 numbers of geophone. The source offset adopted for active recording was 7.2 m. The processing scheme used in the study was termed as passive-with-active (PWA) scheme. Yoon (2011), in the study to develop a composite dispersion curve by conducting combined active-passive survey, utilized a long recording time of 256 s, at a sampling frequency of 320 Hz, for collecting passive surface wave data which were mostly traffic originated and from Pacific Ocean. In case of passive roadside survey, acquisition time is suggested to be set in a way such that atleast one vehicle should pass the nearby the receiver spread during the recording time of surface waves, and hence the acquisition depends largely on the volume of traffic on the nearby road beside which the survey is conducted.

2.6.2.3 Sampling Frequency

Sampling frequency is another important parameter of field data acquisition, which is defined as the number of samples or data collected per second during the recording process to gather the wavefield propagation in digitized form. According to Nyquist theorem, the sampling frequency has to be atleast twice that of the maximum observable frequency in the wavefield to successfully convert it from analog to digital form (Foti *et al.*, 2014). An insufficient sampling frequency create aliasing in the recorded signal due to which all the frequency components of the signal will not be sampled or recovered properly. Hence, setting optimum sampling frequency during the recording process needs adequate knowledge and experience to sample the required set of wavefields and to avoid the unnecessary ones. Gosar *et al*. (2008), in the work of comparing active and passive

MASW test results, adopted sampling frequency of 2000 Hz and 500 Hz for collecting active and passive field data, respectively. Picozzi *et al*. (2009) applied a sampling rate of 200 Hz in his work for site characterization by ambient noise. Yoon (2011) utilised a sampling frequency of 320 Hz for recording sea wave sourced passive surface waves. Normally, to record passive sourced signals, sampling frequency is set much lower than to record active signals attributed to the objective of collecting lower frequency component of passive signals. However, there is no standard guideline for selecting an optimum range of sampling frequency for a typical passive MASW survey, and the same is selected on a trial-and-error basis.

2.6.3 Signal and Vertical Stacking

In surface wave techniques, it is often required to increase the SNR of the useful signal when there is a dominant unwanted ambient noise environment effective during data acquisition. This can be achieved by a process known as 'vertical stacking' that implies summing of multiple signals by repeating the recording of the test data in a synchronised manner. By this summation process, the amplitude of the coherent signal increases with number of stacking applied while the amplitude of incoherent noise reduces (Foti *et al.*, 2014). Researchers adopt signal stacking during data recording process to obtain clear and clean raw data, to ensure easier and accurate processing in the subsequent stages. However, there is no standardization on optimum number of vertical stacking and found to be mostly site specific. Xia *et al*. (2004a) reported use of vertical stacking of 6 active raw data to enhance the SNR value. Gosar *et al*. (2008) used 10 number of active source hit stacking to avoid the effect of ambient noise contamination upon field record. Moura *et al*. (2012) used 8 numbers of records for vertical stacking for earthquake site response measurements in an urban area of Porto, North Portugal. Zekkos *et al*. (2014) used 5-8 numbers of stacking,

depending upon surrounding noise situations for active survey, and 20 stacking for passive surveys. Importantly, Park and Miller (2008) discouraged the use of vertical stacking during recording of field data in passive MASW survey owing to the complex wavefield induced from multiple sources and randomness of wave signals in respect to its occurrence, arrival time, and source locations.

Vertical stacking is also available as a tool in most of the analysis platforms to enhance the quality of resultant dispersion image. In this, each raw field data are separately processed and corresponding dispersion images are obtained. The dispersion images are then stacked (superposition of energy at various combination of frequency and phase velocity) to obtain the final dispersion image which normally has better resolution and increased SNR than the dispersion images before stacking. In an active survey, dispersion image stacking may not be a mandatory requirement, as the field record is expected to contain mostly the active source generated major surface wave event. On the other hand, in passive survey, major surface events may not be distinguished during data acquisition. In such cases, vertical stacking of dispersion images is beneficial, as it constructively stacks surface waves coming from major source points resulting in better dispersion image. Normally, greater the number of stacking, the better is the quality of dispersion image. Park and Miller (2008) made use of 10 numbers of dispersion image stacking for the pioneering study in passive roadside survey. Park (2010), in the study for detection of source location in passive roadside survey, used 70 sets of dispersion images obtained from a single long record of 120 s, for a single stacking.

2.7 Combined Active and Passive MASW Survey

It has been learned that both active and passive techniques in MASW survey has their own advantages and disadvantages. Active tests give better resolution in shallow subsurface layers, however, near and far field effects in active tests may cause erroneous results and are of major concerns. The capability of investigating deeper layers of subsoil makes passive methods quite useful over the active method, although it results poor resolution in shallower layers. Further, complex nature of field records and subsequent complicated processing operations raise questions on final V_s profile as well. On the other hand, combined use of active and passive survey may give broader frequency band and fair resolution both in lower and higher frequency domain yielding confidence in the ultimate V_s profile (Tokimatsu, 1995; Rix *et al.*, 2002; Foti *et al.*, 2007; Liu *et al.*, 2005; Park *et al.*, 2005; Foti, 2011b; Zekkos *et al.*, 2014).

Yoon and Rix (2004) recommended that a composite dispersion curve obtained from combining dispersion curve from active and passive test could be fruitful in avoiding the near field effects of the active test and retaining the capacity of deeper subsoil investigation of the passive test. In this regard, the combination should be effectively carried out between the overlapping portion of dispersion curves from active and passive tests. Park *et al*. (2005) utilized active survey for accurate determination of modal nature of dispersion image obtained from passive survey. The study reported the case of misinterpretation of 1st higher order mode dispersion curve as the fundamental mode during passive survey. However, on critically comparing the dispersion curve from passive survey to that obtained from active survey, the authors could truly differentiate between different modes. Foti *et al*. (2007) also recommended the combined use of active and passive methods with particular importance on active test because of the rich data quality in such

tests and in projects where shallow depth resolution is of more importance. Yoon (2011) utilized combined dispersion curves from active and passive methods to obtain a composite dispersion curves from which final shear wave velocity was obtained with greater confidence. The author conducted combined MASW tests at five different test locations in the Western and Southern US with 15 numbers of receivers. The active tests were conducted with a harmonic source with oscillation frequency of 4-100 Hz and a linear receiver array with irregular receiver interval. Passive tests were conducted by deploying circular and cross arrays in the range of 18.3-36.6 m radius/dimension with 12-16 numbers of receivers. Signals were recorded for a recording length of 256 s at a sampling frequency of 320 Hz.

2.8 Inversion Analysis in MASW

In the analyses with surface wave methods, Inversion analysis is the final stage where the shear-wave velocity profile for the investigated substrata is retrieved through a mathematical inversion procedure applied on the dispersion curve. In general, the problem of determining medium parameters from given surface wave dispersion or attenuation curve is termed as Inversion. Surface wave inversion is a non-unique and non-linear problem and categorized as ill-posed problem (Foti *et al*., 2014). In this regard, the primary objective of the all inversion methods is to obtain a final profile with the best possible accuracy, reliability and uniqueness.

2.8.1 Surface Wave Inversion by Empirical methods

The first attempt for the solution of inversion problem was attempted through a numerically simple method known as Steady State Rayleigh method, shortly SSRM (Jones, 1958). This method is the predecessor of the presently popular methods such as SASW and MASW. It is based on two simple

surface wave characteristics; firstly, the ground motion induced strain energy is confined within a depth of about one wavelength from the ground surface and secondly, in a homogenous half-space shear wave velocity is nearly 1.1 times the Rayleigh wave propagation velocity. Thus, shear wave velocity for each point of the dispersion curve may be estimated at a depth equal to a fraction of the wavelength (λ) normally in the range of $\lambda/2$ to $\lambda/3$. The method gives approximate shear wave velocity profile and applicable mostly when the explored site has a normally dispersive characteristic, i.e., increasing stiffness with increasing depth. However, the profile obtained from the method can be fruitfully utilized as an initial profile that can subsequently be used in advanced iterative inversion processes for more confident result (Socco and Strobbia, 2004; Foti *et al*., 2014).

2.8.2 Surface Wave Inversion by Analytical methods

In MASW technique, there are mainly two types of inversion techniques that are commonly used. They are classified as (i) Local Search (LS) iterative methods, and (ii) Global Search (GS) techniques.

In LS methods, iterations are performed based on an assumed initial profile until the final solution converges. The LS method is a much quicker method compared to the GS method, as the number of iterations performed in the former are much lesser. The efficiency of LS methods depends upon the correctness in the adopted initial profile, which should be sufficiently close to the global minimum. The LS approach also makes the solution more biased towards the initial profile (Lai and Rix, 1998). An incorrect initial profile may lead to a failed iteration process without convergence of the estimated and actual profile. The method also has greater possibility of falling

into local minima instead of the global. The most widely used approach in this category is the 'Linearized iterative least square method'. This approach has been used by many researchers with marginal differences in model parameters and inversion strategies (Horike, 1985; Gabriels *et al*., 1987; Xia *et al*., 1999).

GS methods are developed mainly to overcome the mentioned shortcomings of the LS methods. In GS methods, iterations are performed by adopting many initial models and the solutions from each of the profile is retrieved. The true solution of the profile corresponding to the global minima can thereafter be obtained by comparing the local profiles. For the implementation of the global search algorithms, efficient optimization techniques have to be used to provide a guided search in the global population space. The term optimization refers to the finding of the values of input parameters in such a way to get the best possible output results. Some popular optimization techniques are: Monte-Carlo Simulations (Socco and Boiero, 2008), Genetic Algorithm (Pezeshk and Zarrabi, 2005; Dal Moro *et al*., 2007) and Neighborhood Algorithm (Wathalet *et al*., 2004). Monte-Carlo inversion can be defined as a method that uses pseudo-random sampling to search a parameter space to retrieve earth models or other information about the unknowns of interest (Sambridge and Mosegaard, 2002). It is a guided search method, incorporating a scaling method that concentrates sampling in the high-probability density zone (Socco and Boiero, 2008; Leong and Aung, 2013). The method does not imply a uniform sampling unlike it was considered in its early approaches.

Genetic Algorithm is an optimization technique based on the principle of natural genetics and natural selection and survival of the fittest. It is a fully nonlinear direct search method (Sambridge

and Mosegaard, 2002). Here, the solution undergoes a series of genetic operations mainly selection, crossover and mutation, to produce fitter solution in each generation. The process is repeated over many generations until solutions reaching an optimum value of objective function or fitness function is reached. The method has been used for inversion of seismic velocities (Louis *et al.*, 1999), seismic waveform (Stoffa and Sen, 1991) and shallow elastic parameters (Rodrigez-Zuniga *et al.*, 1997).

Neighbourhood Algorithm is a stochastic direct search method. The method attempts to sample the region of multidimensional parameter space that contains models of acceptable data fit or any other objective function and then to extract the best solution from the group of models obtained. The method utilizes previous samples for guiding the search for improved models (Wathelet *et al.*, 2004). The neighbourhood algorithm is reported to provide better result compared to the other stochastic methods (Sambridge, 1999).

One of the primary drawbacks of GS algorithm, apart from its long and slow processing, is that it gives the final solution as a set of acceptable V_s models but not as a single V_s profile. Alhough it is consistent with the non-uniqueness of the solution but it is not easy to handle. For many engineering applications, it is desirable to have a unique V_s profile of the surveyed area. Attributed to this reason, despite many inversion methods have been implemented for interpretation of subsoil characteristics, geophysicists often prefer the LS methods (such as the method of Xia et al., 1999, used in the current work) to the GS methods (Socco *et al*., 2010).

2.9 Practical Applications of Passive MASW Survey

Brandes *et al*. (2011) worked on the characterization of the properties of complex residual soil and rock deposits from volcanic origin on the island of Hawaii with the help of seismic refraction, combined active and passive remote survey. The authors used a linear receiver array with 48 numbers of low frequency geophones placing with an inter-receiver spacing of 1 m. For active tests, a hammer of 5.2 kg-weight was used as the source of signals, while, for passive tests, traffic energy sources from nearby roadways were utilized. Recording time was kept 30 s for each acquisition of passive data. The authors reported existence of fully weathered volcanic rocks and soil with uncommon mineralogy and properties in the site, and the distribution of the same has been identified by the surface wave tests.

Mahajan *et al*. (2011) conducted passive remote experiments for the characterization of sedimentary cover at Himalayan region. In the survey work, two circular arrays with diameters 25 m and 50 m were deployed to collect passive data. In both the arrays, 24 geophones of 4.5 Hz natural frequencies were laid around the circumference of the circular arrays with an inter-geophone spacing of 3.3 m and 6.6 m, respectively. Field data were recorded with a sampling frequency of 250 Hz and long records of 30 s were collected for each setup.

Eker *et al.* (2012), in the study for dynamic soil characterization and site classification, utilized active MASW and passive MAM technique at 51 sites in the northern side of Ankara, Turkey. Surface wave testing was extensively used as the chosen method is particularly suitable for characterization of a site having stiffer layers overlying loose layers that is difficult to recognize via destructive methods. The primary objective of the research was to determine geotechnical and

geological characteristics of the sediments in the region and to classify the site existing with Plio-Quaternary sediments. The researcher used linear receiver array with 12 geophones with 5 m receiver spacing for all the tests. For active MASW test, a recording length of 2 s with a sampling interval of 1 ms was adopted, while, for passive MAM test, a recording length of 5 min with sampling interval of 2 ms had been adopted. The site was classified in terms of average $V_{s,30}$ results after due comparison with the available borehole test results.

Savvaidis *et al*. (2014) conducted extensive experimentation with active MASW and passive MAM technique for the estimation of seismic ground response in Crete, Greece. The authors used a 24-channel seismograph with 4.5 Hz geophone receivers. For the active tests, a 7 kg sledgehammer hitting on a steel striker plate was used as the source. The total recording time was 4 s for active MASW tests and 20 min for MAM tests, with a sampling interval of 2 ms. More than 15 shots were collected at every set up to increase the signal to noise ratio. For both the tests, different receiver spacing was tested depending upon the site requirement. Source offset was also kept at a minimum range of 20 m to avoid near-field effects. Dispersion curve obtained from both the tests were compared and combined to give a composite dispersion curve. The results from the tests were compared with recommendations and clauses from Eurocode (EC8).

Zekkos *et al*. (2014) utilized the methodology of combined active MASW and passive MAM measurements to develop a shear wave velocity model for municipal solid waste landfills. A linear array with 16 receivers placed with 3 m inter-receiver spacing was used for both tests. Signal stacking of 5-8 numbers of record were implemented for each raw active field data obtained with a 44-N sledgehammer. For passive MAM records, 20 numbers of records, each of 32 s length,

were collected from signals received from cultural sources. Importantly, during the processing of the field data, sites that were found to be inversely dispersive, higher modes of Rayleigh waves were selected for analysis.

2.10 Critical Appraisal of Literature and Gap Areas

The study presents a comprehensive review of various aspects of passive MASW, with special emphasis on the parameters affecting resolution of dispersion imaging. The study systematically represents various parameters and their respective importance during data acquisition and data processing during dispersion. Following salient points can be summarised as the gap areas after the critical scrutiny of the literature:

- In MASW surveys, dispersive nature of Rayleigh waves through layered soil strata is utilised for soil characterisation. Dispersion curve is a representation of the variation of Rayleigh wave propagation velocity with frequency and is most crucial for the estimation of final V_s profile. It is affected by a number of field and processing parameters such as source offset, array length, acquisition time, sampling frequency, and vertical stacking. Active MASW survey is the simplest MASW survey and gives high resolution in shallow depth range. The dispersion imaging process in active MASW is also the simplest due to the single source approach. There are many existing literatures which have reported optimum field and pre-processing parameters for the attainment of high resolution dispersion image for active MASW (Taipodia and Dey, 2018; Taipodia *et al*., 2017, 2018a, 2018b, 2018c).
- Passive MASW survey is suitable for investigation of deeper soil layers as it uses low frequency Rayleigh waves generated from ambient passive sources. However, analysis of

passive methods are more complex owing to its large receiver array layout and complicated multisource induced wavefield records. There are continuous developments in the understanding of various characteristics of recorded data and processing tools in passive MASW survey, but it is yet to be developed as a stand-alone technique and is often prescribed to be used along with active or other established mode of surveys.

- Most of the dispersion imaging schemes for passive surveys neglects the source distance from the receiver array in the consideration of plane fundamental mode Rayleigh wave. However, it was reported that closely situated strong sources, which emit waves of long wavelength, causes overestimation in phase velocities owing to the non consideration of the distance parameter in the dispersion imaging process.
- Dispersion imaging in case of passive roadside method have to take care of both offline and cylindrical nature of wavefields by taking both azimuth and distance parameter of the sources. The OC scheme in passive roadside survey was found to give superior performance with high resolution and far accurate dispersion image. However, experimental validations using different positioning of sources with respect to the receiver array (such as intra-line condition), are very rare and require further in-depth study.
- In case of passive remote surveys, it is recommended in most of the literatures to use 2-D symmetric geometrical shapes to account for true azimuthal characteristics of the passive surface waves. Till date, shapes such as cross, circular, square, triangular, L-type etc., have been used in different studies depending upon site conditions and instrument capacities. However, comparison of these experimental results using different types of array type in regard to the enhancement of the resolution of dispersion image is still very few. Further,

there is no experimental study on the effect of size of the array on the resolution of the dispersion image.

- In passive roadside survey, vehicular traffic serves as the sources of wavefield generation. However, there could be multiple numbers of sources on the road surface in the form of potholes, road bumpers, or road cracks, creating the sources of undulations and wave generation. There is no experimental study on the influence of such multiple sources on the resolution of dispersion image and the subsequent V_s profiling.
- In passive roadside survey, the receiver array is normally placed parallel to the road alignment. Therefore, some offline distance always exists in this form of survey. Literatures till date have not provided experimental report on effects of change in offline distance on the dispersion imaging and V_s profiling.
- Vertical stacking is a vital tool for enhancement of SNR of the recorded signals, and, thus, for the improvement of resolution of the dispersion image. However, there is no conclusive recommendation on the optimum number of vertical stacking required for the best resolution in dispersion imaging.
- Literatures recommend combined active and passive MASW survey for better comprehension of modal nature of surface wave, and to enlarge the analysable frequency band in the dispersion image. However, there is neither a direct comparison among active, passive remote and passive roadside MASW in estimation of phase velocity, nor in estimation in final V_s profile.

Passive MASW survey is a recent advancement in the subsurface investigation techniques and has already become popular due to its efficacy in deciphering large investigation depth and availability

of swift processing tools. However, the review indicates that geometrical and processing parameters utilised during passive surveys are merely site specific, without having or following any standard guideline. The method still need further research and analysis, particularly on the aspects affecting dispersion imaging, to develop standard guidelines that can be used in a more general sense.

2.11 Objective of the Present Research

From the literature review, it is clear that dispersion analysis and generation of dispersion image is the most critical stage in the analysis of records obtained from MASW survey. The final V_s profile to be obtained in the inversion stage depends solely on the experimental dispersion curve as an input data. It has also been observed that the resolution of dispersion image from passive roadside data normally lacks in distinctness compared to a dispersion image from active as well as remote survey. Such comparative lack in resolution leads to higher approximation during the extraction of experimental dispersion curve. Further, it has been comprehended that in contrary to the active MASW survey, there are no standard guidelines available with respect to data acquisition, dispersion and inversion analysis for the case of Passive MASW survey. In the urbanized regions and near highways/railways, Passive Roadside MASW survey that utilizes the moving vehicular traffic as a source of signals can be a suitable alternative to the active MASW survey utilizing a user-controlled impact source, which many a times cause a hindrance due to their non-portability issues. In the above deficient circumstances, the objective of the present research is focussed to examine critically the various parameters controlling the resolution and quality of dispersion imaging of passive roadside data, so that a robust and confident guideline

regarding the same can be developed in order to generate accurate and reliable V_s profile irrespective of site and test conditions.

2.12 Scope of the Work

In order to meet the stated objective, the following are adjudged as the important scopes of the present research work on Passive Roadside MASW survey:

- To study the field records in terms of frequency content, energy levels and propagation characteristics, as collected in passive roadside survey, obtained from the passage of vehicles of different genre.
- To study the nature of field records in terms of spectral and contamination characteristics from sites with different traffic volumes.
- To study the effects of receiver array length and acquisition time on the collected wavefield characteristics and subsequent dispersion imaging based on the data collected from sites with different traffic volumes.
- To study the importance of scanning range of frequency and phase velocity during dispersion analysis on the resolution of dispersion imaging.
- To study the influence of different arrivals of wavefront patterns, i.e., inline-planar (IP), offline planar (OP) and offline cylindrical (OC), and their corresponding analysis schemes on the resolution of dispersion imaging.
- To study the significance of dispersion curve selection from the dispersion image, in terms of frequency band and selection density, on the accuracy and reliability of the resultant V_s profile.
- To study the influence of initial earth model on the resultant V_s profile.

- To assess the effect of source location (intra-line or outer-line) and number of sources (single or multiple) sources on the dispersion imaging.
- To identify the influence of offline distance on the usability of passive roadside MASW survey.
- To develop robust guidelines for conducting reliable passive roadside MASW survey.

CHAPTER 3

BACKGROUND THEORY OF MASW

3.1 Introduction

MASW survey, irrespective of its mode (active, passive roadside or passive remote), comprises three primary stages: Data acquisition, Dispersion analysis and Inversion analysis. Data acquisition is primarily related to the field setup and survey conducted to acquire the time-domain signals through a geophone array. Dispersion analysis is used to derive the dispersion image from the collected records and establish the dispersion curve (indicating the relation of phase velocity and frequency with their unimodal or multimodal characteristics). Finally, Inversion analysis uses the dispersion curve, fed into a suitable optimization algorithm, to obtain the subsurface shear-wave velocity profile. This chapter presents brief details of each of these stages towards the attainment of final V_s profile, with special emphasis laid to the theoretical background of dispersion analysis as used in MASW technique. The numerical scheme of dispersion imaging utilised in the Phase-Shift method (Park *et al.,* 1998a) is discussed, which has been implemented in the present study through the software platform, 'SurfSeis'. The modification in the said scheme, for utilisation in passive MASW records, is also elaborated. The primary principles of the inversion technique, involved in the adopted method, for the determination of V_s profile have also been briefly reported.

3.2 Data Acquisition

This is the first stage in MASW survey where multichannel field records are acquired, which are often called as shot gather, or seismic gather, or multichannel seismogram, in conventional seismic

exploration. The process involves generation of surface waves and collection of the same through a network of receivers and a digital acquisition system. Surface waves can be generated by an active source, such as a sledgehammer or weight drop, or can be collected from passive sources such as ambient natural, cultural and traffic activities. The records are collected by a multichannel data acquisition system or a seismograph. The geophone receiver array deployed with an appropriate geometrical configuration is connected to the seismograph through a connecting spread cable, which transmits the recorded field data to the seismograph. The multiple receiver system allows collating the characteristics of collected wavefield propagation through the medium. The details of seismograph, geophones and connecting cable will be discussed elaborately in Chapter 4.

A seismic data recorded by a receiver is termed as 'seismic trace'. It depicts the response of a medium, such as soil substrata, to any disturbance, in the form of a time signal (Fig. 3.1a). The seismic wavefield, in any surface event, causes vibrations (or motions) in soil particles that are detected by the deployed receivers in the field. These vibrations of soil particles is converted into an electric voltage by the receivers and, therefore, the time signal is represented normally in a unit of volts, more commonly millivolts (mV), as shown in Fig. 3.1a. In case of a multichannel recording, a horizontally propagating surface wave (e.g., Rayleigh wave) appears in a linear arrival pattern, as shown in Fig. 3.1b. The phase velocity of the wave can be estimated by determining the slope of the arriving waves along the traces. This forms the background of the 'Dispersion analysis' stage of MASW, which will be discussed in the following section. Thus, seismic data collected through a linear array is a two-dimensional signal and is the function of time and source offsets (distance of source of wave generation to the receiver).

Another significant advantage of multichannel recording is its capacity to identify various surface events and different kinds of seismic wave propagation from a field record. As shown in Fig. 3.1c, different seismic waves namely, air wave, direct wave, surface wave of fundamental and higher modes, reflected, refracted, backscatter waves and ambient noise, are identified in a typical field record. Thus, it gives the opportunity to curtail these noises during data processing (i.e., dispersion analysis) and provide better assurance of a reliable result.

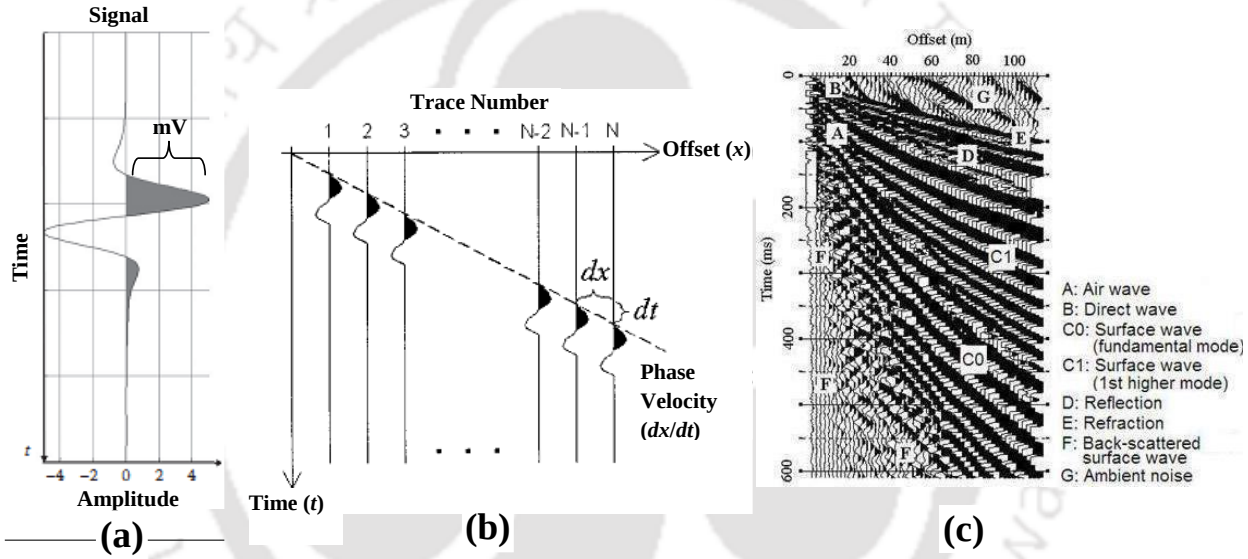

Fig 3.1 (a) A single seismic trace in the form of a voltage wiggle (Foti *et al.*, 2014) (b) Schematic of multichannel recording and phase velocity estimation (Ryden *et al.*, 2004) (c) A typical field record with multichannel recording and various seismic waves (Park *et al.*, 2007)

During the acquisition stage of any surface wave method, the primary objective is to gather field records with dominant surface wave events (i.e., signals) with least contamination from other seismic waves (i.e., noise), thereby assuring high Signal-to-Noise Ratio (SNR). The SNR,

commonly expressed in decibels, is defined as the ratio between the signal power *S* and noise power *N* (Foti *et al*., 2014), and is expressed as

$$\mathrm{SNR}\left[\mathrm{dB}\right] = 20\log_{10}\left(\frac{S}{N}\right) \tag{1}$$

A recorded field data contains both useful signals and unwanted noise. When noises contaminate the signals of the recorded data beyond desirable limit, it affects the output of the adopted method. Increasing SNR in active MASW survey may be possible by utilising impact source of larger weight, or recording during quiet times (e.g., night). On the other hand, these measures cannot be applied to passive MASW survey. However, utilising a technique known as 'Vertical Stacking', the SNR of passive MASW record can be enhanced. It is a method in which multiple field records are stacked, or summed up, so that the useful signals from passive sources get amplified, while the unwanted noises get diminished (Discussed elaborately in Chapter 7).

3.3 Dispersion Analysis

Dispersion analysis is the first and the most critical stage of data processing in MASW method. The objective of the analysis is to obtain an accurate dispersion curve, as far as possible, which can be subsequently utilized for the inversion process to obtain a shear-wave velocity profile of the surveyed area. In general, dispersion curve is defined as the plot between the phase velocity and frequency for a particular mode. When more than one phase velocities exist at a particular frequency, it is called a multi modal dispersion. The slowest one is called as the fundamental mode, the next faster as the first (1^{st}) higher mode and so on (Fig. 3.2). Extraction of accurate dispersion curve (primarily the fundamental mode) is the most critical part in the MASW method as the accuracy of the final V_s profile greatly relies on it. Earlier, it was assumed that the fundamental

mode surface wave is the most dominant in a field record comprising highest energy. Later, it was found that energy of higher modes might become significant and more dominant particularly in the situation of larger source distance and substrata with lower V_s values (Park *et al.*, 1999). The primary techniques for dispersion curve analysis encompasses frequency wavenumber (*f-k*) analysis, slowness frequency (p-ω) analysis, and the phase-shift analysis. However, all the techniques are primarily based on Fourier transformation, in which the time domain data is decomposed into frequency domain, from where dispersion characteristics of surface waves are retrieved.

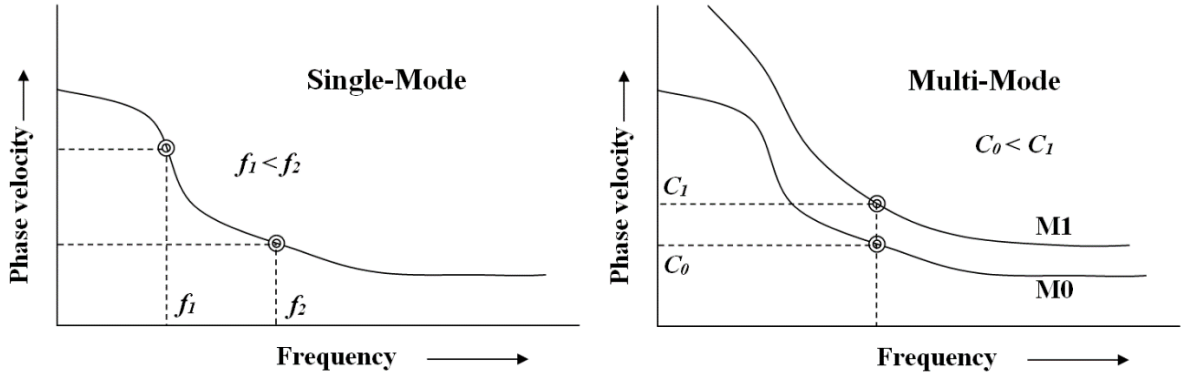

Fig. 3.2 Concept of unimodal and multimodal dispersion

During dispersion analysis, an image space is constructed from where the dispersion trends are identified from the pattern of the peak energy accumulation. The necessary dispersion curve is extracted mostly from the fundamental energy band through the points of spectral maxima. In the imaging process, a multichannel record in space-time (x-t) domain is transformed into either frequency-wavenumber *(f-k)* or frequency-phase velocity *(f-c)* domain. The *f-k* transformation is one of the traditional methods (Nolet and Panza, 1976) and is effective in separating events with

different frequencies, wavenumbers and phase velocities. The *p*-ω (slowness-frequency) transformation (McMechan and Yedlin, 1981) and the Phase-Shift method (Park *et al.*, 1998a) are the recent methods based on transformation in frequency-phase velocity domain.

The Phase Shift method produces dispersion image having higher degree of resolution than the other two mentioned methods (Park *et al.*, 1998a). Here, an *N*-channel record, $mr_N = r_i$, is defined as an array of *N* traces collected by a data acquisition system, where $r_i \ (i=1,2,3,...,N)$ is denoted as the time record for a trace. The frequency-domain representation of this record, after applying the Fast Fourier Transformation, is denoted by $MR_N(\omega) = R_i(\omega) = FFT[r_i]$. The term $R_i(\omega)$ is a complex number whose solution can be written as a product of amplitude $A_i(\omega)$ and phase $P_i(\omega)$. $P_i(\omega)$ is governed by phase velocity (*c*) of each frequency and can be written as

$$P_i(\omega) = e^{-j\Phi_i(\omega)} \tag{1}$$

where, $\Phi_i(\omega) = \omega x_i / c = \omega\{x_1 + (i-1)dx\}/c$ (2)

Here, x_1 is the source-to-first receiver distance, i.e., source offset, *dx* is the inter-receiver spacing, *c* is phase velocity and ω is the angular frequency.

Further, $P_i(\omega) = e^{-j\Phi_i(\omega)} = \cos\Phi - j\sin\Phi$ (3)

Now, $|P_i(\omega)| = \sqrt{\cos^2\Phi - j^2\sin^2\Phi} = \sqrt{\cos^2\Phi + \sin^2\Phi} = 1$ (4a)

and, $|R_i(\omega)| = |A_i(\omega).P_i(\omega)| = |A_i(\omega)|.|P_i(\omega)| = |A_i(\omega)|$ (4b)

As, $|A_i(\omega)|$ does not contain any information of phase velocity, *A* and *P* are independent quantity,

and $|R_i(\omega)|$ can be normalized without loss of significant information on phase, thereby giving

$$R_{i,norm}(\omega) = \frac{R_i(\omega)}{|R_i(\omega)|} = \frac{A_i(\omega).P_i(\omega)}{A_i(\omega)} = P_i(\omega) \tag{4c}$$

Figure 3.3(a) shows a raw field record (r_i) with a surface wave event, while Fig. 3.3(b) shows the record after amplitude normalization ($R_{i,norm}$). The record is an array of normalized sinusoid curves for an arbitrary frequency of 20 Hz propagating at an arbitrary phase velocity of 140 m/s. In such a record, sinusoid curves have the same phase along a slope of the phase velocity, whereas they have different phase along the slopes of other phase velocities. Therefore, if the curves are summed together, within a finite time length (e.g., one period), along the slope of phase velocity of 140 m/s, it will result in another sinusoid curve of finite length whose amplitude (A_s) is *N*. The summation along any other slopes, e.g., along 65 m/s or 500 m/s, will result curves of amplitude lesser than *N*. This is the basic principle of the dispersion analysis employed in MASW method.

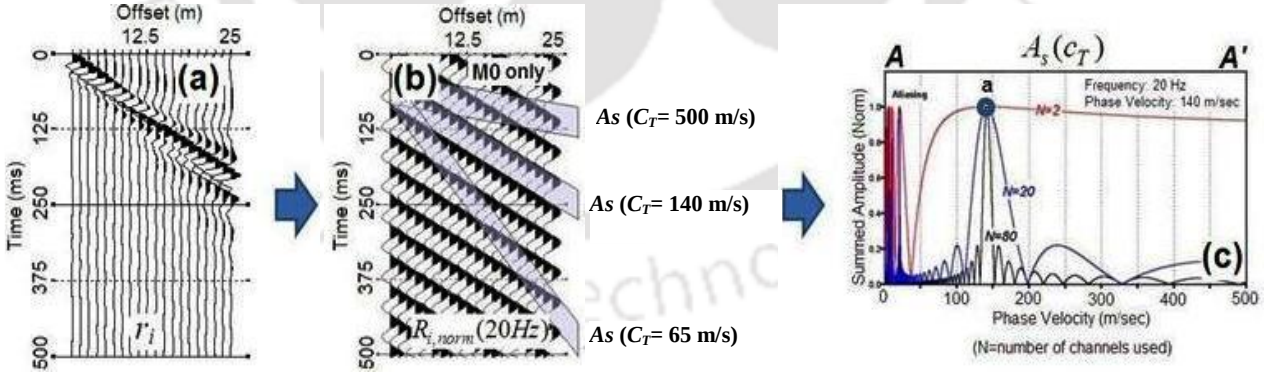

Fig. 3.3 (a) A raw field record (b) Record with normalized amplitude with a frequency of 20 Hz and with phase velocities of 65, 140 and 500 m/s (c) curves of summed amplitudes for different number of traces (Park *et al.*, 1998a)

To search for the true phase velocity, the summation can be performed along many different slopes (i.e., phase velocities), in a scanning manner, with small incremental change (e.g., 5 m/s), within a geologically logical range. The result of each summation, as represented by amplitude (A_s) of summed sinusoid curves, can be then displayed in a 2-D format (i.e., phase velocity versus A_s). In the 2-D scanned curve, the phase velocity that gives the maximum amplitude ($A_{s,max}$) will be the correct value being sought (Fig. 3.3). In the 2-D space, the summed curve having one sharp main lobe with a peak amplitude $A_{s,max}$,along with many side lobes, defines the resolution and accuracy of the analyzed dispersion relationship. For 1-D receiver array, this summed amplitude can be represented as an energy accumulation for a particular frequency (ω) and particular phase velocity (c), and is expressed as:

$$E_{1-D}(\omega, c) = \left| \sum e^{-j\phi_i(\omega)} R_i(\omega) \right| \qquad (5)$$

The method is based on the assumption that fundamental mode dominates in a recorded data over the other higher order modes. It is seen that the sharpness of the peak A_s increases with increase in the number of traces N. This implies that higher number of traces is advantageous for achieving higher resolution in the determination of a phase velocity. In Fig. 3.3(c), A_s has been normalized with respect to N, and, therefore, the peak of the summation of different trace numbers becomes 1 (one).

In many situations, multimodal characteristics (e.g., fundamental and higher order modes) of surface waves dominate in a field record. Higher mode surface waves may generate in cases when a substrata comprises inversely dispersive soil profile, i.e., where soil layer of higher stiffness overlies a soft strata (Stokoe *et al.*, 1994). In such cases, summation of the normalized sinusoidal curves, as stated in the previous section, will result in more than one sharp lobe in the energy-

phase velocity space, representing higher order modes. Figure 3.4(a,b) shows the result of such summations in cases of records with unimodal (*M0*) and multimodal (*M0* and *M1*) wavefield characteristics. In the first case, only one sharp lobe appears at the phase velocity of 140 m/s, representing the dominant *M0* mode; while, in the latter case, two sharp lobes appear at phase velocities of 140 m/s and 220 m/s, representing the presence of both *M0* and *M1* modes. Therefore, in such cases, there will be multiple energy band in frequency-phase velocity space (or, the dispersion image space), as can be observed in Fig. 3.5(a-b).

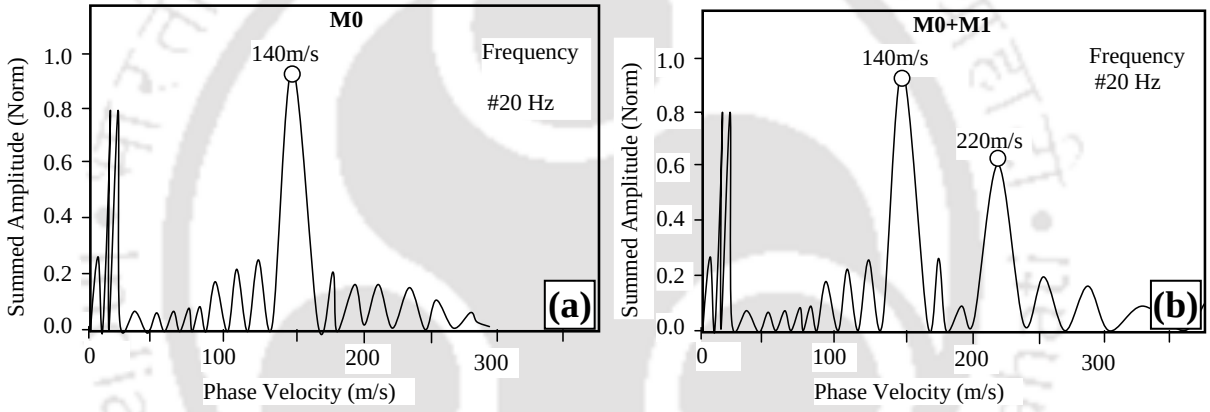

Fig. 3.4 (a) Curves of summed amplitude for only *M0* case (b) Curves of summed amplitude for *M0* and *M1* cases (Park *et al.*, 1998a)

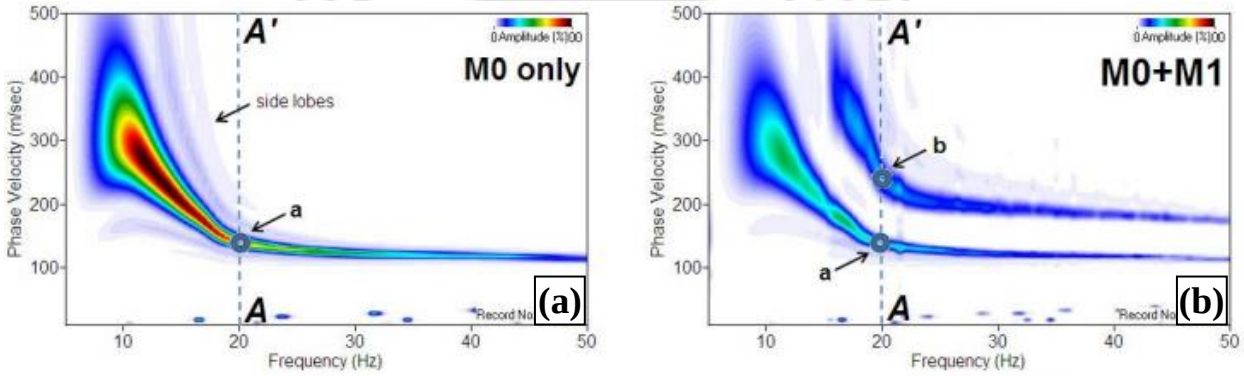

Fig. 3.5 Single and multimodal dispersion characteristics (Park *et al.*, 1998a)

3.4 Dispersion Imaging Process in Passive Roadside MASW

Similar to that of active survey, surface waves are generated when vehicles move over the existing irregularities over the road, comprising joints, potholes, cracks, or speed breakers, and the same is utilized in the Passive MASW method. Therefore, such irregularities, over the surface of the road, serve as the sources of wavefield generation in Passive roadside MASW survey. The energy imparted by the vehicles moving over the road, having different speed and vehicle mass (1000-10000 kg), will be much higher than conventionally used active sources. Such high-energy surface events from traffic sources generate waves of longer wavelength, which can help investigating deeper layers of subsurface strata. However, such passive sources on the road surface is located at some offline distance, with respect to the receiver array. Therefore, an angular measurement or azimuth detection of the sources has to be performed during dispersion analysis process. Following section describes the processing scheme for passive traffic generated surface waves for utilisation in MASW survey.

3.4.1 Modelling Scheme for Passive Surface Waves

Revisiting the shifting property of Fourier transform, Fourier transform of any function $g(t-\delta)$ is expressed as,

$$\hat{F}\{g(t-\delta)\} = \int_{-\infty}^{\infty} g(t-\delta)e^{-i2\Pi ft} \tag{6}$$

Putting $(t-\delta) = u$, the expression is obtained as

$$\hat{F}\{g(t-\delta)\} = \int_{-\infty}^{\infty} g(u)e^{-i2\Pi f(u+\delta)} = e^{-i2\Pi f\delta}\int_{-\infty}^{\infty} g(u)e^{-i2\Pi fu}du = e^{-i2\Pi f\delta}G(f) = e^{-i\omega\delta}G(f) \tag{7}$$

Now, by utilizing the shifting property of the Fourier Transform, the summation procedure can be achieved in frequency domain as

$$
\begin{aligned}
E(V_T) &= \sum_{m=1}^{M} e^{-i\omega\delta_m} R(x_m, \omega) \\
&= e^{-i\omega\delta_1} R(x_1, \omega) + e^{-i\omega\delta_2} R(x_2, \omega) + e^{-i\omega\delta_3} R(x_3, \omega) + \ldots\ldots\ldots\ldots\ldots + e^{-i\omega\delta_M} R(x_M, \omega) \\
&= \left[\begin{array}{l} e^{-i\omega\delta_1} \frac{1}{\sqrt{2\pi}} \int_{-\infty}^{\infty} r(x_1,t) e^{-i\omega\delta_1} dt + e^{-i\omega\delta_2} \frac{1}{\sqrt{2\pi}} \int_{-\infty}^{\infty} r(x_2,t) e^{-i\omega\delta_2} dt \\ + e^{-i\omega\delta_3} \frac{1}{\sqrt{2\pi}} \int_{-\infty}^{\infty} r(x_3,t) e^{-i\omega\delta_3} dt, \ldots\ldots\ldots\ldots + e^{-i\omega\delta_M} \frac{1}{\sqrt{2\pi}} \int_{-\infty}^{\infty} r(x_m,t) e^{-i\omega\delta_m} dt \end{array} \right]
\end{aligned}
\tag{8}
$$

This expression denotes the energy at a particular frequency. For *M* numbers of channels, δ_1, δ_2, δ_3, …, δ_m are the time delays. For the m^{th} geophone, the time delay δ_m is given as

$$
\delta_m = \frac{x_m}{V_T} = \frac{x_o + (m-1)\Delta x}{V_T} \tag{9}
$$

For a particular testing phase velocity, the delay term δ_m increases with the distance of the geophone from the source. The summation of the amplitude is normally carried out at a particular frequency range (viz. 5-50 Hz) and a testing phase velocity range (viz. 10-1000 m/s). The resultant curve of summed amplitude can be displayed in the domain of phase velocity and normalized amplitude.

At a particular selected frequency (say 20 Hz) and a testing phase velocity (say 140 m/s), the obtained dispersion image will only show the peak of the amplitude at those values and nearly zero at all other frequencies (Fig. 3.4, 3.5). Further, the solution of Eqn. 7 becomes

$$
\hat{F}\{g(t-\delta)\} = \text{amplitude term} \times \text{phase term} = e^{-i2\Pi f \delta} G(f) = e^{-i\omega\delta} . a_m \tag{10}
$$

Now, considering an arbitrary k^{th} source with an arbitrary location $L_k = (x_k, y_k)$, having an amplitude a_k^m, phase delay δ_k and mode number *m*, in frequency domain, the excitation can be represented as

$$S_k^m(\omega) = a_k^m . e^{-j(\omega+\delta_k)} \tag{11}$$

The phase delay δ_k will be significant for the sources situated far apart from the receiver array. For an arbitrary i^{th} positioned receiver with its location $L_i = (x_i, y_i)$, the response of the signal in its frequency domain can be represented as:

$$R_i^{m,k}(\omega) = A_{ik}^m . P_{ik}^m . S_k^m(\omega) \tag{12}$$

where, A_{ik}^m is the amplitude modulation factor $\left(A_{ik}^m = \frac{e^{\alpha l_{ik}}}{l_{ik}} \right)$, α is the attenuation coefficient $= \left(\alpha = \frac{\omega}{c_\omega^m . Q} \right)$, c_ω^m is the Phase velocity of the m^{th} mode for a frequency ω, Q is the Quality factor, $l_{ik} = \sqrt{(x_i - x_k)^2 + (y_i - y_k)^2}$, and P_{ik}^m is the Phase modulation factor = $\left(P_{ik}^m = \frac{e^{j\omega l_{ik}}}{c_\omega^m} \right)$

Surface wave amplitude is directly proportional to source amplitude $\left(a_k^m\right)$ and inversely proportional to the distance between source to the receiver position in consideration $\left(l_{ik}\right)$. Both the quality factor *Q* and phase velocity c_ω^m are related to ground materials.

When there is a generation of multiple modes from a particular source, the resultant multimodal surface wave signal, at a particular receiver position (say i^{th} position), is estimated by summing for all existing modes, which is expressed as

$$R_i^k(\omega) = \sum_{m=0}^{M} R_i^{mk}(\omega), \quad \text{for all } (\text{M+1}) \text{ modes} \tag{13}$$

Similarly, in case of existence of multiple sources of wavefield generation, the summation needs to be carried out for all the sources, which will be finally expressed as

$$R_i(\omega) = \sum_{k=1}^{K} R_i^k(\omega), \quad \text{for } K \text{ number of sources} \tag{14}$$

3.4.2 Data Processing

For the calculation of relative energy of the wavefield utilizing a 1-D linear array scheme, at a particular frequency (ω) and with a scanning phase velocity (c), the phase-shift ($\omega\delta_n$) has to be applied to the Fourier transformation of $r_i(t)$, i.e., $R_i(\omega)$. The summation of all such phase-shifted traces deployed in the field, or assumed in the modelling process, gives the required peak energy in case the correct phase velocity is considered. The relative energy at a particular phase velocity and frequency is expressed as:

$$\begin{aligned} E_{1-D}(\omega, c) &= \left| \sum_{i=1}^{N} e^{j\phi_i} R_i(\omega) \right| \\ &= e^{-i\omega\delta_1} R(x_1, \omega) + e^{-i\omega\delta_2} R(x_2, \omega) + e^{-i\omega\delta_3} R(x_3, \omega) + \ldots + e^{-i\omega\delta_M} R(x_M, \omega) \end{aligned} \tag{15}$$

Normally, when there is a single source of wave generation, as in the case of active survey, there are two scanning parameters, namely frequency and phase velocity. Therefore, the required

dispersion image is created by scanning through a preset range of frequency (e.g., 5-50 Hz) and phase velocity (e.g., 50-2000 m/s).

However, in case of passive survey, normally, there is existence of multiple sources of wave generation when moving vehicle pass over various road surface irregularities. Further, in case of passive roadside survey, the receiver array is laid at an offline distance from the centreline of the road. Hence, there exists an angular distance from the source of the wave generation to the mid-point of the geophone array. Therefore, in such a survey, another scanning parameter i.e., the azimuth of incoming waves (θ) requires to be incorporated during phase velocity scanning. For a particular frequency (ω) and a scanning phase velocity (c), the energy $E_{1-D}(\omega,c,\theta)$ is calculated by assuming an azimuth (Fig. 3.6a). Then the summation is carried over a scanning range of phase velocity, followed by a range of azimuth (which is normally 0-180º), considering the movement of the vehicles from both side of the 1-D receiver array. The energy from such summation is represented as

$$E_{1-D}(\omega,c,\theta)=\left|\sum_{i=1}^{N} e^{j\phi_i} R_i(\omega)\right| \tag{16}$$

For a given c and θ, the required phase shift (ϕ_i) for a trace at i^{th} location can be obtained as

$$\phi_i = -\frac{\omega x_i \cos\theta}{c} \tag{17}$$

Finally, all the energy in c-θ space is stacked along the azimuth axis to produce the dispersion image in c- ω space (Fig. 3.6b), and is expressed as:

$$E_{1-D}(\omega,c)=\sum_{i=1}^{N_\theta} E_{1-D}(\omega,c,\theta) \tag{18}$$

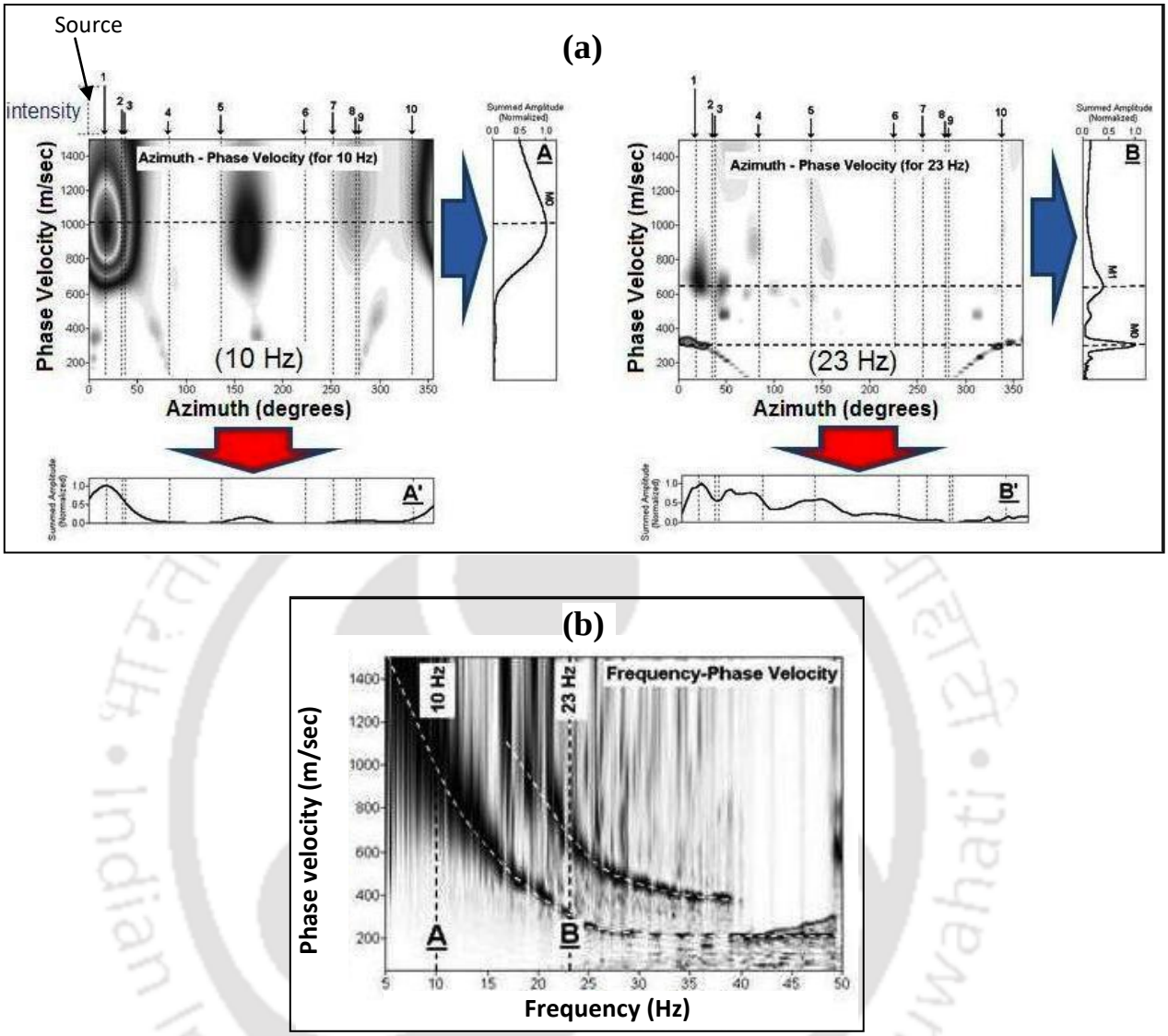

Fig. 3.6 (a) Stacking of energy in phase velocity-azimuth (c-θ) space at two frequencies 10 Hz and 23 Hz (b) Final dispersion image after stacking along azimuth axis (Park *et al*., 2004)

3.5 Different Schemes of Dispersion Imaging in Passive Roadside MASW Analysis

In the case of a passive survey alongside a road, the sources of surface wave generation are usually on the road, since waves are generated when moving vehicles travel over irregularities in the road.

Since the receiver array is always off the road, the wave propagation is rarely in accordance with the inline propagation, except for the cases when the sources are at far-off and large offset distances from the array. If strong waves from nearby source points dominate and their offline nature is not accounted for during the dispersion analysis, the phase velocities are overestimated, approximately in inverse proportion to the cosine of the azimuth ($cos\ \theta$), which can be as high as 30% (Park and Miller, 2008). In addition, the dominating mode of propagation may not only be offline, but also cylindrical when the source of major wavefield generation lies nearby the testing area.

Therefore, depending upon the relative position of the sources and the receiver arrays, three different types of wave propagation may exist in a roadside survey, namely conforming to the Inline Plane (IP), Offline Plane (OP), and Offline Cylindrical (OC) propagation, as shown in Fig. 3.7. The arrival of wavefield generated from distant points from a nearly straight road can be an example of the IP type of wavefield propagation. There can be waves generated at far distances approaching the receiver line with a significant azimuthal angle making an example of the OP type propagation. When the sources on the road are situated very close to the array, e.g., at a distance shorter than a few times the array length from either end or even within the receiver line, the recorded wavefield can be representing an OC type propagation. The waves of OC type propagate into the receiver line with a significant curvature due to the proximity and the offline nature. A considerable amount of recorded energy can be of this origin due to the proximity of the major source points.

The IP waves will make a straight linear arrival pattern on the recorded data with a slope ($S = dt/dx$), which is the same as the inverse of the phase velocity ($1/c$) (i.e., slowness) for a particular

frequency (*f*) (Fig. 3.8). The OP waves will also make a straight linear arrival pattern, but with its slope always smaller than (*1/c*) of the IP case by a ratio of cosine of the azimuth (*cosθ*) (Park *et al.*, 2004). If the offline nature is not accounted, the corresponding velocity (*dx/dt*) will be overestimated by a ratio of *1/cos*θ. The arrival pattern of the OC waves will be hyperbolic with an asymptote, with its slope same as that of the OP propagation with the same azimuth (*θ*).

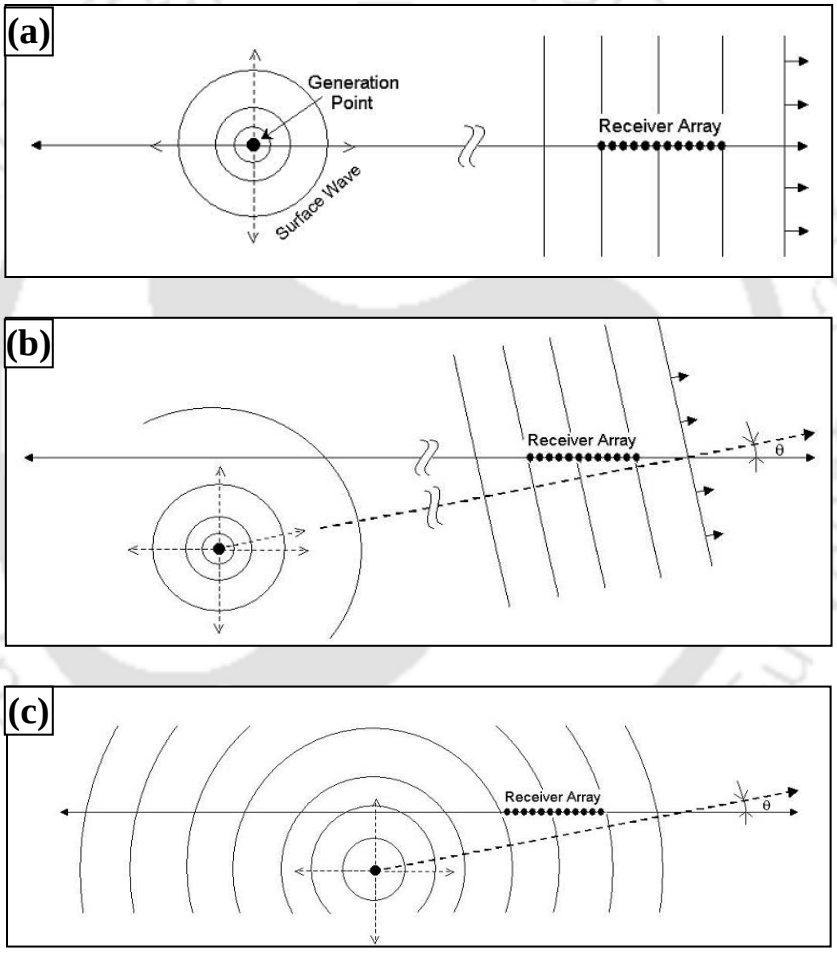

Fig. 3.7 Three different types of possible wave propagation in a roadside survey method (a) Inline plane, IP (b) Offline plane, OP (c) Offline cylindrical, OC (Park and Miller, 2008)

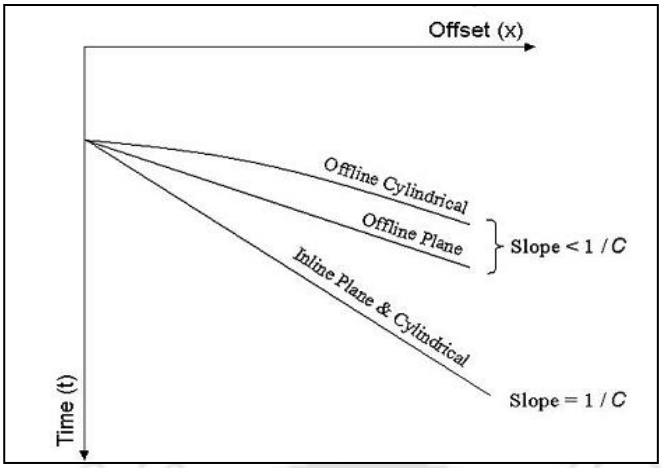

Fig. 3.8 Patterns of different types of wave propagation as appearing in offset and time space (Park and Miller, 2008)

IP waves are the simplest type in a field record that can be processed by any scheme commonly used for active surveys. The offline nature of OP waves is accounted by a scheme that scans through a possible range of incoming azimuths (0-180º) of dominating waves, for each frequency component of the dispersion analysis (Park *et al*., 2004). Subsequently, all of the energy in the phase velocity-azimuth space is stacked along the azimuth axis to account for multiple energy peaks that may represent different modes and sources. The cylindrical nature of OC waves is accounted by an additional scheme that calculates the approximate distance between a specific receiver and a possible source point, which is determined from the consideration of azimuth and approximate distance between the receiver line and the road (Fig. 3.9). The proposed scheme can reduce the overestimation to some extent, indicating the need of a true 2-D array for the most accurate phase velocity estimation.

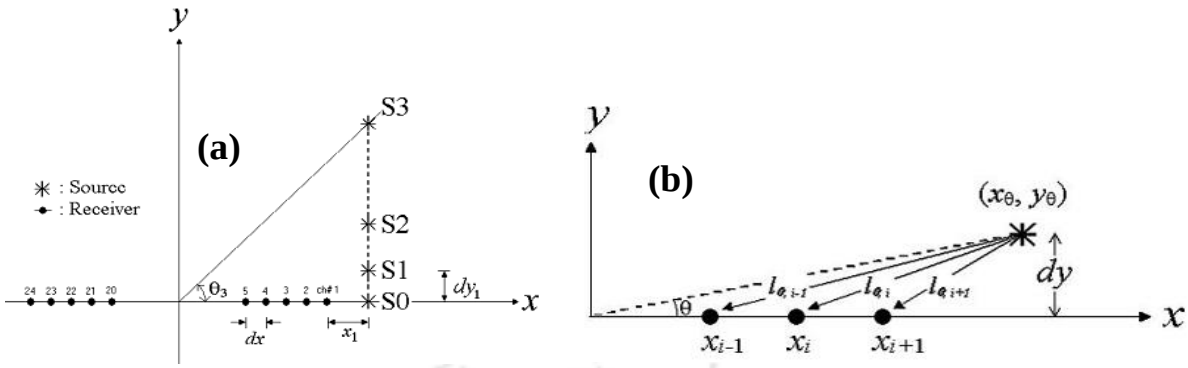

Fig. 3.9 (a) A relative coordinate system considering a linear array and source points with different offline distance and azimuth (b) An illustration of how the offline cylindrical waves are accounted for during the scanning of an azimuth (Park and Miller, 2008)

Theoretical analysis and modelling of experiments suggest that OC scheme should give a superior performance, especially when there are some intra-line source points on the road. Further research has been suggested in comparative study of different influencing conditions for OC and OP schemes. Finite nature of the source distance is inherent to the passive surface wave methods utilizing local traffic noise. The following section describes individual processing scheme for each of the above-mentioned wave arrivals.

3.5.1 Inline Plane (IP) Waves

Park *et al.* (1998a, 2004) provided the scheme that calculates the relative energy for a IP wave, $E_{IP}(\omega,c)$, for a particular frequency ($\omega = 2\pi f$) and a scanning phase velocity (c) in the dispersion image. Firstly, the necessary phase shift ($\phi_i = \omega x_i/c$) is applied to the Fourier transformed record, $R_i(\omega)$, of the i^{th} trace, $r_i(t)$, obtained from an offset x_i. Subsequently, all phase-shifted traces (N)

are summed up, and the absolute value of the summed complex number is determined. The relative energy of the IP signal is expressed as:

$$E_{IP}(\omega,c)=\left|\sum_{i=0}^{N} e^{j\varphi_i} R_i(\omega)\right|+\left|\sum_{i=0}^{N} e^{-j\varphi_i} R_i(\omega)\right| \tag{19}$$

To account for bidirectional nature of incoming waves from both ends of the receiver array, the phase shift followed by the summation is repeated by changing the sign of the phase shift in Eqn. 19. The scheme assumes that major part of the recorded waves is of IP type and any other offline waves of significant energy, if they exist, should appear at higher phase velocities. It therefore tries to extract a curve by following a trend of lowest phase velocity in the energy band of dispersion in the space of $E_{IP}(\omega,c)$.

3.5.2 Offline Plane (OP) Waves

Offline Plane waves can be processed by algorithm based on the conventional 2-D wavenumber (k_x-k_y) method (Park *et al*., 2006; Park and Miller 2008). With the method proposed by Park *et al.* (2004), possible multimodal nature of dispersion can be imaged by stacking energy in the 2-D wavenumber space along the azimuth axis. The method thus considers an additional parameter as azimuth (θ) along which summation of energy is carried over. For each frequency (ω), the energy $E_{OP}(\omega,c,\theta)$, for a scanning phase velocity (c) is calculated by assuming an azimuth (θ), as expressed in Eqn. 20. The calculation is then carried over the scanning range of the phase velocity (e.g., 50-2000 m/s with 5 m/s increment), and then scanned over that of the azimuth (e.g., 0-180º with 5º increments)

$$E_{OP}(\omega,c,\theta)=\left|\sum_{i=0}^{N} e^{j\varphi_{\theta,i}} R_i(\omega)\right| \qquad \forall\ 0\le\theta\le 180^{\circ} \tag{20}$$

For a given c and θ and for a trace at x_i, the necessary phase shift $\left(\phi_{\theta i} = -\frac{\omega x_i \cos\theta}{c}\right)$ is calculated based on projection principle (Park *et al*., 2004). The scanning range of azimuth (θ) is considered only within the two quadrants (i.e., for 180º) due to the linear receiver line. All the IP waves that exist are handled in a precise manner as they are detected during scanning of azimuth near 0-180º respectively.

Finally, all the energy in the c-θ space is stacked along the azimuth (θ) axis for N_o different azimuths to produce $E_{OP}(\omega,c)$, which is expressed as.

$$E_{OP(\omega,c)} = \sum_{i=0}^{N_o} E_{OP}(\omega, c, \theta) \tag{21}$$

This approach constitutes the final dispersion image space, one energy line at a particular frequency, ω, showing the variation with different phase velocities.

3.5.3 Offline Cylindrical (OC) Waves

Offline cylindrical waves are processed in a similar manner to the OP waves (Park *et al*., 2006; Park and Miller, 2008) using Eqns. 20 and 21, only with an additional finite distance ($l_{\theta,i}$) between the source point (x_θ, y_θ) and each receiver point (x_i) for a scanning angle θ. The finite distance is expressed as

$$l_{\theta,i} = \sqrt{(x_o^2 - x_i^2) + y_o^2} \tag{22}$$

where, $x_0 = y_0 / \tan\theta$ and $y_0 = dy$ (Fig. 3.9b)

Next, the phase shift term (in Eqn. 21) is determined as $\left(\phi_{\theta i} = -\frac{\omega l_{\theta,i}}{c}\right)$. The distance $l_{\theta,i}$ may change as the road surface irregularities may exist anywhere on the road. In the software platform used in this study, distance between the centre of the road and the receiver line (i.e., offline distance) can be inserted and it account for the curvature in the arrival pattern of the OC waves.

3.6 Inversion Analysis

Inversion analysis is the final stage of the MASW, or other similar geophysical techniques, based on analysis of surface wave propagation. The objective of inversion analysis is to estimate the shear stiffness profile of the subsurface based on surface wave data by utilizing a dispersion curve obtained from MASW survey. Inversion of measured dispersion curve, through an iterative procedure, results the final shear-wave velocity variation with depth (commonly termed as 1-D V_s profile). Inversion analysis attempts to search for the most probable earth model for which the theoretical dispersion curve matches closest to the experimental dispersion curve. The closeness is established by minimising a mathematical objective function (commonly, Root Mean Square error, or RMSE) that represents the nearness between the two dispersion curves. In general, inversion implies a process of finding the cause for a known result. On the other hand, an opposite process, called as forward modelling, tries to find out the result from the known cause (Fig. 3.10). Similarly, in geophysical investigation, the problem of determining dispersion or attenuation curves, with given medium (subsurface soil) parameters (e.g., V_s, V_p, μ and ρ), is termed as Rayleigh direct or forward modelling. While, the problem of determining medium parameters from given dispersion or attenuation curves is termed as inversion. On a whole, an inversion analysis usually involves one or more of forward modelling techniques in the course of examining possible

candidates of causes. An inversion can be stated as 'Unique' when there is only a single solution to a given problem. If multiple solutions exist for a given problem, the inversion can be stated as 'Non-unique', or 'ill-posed'. Moreover, if a small change in the cause gives only a small change in the result, the inversion is stated to be 'Linear'. An inversion will be appreciated as 'Non-linear' when a small change in the cause results in a large change in the result. Figure 3.10 illustrates each of these terminologies associated with the inversion analysis. Surface wave inversion is kind of a non-unique and non-linear problem and hence categorised as ill-posed problem (Foti *et al.,* 2014).

Inversion of dispersion curves to estimate shear-wave velocity profiles was first attempted by Dorman and Ewing (1962). Inversion of surface wave data to obtain V_s is not a straightforward problem and, mostly, it is solved by an optimization technique. The methods for the solution of an inversion problem via optimisation techniques associated with dispersion curve are mainly categorized into two forms: Local search and Global Search methods (Fig. 3.11). Local Search methods are deterministic methods (e.g., least square method by Xia *et al*., 1999) utilises an iterative scheme to find out the ultimate solution starting from an initial guess. During each iteration, it attempts to find the solution, until the initial guess converges to the solution. However, as the solution is searched in the vicinity of an initial guess, the solution obtained by this approach is not guaranteed to be a global one i.e., extremum (maxima or minima). On the other hand, 'Global Search methods' search for a global solution by exploring the entire solution space and hence are more effective and reliable in finding the global extremum (Fig. 3.11). Random methods such as Monte-Carlo, Simulated Annealing and Genetic Inversion are examples of global search method. However, these methods require significant computational effort and time, unlike the local search

method, which is significantly faster, although the probability of converging to the actual extremum is significantly higher with the global search techniques.

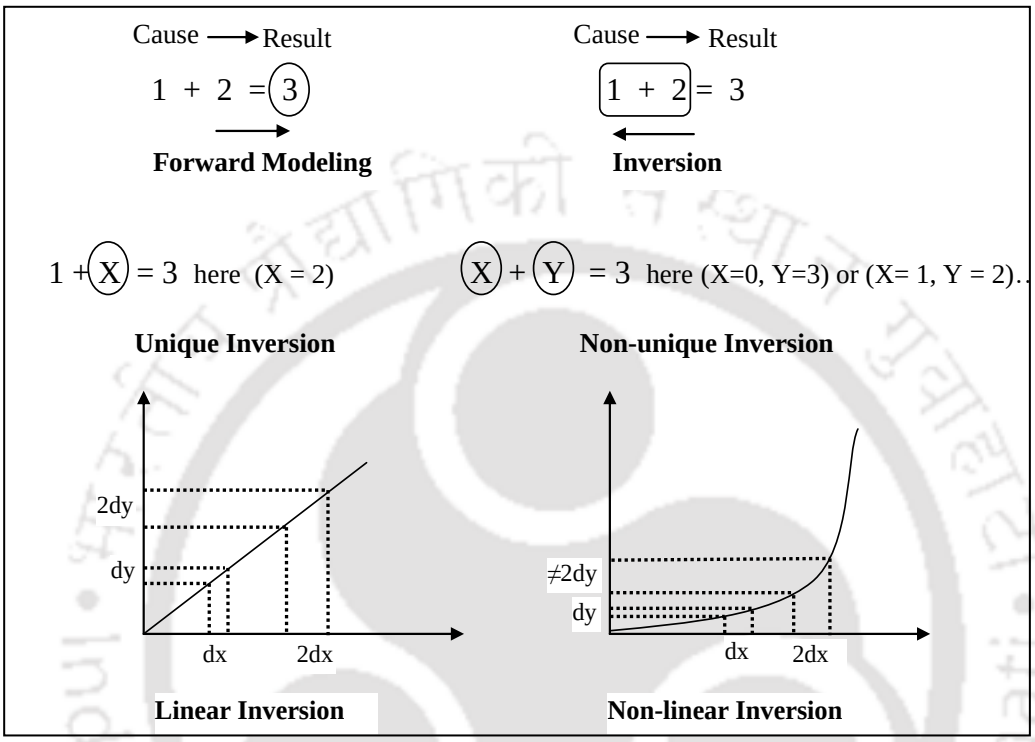

Fig 3.10 General principle of inversion process

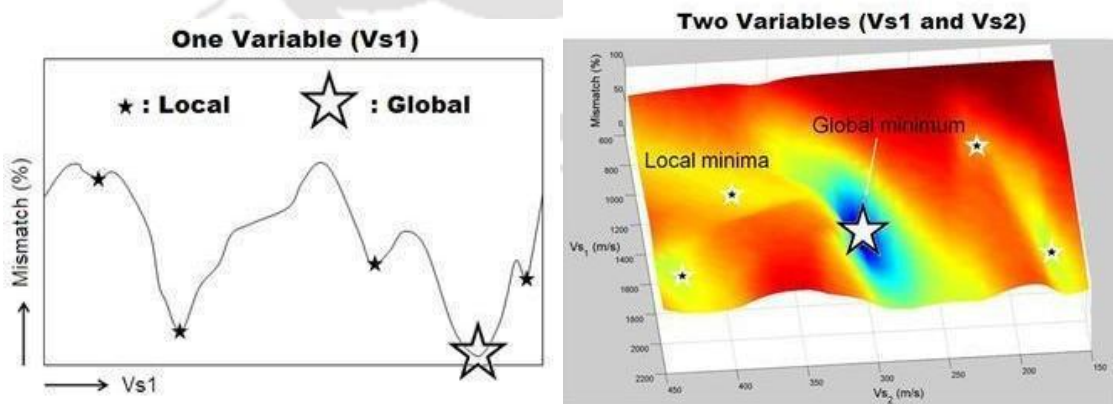

Fig. 3.11 Local and Global minima of an objective function (http://www.masw.com)

In SASW and MASW surveys, the dispersion curves are mostly inverted with the aid of local search based least square method (Nazarian *et al.,* 1983; Xia *et al.*, 1999). In the current work, all dispersion analysis and subsequent inversion of the extracted dispersion curves are carried in *SurfSeis* software platform, which is based on the least square algorithm adopted from Xia *et al*. (1999). As previously mentioned, inversion is an iterative process that requires dispersion data along with estimates of Poisson's ratio (μ) and density (ρ). Among the earth's property, the shear-wave velocity (V_s) is usually estimated from the inversion of the surface wave data. During inversion, normally the fundamental-mode (*M0*) dispersion curve is used to find out the V_s profile. The shape of *M0* curve is influenced mostly by the V_s structure of the earth among all other parameters such as V_p, μ and ρ (Xia *et al*., 1999). Further, it is generally considered that the fundamental mode Rayleigh wave are most predominant in a recorded field data. Consequently, the processing of surface wave data follows the procedure of constructing the *M0* curve that is used to find the earth's V_s structure whose theoretical *M0* curve matches most closely with the actual experimental or measured *M0* curve. The procedure is pictorially explained in Fig. 3.12.

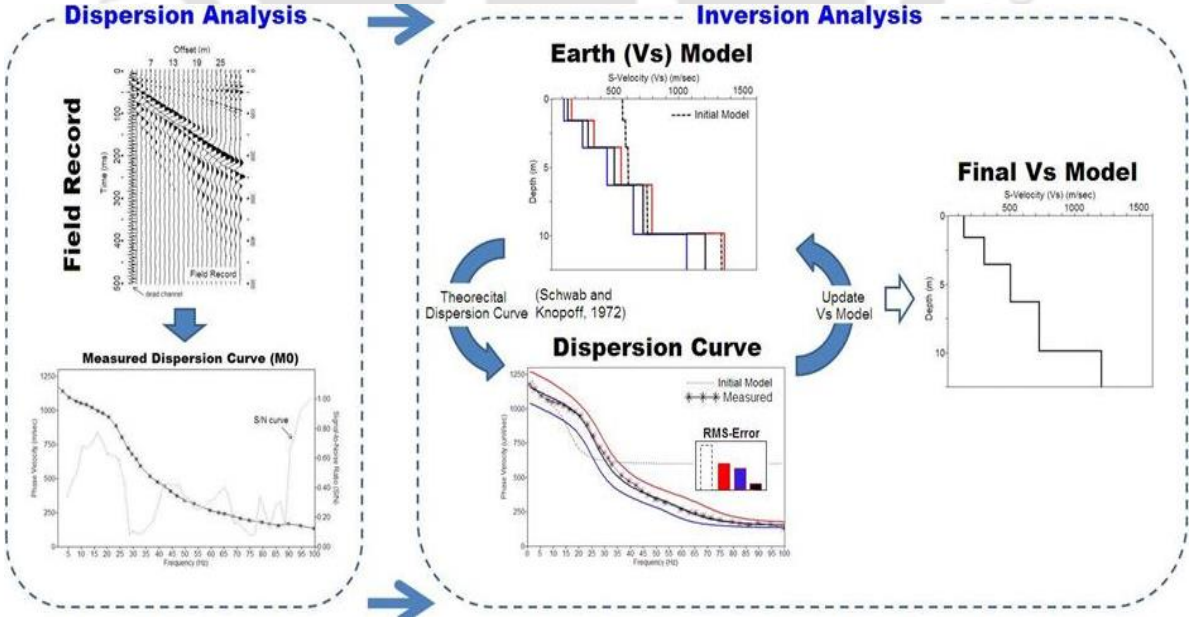

Fig 3.12 Pictorial representation of inversion analysis in MASW (http://www.masw.com)

The key focus of this inversion approach is the optimization technique that searches for the most probable earth model, as efficiently as possible. The dispersion curve constructed during dispersion imaging process, called as measured or experimental dispersion curve, is processed for inversion analysis. The automated process first makes an initial guess of the solution by considering a best suitable initial layered shear-wave velocity (V_s) model, approximated from the measured dispersion curve. The initial primary-wave velocity (V_p) model is determined using the V_s model and a constant Poisson's ratio of 0.4. A continuously increasing density, in the range of 1.5-2.00 gm/cc, is assigned to the earth layers of the model. The maximum depth of investigation is determined from the longest wavelength calculated from the measured dispersion curve. The initial layer model is created by increasing the layer thickness with increasing depth. Then, based on the initial earth layer model, the theoretical Rayleigh wave dispersion curve is constructed by following the analytical technique described by Schwab and Knopoff (1972). To compare the closeness between the two dispersion curves, namely the measured and theoretical, root-mean-square (RMS) error is usually used as an indicator. Based on the obtained RMSE, the initial earth model is updated by varying the layer thickness and shear wave velocities. This process, popularly called as iteration, is repeated until the final solution is obtained, i.e., when preset (tolerance) value of RMS error is attained (Fig. 3.12). The RMS error is mathematically represented as

$$RMSE = \sqrt{\frac{1}{N}\sum_{i=1}^{N}\delta_i^2}, \qquad \text{where} \quad \delta_i = c_i^M - c_i^T \tag{23}$$

where, c_i^M is the i^{th} phase velocity of the measured dispersion curve, c_i^T is the i^{th} phase velocity of theoretical dispersion curve, and N is the total number of data points considered to represent the dispersion curve. The 1-D shear-wave velocity profile pertaining to the tolerated RMSE is

considered as the best possible model for the substrata, which is also demarcated by the close match between the experimental and theoretical dispersion curve obtained from the final iteration. Thus, RMS error serves as a tool for validation of measured and theoretical dispersion curves after each iteration during inversion. The lower is the final RMS error, the greater is the confidence of the obtained V_s profile. Similar approach has been extensively used by earlier researchers for active MASW survey, and the obtained shear-wave velocity profiles were validated with those obtained from seismic bore-hole surveys (Taipodia and Dey, 2018; Taipodia et al., 2018a).

Several notable literatures are available highlighting successful studies related to active or passive MASW surveys while utilizing automated inversion techniques using the least squares based local search algorithms. For all engineering applications, it is desirable to have a unique final V_s profile of the surveyed area. However, global search methods have the disadvantage of resulting in multiple V_s profile that are difficult to address conclusive comparisons. Further, in comparison to local search methods, the global search methods are comparatively slower in process involving much higher number of iterations. Hence, despite many inversion methods implemented for interpretation of subsoil characteristics, engineers often prefer the LS methods (such as the method of Xia *et al*. (1999) used in the current work) over GS methods (Socco *et al*., 2010).

After first developed by Xia *et al*. (1999), Xia *et al*. (2000b) utilized the least square method of inversion via SurfSeis. The author reported the capability of the methodology in many practical field problems, e.g., mapping bedrock layer and locating a steam tunnel in Kansas, mapping bedrock surface in Missouri and mapping dissolution feature in Alabama. Long and Donohue (2007) have extensively used MASW method with Surfseis inversion platform to compare shear

wave velocity profiles obtained from MASW, cone penetration test and cross hole test in eight Norwegian Research sites. In all the results, the author found close agreement between the results from MASW test and other tests. Banab and Motazedian (2010) used Surfseis based inversion in the study for finding efficiency of MASW method in delineating shallow subsoil characteristics at 16 sites possessing sharp velocity contrast, located in the city of Ottawa, Canada. The researchers reported that the primary advantage of random inversion technique as its extra flexibility in updating both the variables in depth and velocity, the feature that does not exist in the generalized inversion technique. However, apart from one lone site, in all other reported sites, the result from MASW tests with generalized inversion technique (i.e., Surfseis) showed appreciable agreement with the results obtained from other exploration techniques. Uma Maheswari *et al.* (2010) used Surfseis for the development of empirical correlations between V_s and SPT-*N* value for different categories of soil in Chennai city, located on the southeastern coast of India, characterized by complex variation of soil conditions. The researchers validated the MASW test results and the inverted shear-wave profiles obtained using the standard inversion adopted in Surfseis by comparing them with available SPT-*N* profiles. The MASW test results obtained through Surfseis were also compared with laboratory Bender element test and were found in close agreement. Brandes *et al*. (2011) have used MASW and automated inversion process through Surfseis for the study of subsoil properties in a young volcanic deposit on the Hawaii Island. The study was conducted to characterize the complex residual soil deposits, particularly for characterizing the strong seismic-motion propagation through the decomposed surface soil and rock sequences. The findings from the study was validated with the borehole profiles at the site and from the findings of the laboratory tests as well. Mohamed *et al*. (2013) used 1-D and 2-D MASW with automated inversion using Surfseis, along with seismic refraction and borehole tests, for site classification in

Egypt based on NEHRP. McGrath *et al*. (2016) conducted an experimental study on the assessment of the repeatability, accuracy, and reliability of the underwater MASW (UMASW) technique. The author utilized automated inversion using SurfSeis programme for the study of the area near Bull Island, Ireland. The shear-wave velocity profiles obtained via MASW methods are compared with the Seismic Cone testing, which resulted good agreement between the two procedures. Anbazhagan *et al*. (2018) have used active, passive roadside and remote method for the characterization of Indo-Gangatic Basin with extensive application of Surfseis and ParkSEIS, which uses the standard automated inversion procedures. The V_s profiles obtained using the automated inversion techniques were found to be in very appreciable agreement with the same obtained using SPT-*N* values for many of the test sites.

3.7 Summary

The dispersion imaging in MASW is the most crucial stage and largely affects the final V_s result. In the present research, the processing of the raw field records have been conducted on the software platform 'SurfSeis'. The dispersion imaging process in the software is based on the Phase-Shift method that is considered to give higher resolution than any other existing methods. The method was originally developed for active MASW records, but later modified for passive MASW records as well. The modified dispersion imaging scheme for passive roadside record takes account of both offline and cylindrical characteristics of the wavefield records and thereby gives more robust result. The software utilises inversion scheme proposed by Xia *et al*. (1999) to finally derive V_s structure of earth from the dispersion curve. The method is based on the 'Local Search algorithm' to find the most probable result with the aid of RMS value as reference and stopping criterion.

CHAPTER 4

FIELD SETUP, INSTRUMENTS AND METHODOLOGY

4.1 Introduction

As already mentioned earlier, the crux of the present research lies with the field experimental investigation based on Passive Roadside MASW Survey conducted at various sites comprising different genres of traffic. This chapter reports the details of the site locations, traffic characteristics, and other details related to the field experimentation, instrumentation and recording parameters adopted at different sites during field data collection. The details of various processing steps of field data with SurfSeis, the adopted software platform, is also briefly presented.

4.2 Details of Site Locations

In the present research, three site locations, inside and around IIT Guwahati campus, have been selected for an extensive passive roadside MASW experimentation. Field tests, and corresponding evaluation of the results from multiple sites, along with their detailed inferences in terms of field recording and data processing, will help to develop robust guidelines for effective and precise passive roadside MASW survey. The locations of the three sites are shown on a map in Fig. 4.1, and are listed as follows:

- **Site 1**: Inside IIT Guwahati campus, along the roadside near the cricket field, between SAC and hostel Siang (26º11'27" N, 91º41'45" E).
- **Site 2**: A part of the road stretch from IIT Guwahati to Amingaon market (26º10'56" N, 91º41'35" E).

❖ **Site 3**: Beside National Highway (NH) No. 31, over a stretch between Jalukbari to Baihata Chariali route (26º12'38" N, 91º41'22" E).

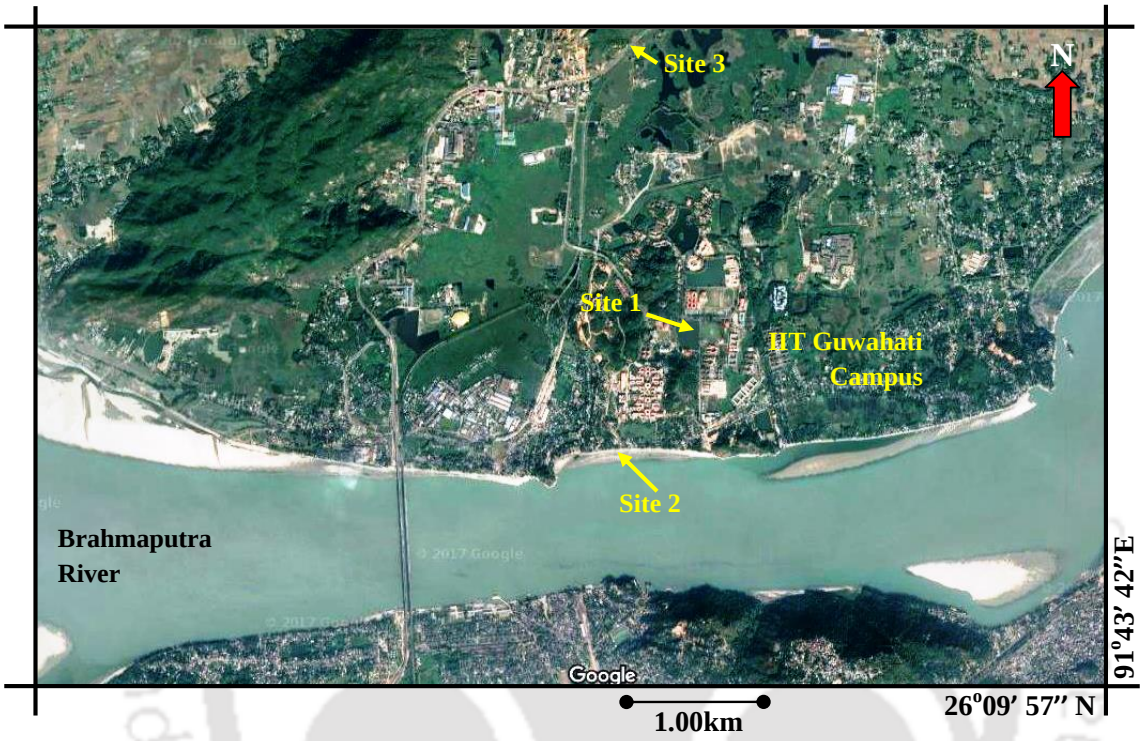

Fig. 4.1 Map showing positions of the Sites 1, 2 and 3 in and around IIT Guwahati campus

All the sites comprised different volumes of traffic: light at Site 1 (less than 50 commercial vehicles per day), medium at Site 2 (50-150 commercial vehicles per day) and heavy at Site 3 (more than 150 commercial vehicles per day). Two primary reasons guided the selection of all these three sites. Firstly, the road beside the site should have a straight alignment as far as possible (23-100 m) so that a linear receiver array can be placed with a constant offline distance. Secondly, there should not be any major intersection road, or other structures, which could hinder laying of the receiver array and could produce traffic waves from unwanted directions. A straight road stretch also helps in switching the recording on the seismograph at appropriate time as any approaching

vehicle can be easily noticed from far away distance. The details of the three sites are presented as follows.

Site 1: The first site is chosen inside IIT Guwahati campus on a road adjacent to the cricket field. The selected road stretch spans from the entrance route of Siang hostel to the SAC building. Inside the campus, the roads were newly repaired and, thus, possess very little cracks or other irregularities, and are sufficiently free from undulations. Moreover, there are no speed breaker or speed inhibitors on the selected stretch, which could have served as a major energy source for wavefield generation. Therefore, to conduct passive MASW experiments, a GI pipe, of approximately 4 m length that almost covered the width of the road, was used whenever a strong wavefield source was desired. This pipe served as a source of wave propagation whenever a vehicle passed over it. The source can also be moved easily and placed in other positions as per the experimental requirements. The pictorial view of the site is shown in Fig. 4.2a. Attributed to very light traffic volume at the site, the experimentation could be conducted in a controlled manner that helped in evaluating many critical parameters of roadside survey. The traffic of the road beside the site mainly comprises private four wheeler vehicles weighing around 1000 kg and institute buses weighing approximately 10000 kg. Beside the selected road stretch, there is a cricket field ground that provided ample space to conduct roadside survey at various offline distances along with passive remote survey as well. The borehole report of a location in the vicinity of the experimental site is represented in Fig. 4.3a. The Standard Penetration Test conducted at the site indicates a loose stratum with smaller SPT-N values until a depth of 10 m from the surface. An increase in the SPT-N values is then observed until a depth of 14 m. Following, there appears a decreasing trend until a depth of 17 m and then it continuously increases until 30 m depth. It reports

the existence of a loose clayey stratum overlying a stiffer sandy stratum. The water table during the time of investigation was found at a depth of 3 m from ground surface.

Site 2: At this site, approximately 100 m of a straight road stretch was available for the field experimentation that can easily accommodate up to a 92 m of linear receiver array i.e., with 24 numbers of geophone at an inter-receiver spacing of 4 m. The road being a fairly busy road provided a good potential and scope for passive roadside survey. The traffic of the road comprises of two wheeler motorcycles, three wheeler light vehicles, four wheeler private cars and average weight buses and trucks (weight less than 10000 kg). Further, in the reconnaissance survey of the road, many irregularities on the road, such as potholes and depressions, were noticed which served as sources of wavefield generation. The width of the road is around 3.5 m with a shoulder width of roughly 2 m along the stretch. The receiver array was deployed along the shoulder of the road and approximately 1.5 m away from the edge of the bituminous road, i.e., an offline distance of 3.25 m from the centre of the road. This geometry was maintained along the whole stretch of the array to make it parallel to the centre of the road. The pictorial view of the site has been shown in Fig. 4.2b. Figure 4.3b represents the detailed borehole report of a nearby location close to the Site 2, as no borehole reports were available for the exact location. The SPT-N value at the site depicts very loose soil until 11.5 m depth from the surface and thereafter continuously increases with depth. The top 3 m layer of the soil is observed to be the filled up soil and classified as SP type. The soil layers below the top layer are mostly loose clayey soil up to a depth of 16 m after which there is a stiffer sandy stratum.

Site 3: The third site has been selected over the stretch of a four-lane National Highway (NH) no. 31. The road has a very busy traffic line and comprises small to very heavy vehicles (weighing more than 10000 kg) travels on it. The roadside area beside the highway has a width of around 5-10 m and suitable for conducting roadside survey. During preliminary survey, it was noticed that there is no major surface sources on the road stretch of the selected site. However, traction of the heavy vehicles plying on the road is found to produce sufficient surface wave energy for passive roadside survey. The pictorial view of site has been shown in Fig. 4.2c. A detailed borehole report is presented in Fig. 4.3c for a nearby area to the Site 2. However, as in the previous case (Site-2), the site of borehole location and the MASW experimental site are not identical. Therefore, the report will only give a general idea about the soil stratigraphy of the experimental site. The borehole log shows stiffer soil strata from the shallower layers with much higher SPT-N values compared to the earlier two sites. The soil in the site is mostly of sandy type with either silt or clay mix in alternate layers. Attributed to the hard rock stratum existing at a shallow depth, the borehole could not be advanced below 15 m depth. The SPT-N values are considered as 'Refusal' attributed to their very high values (greater than 100) beyond 10 m depth.

In summary, the borehole profile, depicted in Fig. 4.3a, is in vicinity of Site-1 for MASW survey, and hence the same is used for validation of MASW profile in the later sections (Fig. 9.17). However, it is to be noted that the borehole profiles for Sites 2 and 3 (Fig. 4.3b and 4.3c) are not exactly located near the MASW survey sites. They are only used to provide an idea about the local geology and geotechnical stratification. However, they are not used for any other validation studies. For Sites-2 and 3, the validation studies are conducted with the active MASW surveys, while for Site-1, both active MASW survey and borehole profile is used for validation study.

Fig. 4.2 Pictorial view of the chosen experimental sites (a) Site 1 inside IIT Guwahati campus (b) Site 2 beside IIT Guwahati to Amingaon Market route (c) Site 3 beside NH-31, between Jalukbari to Baihata Chariali route

Type of Boring: Auger /Wash **Date started:** 21/10/2002

Place: Site-1 IIT Guwahati **Date completed:** 23/10/2002

Description of strata	Depth (m)	Strata	Sample collected (m)	Ground water level	SPT	N-Value
Clay soil grey to brown in colour	1		1.5			3
	2					
Black pit soil	3		3			2
	4		4.5			3
	5					
Clay soil grey in colour	6		6			4
	7		7.5			5
	8					
Clay soil ash in colour	9		9			6
	10		10.5			18
	11					
Clay soil brown in colour (hard soil)	12		12			24
	13		13.5			31
	14					
Silty clay grey in colour	15		15	Ground water level at 3 m		20
	16		16.5			22
Sandy clay ash to grey in colour	17					
	18		18			15
Clay soil grey in colour	19		19.5			17
	20					
Sandy clay grey in colour	21		21			22
	22		22.5			26
	23					
Sandy clay grey in colour	24		24			30
	25		25.5			32
Silty clay grey in colour	26					
	27		27			36
Sandy clay ash in colour	28		28.5			39
	29					
Sandy clay black in colour	30		30			42

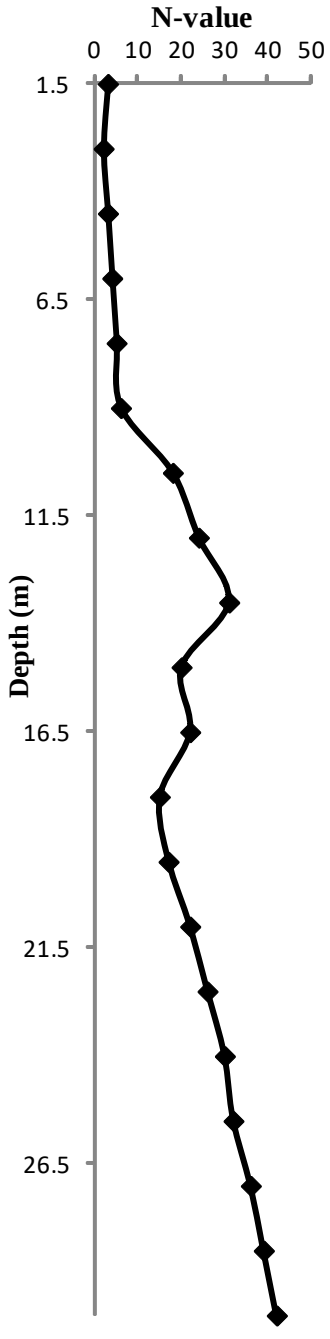

(a)

Type of Boring: Auger /Wash

Place: Site-2 Amingaon Site Date: October, 2009

Description of strata	Depth (m)	Strata	Sample collected (m)	Ground water level	SPT	N-Value
Ash in Colour 'SP' type soil (Filled up soil)	1		1.5			8
	2					
	3		3			1
Blackish to grey in colour 'PT' type soil	4		4.5			0
	5					
Greyish in colour 'CI' type soil	6		6			1
	7					
	8		7.5			2
Blackish to grey in colour 'PT' type soil	9		9			4
	10					
	11		10.5			1
	12		12	Ground water level at 0.4 m		3
Greyish in colour clayey silt with sand 'CI' type of soil	13		13.5			5
	14					
	15		15			8
	16					
	17		16.5			11
	18		18			20
Brownish in colour poorly graded fine to coarse grained sand mixed with silt 'SP' type soil	19		19.5			37
	20					
	21		21			41
	22					
	23		22.5			44
	24		24			48
	25					
	26		25.5			56

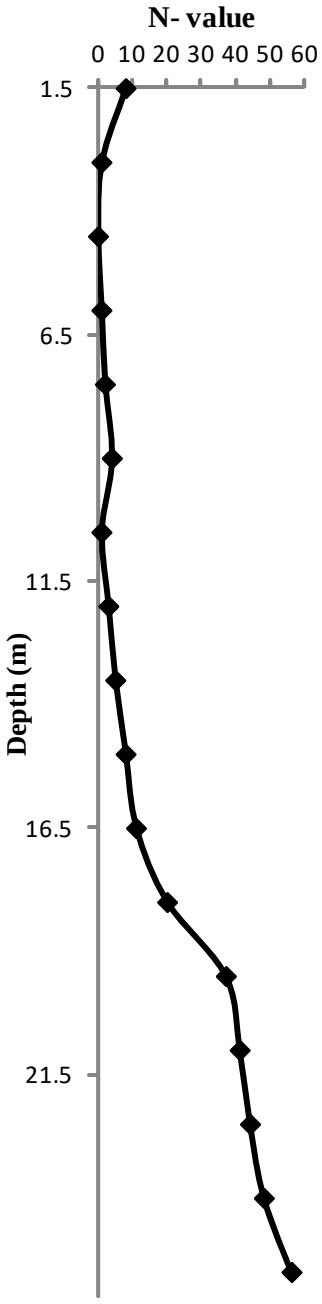

(b)

Type of Boring: Auger /Wash

Place: Site-3 NH 31 Date: Sept, 2012

Description of strata	Depth (m)	Strata	Sample collected (m)	Ground water level	SPT	N-Value
Clayey sand	1		1.5			14
	2					
Poorly graded sand with silt	3		3			15
	4		4.5			18
	5					
	6		6			20
Sandy clay grey in colour	7		7.5	Ground water level at 4 m		54
	8					
	9		9			54
	10		10.5			100
Hard rock strata	11					
	12		12			100
	13		13.5			100
	14					
	15		15			100

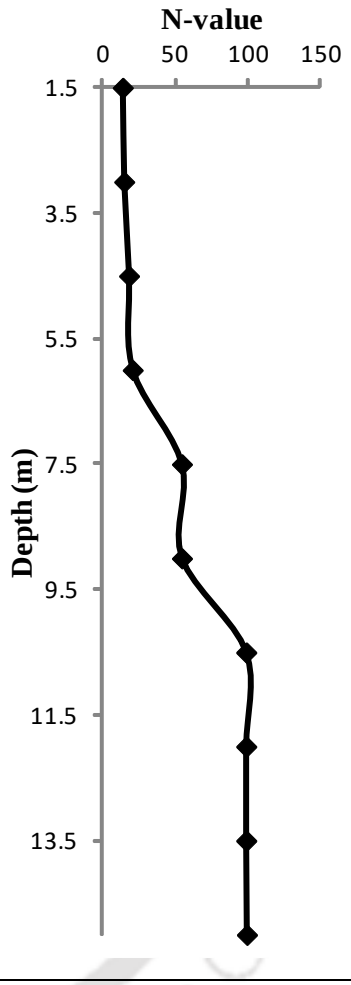

(c)

Fig. 4.3 Borehole log report of nearby area of (a) Site 1 (b) Site 2 (c) Site 3

4.3 Details of Data Acquisition Systems and Parameters

4.3.1 Geophone Receivers

The basic principle of surface wave recording by geophone receivers is already presented in Chapter 2. It has been reported in the existing literatures that natural frequency of geophone

receivers should be as low as possible to record surface waves comprising low frequency components. The natural frequency of the geophones utilised in this work is in the low frequency range of 4.5 Hz (http://www.mae-srl.it/prodotti/showprodotto/500). Low frequency geophones are effective in recording waves of low frequency i.e., larger wavelengths. Such geophones are particularly required in case of passive surveys where attempt is made to collect the passive source generated waves of low frequency for deeper subsoil investigation. The pictorial view of the 4.5 Hz geophones utilised in the present study is shown in Fig. 4.4a, along with a schematic view illustrating its main components. The descriptions of its various parts is already presented in Chapter 2.

Figure 4.4b shows the frequency characteristics of 4.5 Hz geophone, which manifests that although the resonating response of the geophone is obtained at 4.5 Hz, recognizable voltages will be generated even at frequencies as low as 1.6 Hz. For the frequency range 1.6-4 Hz, the generated low voltage can be enhanced by vertical stacking of dispersion image which results in a distinguishable energy trend (or, dispersion band) (Foti *et al*., 2014); the same will be discussed in detail in Chapter 7. Geophones are subjected to deterioration over time thus require regular calibration for their effective performance. The earliest technique of in-situ calibration of geophones was proposed by Asten (1977) for both under-damped and over-damped systems. The calibration of such geophones depend on six constants: the suspended mass, the natural resonant frequency, the mechanical and the electrical damping factors, the inducting time constant of the coil-damping resistance circuit, and the coil transductance. If the suspended mass is known a-priori, the remaining constants are satisfactorily determined by displacing the mass with a known DC current, and observing the time-varying output potential on removal of the steady current.

Following this method, the Bird Dog Test System for geophone testing and calibration is widely used by the WHOI Ocean Bottom Seismograph Laboratory (https://web.whoi.edu/obslab/wp-content/uploads/sites/98/2017/10/Geophone_TestingEDIT-1.pdf). Chevatco (2017) carried out effective calibration of geophone sensors with the help of a seismic shaker, and proposed a new calibration process based on multi-tone excitation coupled with system identification methods for parameter estimation. In the present study, intermittent checks on the frequency-voltage relationship of the geophone receivers were conducted by the service provider, as well as by testing against standard sweeping sinusoidal wave frequencies.

In the literature survey, it has been reported that greater number of receivers are beneficial for generating better and higher resolution of dispersion image. The seismograph employed in the study can accommodate maximum 24 numbers of geophones. To achieve the highest level of accuracy and resolution, all the 24 numbers of geophone have been utilised in all MASW experiments and in all the above-mentioned three sites.

4.3.2 Seismograph or Data Acquisition System (DAQ)

Seismograph is a digital recording system that can record seismic signals generated by the geophones. It is a portable and lightweight instrument and can be easily transported. All the geophone receivers are connected to the Seismograph or Data Acquisition System (DAQ). The signals collected by the receiver geophones are recorded by the DAQ/Seismograph through an analog-to-digital (A/D) conversion process. The primary parameters of a seismograph that can influence the experimental findings are (a) Numbers of recording channels, (b) Accuracy of digitization (dynamic range, distortion), and (c) Sampling parameters (maximum range of

acquisition time, sampling rate). For shallow subsurface applications, seismograph with 24 to 48 number of channel capacity is found to be sufficient. The dynamic range is one of the most critical characteristic of a seismograph that determines the quality of the recorded data, the detectable frequency range (highest and lowest frequency range) and the detectable modes. The A/D accuracy of any data acquisition system is measured in bits, describing the numbers of discrete values that can be sampled within an input range (Foti *et al*., 2014). The seismograph employed in the study has a 24-bit A/D converter that corresponds to a 144 dB dynamic range. It is a make A-6000-S seismograph acquired from Molisana Apprachhiarature Electroniche (MAE), Italy (as shown in Fig. 4.5a, http://www.mae-srl.it/prodotti/pdfprodotto/23).

The power supply to the seismograph is provided through a portable dry cell battery. The geophones are connected to the spread cables as shown in Fig. 4.5b. One such cable can connect a maximum 12 numbers of geophones. The seismograph can connect two such cables giving a total geophone connection of 24 numbers. Figure 4.6 shows a typical passive roadside field record collected with the seismograph employing 24 numbers of geophones, in which a 24-channel time-domain record can be observed.

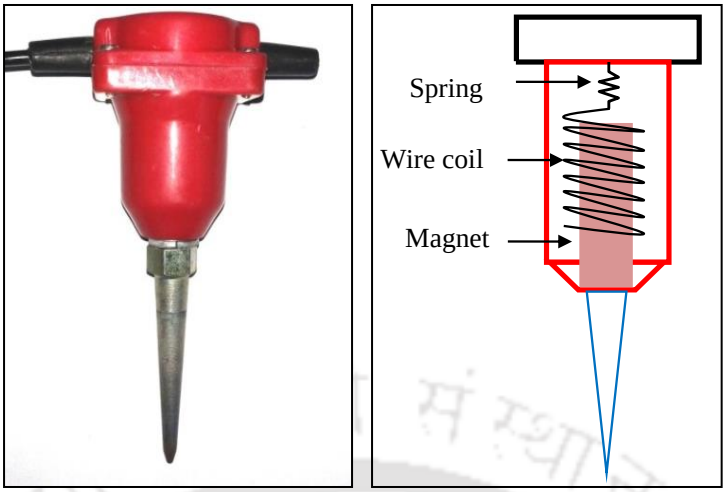

(a)

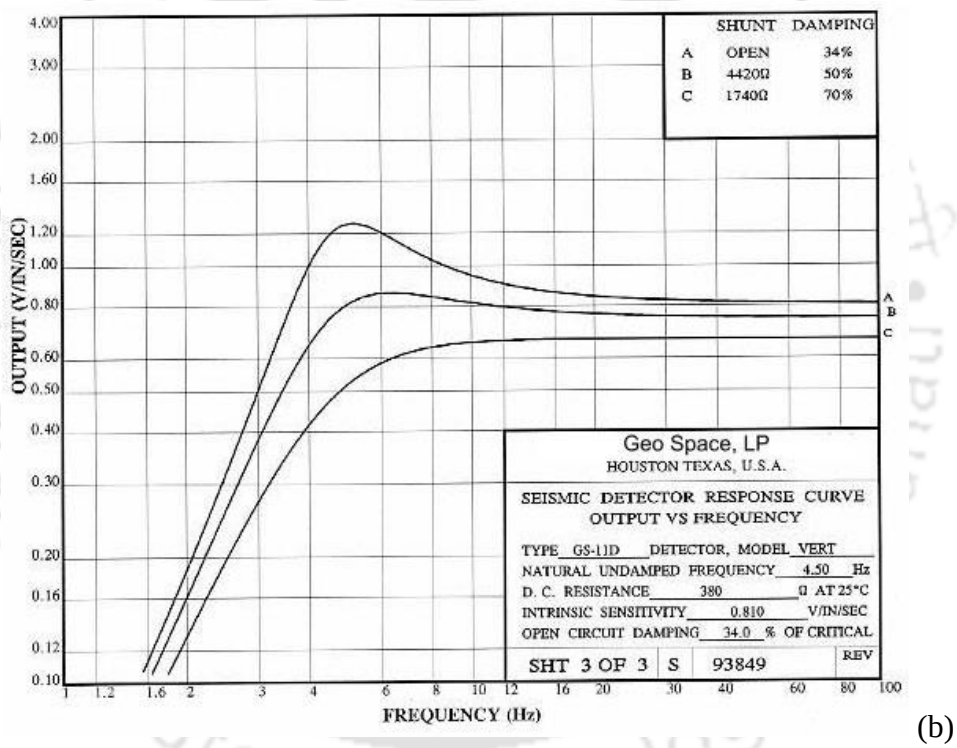

(b)

Fig. 4.4 (a) A typical 4.5 Hz geophone used in the present study and schematic representation (b) Frequency characteristics of 4.5 Hz geophone (as per Impostaziani Sismica GS-11D, MAE, 2011)

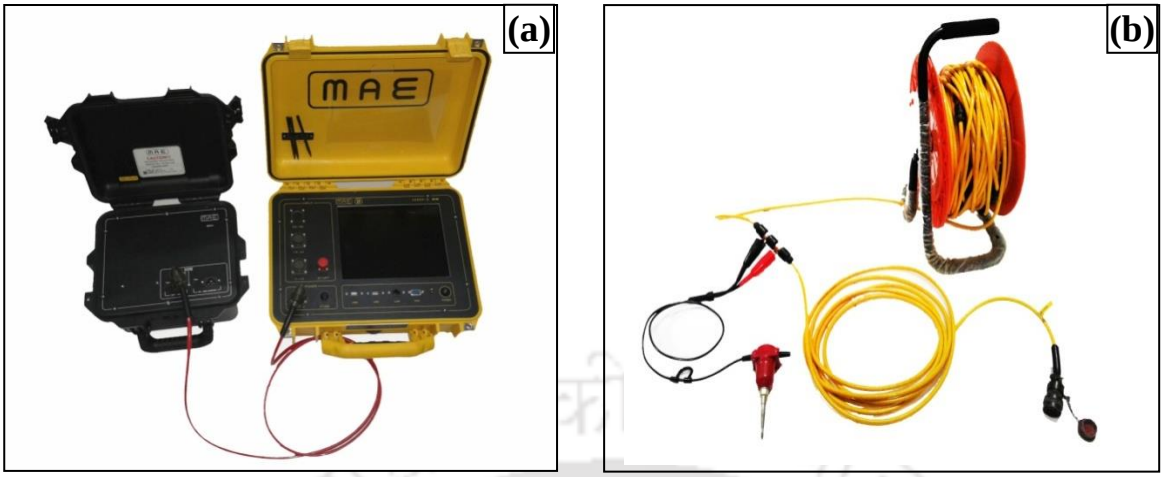

Fig. 4.5 (a) Seismograph connected with a dry cell battery (b) Spread cable used to connect the geophones to the seismograph

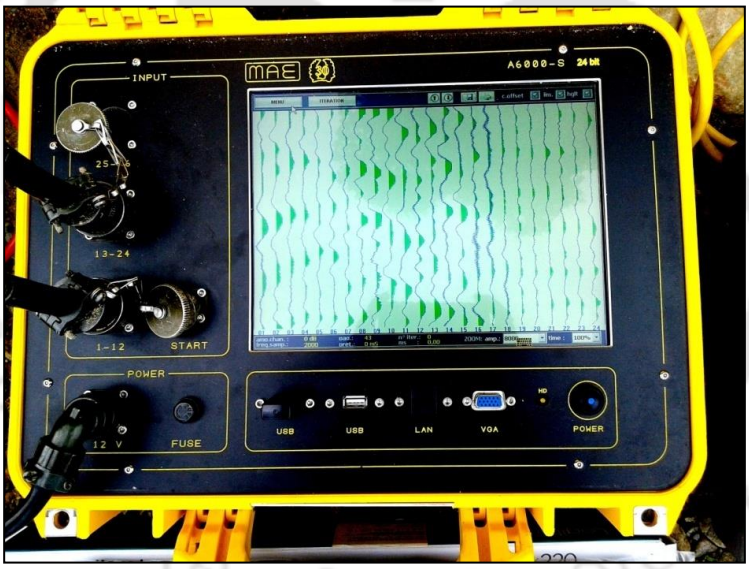

Fig. 4.6 A typical 24-channel passive roadside field record collected with the seismograph

4.3.3 Receiver Array

In passive roadside survey, a linear receiver array is placed at the sites, parallel to the road stretches. Normally, it is recommended that the offline distance (between the array and the road

centre) be maintained fairly constant (viz. within ± 30%) throughout the entire survey. The linear dimension (D) of the array should be at least equal to or greater than the desired maximum depth of investigation (Z_{max}), i.e., $D = mZ_{max}$ $(1 \leq m \leq 3)$ (http://www.masw.com). It is normally considered that the maximum penetration depth of ground roll (Rayleigh wave) is approximately equal to its wavelength. However, the maximum depth up to which V_s can be reliably evaluated is normally considered as half of the longest wavelength (Park *et al*., 1999).

The receiver spacing (dx) is determined by the number of channels or receiver (N) to be utilised i.e., $dx = D/N$. It is usually convenient to select dx as a rounded number (e.g., 1 m, 4 ft, etc.). The receiver spacing (dx) controls the minimum resolvable thickness of shallowest layer to be investigated (Z_{min}) roughly as $Z_{min} = pdx$ $(1/3 \leq p \leq 1.0)$ (Park *et al*., 1999).

In the present research, the selection of length of the receiver array is decided as per the availability of uninterrupted roadside stretches and the attempted investigation depth. The details of various receiver array parameters such as number of receivers, array shape and dimension of the array, adopted in this study, at the three sites, with different mode of MASW surveys, are shown in Table 4.1. It is to be mentioned here that the receiver cable used in this research has a maximum receiver spacing slot of 5 m. Therefore, with 24 numbers of geophone maximum array length that can be accommodated is 115 m. At Sites 2 and 3, receiver array length up to 92 m could be used, given the long stretch of available uninterrupted roadside. On the other hand, at Site 1, due to various field limitations, the longest array length that could be used was 69 m. However, attributed to the availability of a wide space beside the road, a set of roadside survey with different offline distances, a set of active test at the respective positions of roadside survey and a set of remote MASW survey with 2-D circular arrays could also be conducted. Such availability of space at Site 1 proved to be

a major advantage in understanding the influence of offline distances and various validation studies.

Table 4.1 Details of receiver array type and dimension utilized at different sites

Site	Receiver Numbers	Receiver array shape	Dimension or Length of receiver array (m)		
			Passive Roadside	Active	Passive Remote
1	12, 24	Linear for roadside/active; Circular for remote	23, 46, 69	11, 23, 46, 69	18 m diameter
2	24	All linear	23, 46, 92	46	----------
3	24	All linear	46, 92	46, 92	----------

4.3.4 Acquisition (Sampling) Time and Sampling Interval

The acquisition, recording or sampling time and sampling interval are other important recording parameters that influence the passive MASW surveys. The existing literatures report that a recording time (T) in the order of 10 s and a sampling interval (dt) in the order of 4 ms is sufficient for a survey near major highways. It is normally recommended to decide for the total recording time in such a way that there is at least one occurrence of passive surface wave event during actual recording. Therefore, in case of passive roadside survey, there should be a vehicle passing near the surveyed area at least once during the recording time. The longer recording time does not always guarantee an effective recording as it also increases the possibility of recording surface waves generated at different locations (azimuths) on the road and may degrade the overall data quality. However, a longer recording time may be effective when there is a major source point nearby the surveyed area, as it is capable of producing multiple numbers of major surface events from the

same source. A source point of major surface waves is observed when a jolting sound comes from nearly the same spot (azimuth) on the road as vehicles passes through the same. Vertical stacking, during in-situ recording, is strongly discouraged in the literatures, owing to the possibility of recording multi-azimuthal surface waves.

Table 4.2 Details of acquisition time used at different sites for the present study

Site	Survey type	Acquisition time (s)
1	Passive Roadside and Remote	10.8
	Active	1
2	Roadside	0.7-218
	Active	1
3	Roadside	0.7-218
	Active	1

The details of various ranges of acquisition time applied in the present research, at different sites, are presented in Table 4.2. A sampling interval of 4 ms was maintained for all the passive roadside and remote field acquisitions. On the other hand, the acquisition time has been varied between 0.7-218 s at Sites 2 and 3. However, due to very thin traffic volume at Site 1, a longer acquisition time was allowed for passive surface wave recording.

4.4 Analysis Methodology: SurfSeis Platform

This section describes the methodology and steps involved during dispersion and inversion analysis of the seismic raw data collected in the field with various geometrical and recording parameters as reported in previous sections. As already mentioned, during the dispersion analysis,

a phase-velocity versus frequency image is obtained from the propagation characteristics of dispersive surface waves through wavefield transformation methods. Thereafter, from the dispersion image, a dispersion curve is selected along the points of spectral maxima. During inversion analysis, through an iterative procedure, the measured dispersion curve is inverted to obtain shear-wave velocity profile against subsurface depth. In this study, a commercialized software, 'SurfSeis' v3.45 and v5, have been used for the processing of raw field records collected from all the three sites. A brief description of the working procedure of the software as used in the processing of raw field records obtained from passive roadside survey is reported in the following section.

4.4.1 Importing Data

SurfSeis supports data in SG2 format. When such data is imported from storage drive, first step is to assign the geometrical shape and size to the imported data, e.g., geophone spacing, geophone number, offline distance, as has been used in the field experimentation. Once these are assigned, the data gets prepared for dispersion analysis.

4.4.2 Dispersion Analysis

When the "Dispersion" button in the analysis menu is selected, a dialog box pops up that allows selecting a file containing the seismic shot records. After selecting the desired file, it leads to the parametric control table where different processing parameter has to be set as per requirements. The "Dispersion" option in the analysis section gives complete flexibility to select key processing parameters, e.g., scanning range of frequency, velocity range, azimuthal range and their scanning increments, and offline distance. Once these parameters are appropriately selected, the file can be

processed for dispersion imaging. After the end of the scanning process, the dispersion image will appear, from which the dispersion curve has to be manually selected along the points of spectral maxima (with visual recognition) such that a high SNR, close to '1', is maintained for each of the selected points.

4.4.3 Inversion analysis

After the dispersion curve is selected and saved for further processing, the window automatically leads to the inversion stage. The "Run" button initiates the inversion process, searching for a V_s profile whose theoretical dispersion curve best matches to the measured dispersion curve, while using the root-mean-square error (RMSE) as a guide and stopping criterion (Xia *et al.,* 1999). At each iteration, a theoretical curve is calculated based on a layered earth model and compared to the experimental curve. After each iteration, the theoretical curve (marked as "Current") is compared to the experimental curve (marked as "Measured"), and the V_s profile for the theoretical curve is compared with the initial V_s profile. The iterations continue until either the minimum RMSE (E_{min}) is achieved or the maximum number of iteration (I_{max}) is reached, whichever is attained earlier. If the experimental curve is fairly accurate, then the RMSE usually drops rapidly during the first few iterations. A high quality dispersion curve usually is characterized by a consistent and smooth change in phase velocity with frequency. For such high quality dispersion curve, E_{min} is usually attained after just a few iterations and the analysis is completed. A step-by-step procedure of the working of "SurfSeis" is included in **Appendix**.

CHAPTER 5

CRITICAL ANALYSIS OF RAW WAVEFIELD RECORDS FROM PASSIVE ROADSIDE MASW SURVEY

5.1 Introduction

In MASW survey, a good quality data is considered to be the one in which surface wave event is the most significant. Such a signal normally possesses a high SNR value. On the other hand, a bad quality signal is the one which is highly contaminated by the effects of various noises and possesses poor SNR value. Noise in MASW survey implies body waves, air waves, backscattered waves and higher mode surface waves. Thus, in MASW, the fundamental mode surface waves are considered as signal during dispersion curve analysis, ignoring all other contamination as 'noise'.

Quality of raw field records play the foremost important role in the resolution of dispersion imaging in the passive MASW survey. Field record containing surface wave energy with high SNR is mandatory for obtaining dispersion image with good resolution. In active MASW survey, the quality of field record is controllable and editable by the surveyor, which is attributed to the use of an active source of wavefield generation. However, in the case of passive surveys, the quality of raw field data is not under the direct control of the investigator, since the occurrence of surface wave events from natural or cultural sources are independent phenomenon and may not always occur in the favour of MASW survey being conducted. Therefore, obtaining dispersion image with high resolution is a challenge in passive surveys in almost every field situations. However, detailed study of the raw field records, and evaluating the critical parameters affecting

its quality, will be beneficial for the effective recording of field records of desired quality as well as deciding for optimum processing parameters for the improvement of dispersion imaging.

5.2 Scrutiny of Wavefield Records from Various Sources at Site 1 comprising Light Traffic Volume

It is foreseeable that different traffic characteristics will produce raw field records with different wavefield characteristics. The primary factors which affect the wavefield characteristics are weight and speed of vehicles, numbers of vehicles crossing the receiver array during recording and the source characteristics upon the road surface (such as the size and positions of road irregularities). From the elementary physics, it is known that the kinetic energy generated by a moving vehicle is a function of two parameters, namely the mass and velocity of the moving object. The popular correlation is represented by Kinetic Energy = $0.5mv^2$, where m and v are mass and speed of the vehicle, respectively. A vehicle of larger weight produces greater impact on passing over a road surface source (i.e., irregularity) than a vehicle of lesser weight. A greater impact generates wavefields of high energy with long wavelengths and can be effective for exploration of deeper soil layers. Thus, a vehicle moving with high velocity produces wavefields of high energy and long wavelengths favourable to passive MASW survey. Considering different weight and speed of the vehicles, a comparison of energy generation on passage of different vehicles over road irregularities is shown in Table 5.1. It is normally assumed that out of the total kinetic energy generated by a vehicle, only 10% of the energy will lead to the generation of the surface waves (http://www.masw.com). From the table, it can be comprehended that even a small car with a moderate speed can generate a much higher level of energy than conventionally utilized weight

drops of smaller mass. Hence, such wavefields from traffic sources can be highly favourable for passive MASW survey.

Table 5.1: Comparison of energy generation by various sources

Source Type						
Weight drop (V_{max} = 10m/s)		Vehicular speed in kmph (m/s)	Small lightweight vehicle: Small four-wheelers (Mass = 1000kg)		Large heavyweight vehicle: Truck, Bus, Road roller (Mass = 10000kg)	
Mass (kg)	Energy (J)		Total Energy (J)	10% of Total Energy (J)	Total Energy (J)	10% of Total Energy (J)
5	250	20 (5.56)	15456.8	1545.68	154568.0	15456.80
10	500	30 (8.33)	34694.45	3469.44	346944.5	34694.45
20	1000	40 (11.11)	61716.05	6171.60	617160.5	61716.05
40	2000	50 (13.89)	96466.05	9646.60	964660.5	96466.05
100	50000	60 (16.67)	138944.45	13894.45	1389444.5	138944.45

Site 1 inside IIT Guwahati campus, comprising a very light traffic volume, was selected to critically assess the influence of traffic genre on the emergence of wavefield characteristics. This condition was favourable for conducting the experimentation in a very controlled manner in two primary ways. Firstly, passive roadside field data could be recorded with desired number of vehicles passing through the array (e.g., single or multiple); and, secondly, the field data could also be recorded aiming for vehicles of desired weight (e.g., car, bus). The following section presents comparative study of field records obtained from various surface sources generated by various genres of vehicles.

5.2.1 Critical Analysis of Raw Field Records obtained from Active Source

For the detailed comparison of different source originated wavefield records, firstly, a set of records obtained from active MASW test is presented in this section. The records were acquired at Site 1 exactly at the positions of roadside survey. The schematic of the test set up is shown in Fig. 5.1. Figure 5.2 shows the raw field records obtained from a set of active tests, conducted with 4 m and 16 m source offsets, using a 46 m receiver array spread with 24 numbers of receivers. Both the records were obtained through striking a 10 kg sledgehammer on a metallic blasé plate made of cast steel. In both the records, the single surface wave event generated by the hammer blow is clear and distinct, and it is observed that there is a bare minimum presence of ambient noise in the record. In the wavefield record generated out of a 4 m source offset (Fig. 5.2a), the arrival of some non-planar waves can be observed in the first few receivers closest to the source in the form of the irregular wave spikes manifesting the near-field effect. As a consequence of near-field effects, the receivers of the array, closest to the source, record underdeveloped portion of the wavefields of non-planar characteristics. In the other record generated from a 16 m source offset (Fig. 5.2b), the wavefield recorded is observed to be of truly planar characteristics. Moreover, the wavefields are observed to be originating approximately from 0 ms and 150 ms in the cases of 4 m and 16 m source offset, respectively, signifying the time delay for the first arrival of wavefield signatures to the receiver spread.

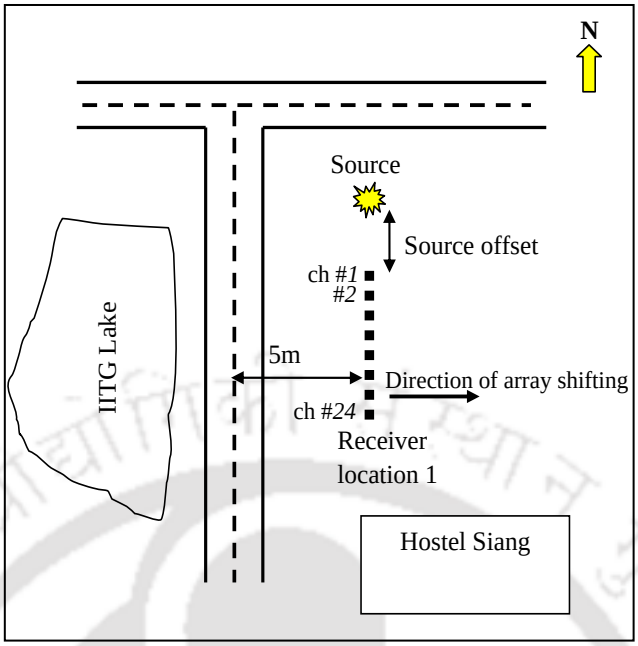

Fig. 5.1 Schematic view of the active MASW survey conducted at Site 1

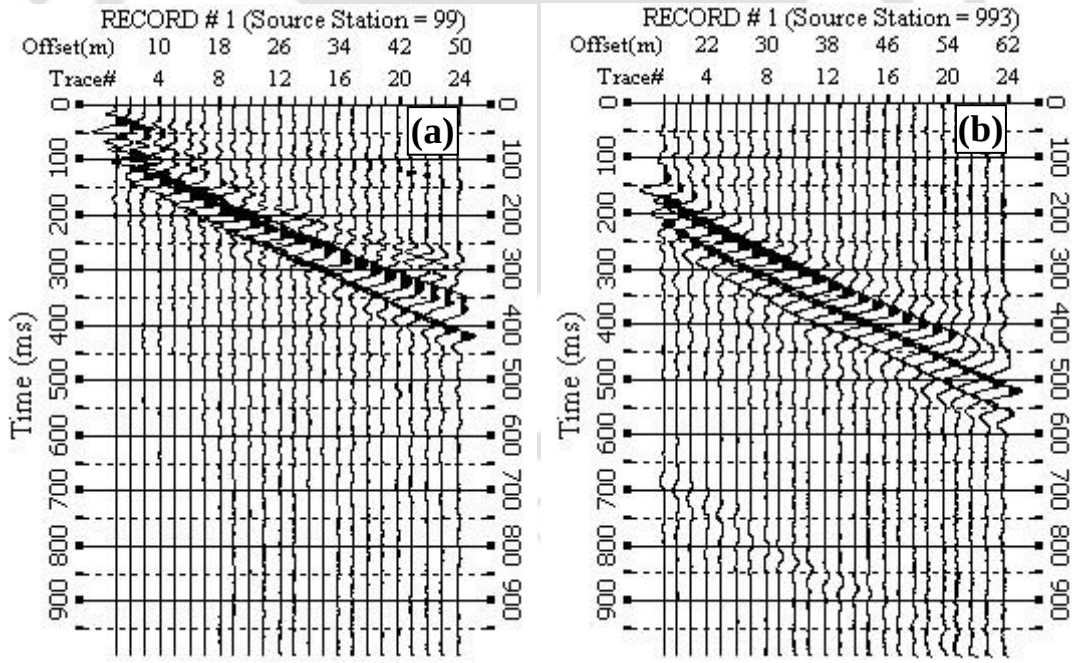

Fig. 5.2 Raw wavefield records from active survey with source offset at (a) 4 m (b) 16 m

Figure 5.3 shows the frequency–amplitude spectrum of both the records in absolute amplitude and normalized amplitude domain. It represents the energy content of the wave signals received by each receiver shown by different coloured lines. Based on the inspection of the frequency spectrum of a record, the optimum scanning frequency range required during dispersion analysis can be identified. In a field record, where surface wave events are significant, the amplitude spectra of the same shows the offset-dependent spectral characteristics of the surface wave events and help in recognizing the optimum spectrum during dispersion analysis. The optimum frequency range can be identified as the portion in the frequency spectrum where majority of the receivers show largest amplitude bands.

It can be observed from Fig. 5.3 that the energy content in case of 4 m source offset record is much higher than the 16 m source offset record, attributed to the proximity of the source of impact to the receiver array. Figures 5.3a and 5.3c shows the frequency spectrum of the 4 m source offset record in absolute and normalized amplitude domain, respectively. The frequency band in both the images span over a wide frequency range from 5-100 Hz, with high amplitudes shown by each of the traces. For the 16 m source offset record (Figs. 5.3b and 5.3d), the most dominating frequency band is found to be in the frequency range of 5-50 Hz. Overall, the optimum analysable frequency band is observed in the range of 5-50 Hz for both the records. The peak amplitudes for the two records are found to be approximately 9830 mVs and 4914 mVs for the cases of 4 m and 16 m offset locations, respectively. The higher range frequency band of the image (> 70 Hz) is observed to be mostly clean and silent, implying that no major contamination from high frequency noise sources have occurred. The dispersion images from the two field records are shown in Fig. 5.4. Attributed to the rich surface wave data in both the records, the dispersion images obtained are

superior in resolution. However, in the dispersion image from 4 m source offset (Fig. 5.4a), some irregularities in the energy band is observed in the lower frequency band below 10 Hz, attributed to the near field effect. Based on the qualitative characteristics of the dispersion trends (as shown in Fig. 5.4), it can be stated that beyond 10 Hz frequency, the dispersion images (obtained from 4 m and 16 m source offsets) are equally suitable for a proper dispersion curve extraction, as they show a clear, thinner and continuous energy band on the dispersion image. Further, thinner dispersion bands aids in the extraction of dispersion curve with more certainty, which, for this case, can be achieved for frequencies above 10 Hz. Earlier literatures have revealed the importance of clarity of dispersion band and subsequent ease of extraction of dispersion curve with high SNR (Park *et al*., 1998a; Uma Maheswari *et al*., 2010; Taipodia *et al*., 2017). However, it is to be noted that the 10 Hz frequency, as mentioned here, is not chosen or suggested as a universal cut-off frequency, as dispersion images generated from different other test conditions might lead the user to choose a different cut-off according to the best possible judgment.

5.2.2 Critical Analysis of Raw Field Records from Zero Traffic and Single Lightweight Vehicle Scenarios

In this section, the influence of the presence and absence of vehicular movement on the recording of wavefield data is presented. Figure 5.5 shows the schematic of the passive roadside survey at the site, conducted with a 46 m linear array comprising 24 numbers of receivers and placed at 5 m offline distance.

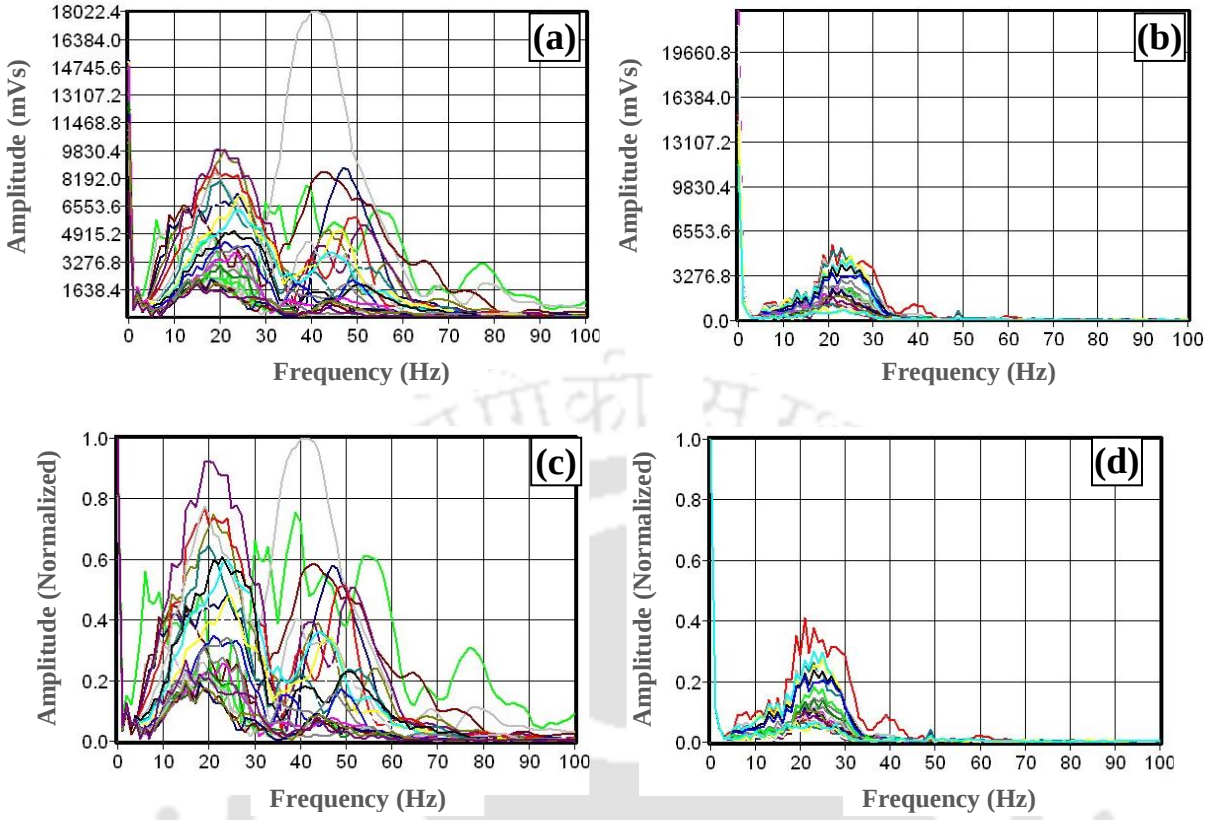

Fig. 5.3 Frequency spectrum of active field records in absolute amplitude domain at (a) 4 m source offset (b) 16 m source offset, and in normalized amplitude domain (c) 4 m source offset (d) 16 m source offset

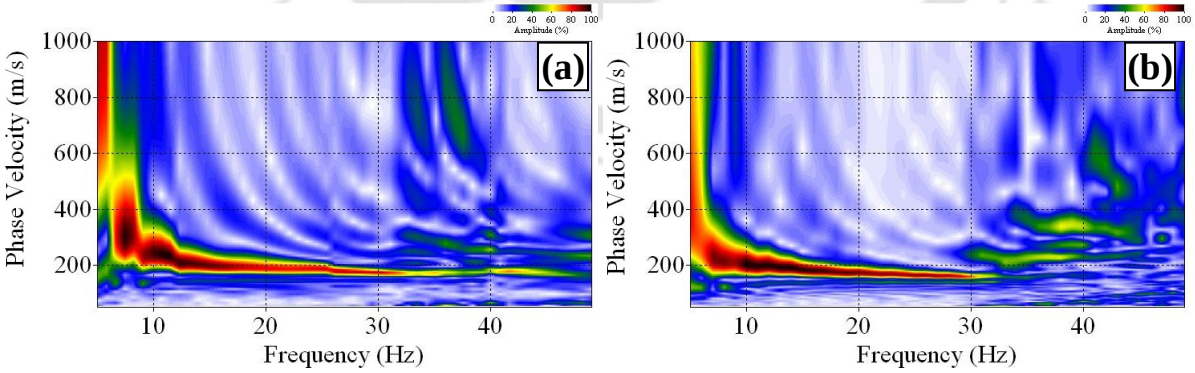

Fig. 5.4 Dispersion images from active field records with source offset at (a) 4 m (b) 16 m

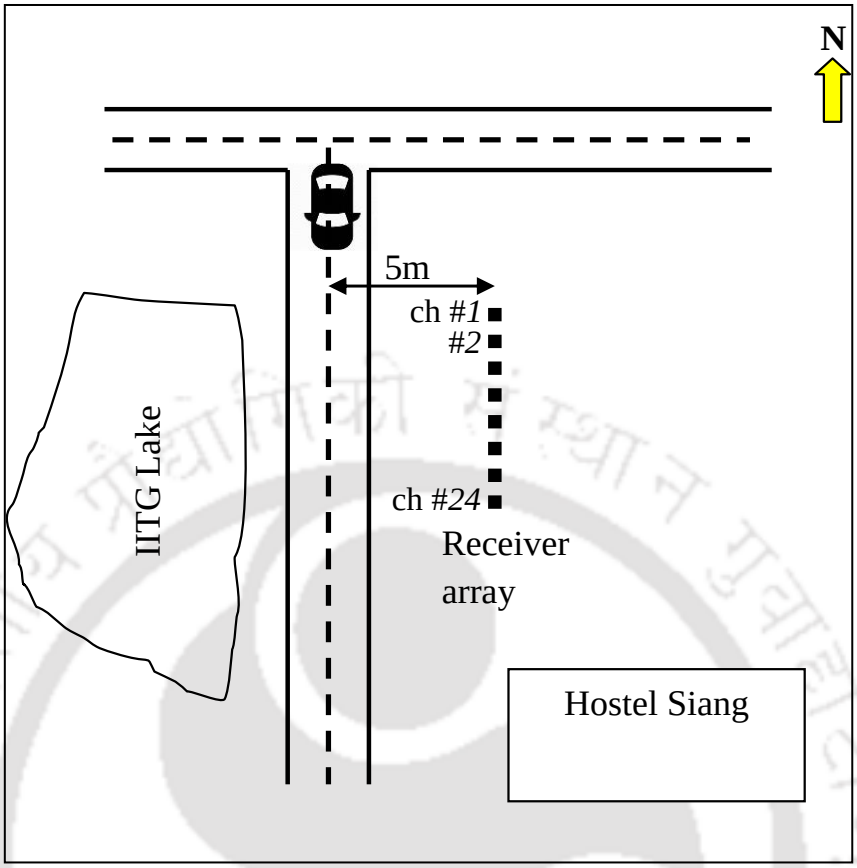

Fig. 5.5 Schematic of the Passive roadside MASW survey without prominent source at Site 1

The first raw field record, shown in Fig. 5.6a, was collected cautiously when there was no vehicular movement on any of the nearby roads. The test was done to check the existence of any ambient noises other than the traffic, which may be recorded in any normal roadside recording. It is observed from the enlarged view of the field record, in Fig. 5.6c, that even with the most silent traffic environment, some microtremors are recorded. The same is manifested in the form of the meagre energy accumulation in the lower frequency band (< 12 Hz) of the dispersion image, as shown in Fig. 5.8a.

In Fig. 5.6b, a typical raw field record is shown that was collected when one lightweight four-wheeler vehicle, weighing around 1000 kg, passed along the receiver array at a speed of approximately 40 kmph. The identical receiver configuration, as used for the zero-traffic scenario, was maintained. Fig. 5.6d represents an enlarged view of the record, extracted between 3000-5000 ms, where it can be observed that all the created wavefields are of nearly identical magnitudes, and no noticeable strong surface event occurred during the recording, which is attributed to the absence of any prominent source on the road surface near the surveyed area. These wavefields are created during movement of the vehicle on the visually unrecognizable tiny surface sources, close to each of the receivers in the array, which created a packet of intra-line sources (details of intra-line sources are presented later in Chapter 9). From the absolute and normalized frequency spectrum of the two records (Fig. 5.7), the very weak signals in case of the first record (zero traffic condition) and comparatively recognizable signals of the second record (single vehicular passage without any prominent source) can be observed in terms of their energy amplitudes. Peak amplitudes of the wavefields in the two records are 0 (approximately) and 2184 mVs ($1/3^{rd}$ of 6553.6 mVs), respectively. Dispersion image in the case of the second record (single vehicular traffic) shows a marginal improvement in the lower frequency band, attributed to the comparatively stronger wavefield from the vehicular movement (Fig. 5.8).

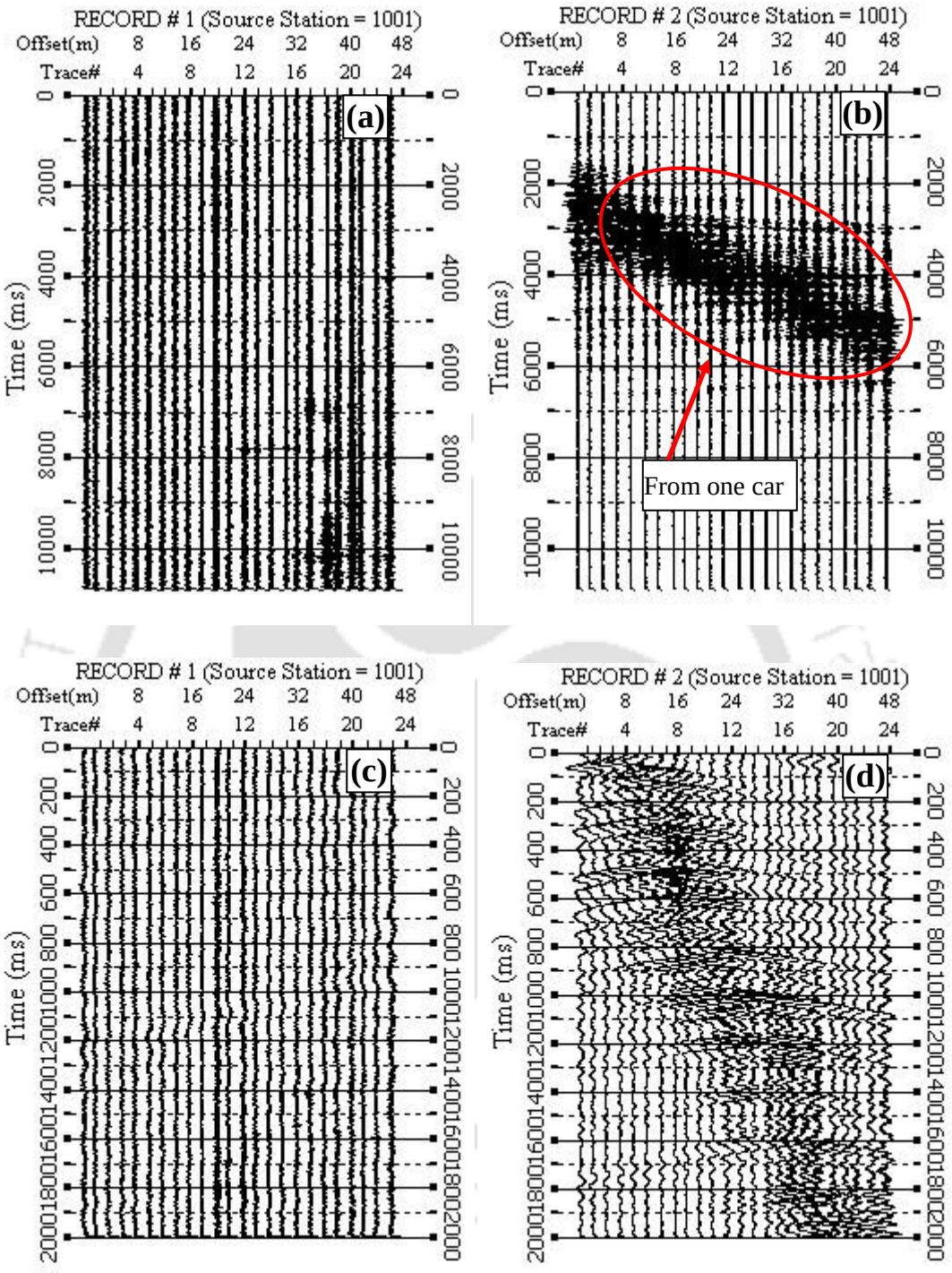

Fig. 5.6 Raw field record (a) during no vehicular movement **(**b) with the passage of one vehicle (c) enlarged portion of record 'a' between 0-2000 ms (d) enlarged portion of record 'b' between 3000-5000 ms

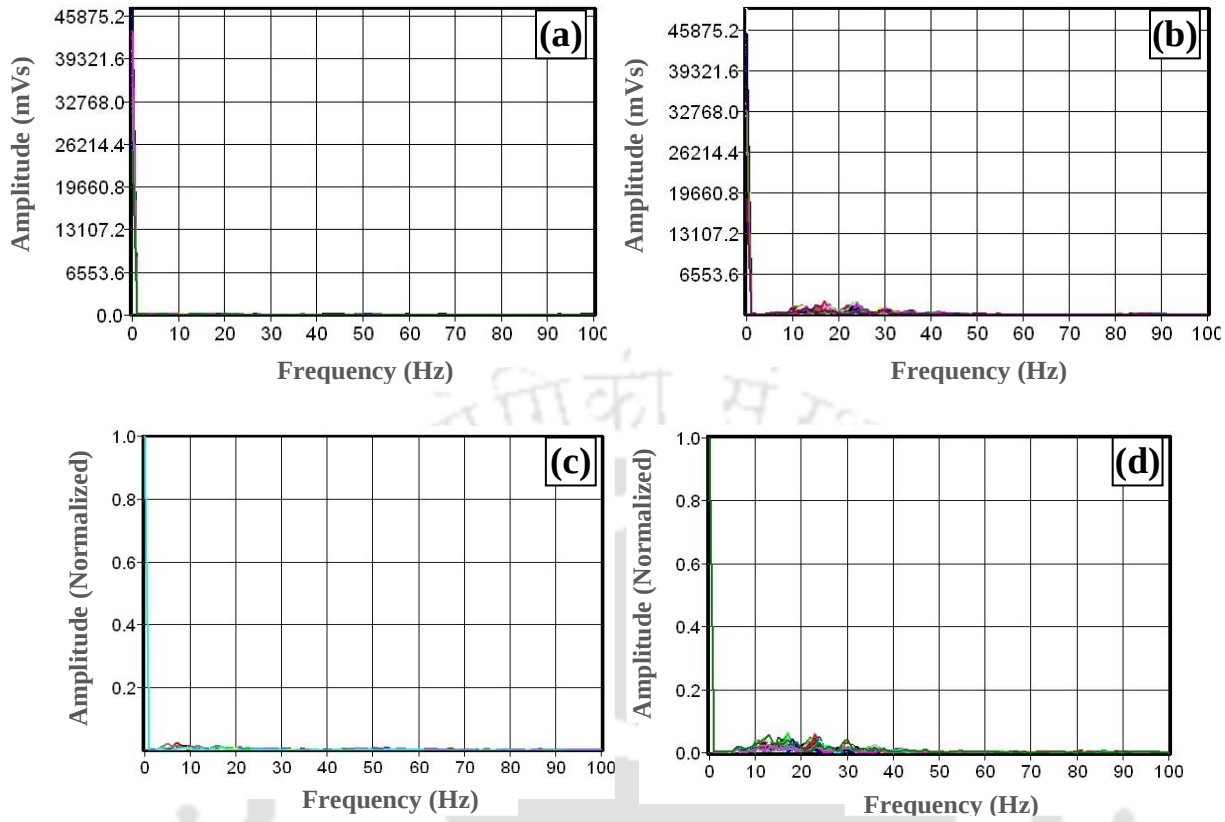

Fig. 5.7 Frequency spectrum of field record in absolute amplitude domain (a) with no vehicular movement (b) with one vehicle passing on the road, and in normalized amplitude domain (c) with no vehicular movement (d) with one vehicle passing on the road

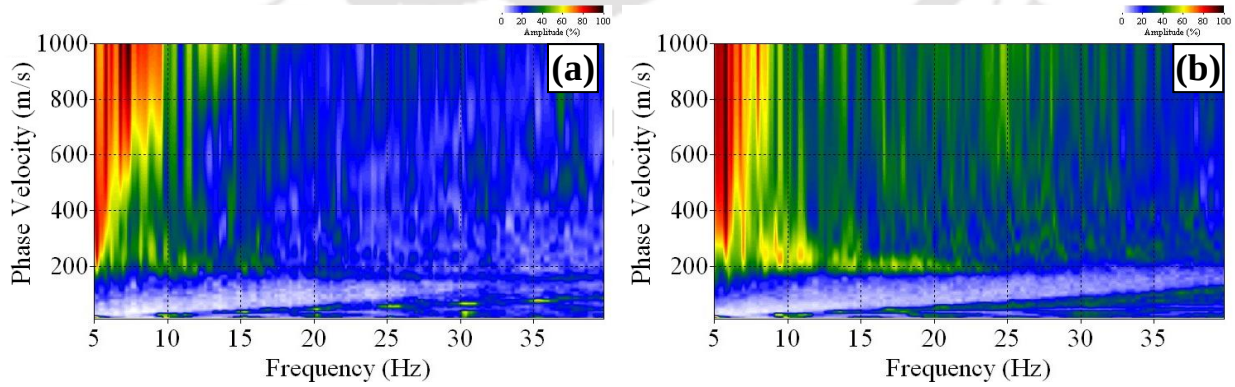

Fig. 5.8 Dipsersion images corresponding to the wavefield signature collected during (a) no vehicular movment (b) single vehicular traffic but without prominent source

5.2.3 Critical Assessment of Raw Field Records from Single Heavyweight Vehicle

Figure 5.9 shows two field records collected from the motion of a single heavyweight vehicle, having mass more than 10000 kg, and passing along the receiver array. The experiments were conducted with the same geometrical configuration, i.e., 46 m array length with 24 numbers of geophone laid at 5 m offline distance. As shown in Fig. 5.9a, the record was collected when a school bus was crossing the receiver array. The enlarged view of the record (Fig. 5.9c) shows similar nature of wavefields as observed, in the previous section, for a lightweight vehicle movement. As already mentioned, there was no major source on the road surface to produce strong surface wave events. However, movement of the heavy bus created wavefields with high energy that can be observed in the frequency spectrum of the record, as shown in Fig. 5.10a and Fig. 5.10c. The peak amplitude in this case reached as high as 19660 mVs, in comparison to mere 2184 mVs in the previous case portraying the passage of lighter vehicle. The dominating frequency band of the record is found out to be in the range of 5-40 Hz.

Figure 5.9b shows a field record acquired during the passage of a heavy road roller through the receiver array. A significant amount of wavefields were recorded, as compared to previous case (passage of a school bus), which is attributed to the severe vibrations caused by the heavy road roller during its movement. The wavefields largely resemble to a set of stationary waves due to very slow movement of the road roller. However, there is absence of relatively stronger wave packets in the record, and all the events are of nearly equal magnitude. In the enlarged view of the record, as shown in Fig. 5.9d, all the wavefields are observed to be very densely spaced and no proper dispersion nature can be spotted in the time domain data, unlike that observed for a typical case of active MASW field record. Several superposition of the wavefields occurred mainly for

the reason of closely situated sources on the road surface (azimuth less than 90° apart), which produces wavefields nearly at the same time.

Figure 5.10b and 5.10d shows the frequency spectrum of the record of road roller in absolute and normalized amplitudes. It can be observed, from the images, that the energy content of the wavefields originated from the motion of road roller is significantly higher than that originated from the motion of the school bus. The peak amplitude recorded for the case of a road roller movement is approximately 39321 mVs, as compared to 19660 mVs recorded upon the passage of the school bus. Further, the frequency spectrum of the record is comparatively much wider in case of the road roller motion, and is observed to be in the range of 5-90 Hz.

Dispersion images for both the records (from bus and road roller) exhibited significant energy accumulation, attributed to the large energy content in the raw data. Compared to the data originated from road roller (Fig. 5.11a), the dispersion image obtained from the field data originated from the moving bus shows (Fig. 5.11b) better resolution, in spite of lesser energy. During the motion of the road roller through the road section, it created a large number of major surface wave events owing to the multiple interactions of the heavy wheels with the pavement surface, leading to a continuous generation of strong signals in extremely close time interval. Therefore, before any individual strong signal could reach the geophone array, it suffered severe contamination due to the successive strong signals overlapping over a very short time-lag. Hence, the resolution of the dispersion image reduced, which is attributed to the closely spaced pseudo-source phenomenon.

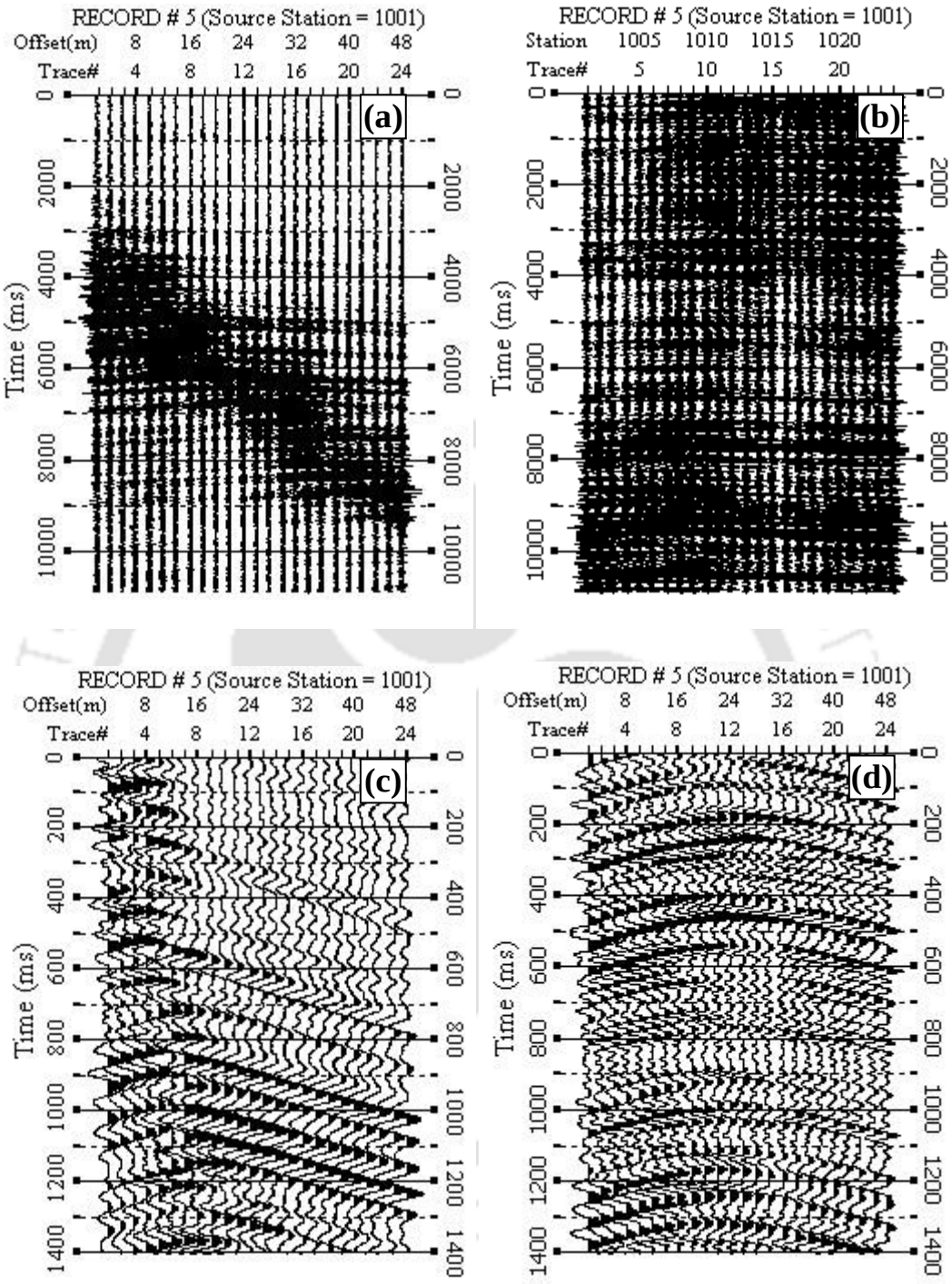

Fig. 5.9 Raw field record (a) acquired during the passage of school bus (b) acquired during the passage of a heavy road roller (c) enlarged view of record 'a' between 3000-4400 ms (d) enlarged view of record 'b' between 0-1400 ms

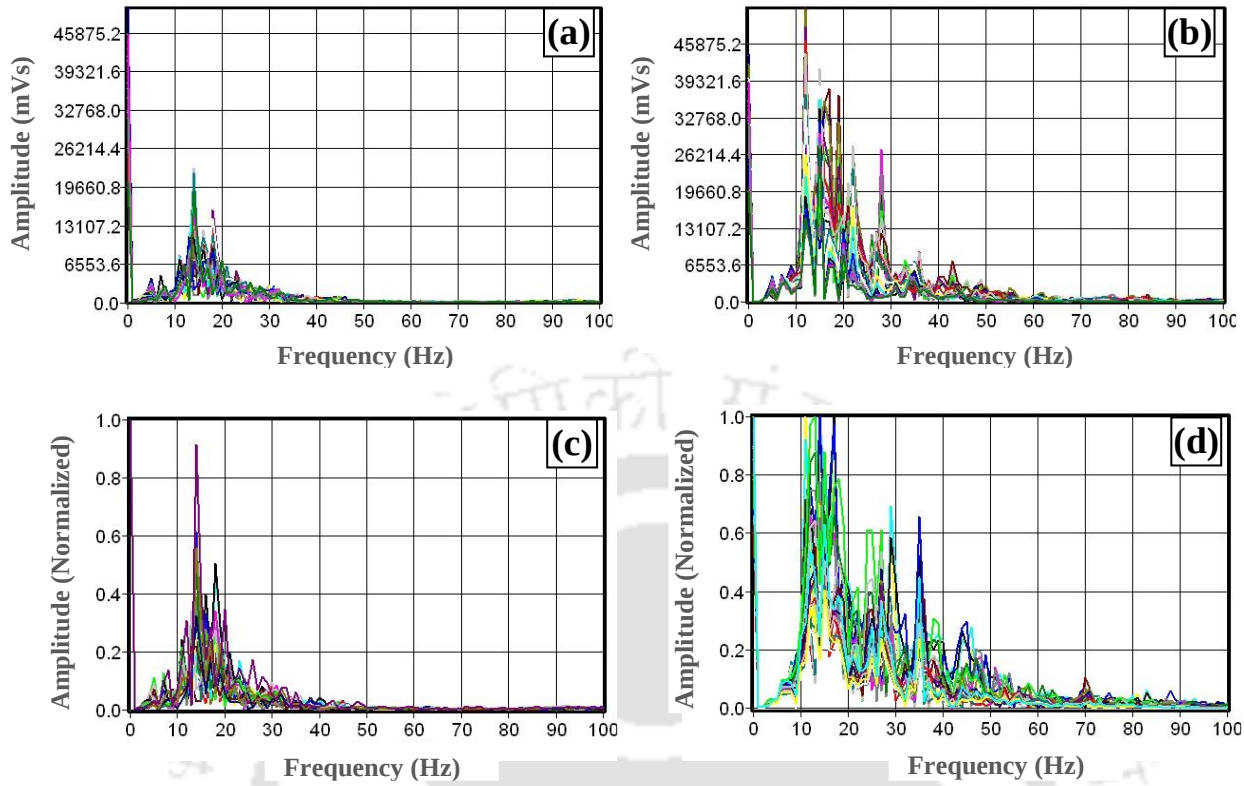

Fig. 5.10 Frequency spectrum in the absolute and normalized scale (a,c) due to the passage of a school bus (b,d) due to the passage of a heavy road roller

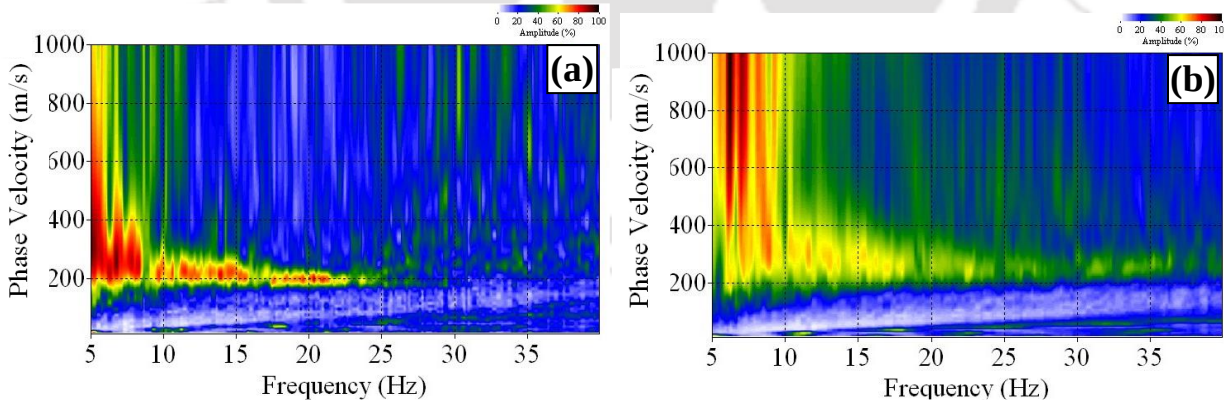

Fig. 5.11 Dispersion images corresponding to the wavefields generated from the passage of (a) School bus as in Fig. 5.8a (b) Road roller as in Fig. 5.8b

5.2.4 Critical Assessment of Raw Field Records from Multiple Vehicle Movements

In most of the practical scenarios, there will be multiple vehicular movements on the road, thereby producing overlapping wavefields with different energy contents and originating from different sources. Therefore, it is important to study the wavefield records generated from the movement of multiple vehicles for better comprehension of their propagation and arrival patterns.

Figure 5.12a shows a raw field record when two cars crossed the receiver array during data acquisition. Both the vehicles were light cars of approximate weight of 1000 kg and moving with velocity of 30-40 kmph. Two packets of wavefields are observed; the first one travelling from left to right of the geophone array in the time frame of 2000-6000 ms, while the second one travelling from right to left of the geophone array in the time frame of 7000-10400 ms, thus manifesting the opposite directional motion of the two cars. Thus, the two wavefields were recorded without being overlapped onto each other. The characteristics of both the wavefields are similar to the one as described in Section 5.2.2 pertaining to the motion of a single vehicle.

On the other hand, in the record shown in Fig. 5.12b, two vehicles coming from opposite directions crossed each other during the recording of the signal. Wavefields from both the vehicles, propagating from either directions into the array, overlapped at 4000 ms with each other, in the time frame of 6000-8000 ms.

From the frequency spectrum of the records, the dominating frequency band in both the records is found to be in between 10-30 Hz (Fig. 5.13). It can be noticed that the peak energy amplitudes, in both the cases, were very low and in the range of 3276 mVs, attributed to the non-existence of

major sources on the road surface. Dispersion images from the two records (Fig. 5.14a and 5.14b) provides no significant information about dispersive behaviour of surface waves; only some minor energy accumulations can be observed in the two images without any regular trends. The influence of the varying overlapping of the wavefields on the difference in the resolution of the two dispersion images could not be well distinguished, although it is evident and expected that the non-overlapping record will certainly contribute better in achieving a better quality dispersion image. Further, on vertically staking 10 numbers of such dispersion images, the final dispersion image is found to be having better resolution with a continuous energy trend than all the individual dispersion images (Fig. 5.14c). This indicates the importance of vertical stacking in obtaining high resolution dispersion image, which will be discussed in sufficient detail in Chapter 7.

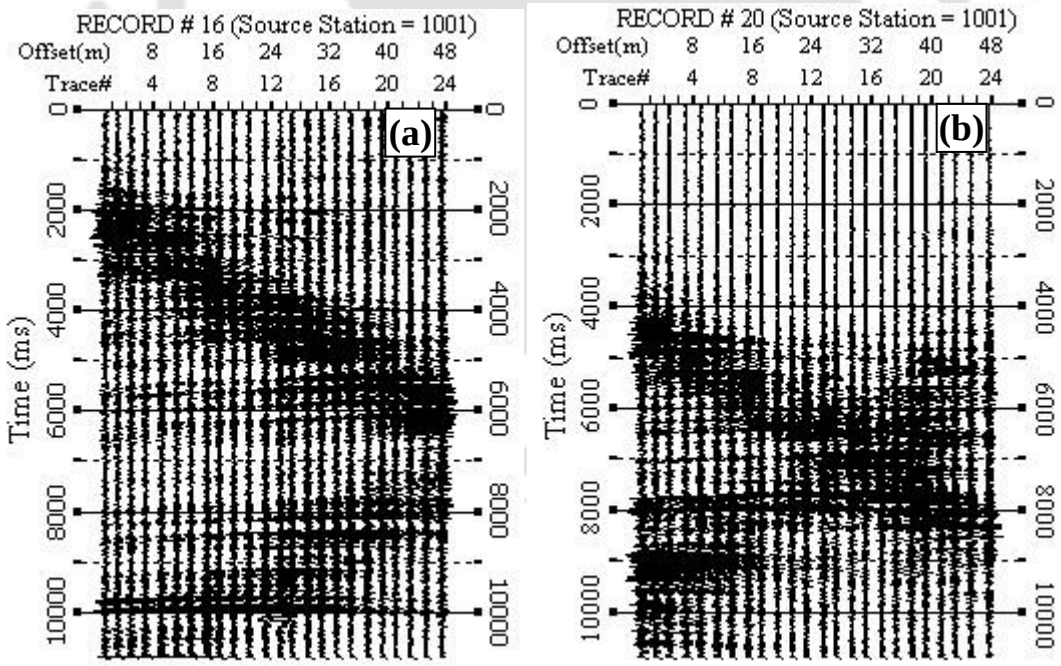

Fig. 5.12 Raw field record during motion of two cars passing along the geophone array and moving in opposite direction (a) without overlapping wavefields (b) with overlapping wavefields

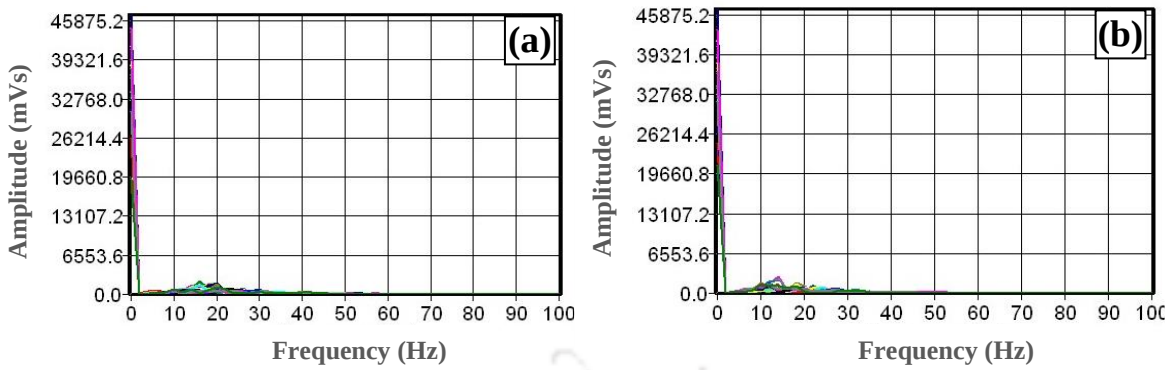

Fig. 5.13 Frequency spectra of the field records due to the motion of two cars passing along the geophone array and moving in opposite direction (a) without overlapping wavefields (b) with overlapping wavefields

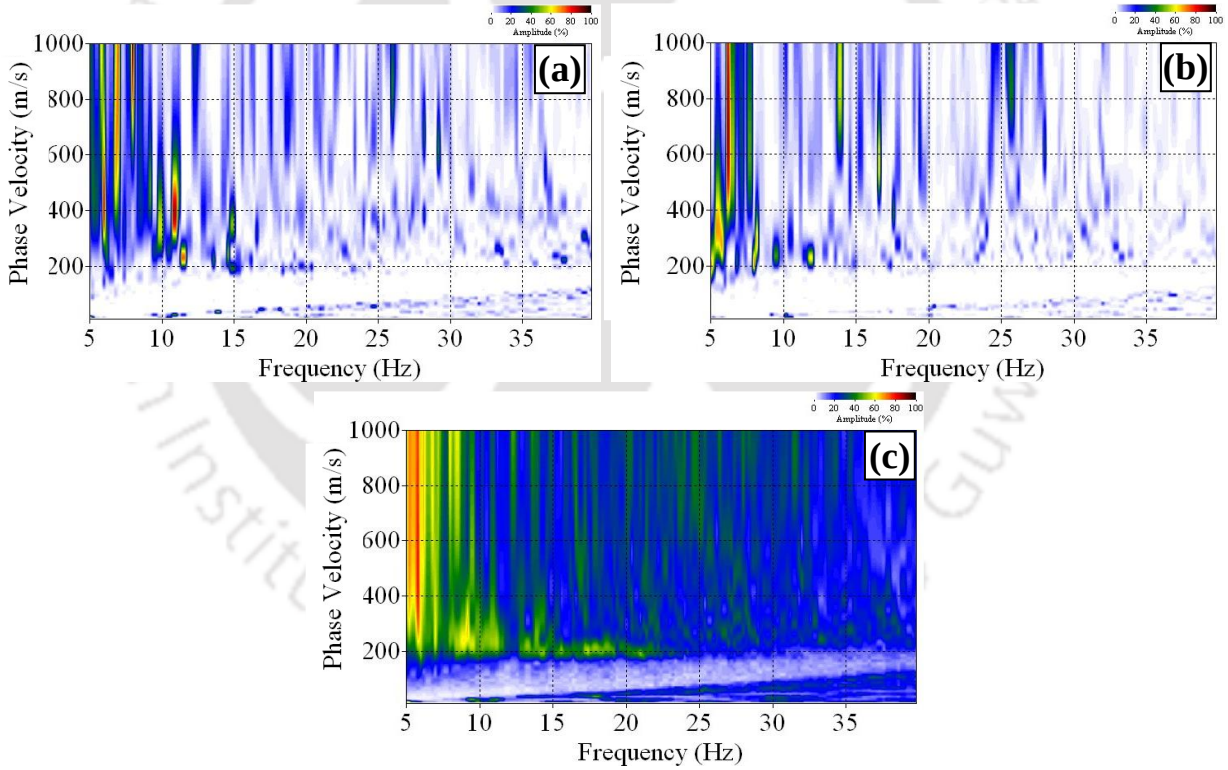

Fig. 5.14 Typical dispersion images as (a) obtained from wavefield record as shown in Fig. 5.12a (b) obtained from wavefield record as shown in Fig. 5.12b (c) obtained by stacking 10 dispersion images generated from raw overlapped wavefield records of lighter vehicles moving simultaneously in opposite directions as shown in Fig. 5.12b

5.2.5 Critical Assessment of Raw Field Records from a Strong Surface Source of Wavefield Generation

In all of the situations described in the previous sections, no prominent strong wavefield sources were present on the road surface, due to which no dominant major surface wave event was produced during the recording of the field data. In this section, the characteristics of field records possessing major surface events, from a prominent strong source on the road, shall be discussed. For this scenario, experiments were conducted at Site 1, in a fully controlled mode, with a known position of a strong source of surface wave generation. During the recording, very limited numbers of vehicles were allowed to pass along the receiver array. As already mentioned in the Chapter 4, the source was a GI rod of approximately 4 m length and 3 cm diameter, placed at a 20 m offset from 1st geophone. The acquisition time for the records was set at 10.4 s, which is sufficient for an incoming vehicle to pass through the placed source. The schematic of the test arrangement is shown in Fig. 5.15.

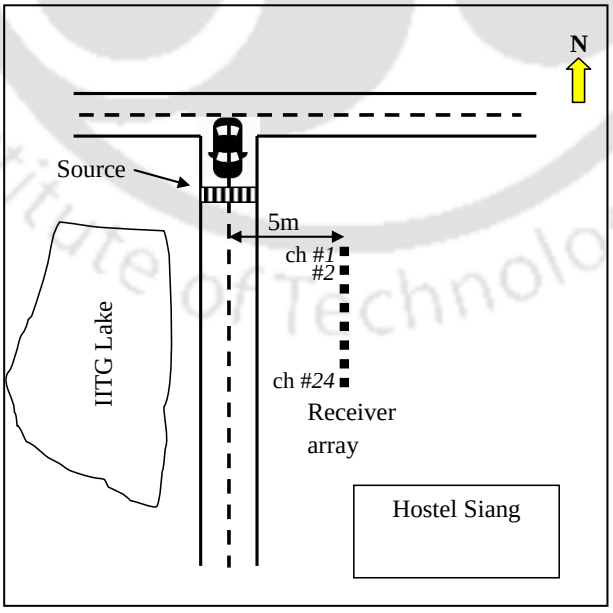

Fig. 5.15 Schematic of the Passive roadside MASW survey with a prominent source at Site 1

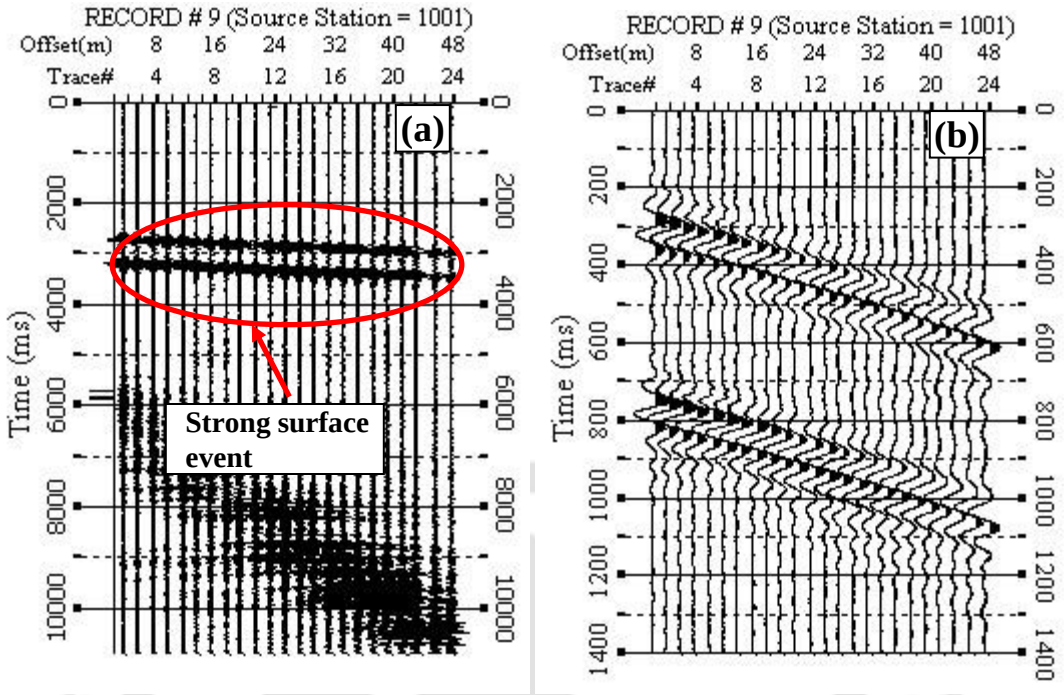

Fig. 5.16 Passive roadside field record under a strong surface event in a controlled environment (a) Full data acquisition time of 10.8 s (b) Enlarged view of the record between 2400-3800 ms

Figure 5.16 shows a field record obtained from the survey with aforementioned field setup. As shown in Fig, 5.16a, in between 2000-4000 ms, two narrowly spaced wavefields with a progressive arrival pattern and a mild gradient can be observed. These two wavefields are created by the front and rear axle wheels of the vehicle, respectively, while passing over the GI rod. The time gap observed between the two wavefields implies the amount of time required for the two set of wheels to pass over the placed source, one after the other. An approximate calculation is shown for the establishment of the above assumption.

From the above time record display, it is observed that:

Average velocity of vehicles passing through the road stretch =25 km/hr or 6.94 m/s.

Time of occurrence of the two wavefields has a time gap= 400 ms (0.4 sec) [Fig. 5.16b]

(The first event occurs at around 2300 ms and the second event occurs at around 2700 ms)

The distance between the wheel base of vehicle passing by the stretch = 2.4 m

So, the time lag between the rear axle to pass the GI rod after front axle = (2.4/6.94)

= 0.35 sec (≈ 0.4 sec)

Hence, this calculation establishes the assumption that the two wavefields are produced by the front and rear axle wheels, respectively, during the passage over the GI rod. This also highlights the fact that in case of passive roadside survey, the road surface irregularities (e.g., road cracks, speed-breakers etc.), forms the major sources of wave generation.

From the absolute and normalized frequency spectrum of the collected records (Figs. 5.17a and 5.17b), the dominant frequency band is found to be 7-60 Hz, with peak amplitude reaching approximately a magnitude of 4369 mVs. The dispersion image from the record (Fig. 5.18) shows an improved energy band, as compared to the dispersion image formed without a strong source scenario (Fig. 5.8b). However, it is observed that even with the presence a strong source of wavefield generation, the resolution of dispersion image is not appreciable, attributed to the field record that is generated by the lesser weight of the vehicle. Hence, it is understandable that either, a very strong impact by heavier vehicles, or, multiple numbers of vertical stacking, are required for obtaining dispersion image with superior resolution.

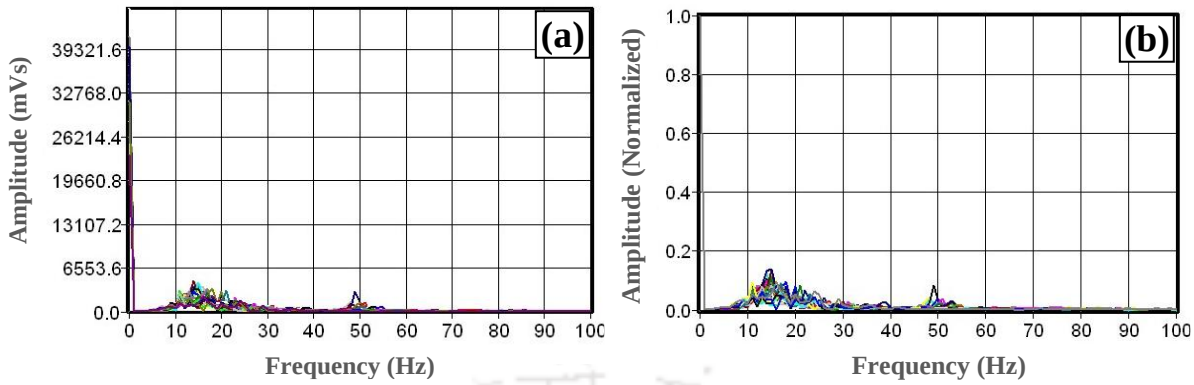

Fig. 5.17 Frequency spectra of the field record with a strong wavefield source during the passage of a single lightweight vehicle (a) Absolute amplitude scale (b) Normalized amplitude scale

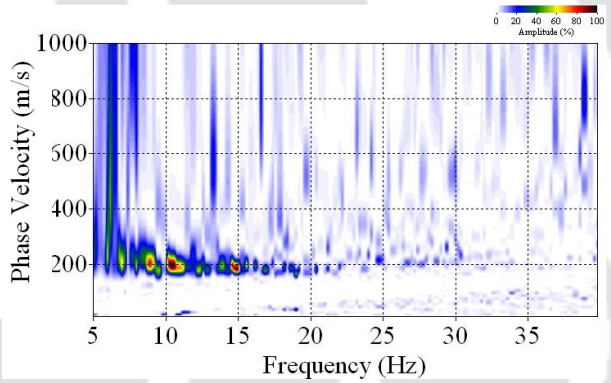

Fig. 5.18 Dispersion image generated from the passage of a lightweight vehicle passing over a strong source of wavefield generation along the geophone receiver

5.2.6 Comparison of Frequency Spectrum of Wavefields from Different Sources

A compartive analysis of frequency and amplitude spectrum of the wavefields originated from different sources, including active and various traffic sources, will be presented in this section. The study will help in selecting the optimum range of frequency band during dipserion analysis of field records produced by different types of sources. Further, it will help in better undertanding of the

strength of various passive sources, upon which the field setup and acquisition paramters (such as array length, acquisition time and others) depend.

Table 5.2 Variation of frequency band and amplitude with source type

Type of MASW Survey	Source type	Source offset (m)	Traffic type	Major Frequency band (Hz)	Largest measurable wavelength (m)	Peak Amplitude
Active	10 kg sledge-hammer	4	NA	5-100	37.6	9830
		16		5-50	31.2	4914
Passive Roadside	No major surface event source	Unknown	No vehicle	3-20	----	~ 0
			A lightweight car	10-40	21.4	2184
			A heavy bus	5-40	32.4	19660
			A road roller	5-90	30.2	39321
	With one major surface event source	20	A lightweight car	7-60	33.1 (46 m array) 51.5 m (69 m array	4369

Table 5.2 shows the range of dominating frequency band from various soures of wavefield generation (active and passive roadside) from the experimentations conducted at Site 1 inside IIT Guwahati campus. When a sledegehammer is used as the active soure, with 4 m source offset from the reciever array, the dominating frequency band is observed to be lying between 5-100 Hz. However, when the source offset is increased to 16 m, the major frequency band reduces to a frequency range of 5-50 Hz. This observation implies the fast attenuating property of high

frequency Rayleigh waves, owing to which the waves with frequencies above 50 Hz are damped out before reaching the reciever array. Further, it may be noted that the peak amplitude recorded for 4 m source offset is almost double than that recorded with 16 m source offset. During recording of passive surface waves wtihout any traffic noise, the miniature vibrations recorded in the frequency band of 3-20 Hz signifies the existence of very little and insignificant ambient and natural vibrations. A peak amplitude almost half of that produced from an active survey, with 16 m source offset, is observed to be generated when a lightweight car, weighing around 1000 kg, passes through the reciever array, with the road surface being devoid of any prominant irregularity; the dominant frequncy bandwidth in this case is found in the range of 10-40 Hz. With the movement of heavier vehicle, such as bus or trucks, weighing around 10000 kg, the peak amplitudes recorded are noticeably higher in comparison to the smaller lightweight vehicles. The records of the heavier vehicles revealed the presence of low frequency components of surface waves. Specifically, it was observed that the slow movement and large vibrations of the road-roller created a wide bandwidth of frequencies from 5-90 Hz. In comparison to the scenario with the absence of any prominent surface source, the presence of a major surface event source on the road stretch, at an approximate source offset 20 m, leads to enhanced frequency and amplitude spectrum of the record. This highlights the importance of a major source point or irregularity on the road surface towards the generation of favourable frequency band of wavefield, which can be succesfully utilized for passive roadside survey. The corresponding largest measurable wavelength from the fundamental mode dispersion curve, obtained from the field records from each of the above field situations, are also included in Table 5.2. It can be clearly observed that with the increase in the weight of the vehicle, the measurable wavelenth of the wavefield also increases. The wavelength of the wavefield generated from the passage of a lighweight vehicle over a

prominent surface source is observed to be comparable to the wavelength generated by a heavier vehicle passing over a road surface without prominent surface source. Further, it is noted that the the largest measurable wavelength increases with increase in the length of the receiver array.

5.3 Study of Wavefield Records from Sources at Site 2 comprising Medium Traffic Volume

In this phase of study, the raw field data recorded from the Site 2, situated near a major district road, from IIT Guwahati campus towards Amingaon, was selected. The various details, along with the pictorial view of the site, is already presented in Chapter 4. The detailed schematic diagram of the same is shown in Fig. 5.19, for better representation of the features at the site. For every sets of experiments, the receiver array was placed at an offline distance of 3.5 m from the centre of the road. Vehicles such as two wheeler bikes, three wheeler tempos, private cars, mini truck and buses, constituted the traffic volume of the road. However, to record the highest possible energy from the sources, recordings were carried out by cautiously and intentionally avoiding the passage of small vehicles (including bikes and tempos), while taking into account the wavefields generated by the heavier vehicles.

Two examples of typical raw field records collected from the site are shown in Fig. 5.20. The records shown were obtained using a 46 m receiver array over an acquisition time of 2.8 s. While registering the first record (Fig. 5.20a), more than two vehicles crossed the receiver array, which is manifested by the two major wavefield regions. However, no major surface event was created by the vehicles during the recording. On the other hand, in the second record (Fig. 5.20b), one major surface event was recorded in the early part of the recording time in between 0-

400 ms, marked by the red oval shape in the figure. Attributed to of the medium traffic flow on the road, it became possible to obtain records of marginal contamination, avoiding substantial overlap and superposition of wavefields.

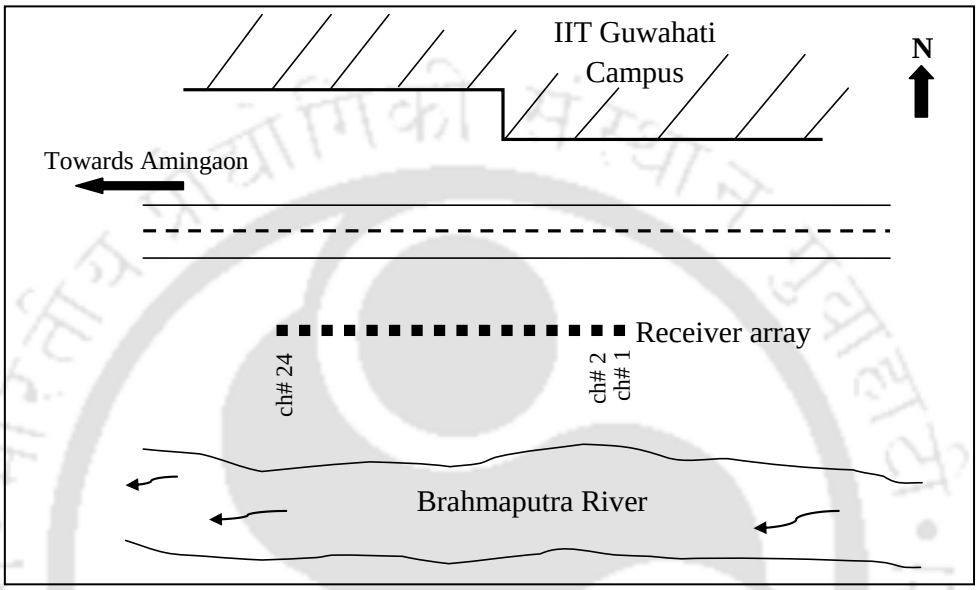

Fig. 5.19 Schematic view of the passive roadside MASW experimentation conducted at Site 2

Figure 5.21 shows frequency spectrum of the two records in absolute and normalized amplitude scales. The first record covers a wide frequency band in the range from 10-80 Hz. In the second record, the frequency range further widens and covers almost from 7-100 Hz. The peak amplitude in the second record is almost double than the first record, owing to the presence of the strong surface wave event, as mentioned earlier. Thus, the strongest wavefield recorded is in between 10-20 Hz for the second record. Dispersion images for these field records, with different ranges of varying parameters, are presented in Fig. 5.22. The energy band, in the dispersion images, from the two records (Fig. 5.20a and 5.20b) lacks continuity and resolution, which inhibits the accurate extraction of a dispersion curve. However, the dispersion image obtained from stacking 10

numbers of dispersion images is of much better resolution as compared to individual dispersion images. Further details related to these dispersion images will be dealt in Chapter 6.

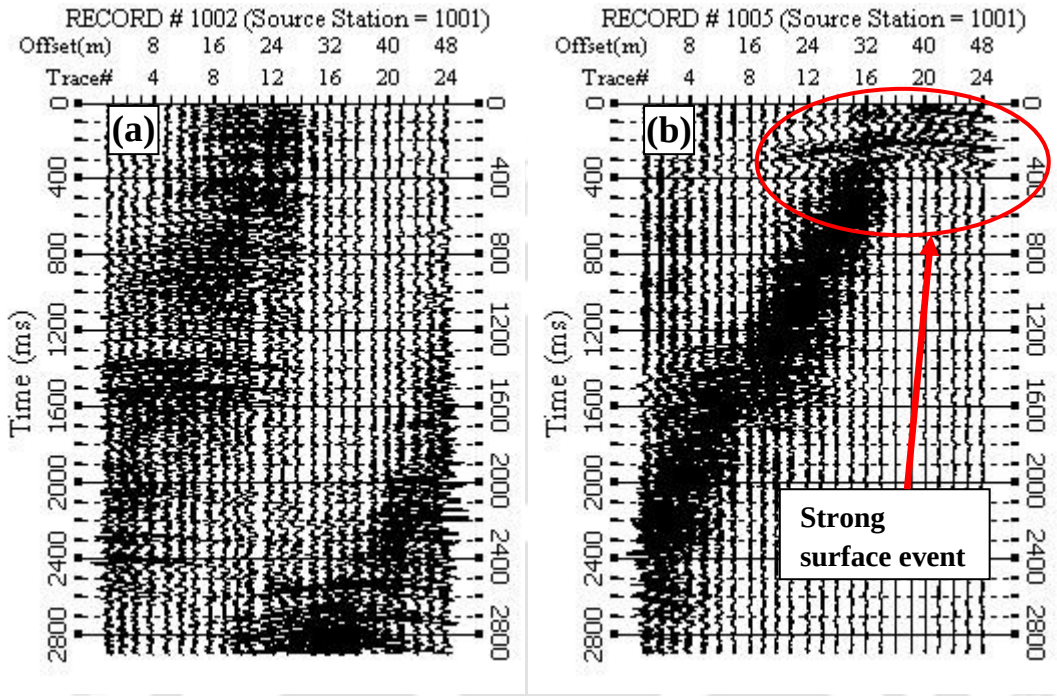

Fig. 5.20 Wavefield record obtained from Site 2 (a) with no significant surface event (b) with some noticeable surface event at the beginning of the record

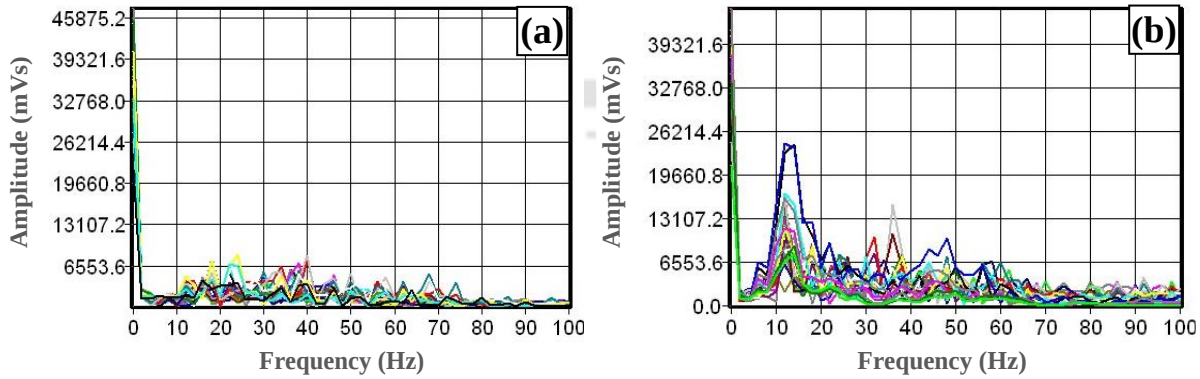

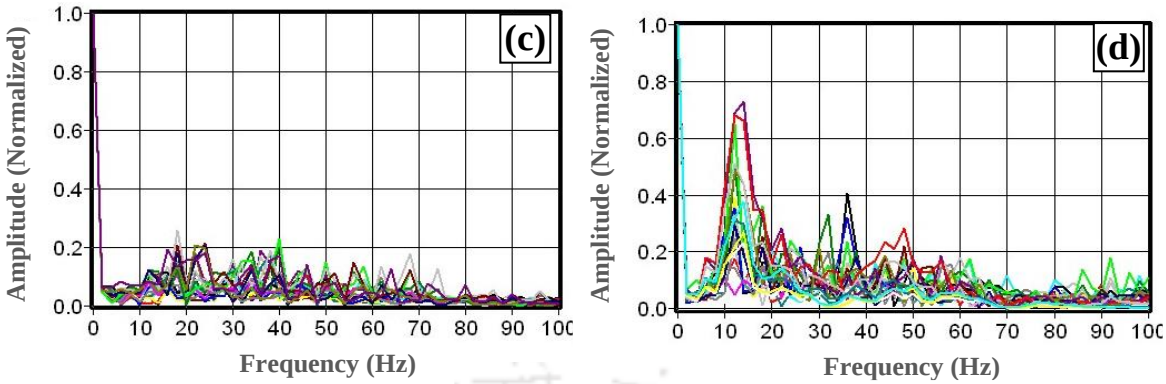

Fig. 5.21 Frequency spectrum of field record in absolute and normzlied amplitude domain (a,c) for the record with no significant surface event (b,d) for the record with some significant surface event

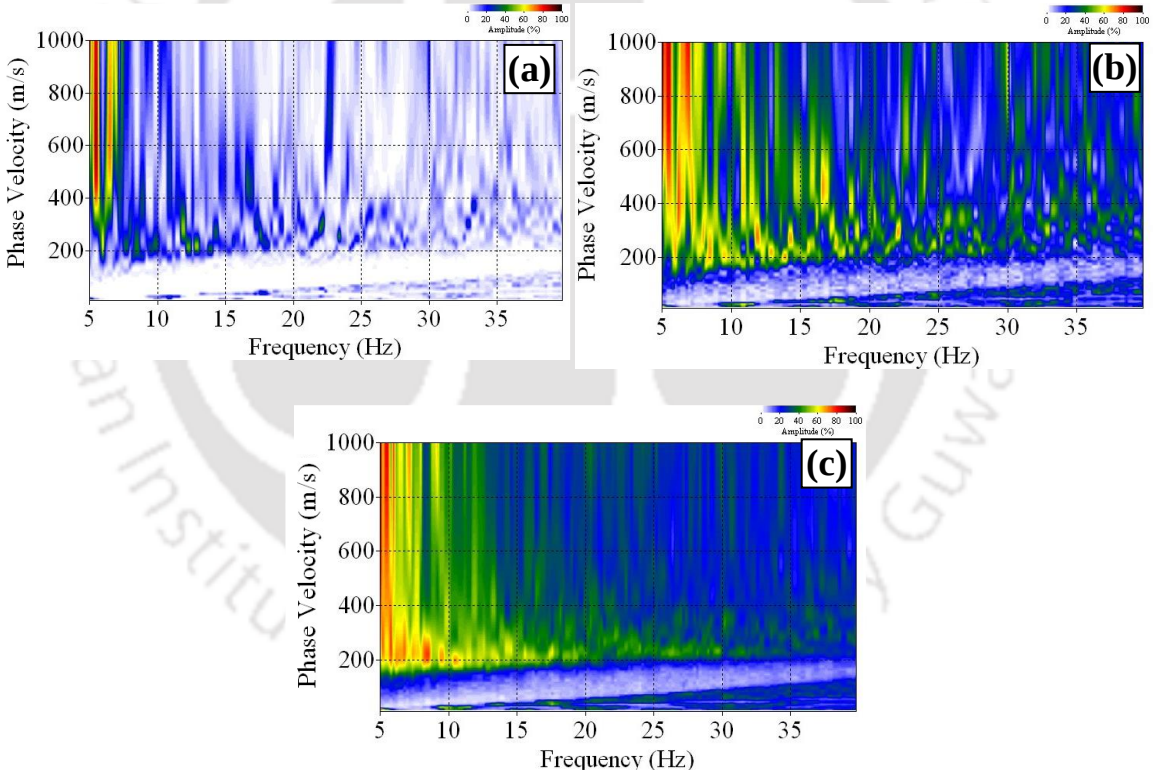

Fig. 5.22 Typical dispersion images as (a) obtained from wavefield record as shown in Fig. 5.20a (b) obtained from wavefield record as shown in Fig. 5.20b (c) obtained by stacking 10 dispersion images generated from the raw overlapped wavefield records of lighter vehicles moving simultaneously in opposite directions as shown in Fig. 5.20b

5.4 Study of Wavefield Records from Sources at Site 3 comprising Heavy Traffic Volume

In order to further examine the usability of passive roadside survey in diverse practical scenarios, a set of experiments were conducted at Site 3, i.e., at the site nearby NH-31, supporting a heavy traffic volume comprising of multitude of vehicles of different weights, speeds and tractions. In the reconnaissance survey of the site, it was observed that the road-surface is fairly plane, and does not have any distinct irregularity on it to serve as source of strong wavefield generation. However, it was expected that the tractive effort of vehicles, application of brakes, and induced mechanical vibration of vehicles should produce wavefields of favourable characteristics for Passive Roadside MASW survey. The site has a fairly unobstructed space beside the road for laying the receiver array and there is no public or commercial institution at the site, thus aiding an uninterrupted experiment. It is a four-lane highway, with each lane of 7 m width. The roadway consists of a divider, or median, of 2.5 m width, between the two lanes. Further, it is to be noted that there is a railway track at around 25 m from the roadway. As the movement of heavyweight trains can also severely affect the raw data, so the data were recorded during the times when no train was passing by. The schematic diagram showing various details of the site is shown in Fig. 5.23.

Figure 5.24 shows two field records obtained from the site, using a 46 m receiver array with 1.4 s recording time. In Fig. 5.24a, the record can be seen with fairly progressive wavefield phases, having many events reaching to the farthest of the receivers in the array. In Fig. 5.24b, however, it can be noted that there are many events that occurred at nearly same time, and thus got overlapped and superimposed, thereby contaminating each other. It can be observed that waves arrived from both the directions of the array and resulted in overlapped contamination,

approximately at the central channels of the array. Therefore, at such a site beside a road supporting heavy traffic volume, to avoid such wavefield superposition, it will be suitable, and is advisable, to restrict the recording of data for very limited time (e.g., 1-2 s). Based on the frequency spectrum of the record, as shown in Fig. 5.25, the dominating frequency band of the record is found to be in the range of 10-30 Hz. The peak amplitude of the recorded wavefield is very high, attributed to the movement of heavy vehicles with very high speed (approximately thrice than that observed at Site 2, as reported in the previous section). The dispersion images from the two records shows similar characteristics as observed in Site 2 (Fig. 5.26). Both the images shows irregular energy trend, despite comprising high energy content, and thus manifest deficiency in several frequency contents. Again, with vertical stacking of 20 numbers of dispersion images, the resolution was significantly improved, highlighting a continuous energy trend (Fig. 5.26c). Further details regarding the same will be provided in Chapter 6.

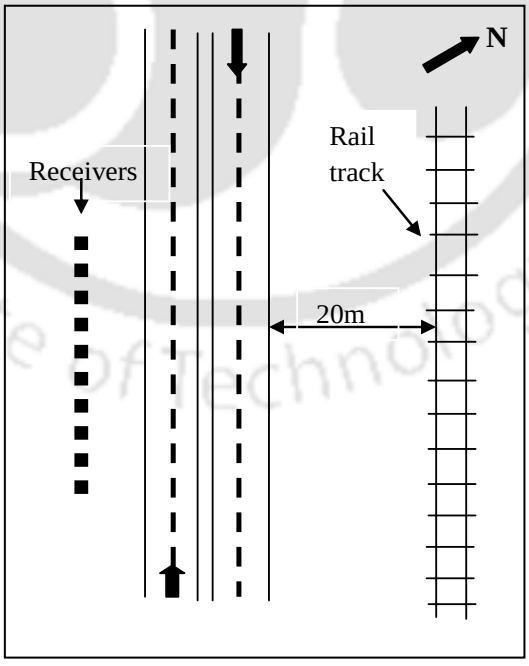

Fig. 5.23 Schematic view of the passive roadside MASW experimentation conducted at Site 3

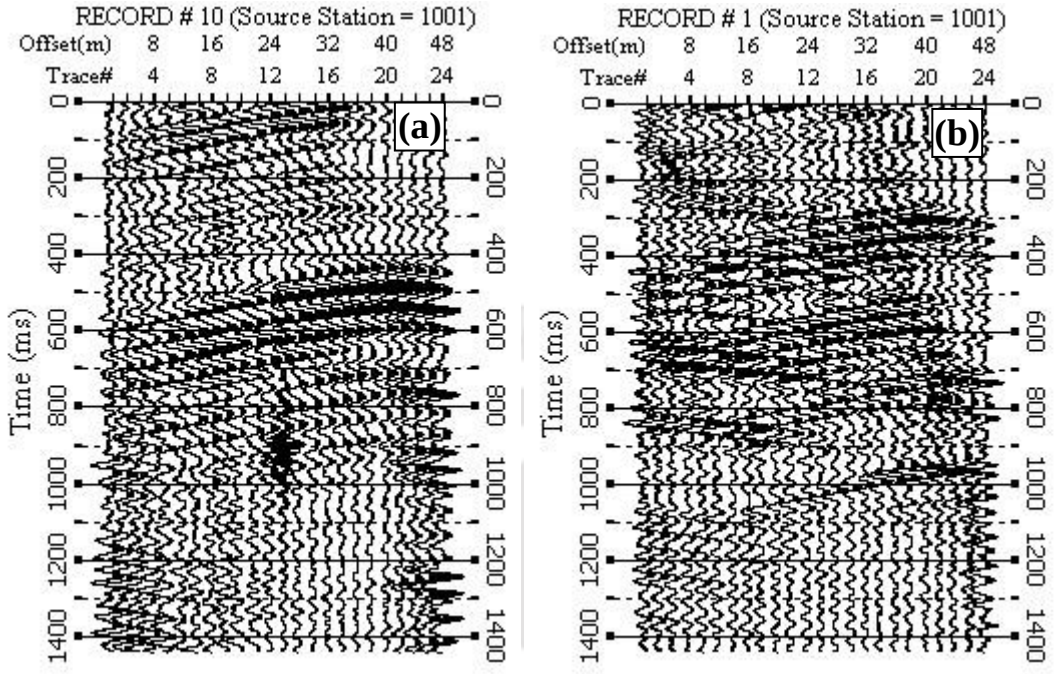

Fig. 5.24 Wavefield record obtained from Site 3 (a) fairly progressive phase propagation (b) severely contaminated phases due to simultaneous arrival of waves from different directions

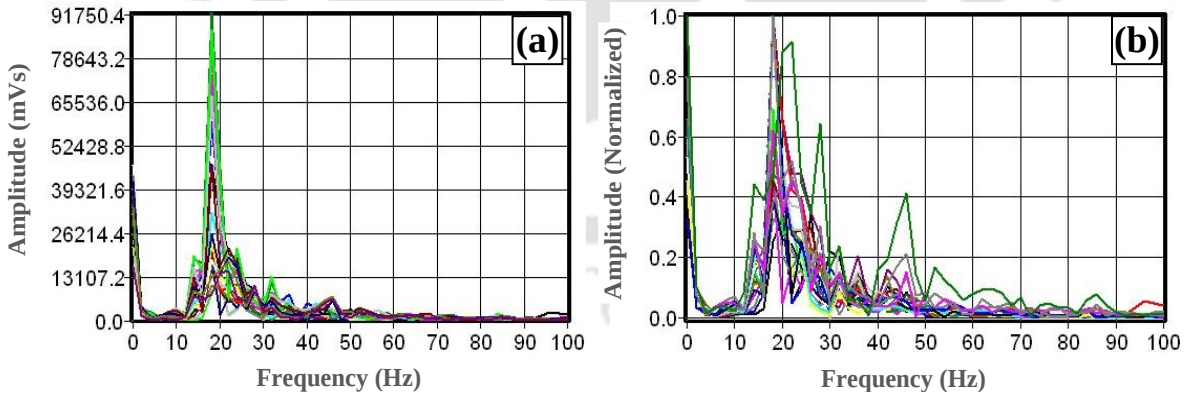

Fig. 5.25 Frequency spectrum of the wavefield record shown in Fig. 5.24a in (a) absolute amplitude scale (b) normalized amplitude scale

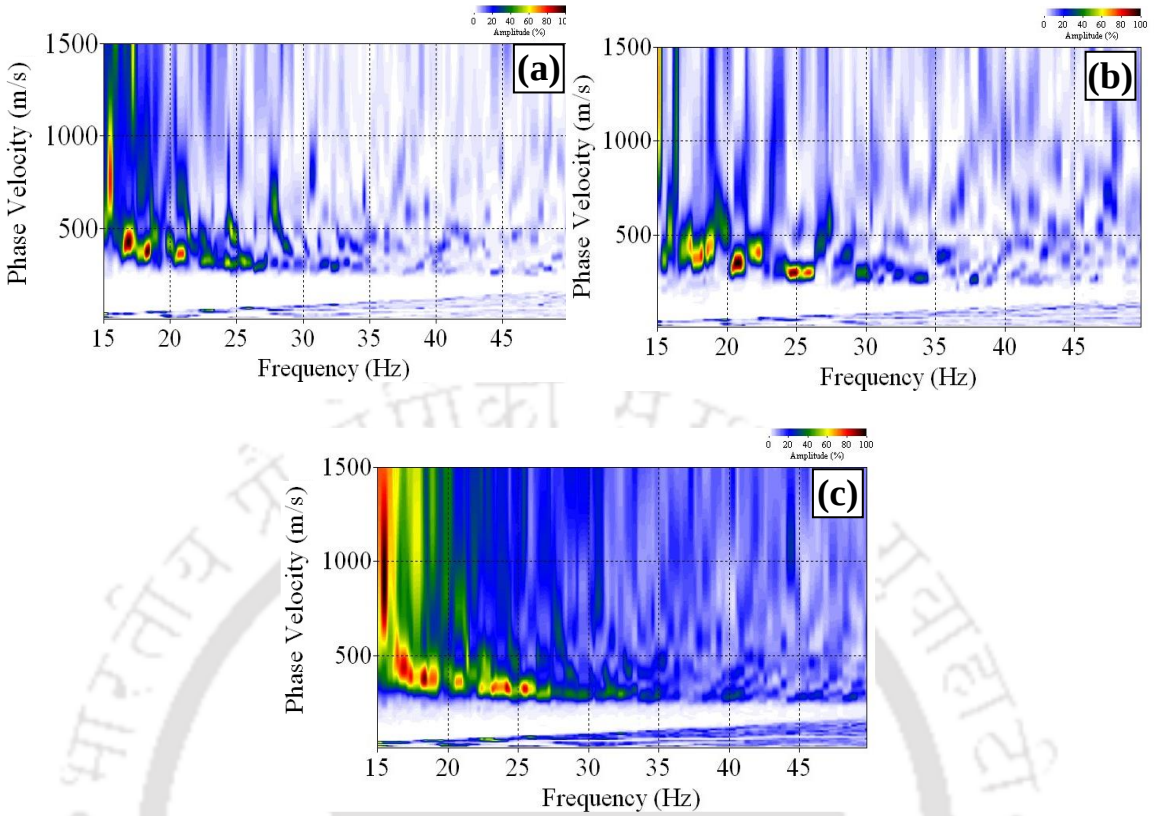

Fig. 5.26 Typical dispersion images as (a) obtained from wavefield record as shown in Fig. 5.24a (b) obtained from wavefield record as shown in Fig. 5.24b (c) obtained by stacking 20 dispersion images generated from raw wavefield records of multiple vehicles moving simultaneously

5.5 Summary

Unlike an active MASW survey, the quality of raw field records in a passive MASW survey is not really controllable by the investigator. However, a detailed study of the site characteristics, available source locations, volume of traffic and a-priori field studies (borehole surveys or active MASW surveys) may help in collecting optimum passive roadside field records, suitable for generating dispersion image with higher resolution. It is observed that even without the presence of major surface sources on the road, traction of heavyweight vehicles, such as a bus, produces significant energy, much greater than that generated by conventionally used drop hammers in

active survey. Surface wave events created by such heavyweight vehicles may be sufficient to produce dispersion image with high resolution. However, surface wave events created by smaller lightweight vehicles, such as a car, were found to be insufficient to produce a continuous energy band in dispersion image, irrespective of presence of strong surface source. Hence, through this study, it is recommended to carry out sufficient numbers of vertical stacking (10 to 20 numbers) at sites where the traffic comprises only smaller vehicles. At sites with medium to heavy traffic volume, it was found difficult to record raw field data without wavefield contamination. At such sites, it is necessary to cautiously record field data with smaller recording time, in the range of 1-2 s, to avoid wavefield contamination. Further, vertical stacking at such sites, as well, becomes a primary tool to obtain dispersion image with higher resolution.

CHAPTER 6

INFLUENCE OF DATA ACQUISITION PARAMETERS ON DISPERSION IMAGING IN PASSIVE ROADSIDE SURVEY

6.1 Introduction

In passive MASW survey, data acquisition or recording parameters significantly affect the raw field data and, hence, the subsequent dispersion image processing. In general, the primary acquisition parameters in passive roadside survey conform to the type of seismograph, characteristics of the receivers and its natural frequency, receiver numbers, inter-receiver spacing, length of array, acquisition or recording time and the sampling frequency. Out of these, the first two are primarily manufacturing parameters and beyond the control of user during any field works. However, the remaining are the field geometrical and recording parameters that can be applied in a variety of ways for the optimum recording. In this section, the influences of the two vital geometrical and recording parameters, namely the length of receiver array and the acquisition time, on the resolution of dispersion imaging are presented.

6.2 Influence of the Length of Receiver Array

Generally**,** a longer receiver array is assumed to give better results in terms of resolution of dispersion image and greater investigation depth (Park *et al.*, 2001). However, using a long receiver array for field survey may not be always feasible especially in congested urban areas, attributed to various obstructions making hindrance in its laying. Moreover, it is also highly laborious to lay a longer receiver array repetitively during field survey. Hence, it will be immensely

beneficial if a short receiver array can also possibly be used to retrieve similar and/or desired result as that of long receiver arrays. Therefore, study on the use of shorter receiver array or lesser inter-geophone spacing becomes an important area for research.

In this study, different receiver spacing, i.e., 1 m, 2 m, 3,m and 4 m were tested at the three sites (as mentioned in Chapter 4) with 24 numbers of geophones, thus producing receiver arrays of length 23 m, 46 m, 69 m and 92 m respectively. The primary objective of the study is to determine the influence of the length of receiver array on dispersion image resolution and on the resultant V_s profile. The study will also help in exploring into the possibilities of using shorter array length in congested urban areas where it is difficult to obtain sufficient space for laying longer receiver array.

The dependency of receiver array length on resolution of dispersion images was first studied by Park and Miller (2008) on synthetic records and reported superior result in case of higher array length with greater inter-geophone spacing. In the dispersion imaging process, the most important stage is to select the points on the dispersion image with maximum signal to noise ratio (SNR) which helps in attaining minimum RMS error in the inversion analysis. For this purpose, it is imperative that the modal energy band should be as thin as possible to precisely locate the accurate dispersion curve as the peak of the energy band on the dispersion image. Such a selection ensures minimum error in the phase velocity estimation with respect to the corresponding frequency. In a wider energy band, the uncertainty of the dispersion curve selection increases.

6.2.1 Critical Assessment of the Study Conducted at Site 1 (Light Traffic Volume and Controlled Experimental Condition)

In an effort to critically examine the influence of length of the receiver array (or inter-receiver spacing) on raw data characteristics and on the resolution of dispersion image, an extensive experimentation programme was conducted at Site 1, i.e., the controlled experimentation site inside IIT Guwahati campus. In the experiment, 24 numbers of receivers were placed with different inter-receiver spacing, i.e., 1 m, 2 m, 3 m, yielding an array length of 23 m, 46 m and 69 m, respectively. Experiments with further increase in the array length could not be performed due to the physical limitations of the site. For the particular experiments, all the receiver arrays were laid at an offline distance of 5 m from the centreline of the road. It is to be mentioned here that prior to the placing of the array, the centre of all the arrays was fixed at a particular location so that all the three arrays share one common midpoint for the eventual estimation of the shear wave velocity profile.

Raw field records from different lengths of arrays are presented in Fig. 6.1. All the three records consist of two major surface events, produced from two major sources from the nearest road. As observed in Fig. 6.1a, representing the record for 23 m array, one major event was present in between 2000-3000 ms, and another between 4000-5000 ms. The latter surface event is more distinct and sharper in all the cases, depicting its closeness to the placed receiver array. The portion of the stronger surface event from each of the record was extracted, and is shown in a separate enlarged view beside each raw field record, as in Fig. 6.1b (4000 - 5400 ms of Fig. 6.1a), 6.1d (4600 - 6000 ms of Fig. 6.1 c) and 6.1f (4000 - 5400 ms of Fig. 6.1c). Each such enlarged view of the records is focussed only on the time segment of 1400 ms around the main event, so that the

typical characteristics of each of the records can be critically compared. The enlarged records reveal two important observations. Firstly, one of the wavefield is generated from a source that is situated on the road surface, within the length of the array spread, and will be hereby termed as 'intra-line source'. The presence of intra-line sources can be comprehended from the curved wavefield signatures emanating from an internal geophone and progressing towards both the ends of the array. In this case, the source was at a position near the middle of the receiver array, close to the 8^{th} and the 9^{th} receiver, and thus the wavefield can be found to initiate between these geophones before spreading to the edges (Fig. 6.1b, 6.1d, 6.1f). Further details of such intra-line source and its significance will be discussed elaborately in Chapter 9. Secondly, the wavefield can actually be recognised as comprising a pair of two smaller wavefields generated from front and rear axle wheels, respectively, of the vehicle. However, as can be seen in Fig. 6.1b, the two pairs are very closely spaced and are not adequately separated. With increase in the length of the array and inter-receiver spacing, the separation between the pair of the wavefield increases and can be distinctly observed in Figs. 6.1d and 6.1f. It is, thus, understandable that closely spaced receiver array is not able to receive and record the wavefield in a fully developed form. In contrary, the wavefield was recorded in its completely developed form when a larger inter-receiver spacing was used. Further, with increase in array length, the curvature, or the slope, of the wavefield increases, showing the higher duration of time required for the propagation of the surface wave to the various geophone receivers.

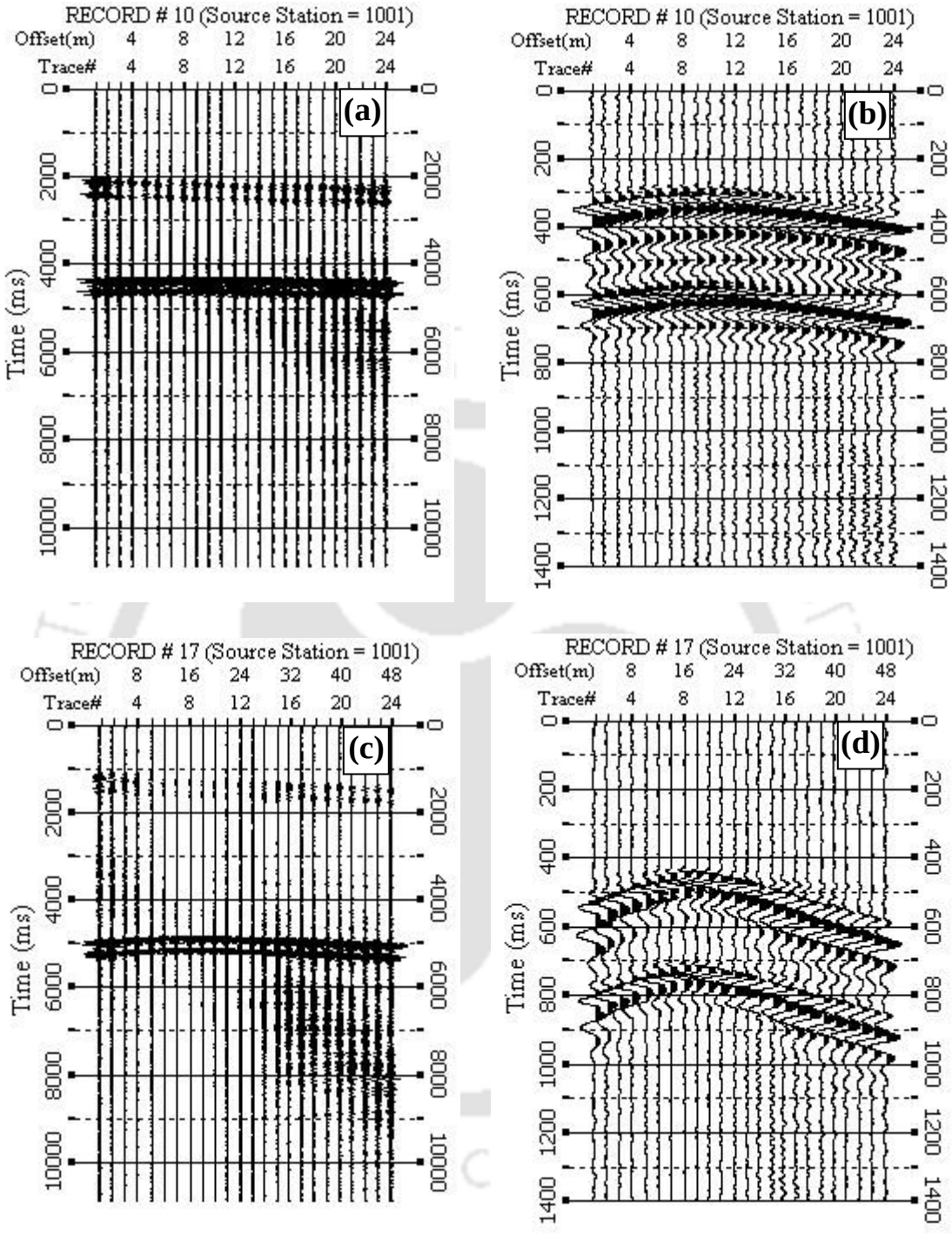

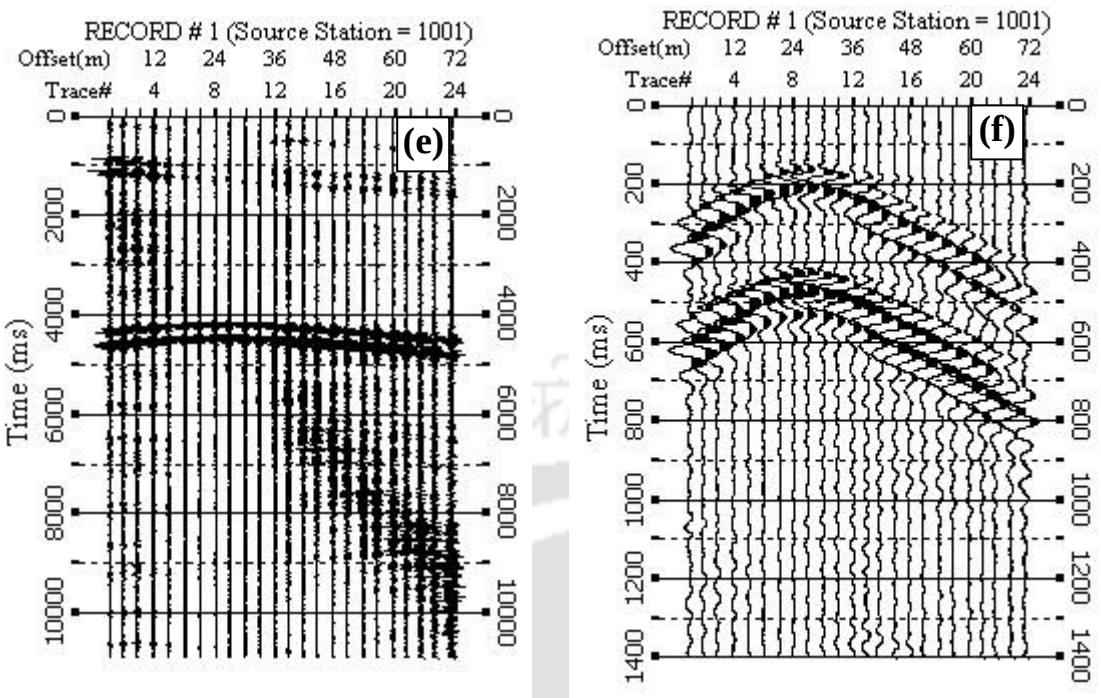

Fig. 6.1 Influence of inter-receiver spacing and 24 geophone receiver array length on wavefield characteristics (a) 23 m array length (b) enlarged portion of major surface event (4000 - 5400 ms) of Fig. 6.1a (c) 46 m array length (d) enlarged portion of major surface event (4600 - 6000 ms) of Fig. 6.1c (e) 69 m array length (d) enlarged portion of major surface event (4000 - 5400 ms) of Fig. 6.1e

Based on the wavefield signatures highlighted in Fig. 6.1, Fig. 6.2 shows the dispersion images obtained from array lengths of 23 m, 46 m and 69 m, respectively. It can be clearly observed that there is significant enhancement in the quality and resolution of dispersion image with the increase in array length. The resolution of dispersion image obtained from the field record of 23 m receiver array (Fig. 6.2a) is significantly poor. This is attributed to the fact that smaller receiver array poorly samples high wavelength or low frequency wavefield, due to which aliasing of the signals appear in lower frequency band. The lowest frequency at which phase velocity can be approximately selected is 15 Hz. With increase in the receiver array lengths, the lower limit of the frequency band

for decipherable phase velocity estimation encompasses further lower magnitudes. With array lengths of 46 m and 69 m, the lowest frequency achieved is approximately 9 Hz and 6 Hz, respectively, which will greatly aid in deeper subsoil investigation (Fig. 6.2b and 6.2c). A typical dispersion curve selection from the dispersion image, resulting from 46 m array, is shown in Fig. 6.2d.

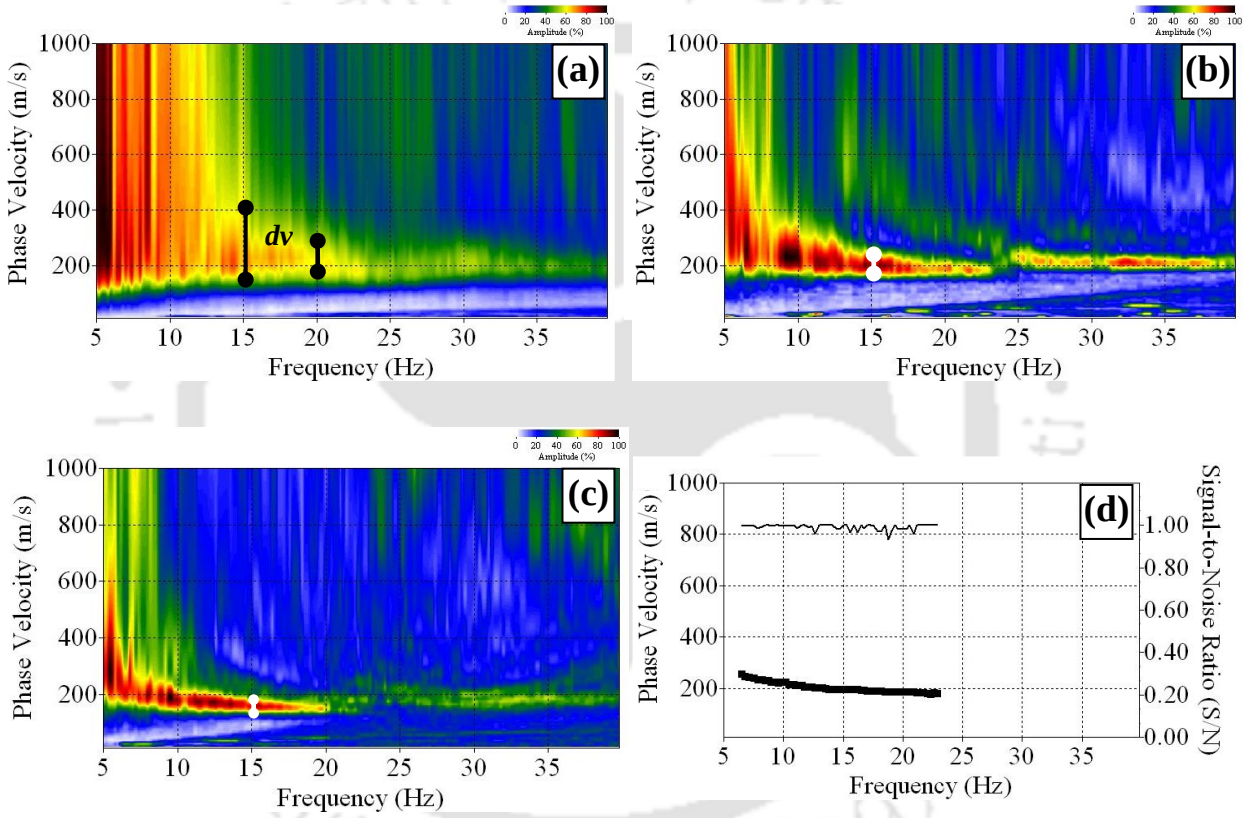

Fig. 6.2 Dispersion images obtained from array lengths of (a) 23 m (b) 46 m (c) 69 m (d) A typical dispersion curve selected from the dispersion image generated by a 46 m array

Evaluation of the resolution of the dispersion images can be done by a method inspired by the theory proposed by Zhang *et al.* (2004). According to this theory, resolution of the dispersion image can be defined as the resolvable capabilities along both the velocity and frequency axes.

Hence, based on the width of the energy band in the dispersion image, resolution of dispersion image can be quantified. On the dispersion image shown in Fig. 6.2a, the width of the energy band along the velocity axis is defined by a term *dv*. In the figure, the value of *dv* at 15 Hz is almost 200 m/s. On the other hand, in Fig. 6.2c, the value of *dv* at exactly the same frequency, i.e., 15 Hz, is mere 25 m/s. It is already mentioned that narrower the energy bandwidth, easier and accurate will be the extraction of the dispersion curve from the dispersion image. Hence, based on the value of *dv*, the resolution and quality of a dispersion image can be defined. For different array lengths, various values of *dv* on dispersion image, at different frequency coordinates, are listed in Table 6.1. It can be observed that the values of *dv* is much greater in low frequency region than in the higher frequency region, indicating greater possibility of errors in the estimation of phase velocity at lower frequencies, i.e., higher wavelengths, which will affect the accuracy of deeper layer information of an inverted V_s profile.

Table 6.1 Values of *dv* at different frequency coordinates for different receiver array length

Array length (m)	Value of *dv* (m/s) at frequency co-ordinate of			Quality of dispersion image
	10 Hz	15 Hz	20 Hz	
23	Unrecognizable	200	80	Poor
46	80	50	30	Fair
69	40	20	10	Good

Shear wave velocity profiles obtained by the inversion of dispersion curves with highest SNR, extracted from dispersion images corresponding to different receiver lengths, are shown in Fig. 6.3. As already indicated earlier, short receiver arrays, such as the 23 m array, yielded poor resolution in lower frequency band of the dispersion image, and as a result, the extraction of

dispersion curve extraction was not precisely possible from this region. This finally resulted in attaining lesser investigation depth compared to V_s profile obtained from the longer array lengths. With increasing length of the receiver array, the depth of investigation significantly increases, attributed only to the effective selection of dispersion curve from dispersion image with enhanced resolution, particularly in the lower frequency bands. With 23 m, 46 m and 69 m receiver arrays, the depths of investigation achieved are approximately 6 m, 15 m and 18 m, respectively. Further, shear wave-velocity profile obtained from active MASW survey employing 69 m array is also included. It can be observed that there is an appreciable agreement with the corresponding profile obtained from the passive survey, thereby indicating the reliability of the adopted passive technique.

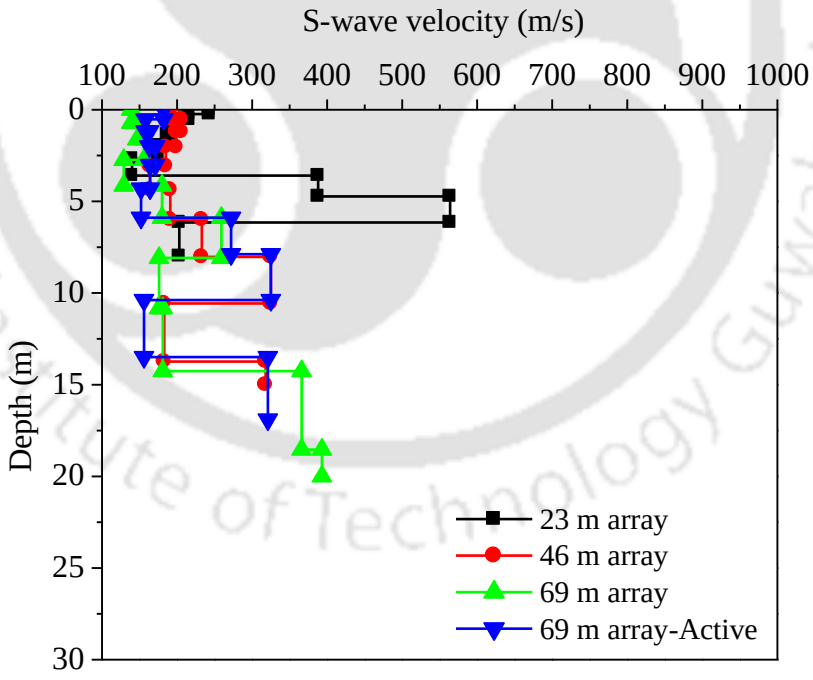

Fig. 6.3 Comparison of the shear-wave velocity profiles obtained from varying lengths of receiver arrays used in passive roadside survey, as well as from active survey

For the three receiver arrays used in the experimentation program, Table 6.2 represents the coordinates of the first point of the extracted dispersion curve in terms of lowest frequency, the corresponding phase velocity and the estimated wavelength. From the table, it can be observed that the longest wavelengths that could be collected from the receiver arrays of length 69 m, 46 m and 23 m, without being aliased, are 50.4 m, 41.6 m and 17.3 m respectively. Thus, the average ratio of longest measurable wavelength to the receiver array length is approximately 0.8. Therefore, it can be stated from the study that with a receiver array of length **X**, the longest wavelength that can be sampled is 0.8**X**.

Table 6.2 Comparison between receiver array length, longest wavelength recorded and depth of investigation

Receiver array length (m)	Characteristics of the first point of extracted dispersion curve			Depth of investigation (m)	Ratio of the longest wavelength to array length	Ratio of the depth of investigation to longest wavelength
	Frequency (Hz)	Phase velocity (m/s)	Wave-length (m)			
69	5.5	288	50.4	17.7	0.73	0.35
46	6.5	272	41.6	14.6	0.90	0.35
23	12.6	218	17.3	6.2	0.75	0.36

Moreover, it is known that the longest wavelength is directly related to the attainable depth of investigation. The depths of investigation obtained from the three receiver array lengths, 69 m, 46 m, and 23 m, are determined as 17.7 m, 14.6 m, 6.2 m, respectively. Therefore, the average ratio of investigation depth to the longest wavelength recorded without aliasing is 0.35-0.4. In other words, if the longest wavelength recorded by an array is λ, then the attainable maximum investigation depth, with good resolution, is 0.4λ. Park *et al.* (1999) reported that the maximum

depth for which shear wave velocity can be estimated is half the longest wavelength. Therefore, the results from current study show a more conservative outcome.

It is to be noted that the shear wave velocity profile for 23 m array (as shown in Fig. 6.3) deviates significantly from the other two profiles beyond 4 m depth, thus manifesting an incorrect representation of the true soil profile. This is possibly due to the approximate selection of the dispersion curve towards lower frequency band that possessed large energy bandwidth. The shear wave velocity profile from 43 m and 69 m very closely matches with each other. Hence, for a subsoil exploration testing, while aiming for a depth range of 15-20 m at a particular site, it is recommended to utilize a linear receiver array of at least 46 m to obtain reliable and satisfactory results.

6.2.2 Critical Assessment of the Study Conducted at Site 2 (Medium Traffic Volume)

The experimentation for the aforementioned aspect was conducted at Site 2 carrying medium traffic volume. The tests were conducted with 24 numbers of receivers laid at an inter-receiver spacing (*dx*) of 1 m, 2 m and 4 m, resulting in the receiver array length of 23 m, 46 m and 94 m, respectively. The array was placed at an offline distance of 3.5 m from the centreline of the road. Other details of the site, along with a pictorial view, are already reported in Chapter 4. At each set up of the receiver array, field records were collected at different acquisition time ranging from 0.7-218 s. However, as the objective of this section is to reflect the effect of receiver array length on the dispersion imaging, the results from only two recording times, i.e., 5.4 s and 10.8 s, are presented.

The result from the experimental work shows a significant dependency of the resolution of dispersion imaging on the array length. As shown in Fig. 6.4a, the dispersion image generated from raw records, acquired from a 23 m receiver array and 5.4 s recording time, has high energy content, but with indistinct dispersion trends. The most recognisable energy trend is observed at a frequency band of 8-15 Hz. It has a thick energy band, possibly of fundamental mode, but lacks a noticeable pattern, and hence very difficult to precisely locate the points of dispersion curve on the image. In lower frequency band lesser than 8 Hz, aliasing of the energy band has occurred, attributed mainly to the use of smaller receiver array incapable of sampling waves of lower frequency (i.e., longer wavelength). Moreover, in higher frequency region beyond 20 Hz, the image contains significant energy, but without recognisable pattern of higher mode dispersion trends as well. The problem arises due to recording of undesirable signals of high frequency of the wavefield by a shorter array.

With the increase in receiver spacing and array length, the undesirable energy accumulation on the dispersion image can be avoided, resulting in a more distinguishable, clearer and thinner dispersion band, as shown in Figs. 6.4b and 6.4c, representing the dispersion images corresponding to 46 m and 92 m array, respectively. The records from 92 m receiver array have produced the better dispersion imaging compared to the 23 m or 46 m receiver arrays, exhibiting a thinner and distinct fundamental mode energy band over a large frequency bandwidth of 5-20 Hz. However, the image obtained from 46 m receiver array is also found to be usable, as the energy band and its peaks are fairly distinct in the frequency band approximately spanning over 6-13 Hz (Fig. 6.4b). While maintaining the highest SNR value close to the value of 1 (or 100%), a dispersion curve is extracted from the obtained dispersion image, and is shown in Fig. 6.4c, which is further used to obtain shear

wave velocity profile of the site. The dispersion images obtained from field records acquired for 10.8 s recording time also shows similar characteristics to that obtained from a 5.4 s recording time (Fig. 6.5b). It is worth mentioning that all the dispersion images presented herein are the final dispersion images obtained after 10-20 numbers of vertical stacking. The topic of vertical stacking will be discussed in detail in Chapter 7.

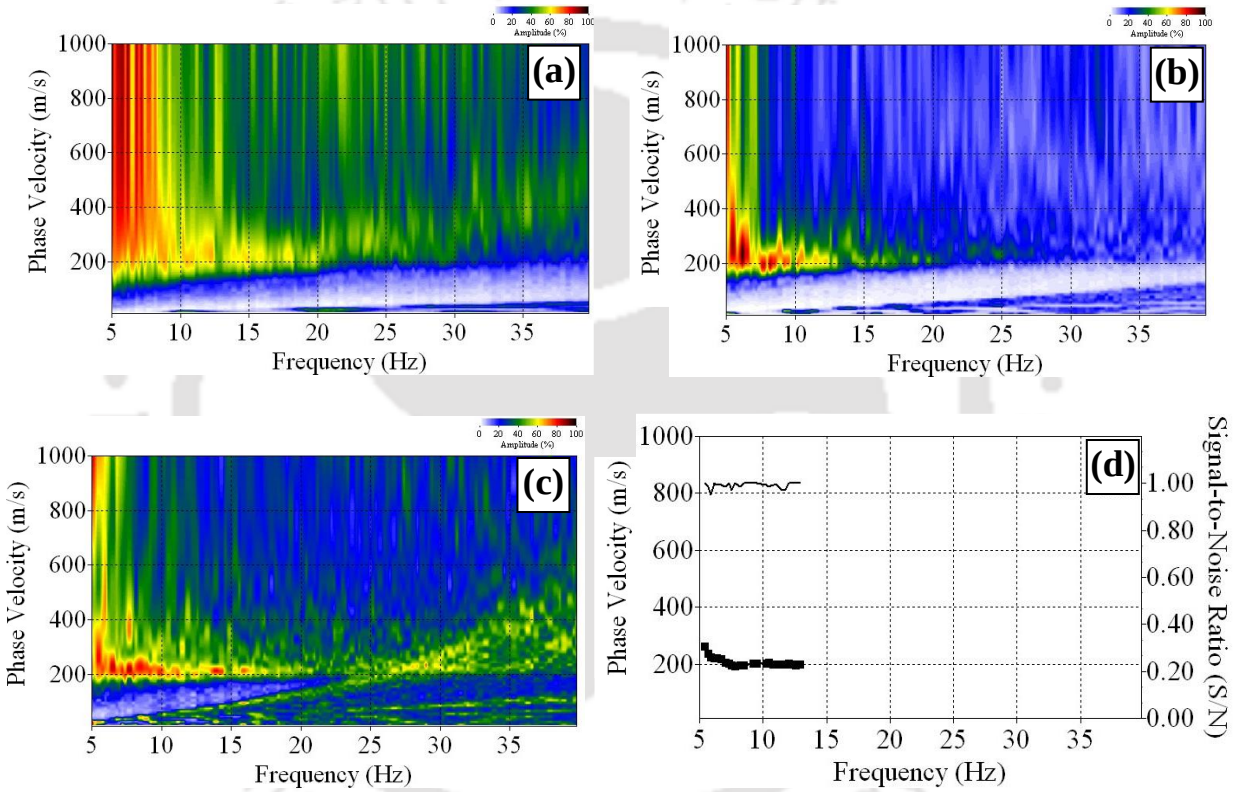

Fig. 6.4 Dispersion images from wavefield records collected at Site 2 with an acquisition time of 5.8 s for array lengths of (a) 23 m (b) 46 m (c) 92 m (d) A typical dispersion curve extracted from the dispersion image produced out of a 46 m array

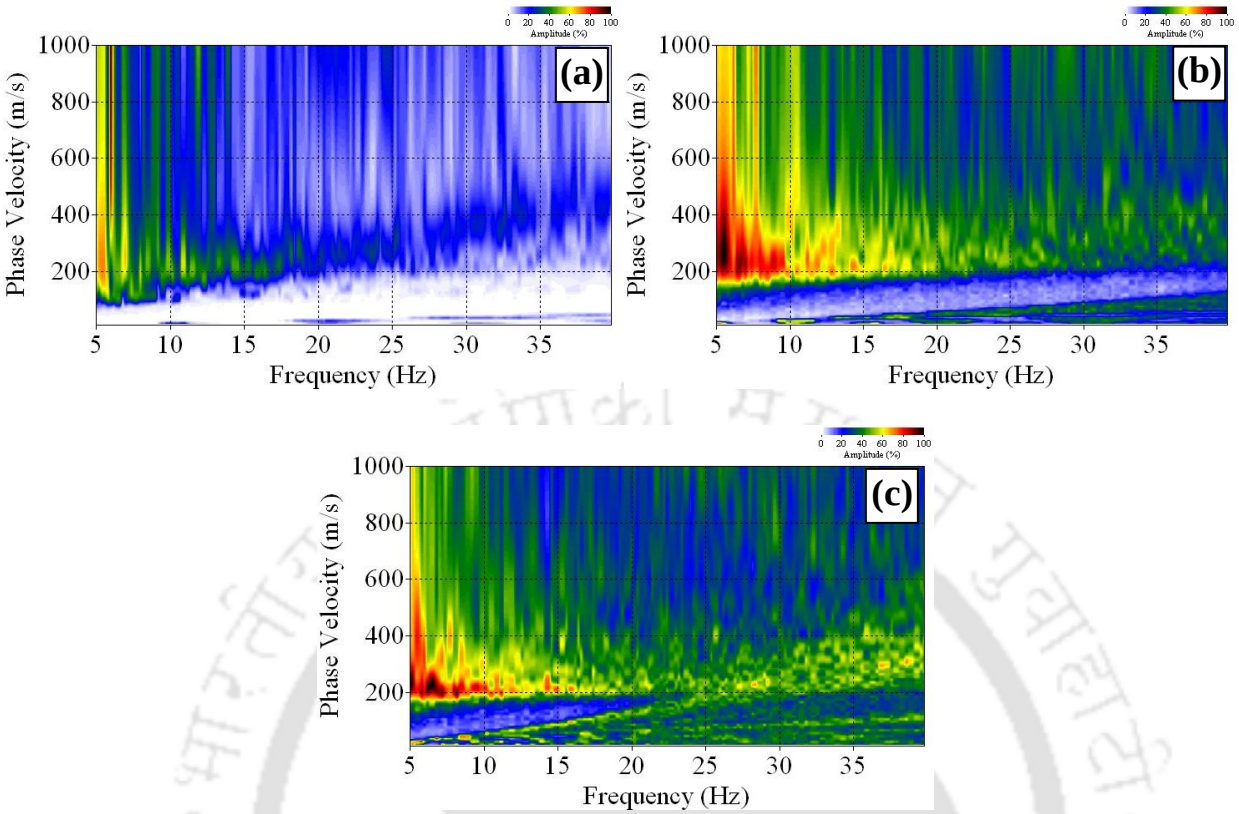

Fig. 6.5 Dispersion images from wavefield records collected at Site 2 with an acquisition time of 10.8 s for array lengths of (a) 23 m (b) 46 m (c) 92 m

6.2.2.1 Validation with the Results from Active MASW Survey

In the dispersion images obtained from the passive roadside survey from Site 2, the peaks of the fundamental energy band is distinct but lacks the continuity and sharpness, particularly in frequency band above 10 Hz. To validate the results from roadside survey, an active test, with 46 m long receiver array, 24 numbers of geophones and 6 m source offset, was performed at the site, with an objective mainly to obtain a dispersion image of enhanced resolution in higher frequency ranges. The dispersion image obtained from such a test is shown in Fig. 6.6a. The image has a similar energy trend as observed in dispersion image from the roadside survey. Existences of some higher mode energies is also observed, unlike in the passive roadside dispersion image. Peak points

of the energy band are observed in the phase velocity range of 200-300 m/s, much similar to the dispersion images obtained from roadside survey. The corresponding extracted dispersion curve is shown in Fig. 6.6b, which is obtained by maintaining the highest SNR value close to the value of 1 (or 100%), at every selected frequency points.

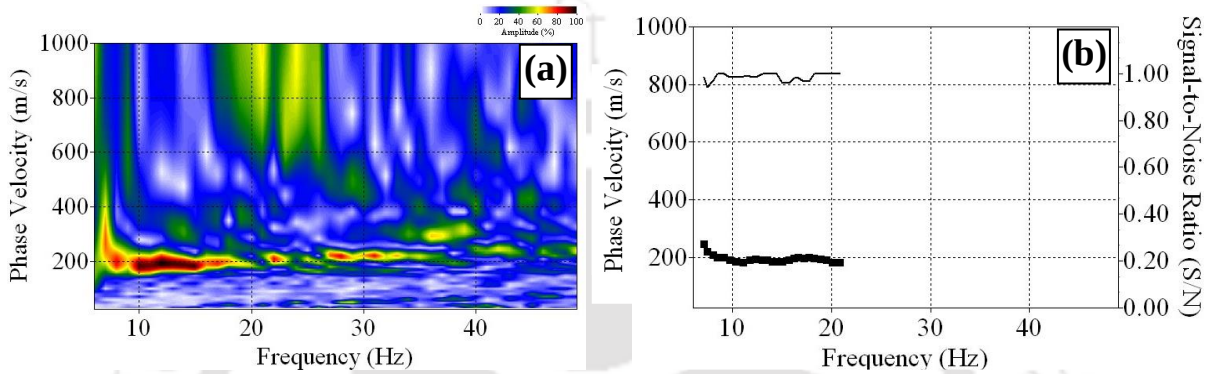

Fig. 6.6 Outcomes of the active MASW test conducted at Site 2 as a validation study against passive survey (a) Dispersion image (b) Corresponding extracted dispersion curve

Fig. 6.7a highlights the comparison of shear wave velocity profiles obtained from the two types of tests conducted at Site 2. At the first 2 m depth from the ground surface, some minor deviations in the shear-wave velocity values between the two profiles can be observed. However, in all other depth ranges, shear wave velocity profiles from both the surveys show good agreement with each other. Figure 6.7b shows the percentage variation of the two shear-wave velocity profiles obtained from the passive roadside and active survey. It can be observed that the highest deviation between 0-2 m depths is nearly 47%. Such difference of V_s values between roadside and active surveys may be attributed to the comparatively irregular selection of dispersion curve from the dispersion image generated out of a roadside survey, which exhibited a notable irregular energy band, unlike the continuous band as observed in the dispersion image from active survey. However, in all other

depth ranges, the differences in shear wave velocities are minimal, which is portrayed by the closeness of the profile towards the zero difference line. In both the V_s profiles, it is perceived that the top 2-3 number of soil layers (up to 3-4 m) has high shear wave velocity that signifies the higher stiffness of the shallow layers of the road, which is built up on the river embankment. Beyond 4 m depth, shear wave velocity significantly decreases within the depths of 5-8 m, manifesting comparatively loose soil of the ground below the base layer of the road. This characteristic of the subsoil is expected and, geologically, suiting for the site. The lower layers of the embankment are expected to have high moisture content due to long-term ingression of water from the river, thereby deteriorating the stiffness of the compacted soil. Importantly, the highest wavelength of the wavefield obtained during dispersion curve selection and the corresponding depth of investigation from the roadside survey are obtained to be 46.91 m and 15.5 m respectively. Thus, the ratio between longest measurable wavelengths to the receiver array length is 1 and the ratio between depths of investigation to the highest wavelength is 0.31. With increase in the receiver array length to 92 m, the longest wavelength recorded was found to be nearly same with 46 m array length.

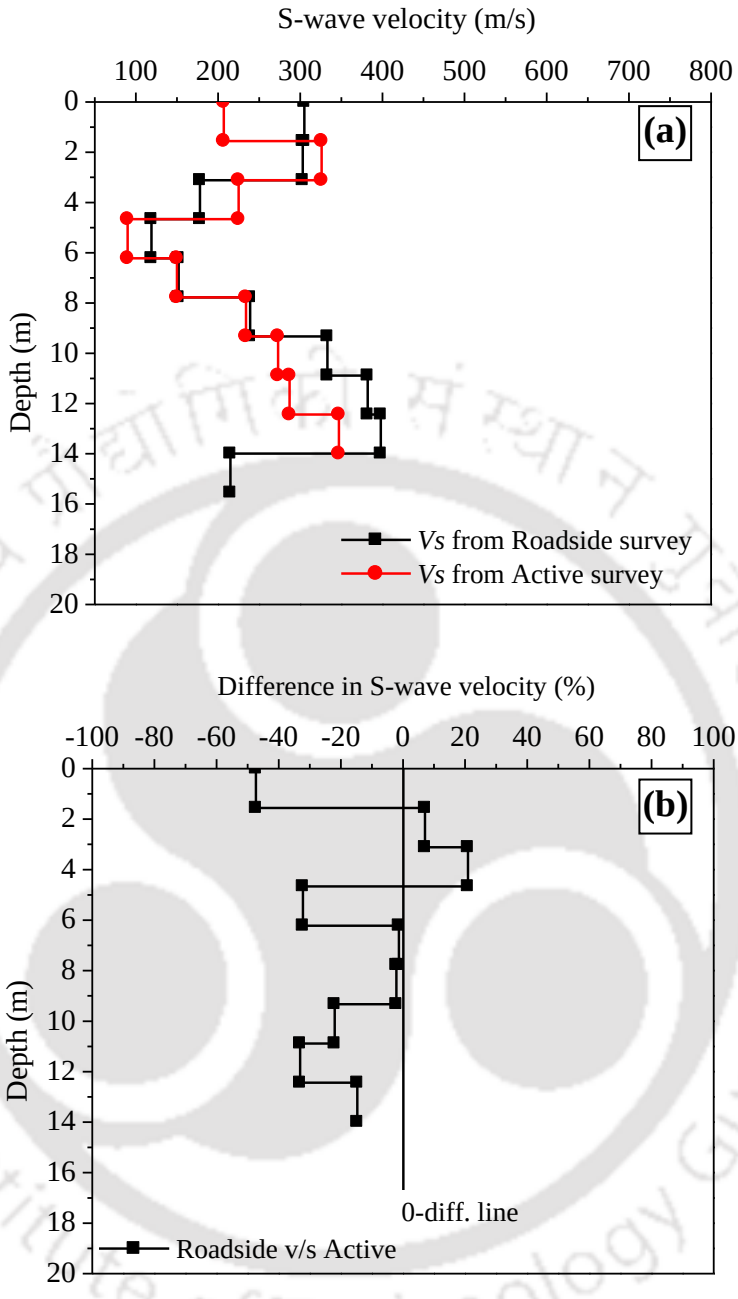

Fig. 6.7 (a) Comparison of S-wave velocity obtained from Roadside and Active survey at Site 2 (b) Percentage difference in S-wave velocity profile from Roadside and Active surveys

6.2.3 Critical Assessment of the Study Conducted at Site 3 (Heavy Traffic Volume)

Studies similar to the ones described in the previous sections were also conducted at Site 3, which is situated near national highway NH-31. It is already reported in Chapter 5 that the raw field records from this specific site contain significant surface energy from the motion of heavy vehicles on the road. In the current study, two lengths of 24 numbers of geophone receiver arrays were chosen, i.e., 46 m and 92 m, using 2 m and 4 m as inter-receiver spacing, respectively. The arrays were placed at an offline distance of 10 m from the centre line of the nearest lane of the road. From the above two studies, it became evident that the receiver array of length of 23 m is not effective in roadside survey for extracting reliable results in dispersion imaging as well as in shear wave velocity profiling. Hence, in this study, utilization of shorter receiver spacing in the order of 23 m is avoided.

Typical raw wavefield records from the two arrays are shown in Fig. 6.8. As sufficiently large numbers of vehicles pass through the site, the wavefield produced from one vehicle, from a particular surface source, has a greater possibility to be contaminated by the wavefield produced by another vehicle with another particular surface source. It is observed that in almost all of the cases, in comparison to the 92 m array length, the 46 m array have recorded comparatively cleaner records, as shown in Fig. 6.8a. Therefore, a relatively shorter array (i.e., 46 m) can record comparatively cleaner records without being contaminated from other incoming waves, particularly in a site comprising heavy traffic volume. However, in the previous sections, it is already established that the shorter receiver array length of 23 m is insufficient to produce high-resolution dispersion image. Hence, receiver array length of 46 m is found to be optimum for

recording cleaner field records. On the other hand, in case of the long 96 m array, the records are mostly of the type shown in Fig. 6.8b, exhibiting severe contamination from other incoming waves.

The dispersion images obtained from the two sets of arrays are shown in Figs. 6.9a and 6.9b. Expectedly, the resolution of dispersion image obtained from 46 m receiver array is found to be better than the 96 m array. The dominant frequency band is observed to be evident in the dispersion image over a frequency range of 15-30 Hz.

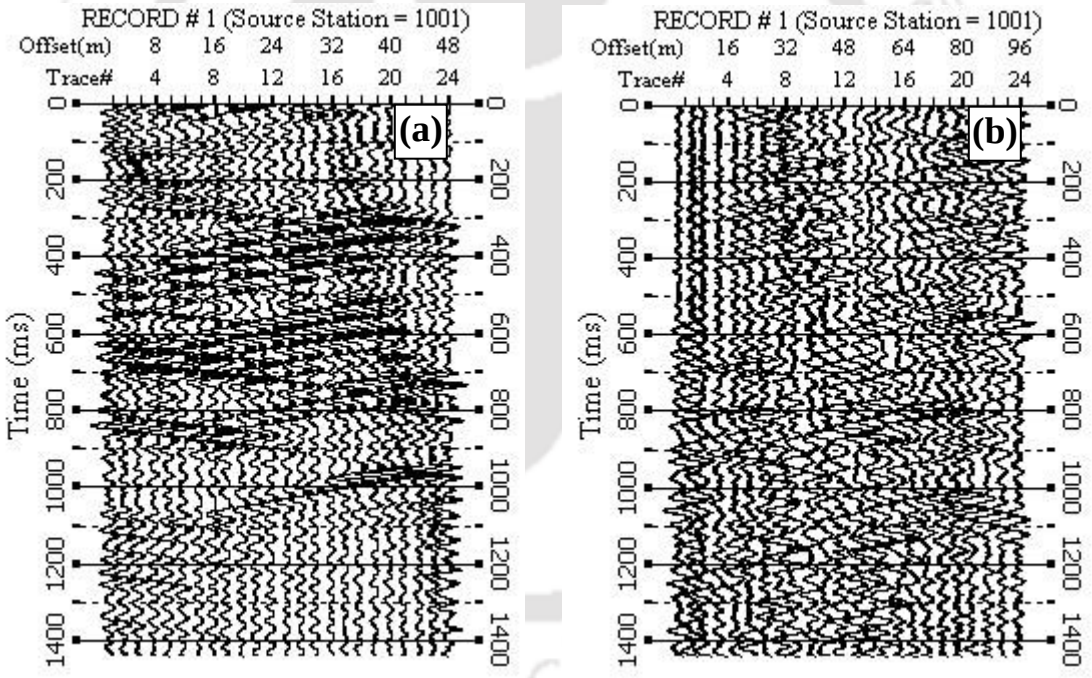

Fig. 6.8 Typical wavefield records at Site 3 collected using (a) 46 m reciever array (b) 92 m reciever array

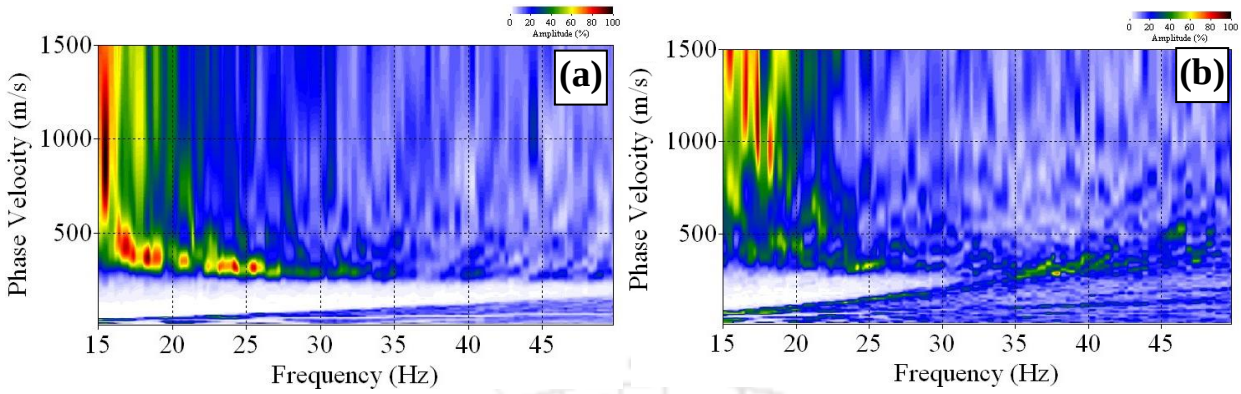

Fig. 6.9 Dispersion images obtained at Site 3 using the wavefield records of Fig. 6.8 (a) 46 m receiver array b) 92 m receiver array

6.2.3.1 Validation with the Results from Active MASW Survey

A set of active MASW survey were conducted at the site for better understanding of the wavefield propagation, contamination and its dispersive nature. The tests were conducted with 2 m source offset and 46 m receiver array, so that a direct comparison can be made between the results already obtained from roadside survey using the same length of array. Two typical raw field records collected from the site with an active source of 10 kg sledge hammer are shown in Fig. 6.10. The ambience of the site was noisy from incoming traffic generated vibrations and is manifested in the record shown in Fig. 6.10a. Beyond 16 m offset, i.e., from the 8th receiver position, the active wavefield was severely contaminated from traffic originated surface waves of large amplitudes. With many trials and efforts, a comparatively cleaner field record was obtained, as shown in Fig. 6.10b, which was primarily used for further processing.

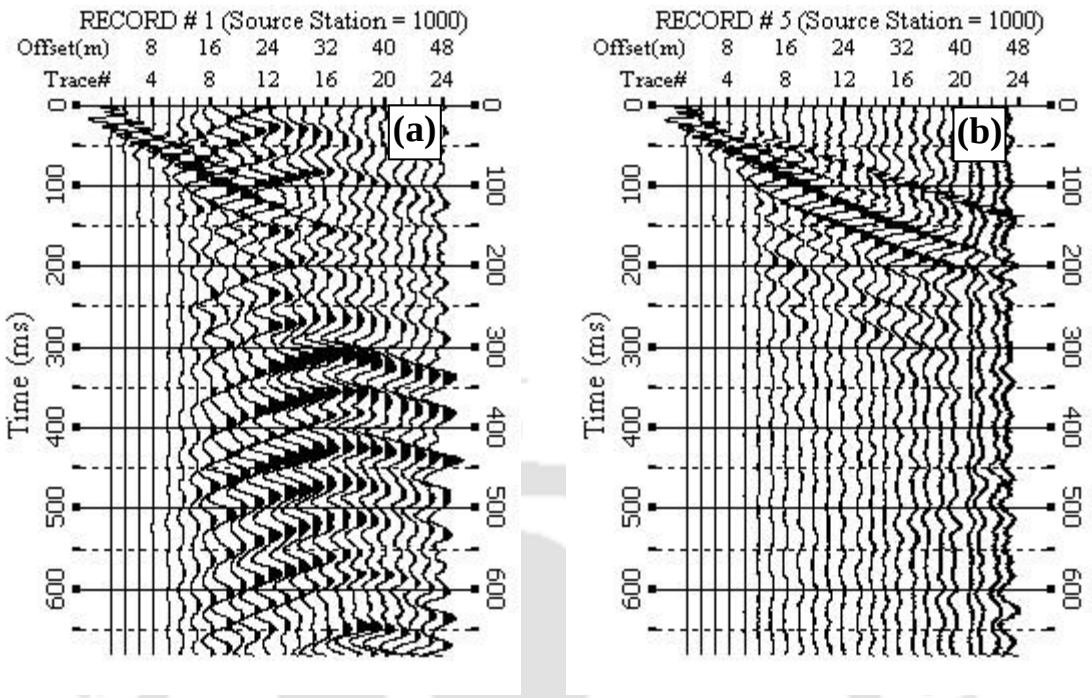

Fig. 6.10 Raw field record obtained from active survey at Site 3 (a) Active surface event severly contaminated from traffic noise (b) A carefully obtained cleaner record from the most possible calm ambience

Fig. 6.11a exhibits the dispersion image obtained by processing the raw field record shown in Fig. 6.10b. The energy trend is appreciably similar to that obtained in the dispersion image from roadside survey. However, the low frequency band is observed to have better resolution in case of active dispersion image, which is primarily attributed to the better quality of raw field data and better control in the processing parameters. The selection of dispersion curve on the dispersion image is shown in Fig. 6.11b. The selection was restricted to a frequency band of 16-31 Hz, since the energy peaks are indistinct beyond this range. The SNR value for all the selected points of the extracted dispersion curve has a value close to 1.

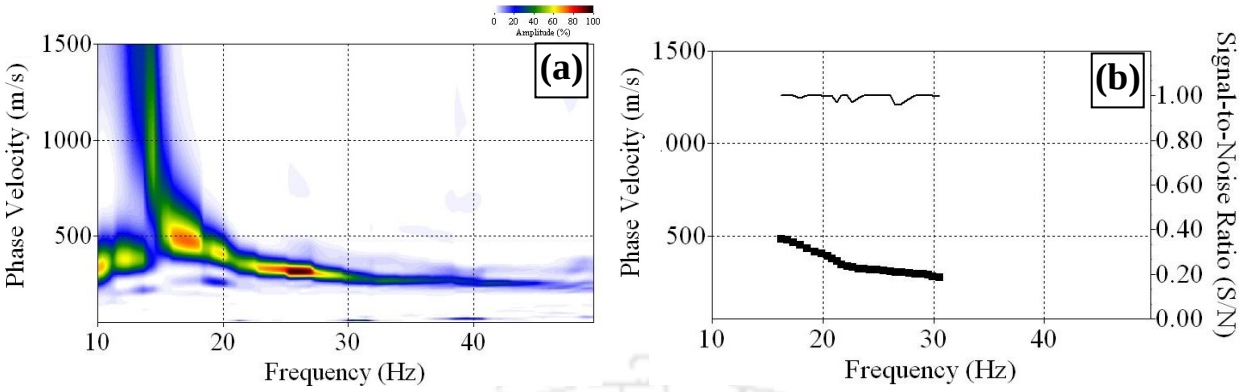

Fig. 6.11 (a) Dispersion image obtained at Site 3 from active MASW test (b) Dispersion curve extracted from dispersion image of active test

Shear wave velocity profiles obtained from passive roadside and active survey are presented in Fig. 6.12a. Some similar deviations in V_s values are observed in the top layers of the two profiles as observed in the case of Site 2, in the depth ranges of 0-2 m and 2-3 m. Figure 6.12b, depicts the percentage variation of shear wave velocities between the two profiles. Major deviations between the two profiles are found to be 47 %, and 36 % in the depth ranges of 0-2 m and 2-3 m respectively. These variations are attributed to the irregular selection of the energy points, leading to imprecise extraction of the dispersion curve from the dispersion image (generated from the passive roadside survey exhibiting a discontinuous fundamental mode energy band). In other layers, the shear wave velocities well converge to each other. For the marginally better resolution in lower frequency band of the dispersion image from active survey, a slightly higher investigation depth, than the roadside survey, has been attained (not shown in the figure). Further, the highest wavelength in the wavefield (based on the selected dispersion curve) and the corresponding depth of investigation from passive roadside survey are obtained to be 25.9 m and 9.1 m, respectively. Therefore, the ratio of attainable depth to longest wavelength is 0.35, while the ratio of longest recorded wavelength to the receiver array length is found to be 0.6.

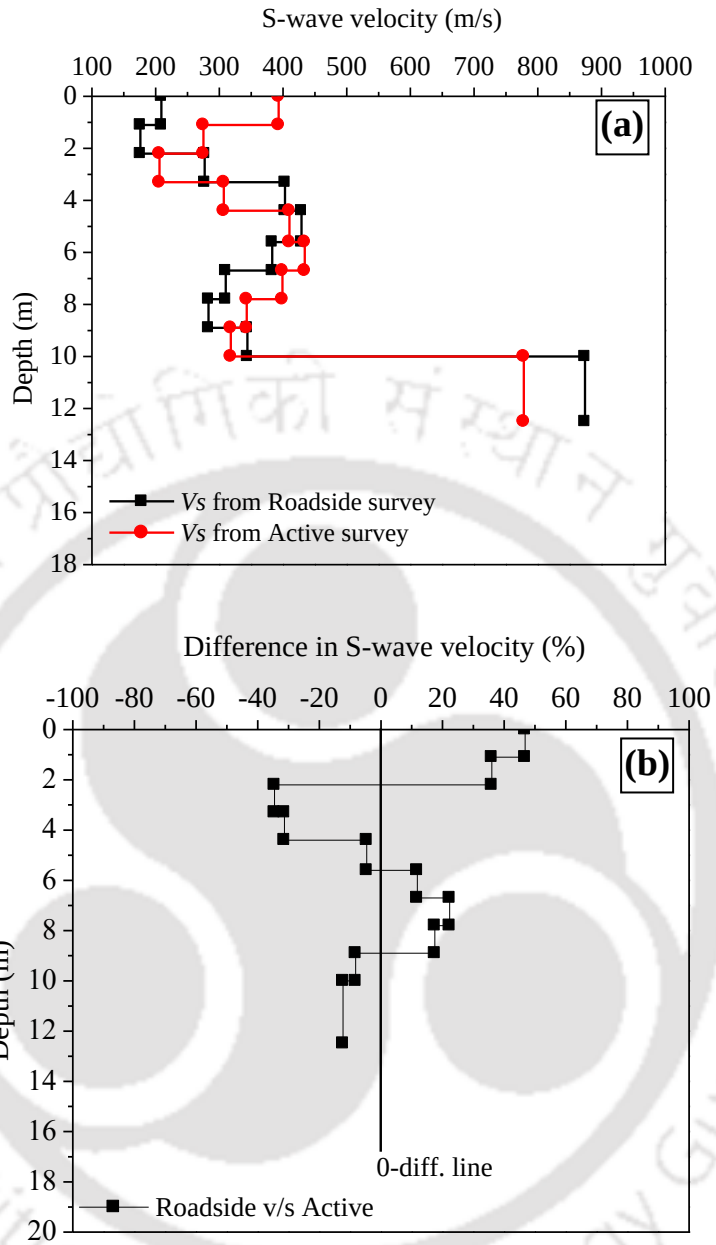

Fig. 6.12 (a) Comparison of shear-wave velocity obtained from Roadside and Active survey at Site 3 (b) Percentage difference in shear-wave velocity profile from Roadside and Active surveys

6.3 Influence of the Length of Acquisition Time

Data acquisition, or recording, time is the time span specifically set on the seismograph to record seismic data from the surface wave events. An optimum acquisition time is dependent on the time of occurrence, distance of origin of the surface wave event from the receiver array and the length of receiver array. A shorter array will certainly need a lesser time, while a longer array will need relatively longer time for collecting the surface wave data. Park and Miller (2008), through the work related to roadside MASW survey, suggested to maintain an acquisition time in such a way that at least one vehicle should pass through the receiver array during the recording process. It was also reported that an acquisition time of 10 s, with a sampling interval of 4 ms, is sufficient for optimum recording of passive surface waves. With an objective to identify an optimum acquisition time, experimentations were conducted at different sites (Site 2 and Site 3) for varying traffic conditions, utilizing different receiver array lengths, to examine critically the influence of acquisition time on dispersion imaging.

In the seismograph system employed in this study, eight different limits of acquisition times are available, as listed in the Table 6.3. The table also shows the sampling rates and total number of samples associated with each acquisition time. All these acquisition times were used for different receiver array lengths, i.e., 1 m, 2 m and 4 m respectively, on both the sites and the respective dispersion images were obtained. The study was not conducted at Site 1 (inside IIT Guwahati campus) due to very light traffic volume.

Table 6.3 List of acquisition times and sampling rate available in the seismograph system

SL. No	Acquisition time (s)	Sampling rate (samples/s)	Sampling interval (ms)	Total number of samples
1	0.7	30000	0.033	21000
2	1.4	15000	0.066	21000
3	2.8	7500	0.133	21000
4	5.8	3750	0.266	21750
5	10.8	2000	0.5	21600
6	21.8	1000	1	21800
7	43.6	500	2	21800
8	218	100	10	21800

6.3.1 Critical Assessment of the Study Conducted at Site 2 (Medium Traffic Volume)

The experimentation work for the study was conducted at Site 2, i.e., adjacent to the road from Amingaon to IIT Guwahati. At least 10 field data sets were recorded at every preset acquisition time (as mentioned above), so that sufficient data is attained to carry out an effective vertical stacking during data processing. It was reported in the previous sections that in the case of medium to heavy traffic volume conditions, quality of field data may deteriorate due to excessive contamination from unwanted incoming waves. Hence, a sufficient number of records are needed to be collected so that there remains some good number of data after discarding the unusable ones. Further, dispersion image obtained through multiple vertical stacking of the records will give reliable results and will help in studying of the current parameter.

Figure 6.13, 6.14 and 6.15 represents the dispersion images obtained from wavefields generated at Site 2 utilizing different acquisition times, while using 23 m, 46 m and 92 m receiver arrays, respectively. In all the cases, it is observed that with very limited acquisition time of 0.7 s, the

dispersion images could not yield any significant or meaningful information. Particularly, the shorter array of 23 m could not record the actual propagation and dispersive characteristics of the wavefield in such a short time span. Normally, a shorter receiver array is capable of sampling and collecting the shorter wavelength or high frequency components of a wavefield. However, the high frequency waves propagate slowly through the shallower layers of soil, i.e., they possesses low phase velocity. Hence, during the short time interval, all the high frequency components of the wavefield could not fully arrive to the receiver array, thereby resulting in a poor dispersion image of the type shown in Fig. 6.13a. In the figure, the most prominent energy spikes of interest are observed in the frequency band of 15-20 Hz, although with very little clarity. On the other hand, a longer array is capable of sampling longer wavelength, or lower frequency components, of the wavefield. As the waves of longer wavelength travels faster through the subsoil, they reach sufficiently earlier to the receiver array. Hence, in spite of very short duration of acquisition, some dispersive pattern of waves can be observed on the dispersion image from 46 m receiver array, as shown in Fig. 6.14a, attributed to the sampling of waves in the frequency band of 10-15 Hz.

Pertaining to the same conceptual understanding, similar features can be also observed in the dispersion images generated out of the acquisition time of 1.4 s while utilizing 23 m, 46 m and 92 m receiver arrays. With a mere increase in the acquisition time to 1.4 s, the dispersion images for all the three array sets exhibited significantly improved dispersive energy bands. Thus, for the test site (Site 2) comprising particular characteristics of subsoil and traffic volume, 1.4 s is found to be sufficient for all the frequency components of wavefield to reach the receiver array from major surface events and being properly recorded.

For any acquisition time of 2.8 s and beyond, all the obtained dispersion images comprise sufficiently distinct energy peaks. With higher acquisition times, wavefields generated from more numbers of strong source events were recorded. As described in Chapter 5, the existence of a stronger source helps in enhancing the resolution of dispersion image. Thus, when these data are stacked together, waves with higher energy becomes further prominent giving an enhanced dispersion image with further better resolution. However, mere increase in acquisition time beyond 21.8 s does not have further substantial effect on the enhancement of the dispersion image, rather may lead to the degradation of its resolution. This is attributed to the fact that with excessive increase in the acquisition time, wavefield arriving from different sources overlap, leading to the contamination and degradation of the resolution of the dispersion image. Further, it is observed from this study that acquisition time is specifically a site-dependent parameter. Thus, it is comprehended that the primary factor governing the optimum acquisition time for a particular site is the volume of the traffic in the nearby roads and presence of major surface events.

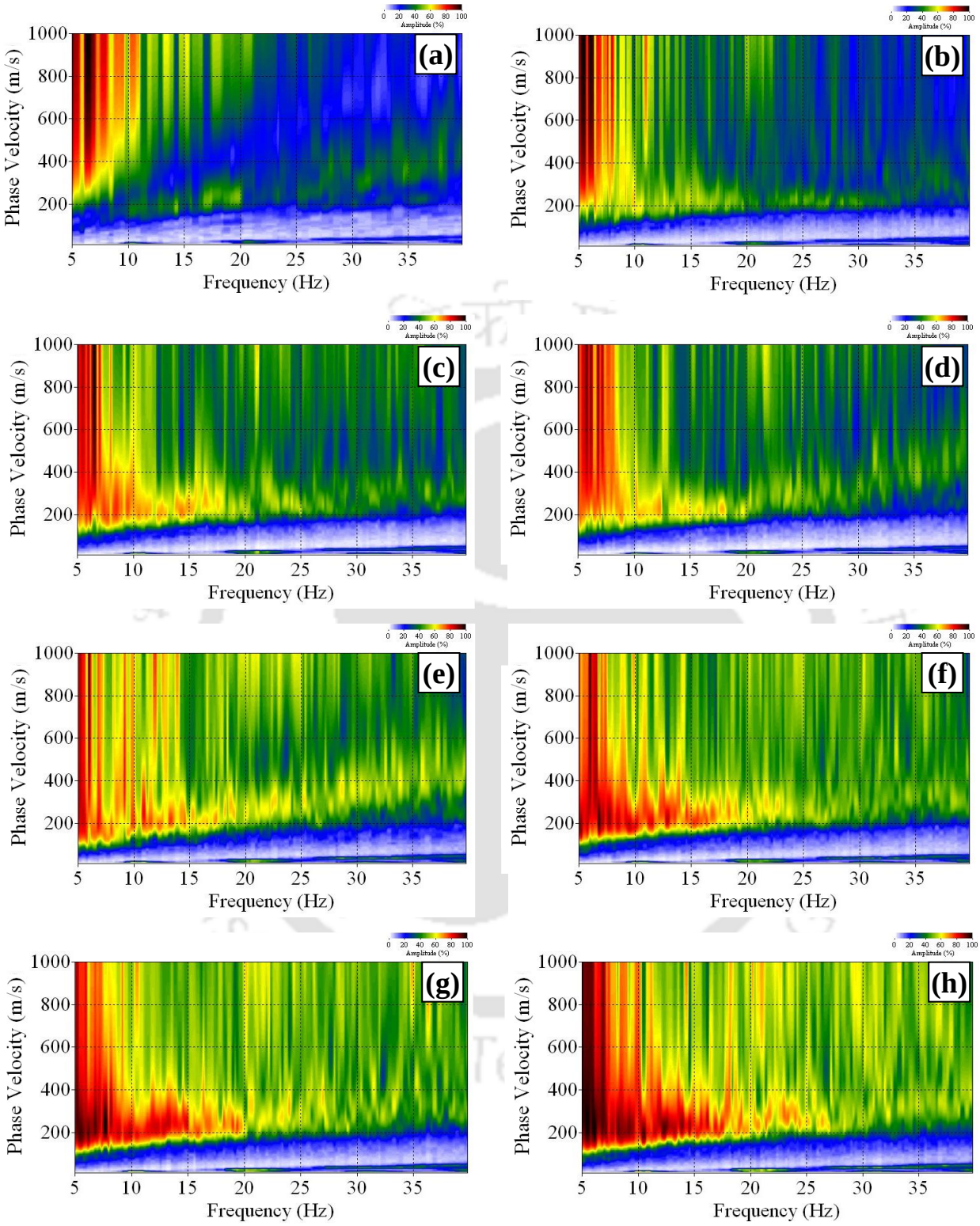

Fig. 6.13 Dispersion images obtained at Site 2 using 23 m array length and with recording times of (a) 0.7 s (b) 1.4 s (c) 2.8 s (d) 5.4 s (e) 10.8 s (f) 21.8 s (g) 43.6 s (h) 218 s

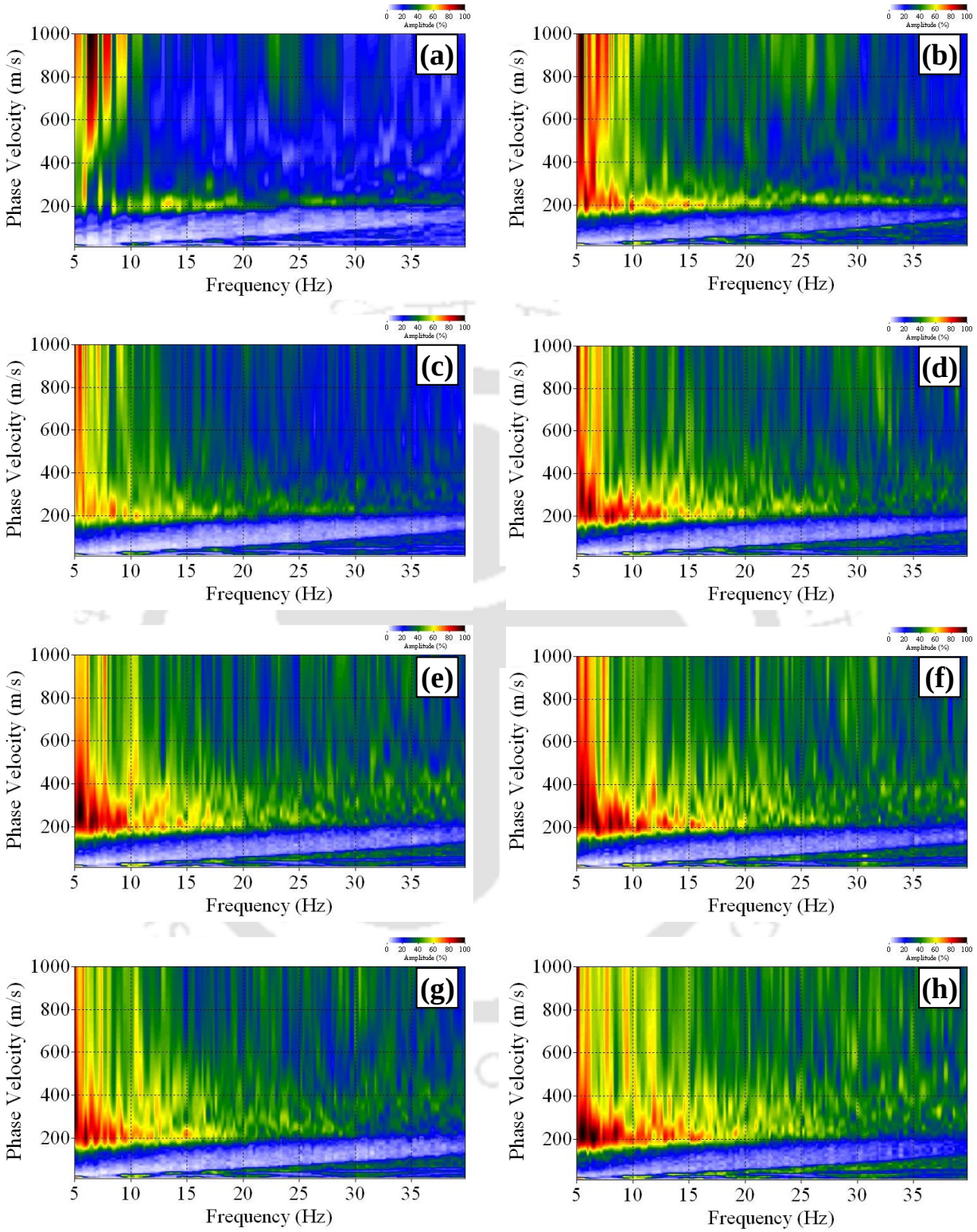

Fig. 6.14 Dispersion images obtained at Site 2 using 46 m array length and with recording times of (a) 0.7 s (b) 1.4 s (c) 2.8 s (d) 5.4 s (e) 10.8 s (f) 21.8 s (g) 43.6 s (h) 218 s

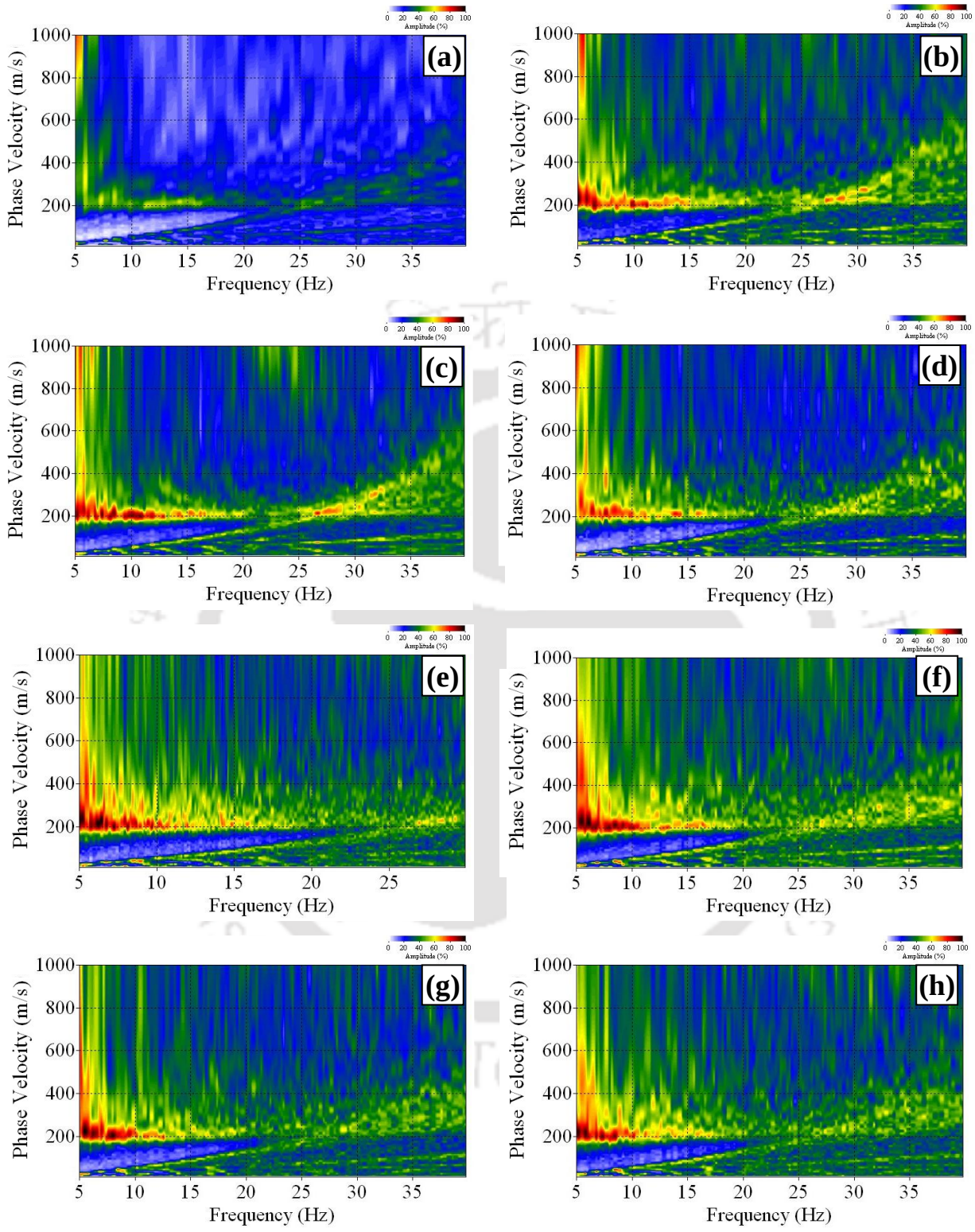

Fig. 6.15 Dispersion images obtained at Site 2 using 92 m array length and with recording times of (a) 0.7 s (b) 1.4 s (c) 2.8 s (d) 5.4 s (e) 10.8 s (f) 21.8 s (g) 43.6 s (h) 218 s

6.3.2 Critical Assessment of the Study Conducted at Site 3 (Heavy Traffic Volume)

In this section, for the current investigative aspects of the study, the results from Site 3, i.e., the site near NH-31, are presented. As already mentioned, this site comprises a heavy traffic volume with significant numbers of medium to heavy vehicles passing through at any instant of time. Hence, a study at the location will certainly help to establish the findings of the previous study based on medium traffic volume.

It is observed in the previous study that mere increase in acquisition time does not improve the resolution of dispersion image, until there is no occurrence of major surface event during the recording. It may rather degrade the resolution of dispersion image by superposition of waves arriving from different micro sources. In heavy traffic flow situations, the possibility of existence of multiple surface events is even higher. The frequent passage of vehicles over closely situated sources may reduce the quality of raw field record and, hence, the resolution of dispersion image. Dispersion images obtained from the field records of 46 m array, with varying acquisition times, are shown in Fig. 6.16. The best dispersion image, with a comparatively continuous energy band, is observed only in case of 1.4 s recording time, as shown in Fig. 6.16a. Therefore, for the present site, a small time-length of 1.4 s is found to be sufficient to record the major surface events for a meaningful dispersion image. Dispersion images from field records acquired at 10.8 s and 21.8 s acquisition times (Figs. 6.16b and 6.16c) have shown deterioration in higher frequency band of the dispersion image. This is attributed to the contamination of higher frequency components of wavefields from waves of other sources due to the longer time of acquisitions.

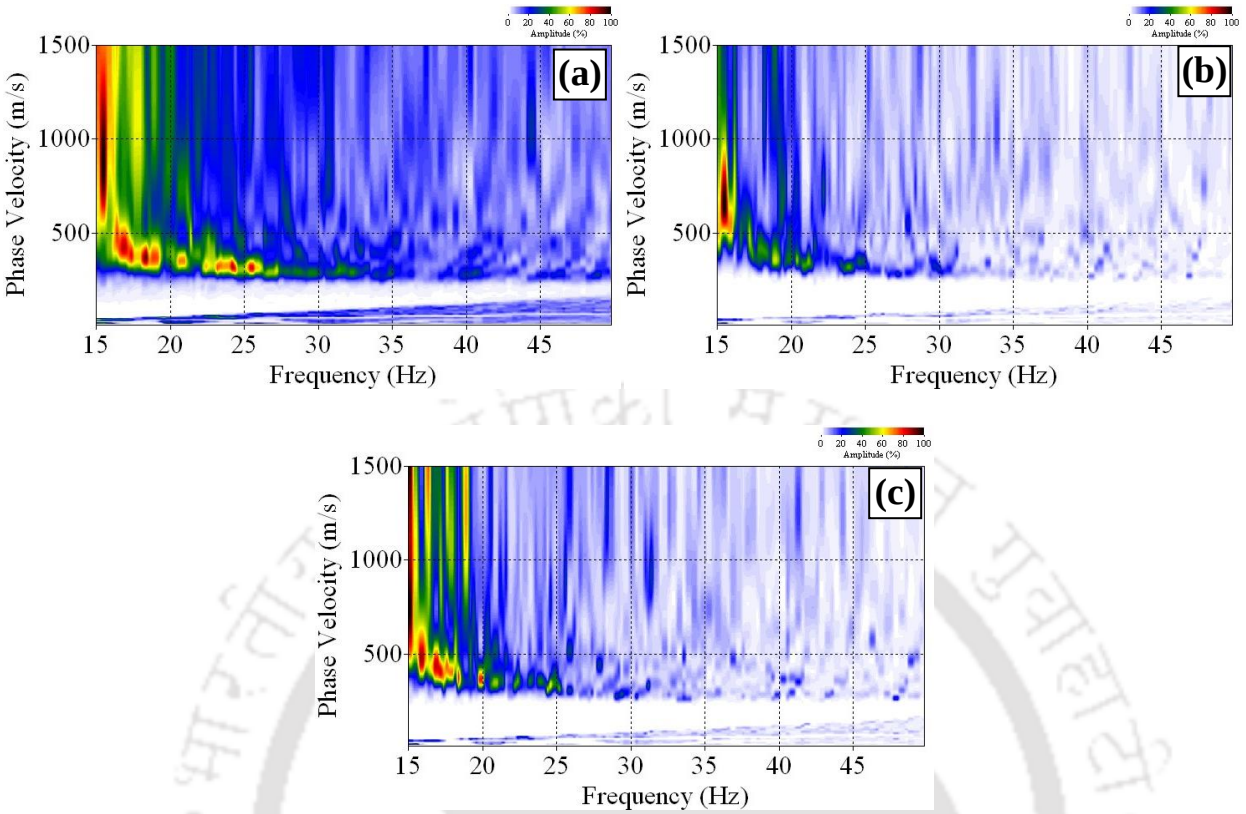

Fig. 6.16 Dispersion images obtained for the wavefields recorded at Site 3 with 46 m array at acquisition times of (a) 1.8 s (b) 10.8 s (c) 21.8 s

Dispersion images obtained from field records collected with a 92 m receiver array with varying acquisition time are shown in Fig. 6.17. The dispersion images did not show any useful dispersive characteristics of surface waves, and are mostly unrecognizable. As it has been observed from the frequency spectrum of the field records presented in Chapter 5 and the corresponding dispersion images from 46 m receiver array, the most dominating frequency band of the field records lies in between 15-25 Hz. The longer receiver array of 92 m could not sample and record the energy characteristics in the higher frequencies or the shorter wavelength components of the wavefields. Further, non-existence of sufficiently stronger surface events, which are capable of producing frequency components lesser than 15 Hz, eventually resulted in indistinct dispersion image.

Consequently, there were no changes in the resolution of dispersion images with varying acquisition time.

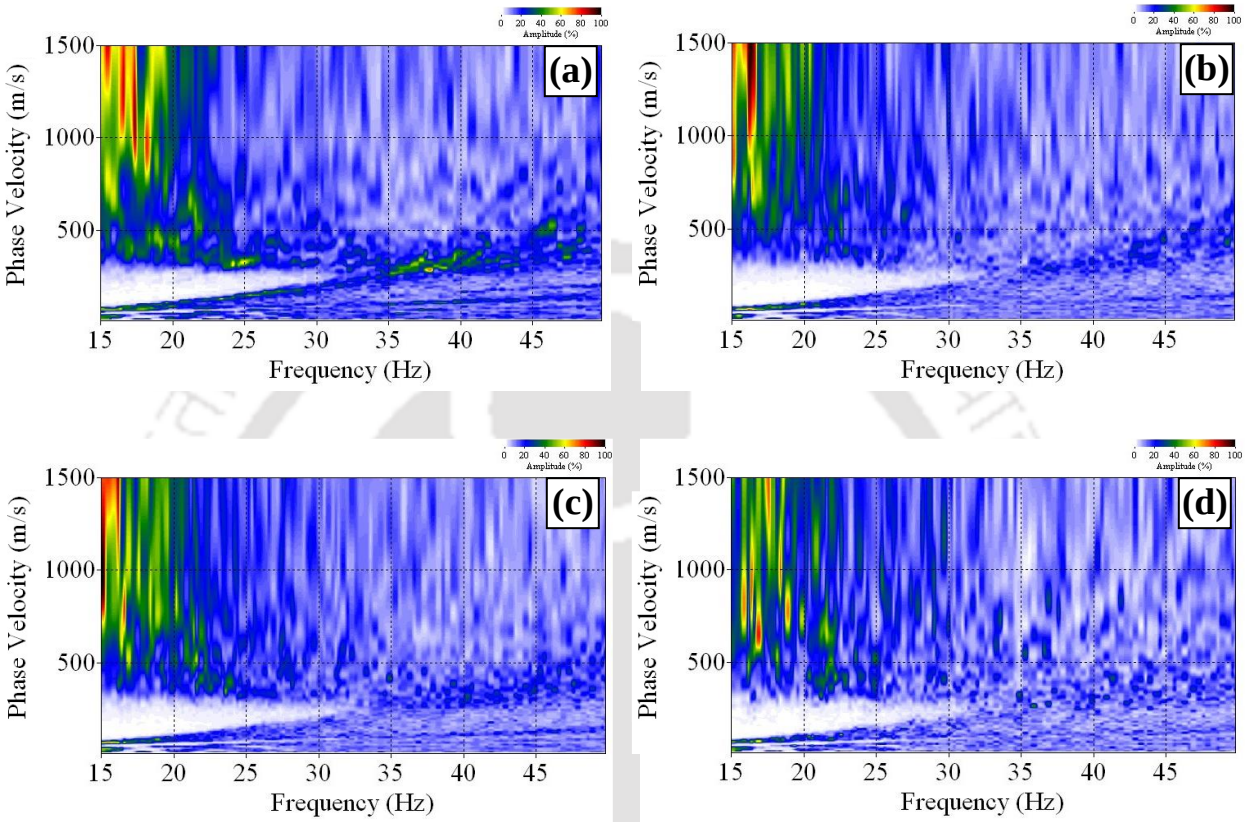

Fig. 6.17 Dispersion images obtained for the wavefields recorded at Site 3 with 92 m array at acquisition times of (a) 1.8 s (b) 10.8 s (c) 21.8 s (d) 43.8 s

6.4 Summary

Receiver array length and acquisition time plays a significant role in governing the resolution of dispersion image. Thicker dispersion energy band and poor resolution in lower frequency bands of dispersion image are found to be the outcome of utilizing smaller arrays. A short receiver array length of 23 m is found to be insufficient to produce dispersion image with sufficient resolution, particularly in lower frequency band, irrespective of the site conditions. With increasing length of

the arrays to 46-92 m, the resolution of dispersion image is found to be continually increasing at the Sites 1 and 2 comprising light to medium traffic volume respectively. The dispersion energy band in the corresponding images becomes progressively thinner with increasing length of the arrays, resulting in high SNR for the extracted dispersion curve. However, at site with heavy traffic volume (Site 3), raw field records from longer receiver array suffers severe contamination which resulted poor resolution dispersion image. At Site 3, a receiver array length of 46 m is found to be optimum. It is observed that ratio between longest measurable wavelength to the receiver array length is approximately in the range of 0.6 to 1. Further, the highest ratio between depth of investigation to longest wavelength is found to be approximately 0.4.

The acquisition time is primarily a site dependent parameter and is largely influenced by the volume of the traffic and numbers of existing sources on the road surface nearby the test site. For light to medium traffic volume site, acquisition time between 2.8-21.8 s have been found to be sufficient. Smaller recording time is effective during raw data acquisition at site with heavier traffic volume case. At Site 3, a mere acquisition time 1.4 s has been found to be sufficient to produce a usable dispersion image.

CHAPTER 7

INFLUENCE OF PROCESSING SCHEMES AND STACKING ON THE RESOLUTION OF DISPERSION IMAGE

7.1 Introduction

Good quality raw field records, obtained by utilising optimum geometrical configurations and acquisition parameters, are to be processed for dispersion analysis. It is the most important stage in MASW survey, as the accuracy of final V_s profile is primarily a function of accurate extraction of dispersion curve. In the process of dispersion analysis, a number of analytical processing parameters largely affect the resolution of dispersion image. It has been experienced during the study that without optimum use of the processing parameters, it is difficult to produce a dispersion image with high resolution, despite having good quality raw field records. The notable parameters that influence the analysis of passive surface wave data are (a) the optimum scanning range of frequency and velocity, (b) precise azimuthal range for scanning major surface events, (c) offline distance that adopts appropriate processing scheme (e.g., IP, OP, OC scheme) for the particular record, and (d) vertical stacking. The significance of these parameters on the resolution of dispersion image will be elaborated in the following sections of this chapter.

7.2 Selecting Site-Specific Best-Suitable Range of Scanning Frequency and Velocity

During the dispersion analysis, the first set of processing parameters to be selected are the best-suitable scanning range of frequency and phase velocity. Every site has its own unique soil

characteristics. At any particular frequency, a site with stiffer soil layers assists the surface wave to propagate with greater phase velocities. On the contrary, at sites comprising loose or relatively less stiff soil layers, surface waves propagate with lower phase velocities, even at lower frequencies. In Chapter 3, it is already reported that during dispersion analysis, scanning of true phase velocity is computed at every frequency component while searching for the greatest amplitude or energy. On the other hand, in Chapter 5, it was observed that different sites yield different types of field record with various nature of frequency-amplitude spectrum. Therefore, it is necessary to identify the best-suitable and geologically feasible range of scanning frequency range and equivalent phase velocity during dispersion analysis.

Figure 7.1a and 7.1b shows dispersion images obtained from Site 1, utilizing different ranges of frequency and phase velocity. The first image refers to the analysis conducted for a frequency range of 5-50 Hz and phase velocity range of 10-2000 m/s. As the site did not comprise soil of very high stiffness (greater than 1000 m/s), it is evident that the wavefield produced by the traffic source did not contain any frequency component having a propagation velocity in the range of 1000-2000 m/s. Figure 7.1b shows a dispersion image, processed with a reduced range of frequency and phase velocity, i.e., 5-40 Hz and 10-1000 m/s, respectively. The resolution of the dispersion image is found to be enhanced, as the peak points on the energy band are notably distinct (the dark coloured region) than the previous scenario. Further, a high scanning range of frequency and phase velocity also prolong the computation time. Under similar scanning ranges of phase velocity and frequency, similar response was observed when the field data from Site 2 (beside IIT Guwahati to Amingaon market road route) was analysed, as shown in Fig. 7.1c and 7.1d.

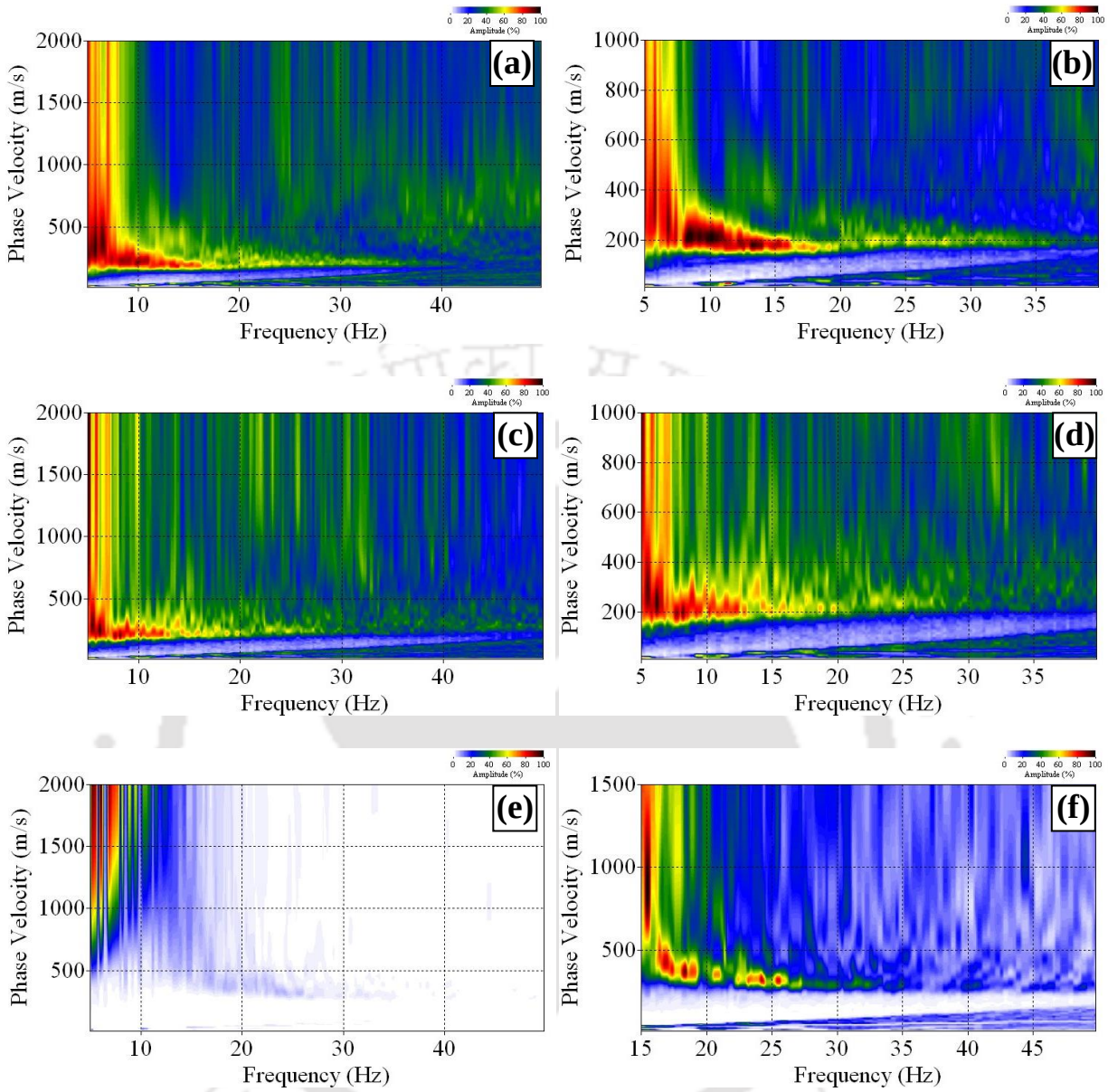

Fig. 7.1 Dispersion image with different phase velocity and frequency range (a and b) Site 1 (c and d) Site2 and (e and f) Site3

However, a different outcome is observed during the analysis of the field records from Site 3, i.e., at the site beside NH-31. From the field data processed using frequency and phase velocity ranges of 5-50 Hz and 10-2000 m/s, respectively, the dispersion image lacks the minimum required resolution for dispersion curve extraction. On examining the image carefully, the dispersive wave

energy can be identified to be starting from approximately 12 Hz frequency. The record, on reprocessing with a curtailed frequency range of 15-50 Hz and 10-1500 m/s, resulted in a significantly better dispersion image with well-defined dispersion energy trend. Because of high magnitudes of normalized amplitude at the lower frequency components of the wavefield (< 15 Hz), as observed in Chapter 5, the energy peaks in the other part of the dispersion image, i.e. in higher frequency band (> 15 Hz), exhibited relatively lesser resolution and sharpness. Further, as the shorter receiver array is not capable of sampling the low frequency wavefields, aliasing occurred on the dispersion image resulting in unrecognisable dispersion band in the stated low frequency zone. However, when the frequency band below 15 Hz is discarded from the analysis (Fig. 7.1f), the corresponding normalized amplitude in the frequency band from 15-30 Hz attained their maximum magnitudes and, therefore, resulted in a dispersion image of better resolution.

It is worth mentioning that the choice of scanning frequency and velocity is site-specific (which depends upon the traffic volumes and subsurface properties) and cannot be recommended equivocally for all sites. As observed from Fig. 7.1, for obtaining an illustrative dispersion image at three different sites, the suitable ranges of scanning frequency and phase velocity are different. Upon observing Fig. 7.1(a-b), for Site 1, it may be noted that the scanning frequency range is comparable, while the scanning velocity range is substantially different. Similar observation can be made from Fig. 7.1(c-d) for Site-2. It can be noted that change in the scanning velocity simply enhances the recognizable thickness of the dispersion band without significantly improving its quality. However, for Site-3, Fig. 7.1(c) clearly shows that the change of scanning frequency has substantial influence as a curtailed range of scanning frequency could illustrate the recognizable energy distribution on the dispersion band. Hence, it can be confidently stated that the choice of

scanning frequency has more dominant effect than the scanning velocity range to obtain a recognizable dispersion band.

7.3 Selecting Site-Specific Appropriate Azimuthal Scanning Quadrant for Dispersion Analysis

Another important parameter to be carefully selected during dispersion analysis is the scanning quadrants for detecting the direction of incoming wavefields from various sources. For passive MASW surveys, it is important to note correctly the direction or orientation of the receiver array with respect to a reference meridian (e.g., geographic North or East). For example, in passive roadside survey, based on the first receiver in the array, it is required to note the direction of receiver array with respect to the geographic North. On the other hand, for passive remote survey, it is required to note the position of first receiver with respect to the geographic East, and sequence of layout of other receivers in the array i.e., clockwise or anticlockwise starting from the 1st receiver. In passive roadside survey, as the receiver array is normally placed parallel to the nearby road, at least two quadrants are normally selected to scan all possible incoming directions of the major surface waves from the road. However, in cases of such passive roadside survey conducted at sites comprising a number of surrounding roads and road intersections, strong surface sources may arrive at the receiver array without being in the range of selected quadrants. In this section, the effects of selection of various quadrants during dispersion analysis are presented. The tests were carried out in a controlled environment, i.e., when the quadrant comprising major wavefield source is already known. A schematic layout of the position of a major surface source on road at Site 1, with respect to the receiver array, is shown in Fig. 7.2a. It is evident that the all the incoming

wavefields from the visible major source and all other minor sources will be arriving at the receiver array from NW-SW quadrants.

In this study, dispersion analysis is performed considering three different quadrants to evaluate the significance of the considered aspect. Fig. 7.2b shows a dispersion image obtained by conducting dispersion analysis considering NE-SE quadrants, i.e., completely ignoring the direction of all major possible incoming waves. As expected, the analysis could not take account of azimuth of any incoming surface waves in the energy estimation for the analyzable range of phase velocity and frequency and, hence, no energy peaks are noticeable in the dispersion image. By changing the quadrant to SE-SW, the analysis could partly take into account the azimuth of the incoming waves (due to SW quadrant); consequently, the dispersion image within the scanning range of phase velocity and frequency range have yielded an improved energy band (Fig. 7.2c). Figure 7.2d shows the best dispersion image obtained when quadrants NW-SW is considered for dispersion analysis that comprises the major source position (in NW quadrant).

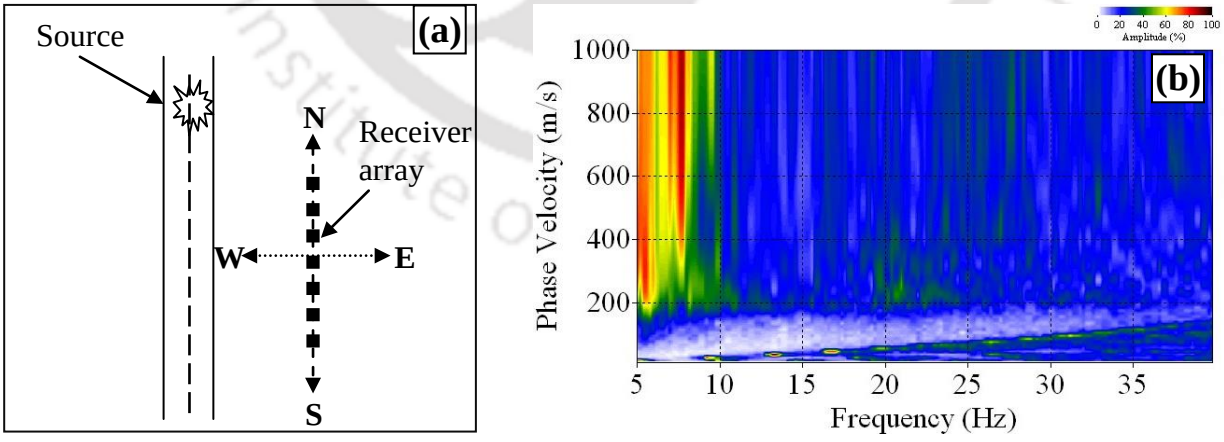

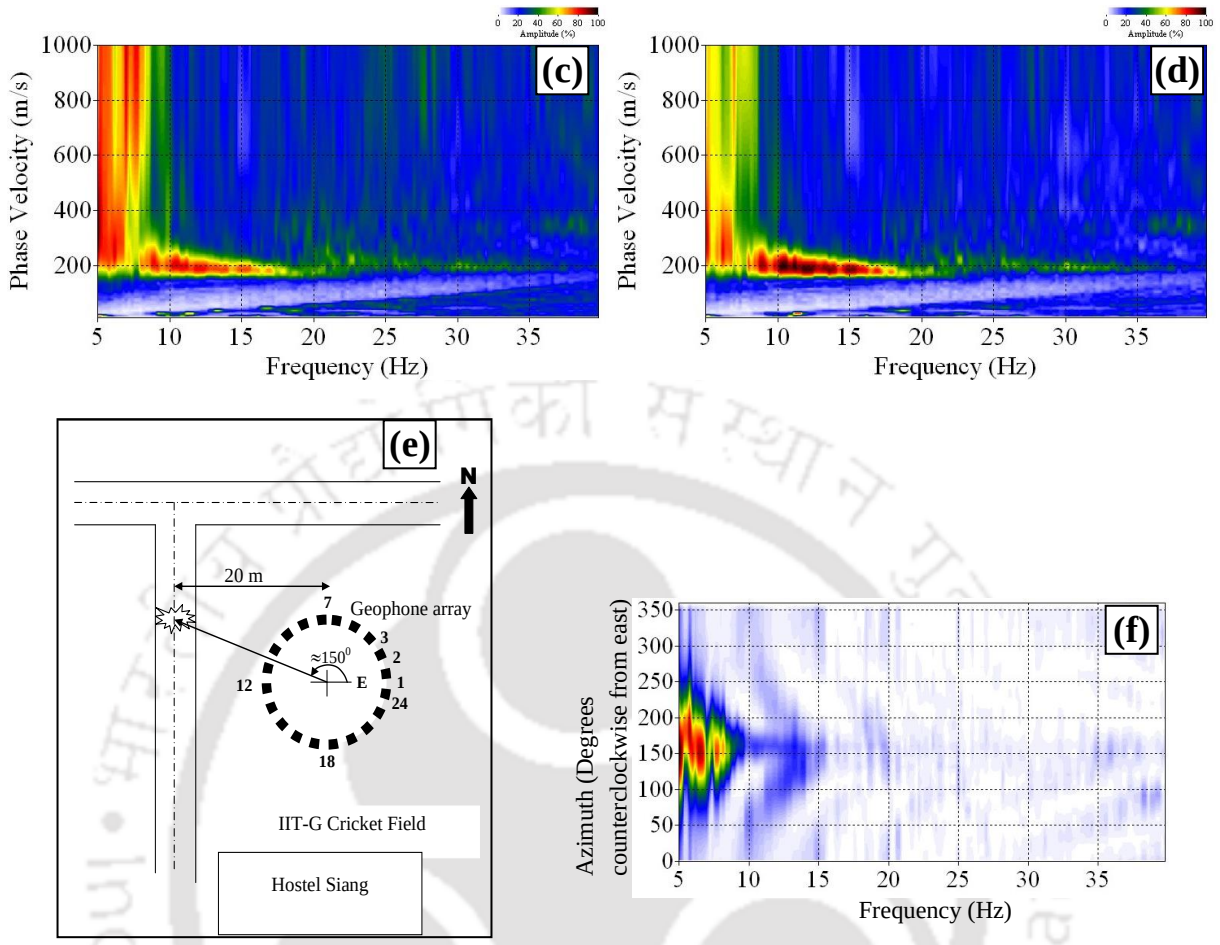

Fig. 7.2 (a) Schematic of source position with respect to the reciever array. (b, c, d) Dispersion images from azimuth scanning analysis in the NE-SE, SE-SW, and NW-SW quadrants, respectively (e) Schematic of Passive remote survey conducted at Site 1 for source detection (f) Azimuth v/s frequency space, showing position and energy of surface sources

With the aid of Passive Remote Survey, the exact azimuth detection of the major surface source was performed at the site, which also served as a validation of the current study. The schematic of the site with various details are presented in Fig. 7.2e. The test was conducted with a circular array of 18 m diameter placed at 20 m away from the centerline of the road. The placed source made an angle of approximately 150º to the center of the circular array, measured anticlockwise from east.

On processing the field data for detection of surface sources, majority of the surface waves shows their origin from the 150º position in azimuth-frequency space, as shown in Fig. 7.2 f. The dominant frequency band is observed in the range of 5-20 Hz.

The selection of the appropriate azimuthal scanning quadrant is site specific as it depends on the orientation of the layout of receiver array with respect to the adjacent road and the corresponding traffic movement. Selecting a pair of appropriate scanning quadrants comprising the major source of surface wavefield in passive roadside survey is found to be important during the dispersion analysis so that the directivity of the travelling signal can be properly incorporated to obtain the maximum propagating energy generated by the source, which would aid in obtaining a higher resolution dispersion image. For this careful consideration of appropriate orientation of receiver array with respect to the reference meridian is important.

7.4 Influence of Processing Schemes: IP, OP and OC

In passive roadside survey, the positions of the sources on the road surface do not qualify as a user-controlled parameter. However, this is the most critical parameter largely affecting the raw field records and the subsequent dispersion imaging. Depending upon the positions of the source, the wavefield recorded by the receiver array can be mainly of three types (Park and Miller, 2008): Inline Plane (IP), Offline Plane (OP) and Offline Cylindrical (OC). If a source is situated at a great distance from the receiver array and in-line with the alignment of the array, the wavefield recorded will be mostly of IP type with planar wavefront, and in such a case, the IP processing scheme is adopted (Park *et al*., 1998a; Louie, 2001; Park *et al*., 2004). This is an equivalent case to that of an active MASW survey when the records are collected having the source of impact placed at a large

offset. When wavefields are recorded from a distant source, but not in the same alignment with the receiver array, then the recorded wave signatures are OP nature. For such scenario, the OP scheme is generally adopted (Lacoss *et al*., 1969; Capon, 1969; Park *et al*., 2006). When the source is situated close to the receiver array, while not being in the alignment of the receiver array, then the wavefields recorded are of OC nature with cylindrical wavefronts (shown in Fig. 3.7 in Chapter 3). Under such conditions, the OC scheme is proposed to be adopted (Park *et al*., 2006; Park and Miller, 2008).

From the study of the raw field records in Chapter 5, it was not possible to classify the characteristics of the wavefield into IP, OP and OC. The records from the intra-line sources may result OP or OC nature of wavefield, although that too could not be classified in the earlier work. The dispersion analysis process that adopts the IP scheme is simpler, as it is similar to an active survey, and consumes significantly lesser amount of computation time.

In this section, the analysis of field data performed with the aid of IP, OC and OP schemes is reported, and the analysis results are mutually compared. For the study, three field situations were selected, as shown in Fig. 7.3, from Site 1 inside IIT Guwahati campus. In the first case, the field records were collected when a road surface source was placed at 20 m offset from the receiver array (possibly comprising IP type wavefield). In the second case, the records were collected from a source situated within the receiver spread, i.e., an intra-line source (possibly comprising OC type wavefield). In the third case, the records have been collected from the same intra-line source when the receiver array is at large offline distance of 15 m (possibly comprising OP type wavefield). While formulating analyzing schemes for passive roadside data with IP, OP and OC wavefields,

Park and Miller (2008) considered an outer-line source with different proximity to the receiver array (Chapter 3, section 3.5). However, in the current study, it was difficult to differentiate the wavefield type (as IP, OP or OC) arriving from an outer line source in the practical field conditions. Therefore, an attempt is made to simulate various conditions of the offline schemes (particularly OC and OP), the intra-line source is used.

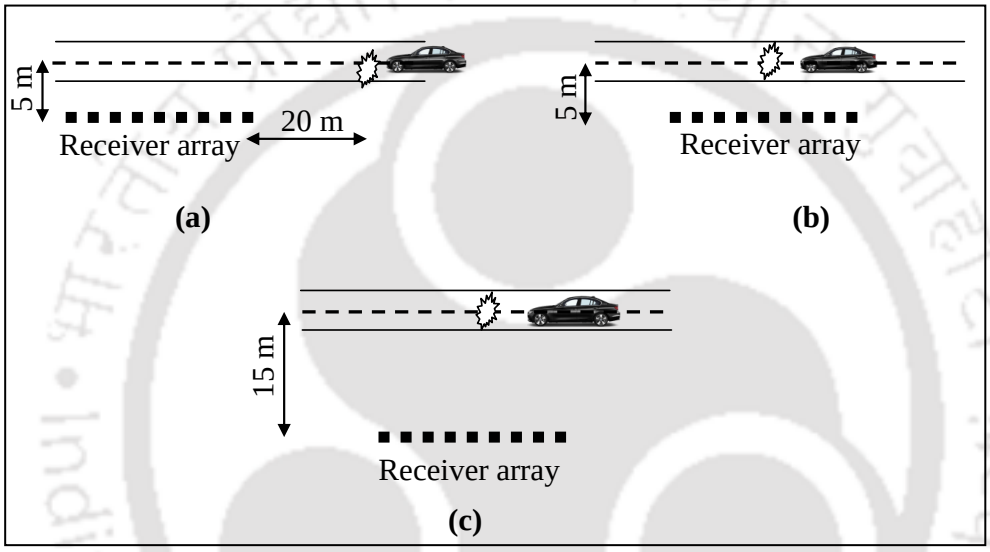

Fig. 7.3 Three different types of field set up for analysis of raw data simulating (a) IP (b) OC and (c) OP waves

In Fig. 7.4, the dispersion images are shown for the records obtained from the situation of an IP type of wavefield arrival (i.e., as per Fig. 7.3a). The record was analyzed with both IP and OC processing scheme in the SurfSeis platform. During roadside analysis, the offline distance takes account of both OP and OC scheme and is used as a source function. Unlike an OC scheme, to simulate the situation of an ideal inline case (as in active survey), during the processing with IP scheme, the offline distance of receiver array from the centerline of the road is not accounted (accordingly, a value of 0 is selected). The final dispersion images from both the processing

techniques shows a notable difference in their resolution. The image obtained from OC scheme (Fig. 7.4a) has more distinct energy peaks compared to the other case, i.e., IP scheme. Further, during dispersion curve selection from the dispersion image generated using IP scheme (Fig. 7.4d), it is observed that the phase velocity are slightly in the higher side as compared to that obtained from OC scheme (Fig. 7.4c), particularly in lower frequency band. It is worth mentioning that the dispersion curve selection made in both the cases has high (approximately 1) and nearly identical SNR values.

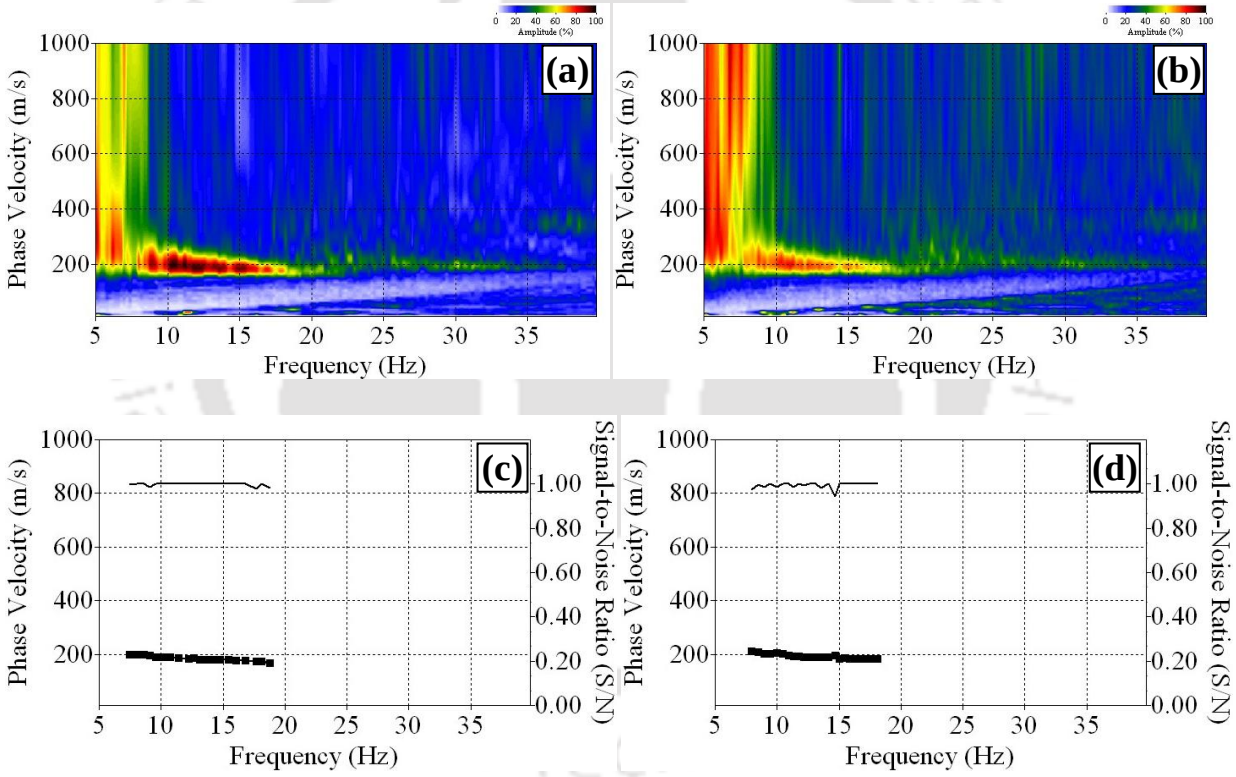

Fig. 7.4 Dispersion image, and the corresponding extracted disperion curves,obtained from the wavefield generated by an approximately aligned source at 20 m offset using (a,c) OC scheme (b,d) IP scheme

In the second case, the study was conducted to check the effect of IP and OC processing schemes for the records obtained from an intra-line source (Fig. 7.3b) from the same site with same geometrical and recording parameters. The final dispersion images from the two schemes are shown in Fig. 7.5. The energy band obtained in case of IP scheme is much broader than the OC scheme. In addition, the energy peaks in the lower frequency band is found to be comprising of much higher phase velocity ranges. The dispersion curve constructions for the two cases, IP and OC, (Fig. 7.5 c and 7.5d, respectively) clearly indicate higher phase velocities when processed with IP scheme.

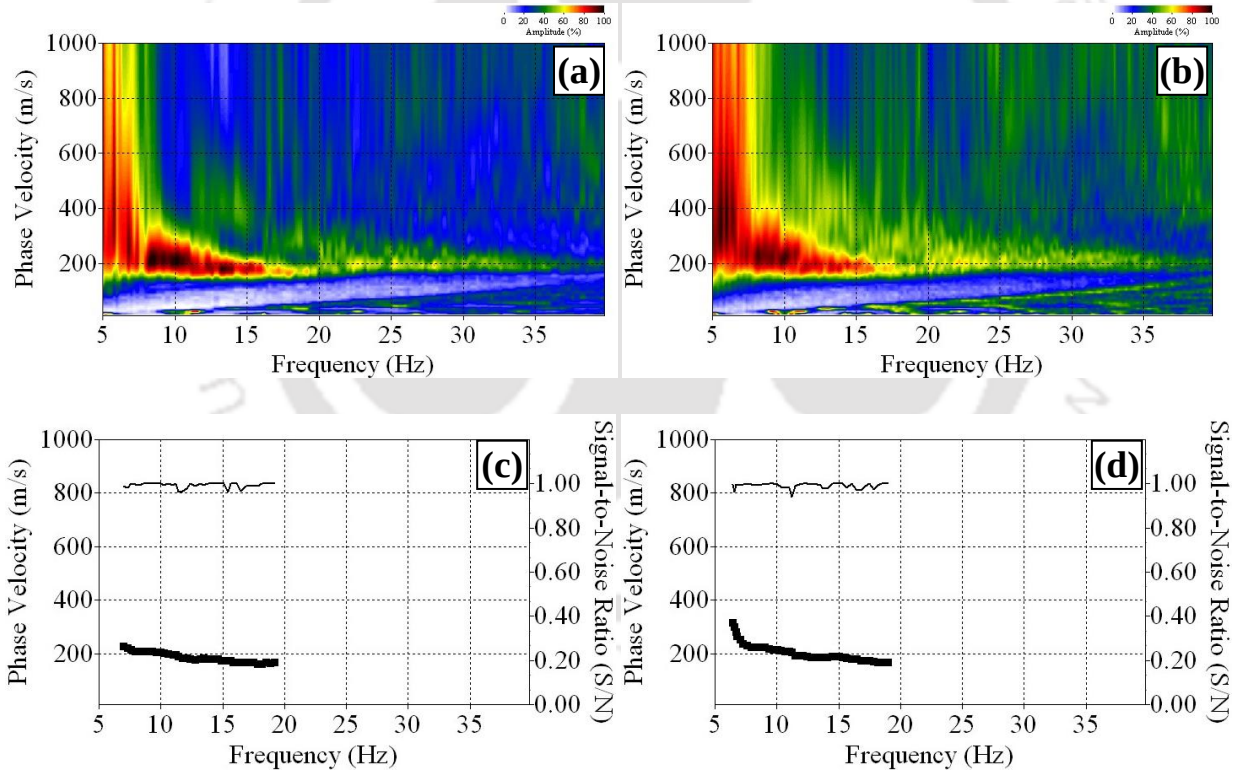

Fig. 7.5 Dispersion image, and the corresponding extracted disperion curves, obtained from the wavefield generated by an intra-line source, at an offline distance of 5 m, using (a,c) OC scheme (b,d) IP scheme

When the receiver array is placed at higher offline distance of 15 m from the centerline of the road (as shown in Fig. 7.3c), the recorded wavefield has greater possibility of being an OP type. As shown in Fig. 7.6a and 7.6b, both the dispersion images obtained using IP and OP scheme exhibited poor resolution at lower frequencies, which is mainly attributed to the remoteness of the sources of wavefield generation from the receiver array. The corresponding extracted dispersion curves are shown in Fig. 7.6c and 7.6d, in which it can be observed that the SNR values are nearly 1 for both the extracted curves, thereby depicting the precision of the selection. However, the phase velocity exhibited in the dispersion curve extracted with IP scheme (Fig. 7.6d) is observed to be marginally higher than that obtained with OP scheme (Fig. 7.6c). Rather, in all the comparisons with IP scheme (Figs. 7.4-7.6), it is observed that the IP scheme provided marginal higher phase velocity values, the distinction being more in the lower frequencies, although all the dispersion curves were extracted with SNR nearly equal to 1. Similar observation is also reported in earlier researches (Park *et al*., 2006; Park and Miller, 2008). Based on the observations, it can be stated that IP scheme of dispersion analysis can be suitably adopted to extract the dispersion curve in various cases of intra-line and outer-line sources, located at different offline distances from the receiver array. Such an adoption may result in marginally higher phase velocities in the lower frequencies, while at the higher frequencies, the difference with the dispersion curves obtained through OC and OP is negligible. Hence, from a practical consideration, the application of OC and OP scheme should be adopted for those site-specific conditions where there is an appreciable difference in the dispersion curve obtained using different schemes.

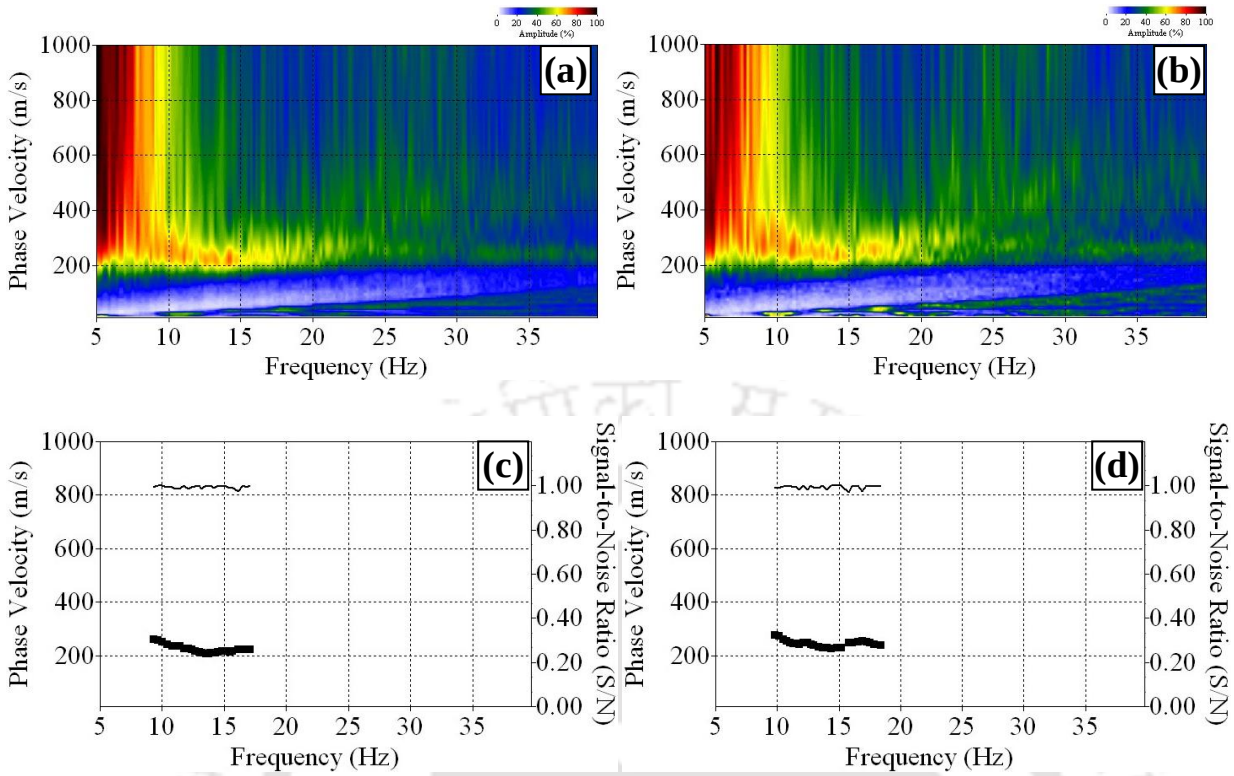

Fig. 7.6 Dispersion image, and the corresponding extracted disperion curves, obtained from the wavefield generated by an intra-line source, at an offline distance of 15 m, using (a,c) OP scheme (b,d) IP scheme

7.5 Enhancement of Resolution of Dispersion Imaging by Vertical Stacking

In all seismic surveys, the primary objective of data acquisition is to obtain an enhanced Signal-to-Noise Ratio (SNR) of the recorded data, which is often hindered by several practical limitations and infeasibilities. However, different types of experimental and/or theoretical techniques can be adopted to enhance the SNR of recorded signal. This can be achieved either by reducing the level of the noise, or by increasing the level of the signal. By acquiring the data during quiet times (e.g., at night) or by using better equipment with a lower inherent noise level, the reduction in noise level can be achieved. On the other hand, increasing the signal level can be achieved by increasing

the energy of the source. However, without opting for the above two experimental solutions, an alternative easier approach, known as vertical stacking, can be very useful in enhancing the SNR of the recorded data. Vertical stacking is primarily the summation of multiple synchronised repetitions of the test data. Normally, vertical stacking increases the SNR by the square root of the number of repetitions (Foti *et al*., 2014). **Vertical stacking** is a technique that enhances the SNR by summing the signals for a number of shots recorded by the same array configuration of the geophones (identical field layout, offline and offset distances). In passive roadside MASW survey, vertical stacking has been utilised successfully in some of the recent studies (Park and Miller, 2008). However, a comparative analysis on the effect of number of vertical stacking on dispersion images has not been reported in the literatures until date. In this study, based on Passive roadside MASW tests conducted at all the three test sites, a detailed comparative analysis has been conducted to illustrate the effect of different numbers of vertical stacking on the resolution of dispersion images. Various geometrical and recording parameters utilised for the detailed comparison of number of vertical stacking is shown in Table 7.1.

Table 7.1 Details of the parameters involved at the three sites for the study of vertical stacking

Site	Receiver array length (m)	Acquisition time (s)	Nature of Traffic volume	Number of Vertical stacking performed
Site 1: Inside IIT Guwahati Campus	46	10.8	Thin	1-15
Site 2: IIT Guwahati to Amingaon road	46	1.4	Medium	1-20
Site 3: Beside NH31	46	1.4	Thick	1-20

In the SurfSeis platform, vertical stacking can be performed mainly by two methods, which are described as follows:

- **Method I**: In this method, all the field records, collected using the same geometrical array shapes and dimensions, are selected in one single file. After setting the requisite geometrical parameters for the composite file, it is processed for dispersion imaging. The process internally develops dispersion images for each of the raw records (called as overtone record or OT) constituting the composite file, and finally generates one resultant vertically stacked dispersion image.
- **Method II**: In this method, each raw record are separately processed for obtaining the individual dispersion images, which are finally combined to form the superposed dispersion image. However, each summation has to be conducted separately and hence the method consumes more computational time.

7.5.1 Applicability of Method I for Vertical Stacking

7.5.1.1 Optimum Vertical Stacking for Light Traffic Site (Site 1)

The detailed study on vertical stacking is conducted on the records collected from the light traffic prevalent at Site 1 i.e., the site inside IIT Guwahati campus. Field records were collected considering the parameters mentioned in Table 7.1. The results shown in Fig. 7.7 are from a source existing outside the receiver array (i.e., outer-line source) at an offset of 20 m. It is observed from the dispersion images (Fig. 7.7) that vertical stacking helps in significantly improving the resolution of the dispersion image obtained from passive data. A dispersion image without vertical stacking shows a very indistinct energy band (Fig. 7.7a) which is not useful for selecting a continuous and regular dispersion curve. Upon increasing the number of stacking, the resolution

of dispersion images continuously increases. Various numbers of stacking has been used in the study, ranging from 1-15. It is observed that 10 numbers of stacked sample shows a better dispersion image than the others generated with lesser numbers of stacking. With further increasing in stacking, an insignificant enhancement in the resolution of dispersion image is observed. The dispersion curves are extracted from each of the analysed dispersion image and are processed for inversion to further study the effect of vertical stacking on the resultant V_s profile. In each case, the dispersion curves were extracted with greatest possible SNR values (approximately 1) and having identical frequency range (i.e., 6.82 – 19.76 Hz). The frequency range is selected on the visibly most dominant part in the fundamental-mode dispersion energy band. For each inversion, maximum number of iterations and minimum RMS value of 20 and 1 m/s have been assigned respectively. The resultant V_s profiles from each of the dispersion curve, produced from different number of vertical stacking, are shown in Fig. 7.8a. A reference V_s profile obtained from an active survey with the same field set up is also included in Fig. 7.8a for better comparison. It is observed that except for the V_s profile obtained from the dispersion image with 3 vertical stacks, the other profiles matches closely with each other and also with the V_s profile from active survey. The percentage difference between each V_s profile obtained from different number of vertical stacking are also compared with the V_s profile obtained from 15 numbers of stacks (Fig. 7.8b). The V_s profiles from 5, 10 and 12 stacks dispersion images are observed in vicinity to the 0-difference line. Figure 7.8c shows a characteristic plot depicting the convergence in the shear wave velocity with the numbers of vertical stacking. It is observed that there exists a well-defined convergence in the shear-wave velocity as the average difference reduces to marginal values with higher numbers of vertical stacking. The near-asymptotic nature of the plot indicates no detrimental impact of over-stacking of data.

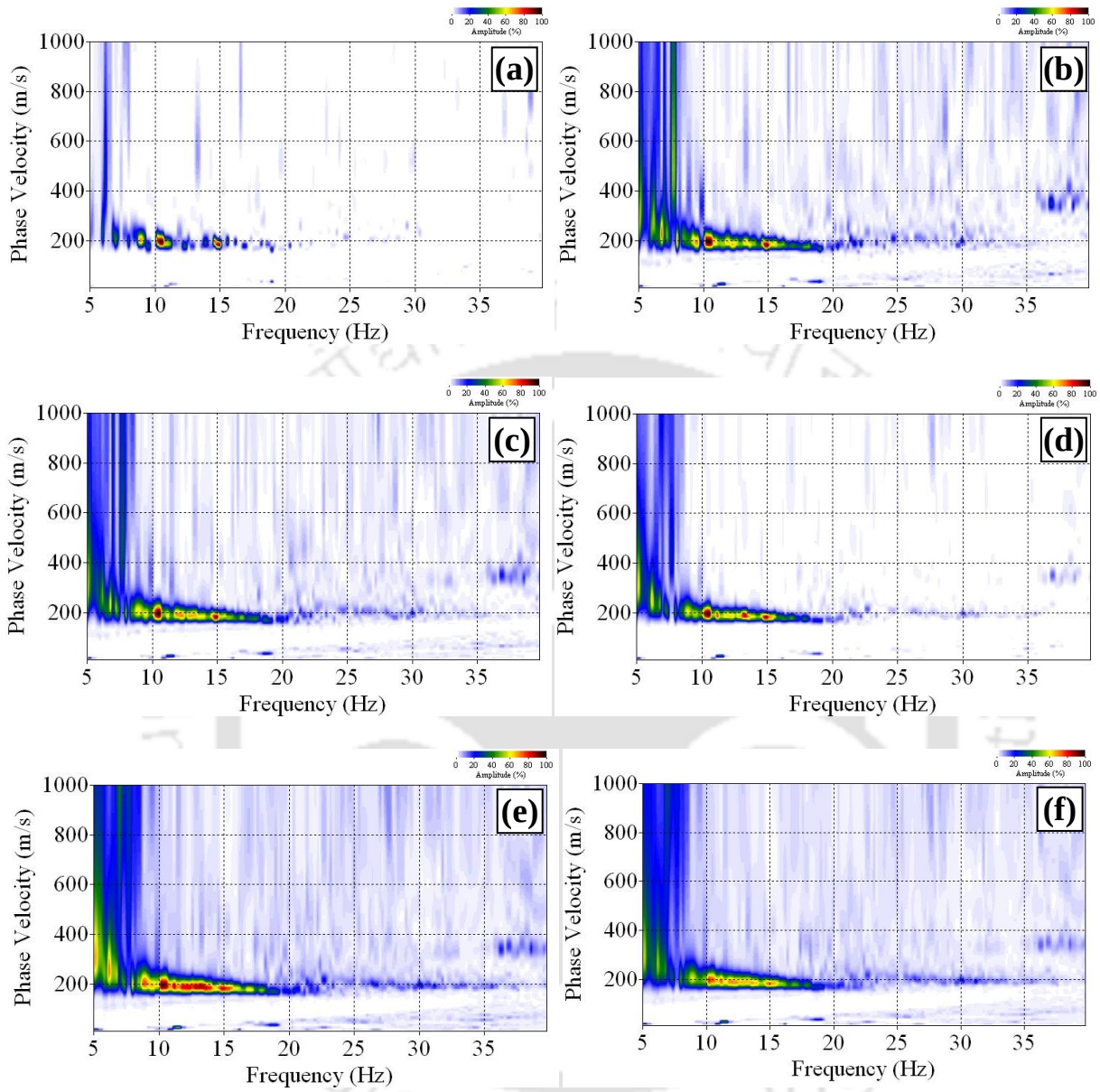

Fig. 7.7 Dispersion images obtained for Site 1 records using outer-line source with 20 m offset and varying numbers of vertical stacking (a) zero (b) 3 (c) 5 (d) 10 (e) 12 (f) 15

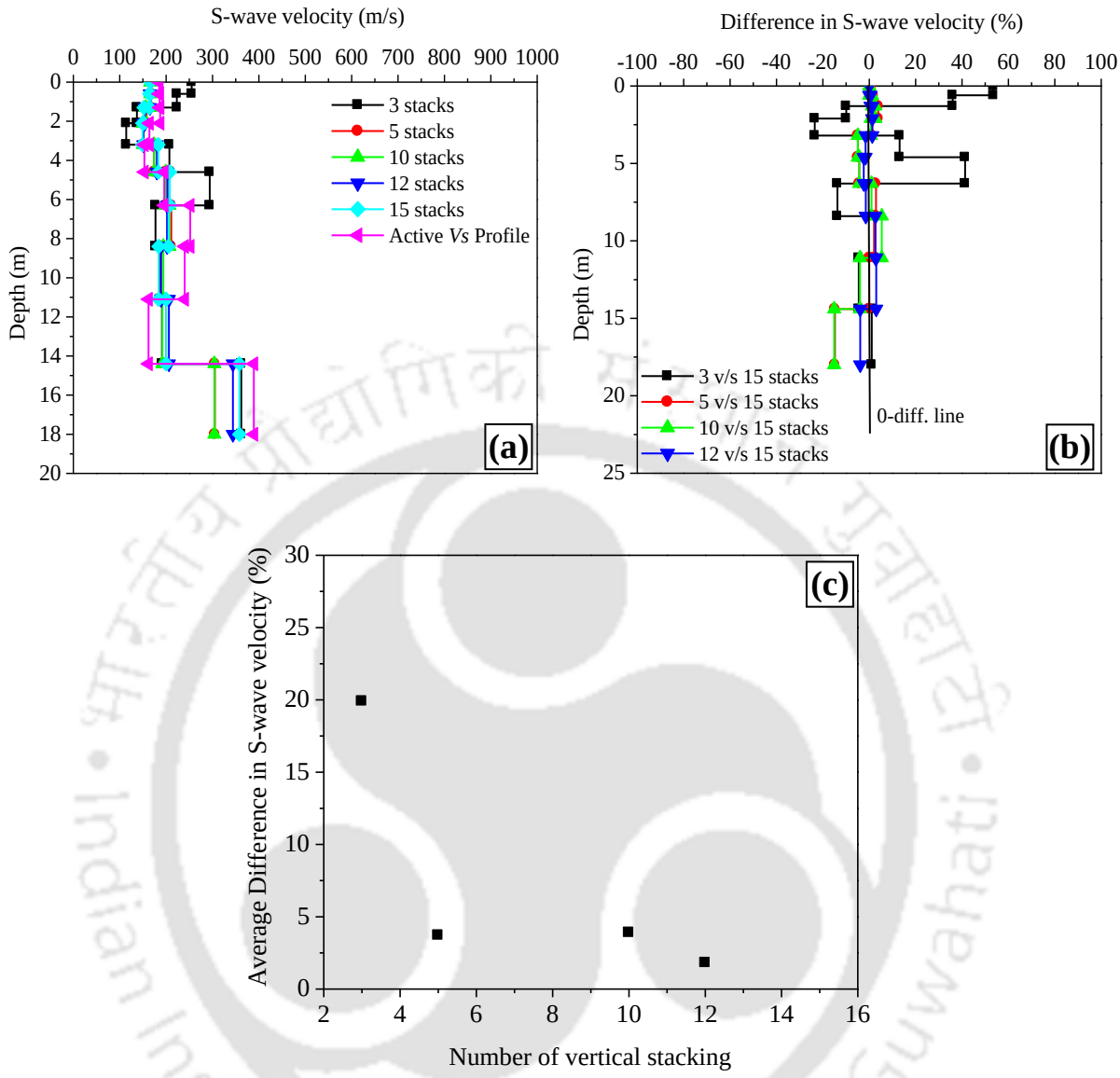

Fig. 7.8 (a) Shear wave velocity profiles obtained from passive roadside survey with an outer-line source with varying numbers of vertical stacking (b) Percentage difference in shear-wave velocity profiles with respect to the same obtained from 15 numbers of vertical stacking (c) Convergence of shear-wave velocity pattern with varying number of vertical stacking

Fig. 7.9 demonstrates the application of vertical stacking on the records obtained from an intra-line source at Site-1. Much similar to the previous case, significant improvement in the resolution of dispersion images with increasing in the number of vertical stacking is noticed in this case as well. Attributed to the benefits of existence of intra-line source, significant resolution enhancement is witnessed in the lower frequency band as well. Figure 7.10a shows V_s profiles obtained from dispersion images with varying number of vertical stacking, along with a reference V_s profile from active survey. The V_s profiles obtained from 10, 12 and 15 stacked are observed to be in close agreement with the V_s profile obtained from active survey. The V_s profiles obtained from 3 numbers of vertical stacking deviates significantly from the other profiles. The deviation is distinctly observed in the Fig. 7.10b, with a highest deviation as much as 110 % in the depth range of 7.5-10 m. The characteristic plot depicting the convergence of shear-wave velocity profiles with varying number of vertical stacking (Fig. 7.10c) has a similar trend as that of the outer-line case.

Fig. 7.11 presents the efficacy of vertical stacking when there is simultaneous existence of both intra-line and outer-line source positions, thereby creating multiple surface wave events upon the passage of vehicles. In such multiple occurrence of surface waves, vertical stacking can effectively enhance the resolution of dispersion image. Existence of the pair of sources also helped in obtaining fair resolution dispersion images even with lesser number of vertical stacking (Fig. 7.11a-7.11c). With higher numbers of stacking, there is further improvement in the dispersion image resolution; although there is no noticeable difference in the dispersion image resolution beyond 10 numbers of vertical stacking (Fig. 7.11d- 7.11f).

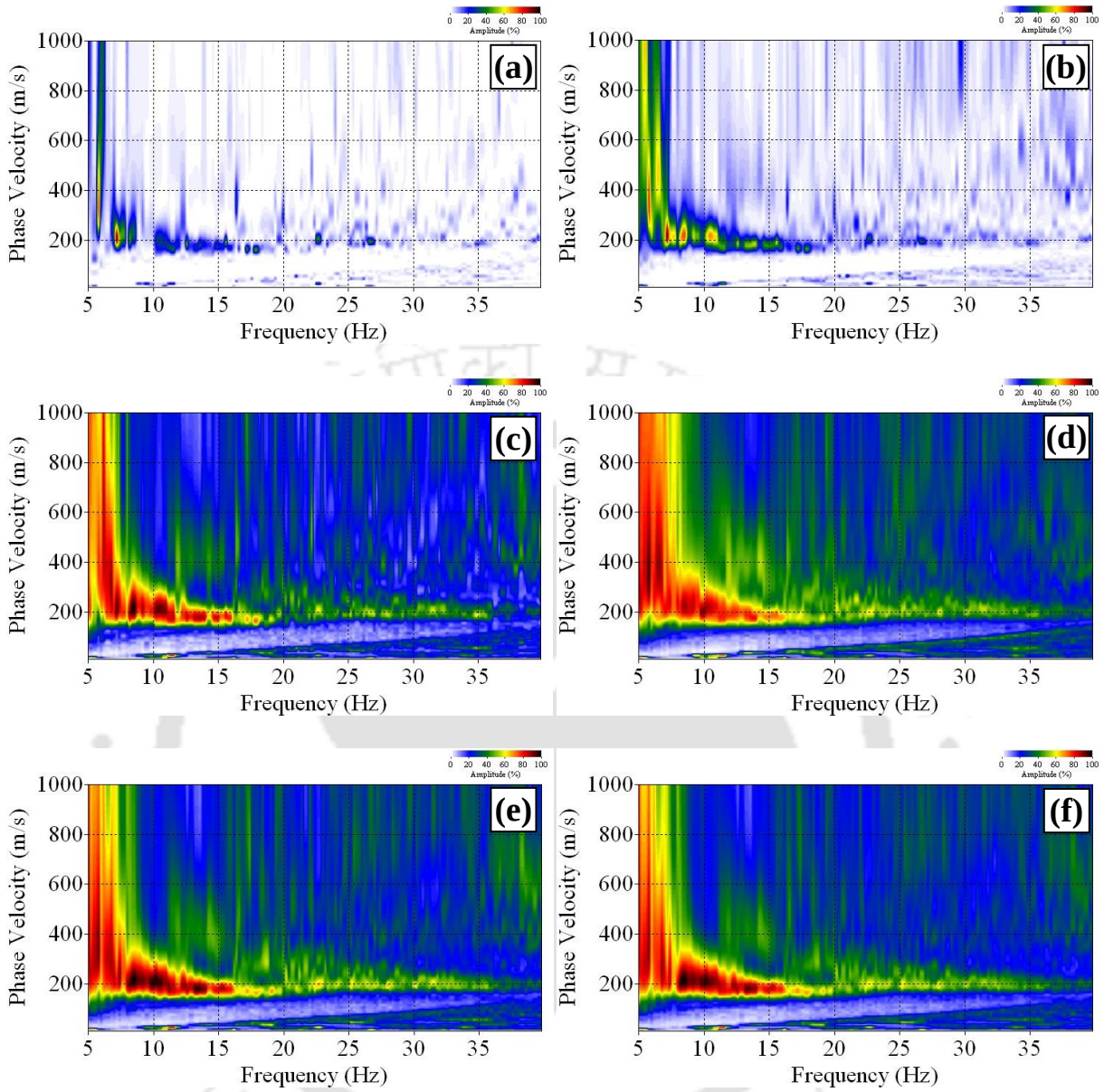

Fig. 7.9 Dispersion images obtained for Site 1 records using intra-line source and varying numbers of vertical stacking (a) zero (b) 3 (c) 5 (d) 10 (e) 12 (f) 15

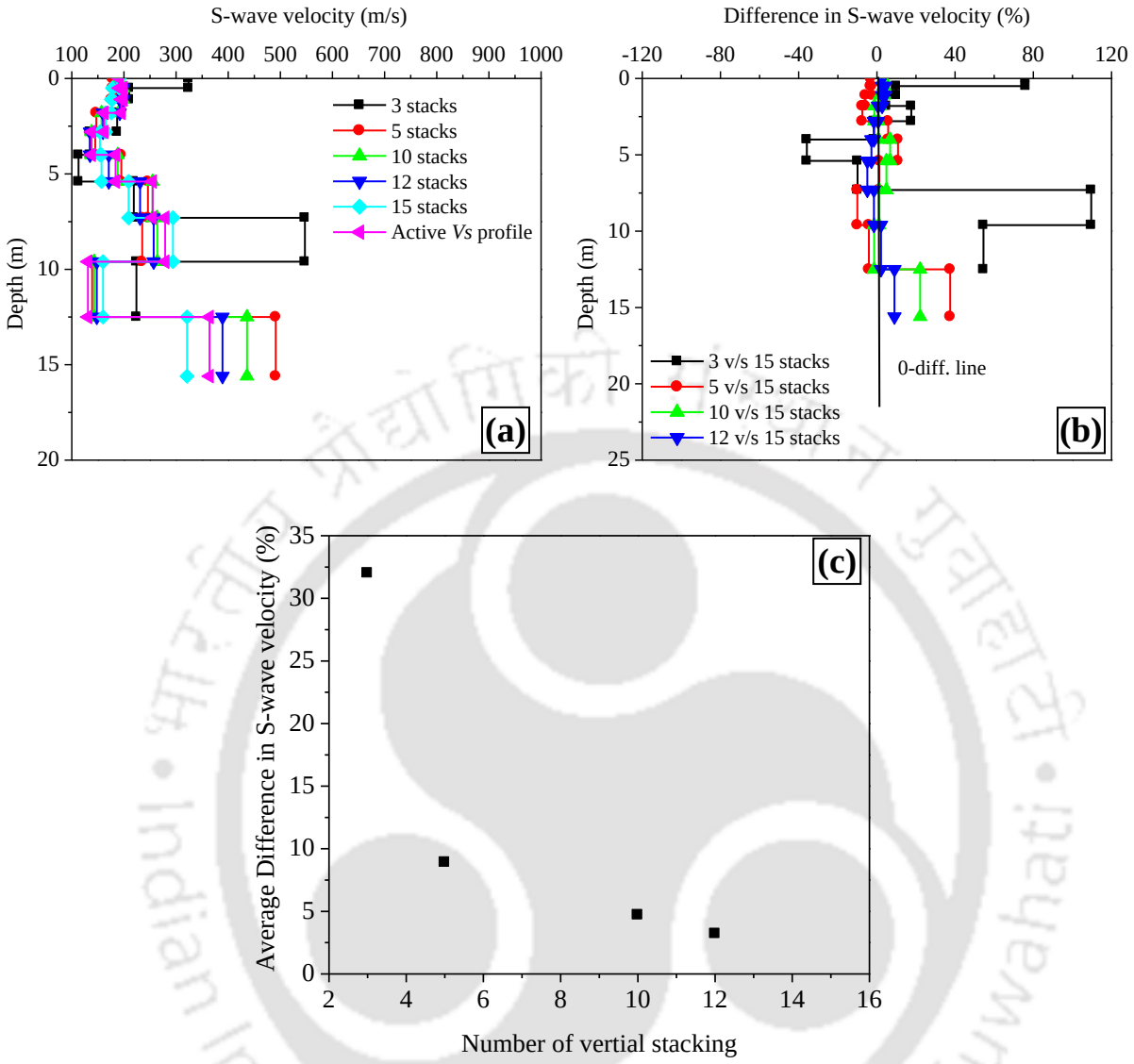

Fig. 7.10 (a) Shear wave velocity profiles obtained from passive roadside survey with an intra-line source with varying numbers of vertical stacking (b) Percentage difference in shear-wave velocity profiles with respect to the same obtained from 15 numbers of vertical stacking (c) Convergence of shear-wave velocity pattern with varying number of vertical stacking

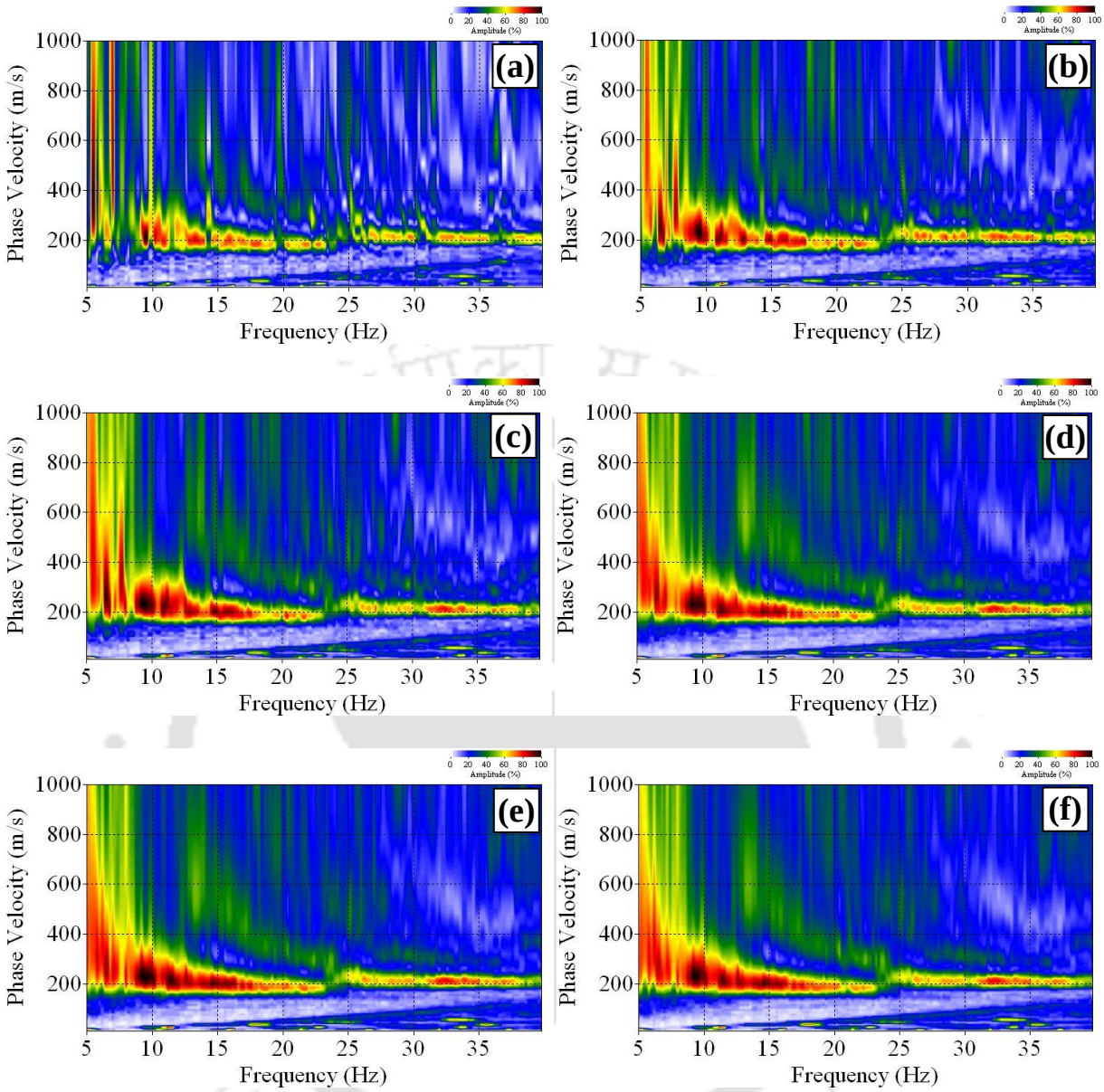

Fig. 7.11 Dispersion images obtained for Site 1 records using both outer-line and intra-line sources, along with varying numbers of vertical stacking (a) zero (b) 3 (c) 5 (d) 10 (e) 12 (f) 15

The shear-wave velocity profiles resulting from dispersion images with 10, 12 and 15 numbers of vertical stacking shows identical results (Fig. 7.12a). The V_s profile from dispersion images with 3 and 5 numbers of vertical stacking shows a maximum deviation of 65% and 20%, respectively, when compared to the V_s profile pertaining to the dispersion image with 15 numbers of vertical stacking (Fig. 7.12b). The characteristic plot depicting the convergence of shear-wave velocity profile with varying numbers of vertical stacking (Fig. 7.12c) show a similar trend as earlier cases. For all the three cases of intra-line and outer-line sources considered, no detrimental effects of overly stacking are observed. In all these three mentioned situations of different source mechanism in the traffic controlled site of IIT Guwahati campus, the optimum vertical stacking number is found to be 10, beyond which further addition of stacking have insignificant effect on improvement of the resolution of dispersion image.

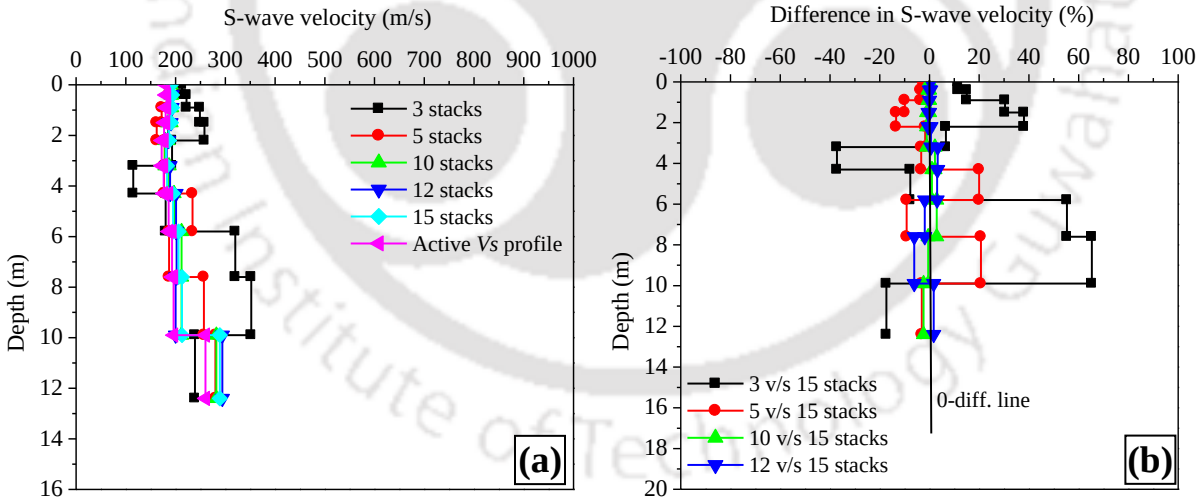

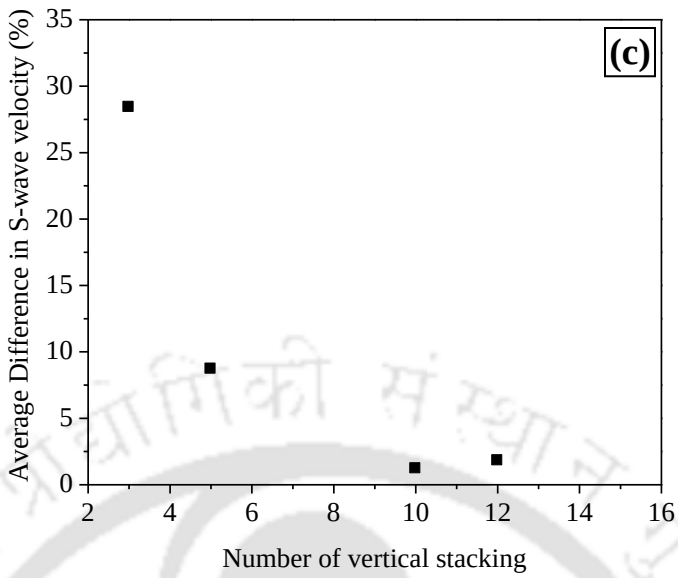

Fig. 7.12 (a) Shear wave velocity profiles obtained from passive roadside survey with simultaneous intra- and outer-line source with varying numbers of vertical stacking (b) Percentage difference in shear-wave velocity profiles with respect to the same obtained from 15 numbers of vertical stacking (c) Convergence of shear-wave velocity pattern with varying number of vertical stacking

7.5.1.2 Optimum Vertical Stacking for Medium Traffic Site (Site 2)

The study on vertical stacking was further carried on field data recorded from Site 2, i.e., at the IIT Guwahati to Amingaon route. The site was dominated by an average traffic flow and was suitable for roadside survey. The field data have been recorded as per the parameters mentioned in Table 7.1. Dispersion images with various numbers of stacking have been shown in Fig. 7.10. Continuous improvement of dispersion image resolution with increasing number of stacking can be observed.

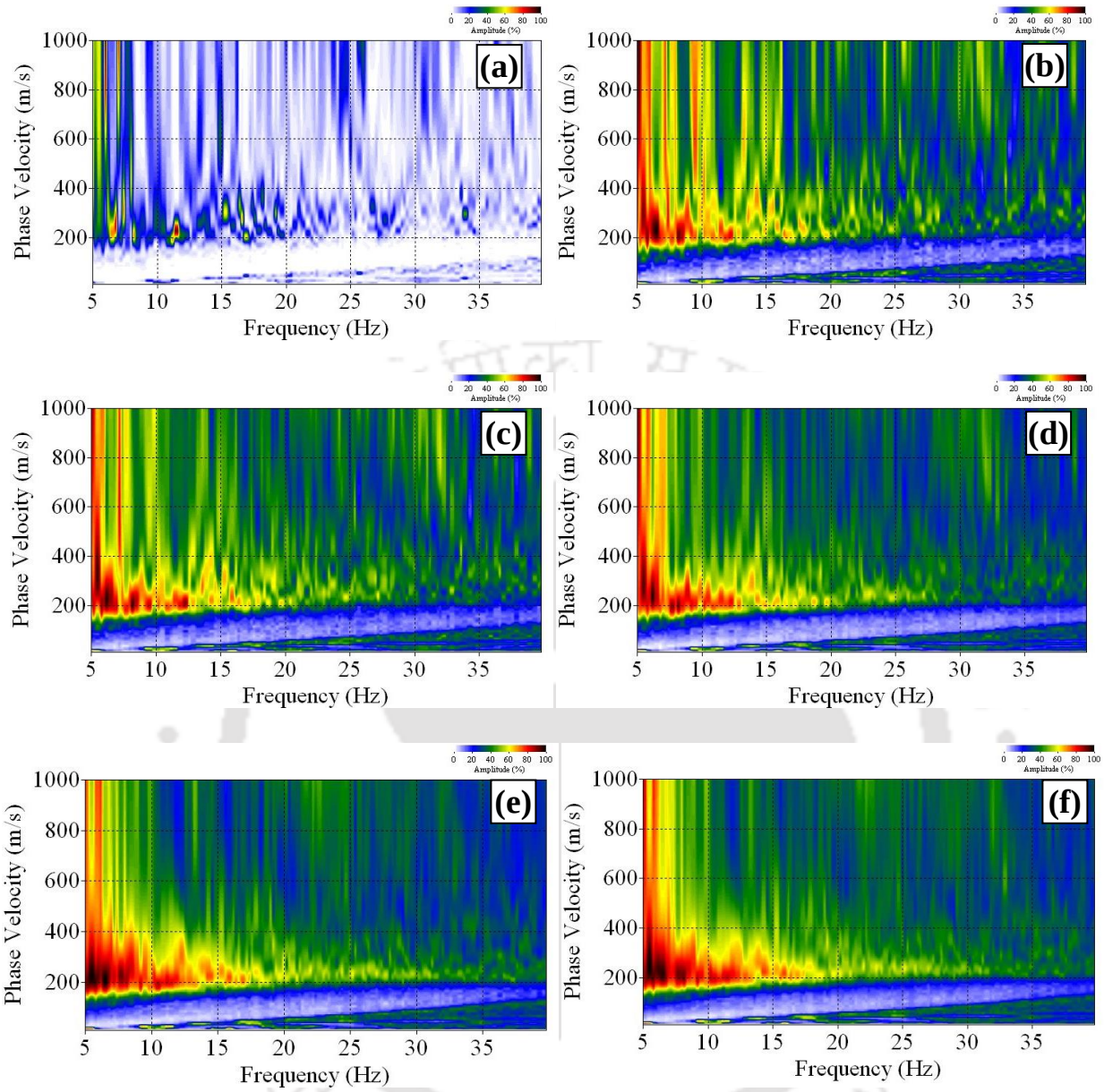

Fig. 7.13 Dispersion images obtained for Site 2 records using varying numbers of vertical stacking (a) zero (b) 3 (c) 5 (d) 10 (e) 15 (f) 20

In spite of recording a fair amount of surface signals in each record, single data, without vertical stacking, could not provide sufficient information of the dispersive properties of the surface waves, as illustrated in Fig. 7.13a. Extraction of an appropriate dispersion curve from the image was not possible due to the irregular and scattered energy bands. With mere increase in vertical stacking

in ranges of 3 to 5 numbers, resolution of dispersion image showed significant enhancement. A maximum of 20 numbers of stacking was applied for the data obtained from this site. It can be observed from the images that with higher number of stacking, the unnecessary energy bands of the dispersion image reduce and the fundamental mode dispersion band becomes prominent. Qualitatively, it is observed that there is no significant improvement in the resolution of the dispersion image beyond 15 numbers of vertical stacks. Similar results on the convergence of the shear wave profiles for increasing vertical stacking was observed for this case as well; however, to avoid repetitive results, the same is not presented herein. The comparison of the shear wave velocity profile obtained from dispersion curve extracted from 15-stack dispersion image and that obtained from active MASW survey is already presented in Fig. 6.7 of Chapter 6, which shows reasonable agreement between the two profiles.

7.5.1.3 Optimum Vertical Stacking in Heavy Traffic Site (Site 3)

In both of the above-mentioned sites (Site 1 and Site 2), the major surface wave sources were present in the form of road surface irregularities, as can be observed in the raw field records already presented earlier in Chapter 5. Attributed to the major surface events created by vehicles passing over those sources, wavefields of strong amplitudes were produced. However, in the Site 3, the nearby road was composed of nearly plane surface without any major sources present on it. In such cases, the optimum number of vertical stacking is expected to be different depending upon the existence of number of major surface wave events in the records.

The field parameters for the study was adopted as mentioned in Table 7.1. The dispersion images with varying number of vertical stacking is presented in Fig. 7.14. In this case, the minimum

number of vertical stacking required for an informative dispersion image is found to be 20. As observed in Chapter 5, the raw field records from the site is vastly filled with surface wave events from the movement of numerous vehicles on the road. However, in none of the field records, a distinctive surface event could be observed. Moreover, in many records, the wavefields were superimposed onto each other, thereby deteriorating the overall quality of the field record. Therefore, a comparatively higher number of dispersion image stacking is found to be required in this case. The comparison of the shear wave velocity profiles obtained from dispersion curve extracted from 20-stack dispersion image and that obtained from active MASW survey is already presented in Fig. 6.12a of Chapter 6, which shows reasonable agreement between the two profiles.

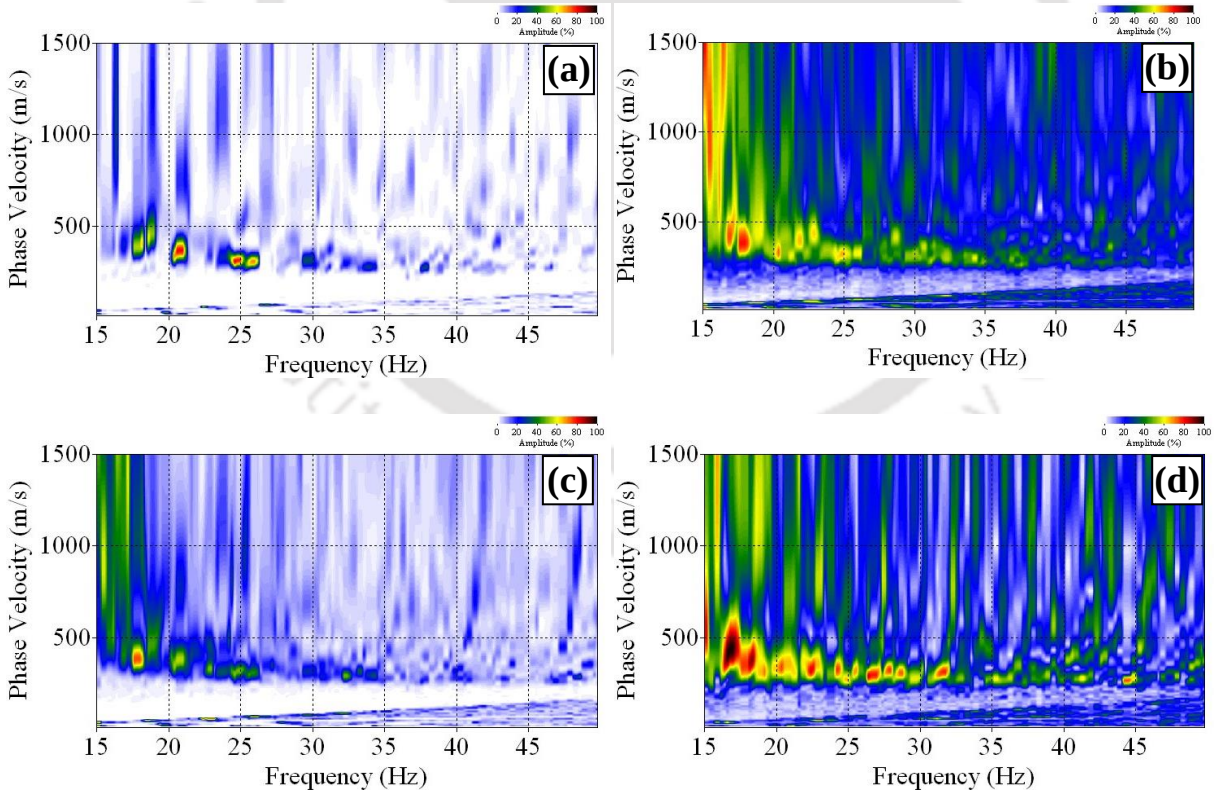

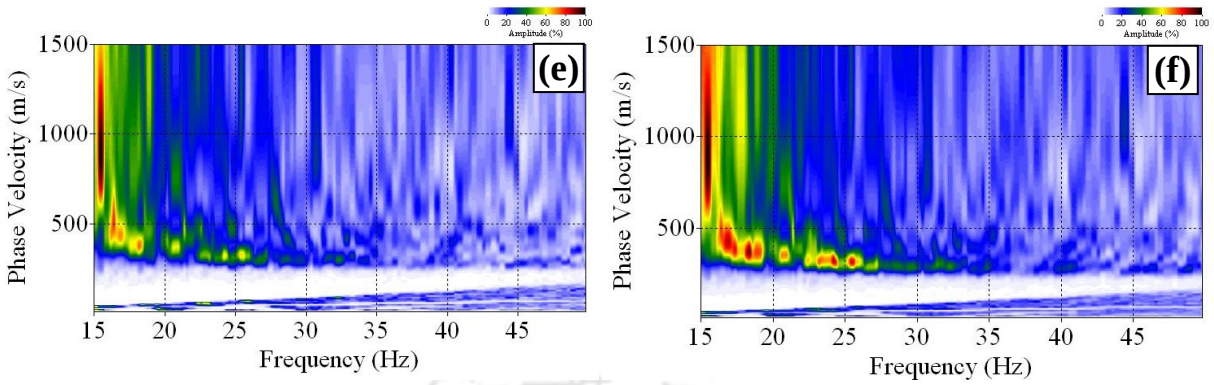

Fig. 7.14 Dispersion images obtained for Site 3 records using varying numbers of vertical stacking (a) zero (b) 3 (c) 5 (d) 10 (e) 15 (f) 20

7.5.2 Applicability of Method II for Vertical Stacking

From the previous section, it was found that for an effective utilisation of Method I for vertical stacking, there should be at least 10-20 numbers of raw field records collected from the site. However, at many sites, particularly in the busy urban areas, it may not be always possible to collect large number of records by spending large amount of investigation time. At such instances, when lesser number of field data are available from a particular site, Method II for vertical staking may be suitably utilised. This section evaluates the effectiveness of Method II for vertical stacking on the resolution of dispersion image.

For the study, field records were collected from Site 1 inside IIT Guwahati campus, using the parameters mentioned in Table 7.1. Two good quality field records, generated by using intra-line source, were selected to apply both the methods of stacking. The dispersion images from these individual raw records are shown in Fig. 7.15a and 7.15b. Although both the images show distinct dispersion energy band, they lack in continuity over the intermediate frequencies. Following Method II, both the dispersion images are stacked vertically to generate the resultant dispersion

image as shown in Fig. 7.15c. For the sake of comparison, similar stacking has been achieved using Method I and the resulting dispersion image is shown in Fig. 7.15d. Attributed to the clear and distinct energy band, the results show that the vertically stacked dispersion image obtained with the aid of Method II yields slightly better results as compared to that obtained by utilizing Method I. The mechanism of stacking significantly improves frequency band of the image in the range of 7-20 Hz. Moreover, the resultant energy band also possesses better continuity in comparison to the band obtained using Method I. A distinct and continuous dispersion energy band helps in the construction of a continuous dispersion curve with high SNR and comprising sufficient number or density of dispersion points, which is essential for obtaining a reliable V_s profile. The details of this aspect are described in Chapter 8. However, it is to be noted that the stacking process also adds other energy accumulations from the two parent images and leads to higher mode contamination, as marked by the oval shape in Fig. 7.15c. On the other hand, vertically stacked dispersion image obtained via Method I (Fig. 7.15d) exhibited little improvement with respect to the two parent images. Although comparatively distinct, the stacked image still shows the lack of continuity between 7-15 Hz frequencies and continues to illustrate less resolution in the higher modes, as observed in the parent images. A comparison of the Figs. 7.15c and 7.15d highlights that even though the adoption of Method II yielded a better resolution dispersion image with a relatively distinct dispersion band, it may be noted that there is insignificant improvement in the energy content in low frequencies lesser than 7 Hz. Hence, it is expected that if a careful extraction of dispersion curve were carried out, the subsequent inversion analysis would not yield a significantly different shear-wave velocity profiles. The same is reflected in the V_s profiles depicted in Fig. 7.16, which shows nearly similar profiles obtained by applying both techniques of stacking. Hence, although Method II improves the resolution of dispersion image and aids in easy

recognition of the dispersion band (even with lesser numbers of stacking), the method does not extra edge Method I in obtaining the V_s profile.

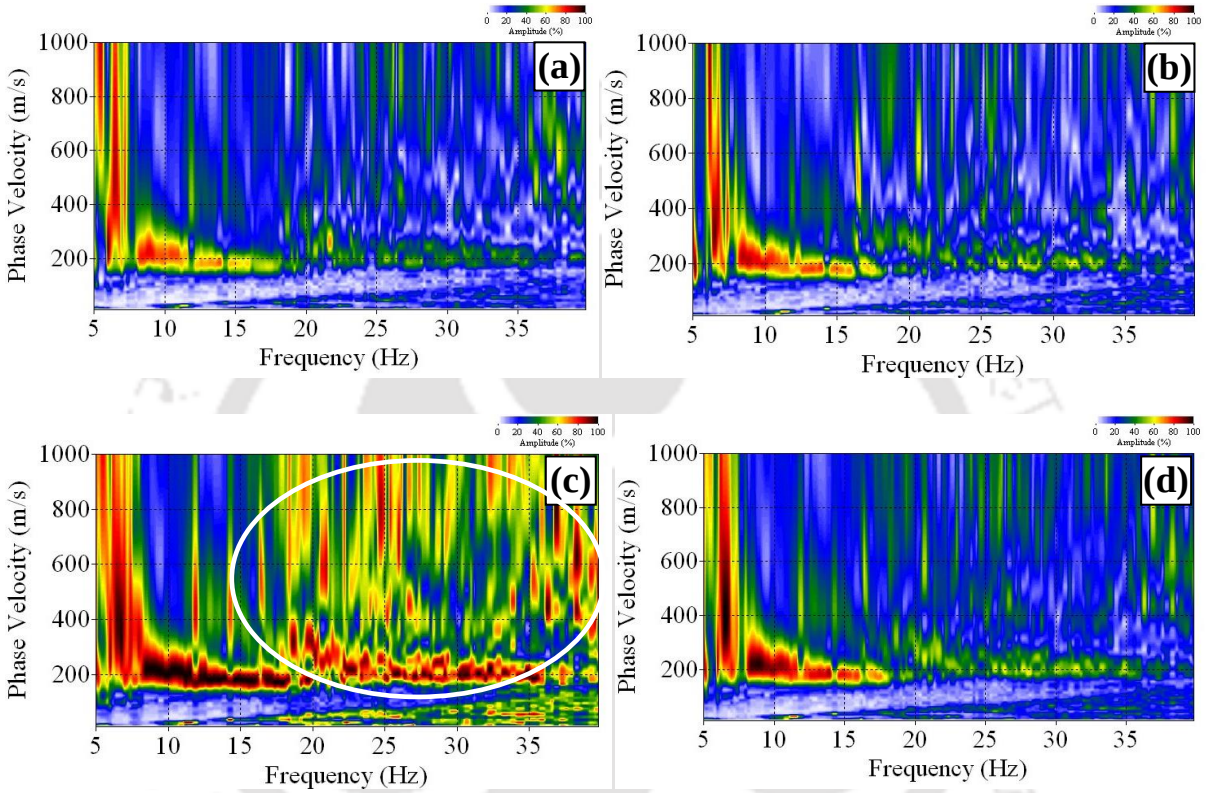

Fig. 7.15 (a and b) Two mutually independent and selected good quality dispersion images obtained using intra-line source at Site 1 (c and d) Vertically stacked dispersion image obtained using Method II and Method I, respectively

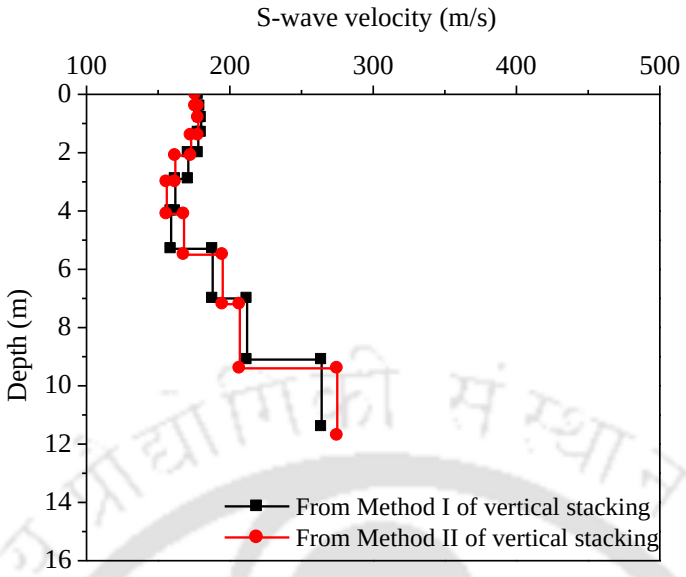

Fig. 7.16 Shear wave velocity profiles obtained from dispersion images produced from an intra-line source and processed through Method I and Method II of vertical stacking

As has been described for intra-line sources, similar exercise have been carried out with the application of the two methods of dispersion image stacking using the results from outer-line sources at the Site 1, utilizing the same geometrical configuration and layout of the array. Following Method II, Fig. 7.17a shows the stacked dispersion image obtained by combining three individual dispersion images from separate field records. It can be observed that the image has a good resolution, distinctly portraying the dispersion energy band spread over a substantially wide frequency range. Some higher energy modes are also nearly recognisable from the image. On the other hand, following Method I, Fig. 7.17b shows a dispersion image by the stacking of 10 raw data gathered from the same set of field experimentation programme (stacking of same mid-station overtones). It can be clearly noticed that this dispersion image is poorer as compared to that produced by Method I stacking procedure. No proper dispersion energy band is visible, especially in low frequency regions, while the higher order dispersion modes are beyond recognition. As for

the earlier case, the shear-wave velocity profiles, obtained from the dispersion images for outer-line sources, stacked using the two different techniques, are presented in Fig. 7.18. Similar to the observation in the previous section, the inferences about the application of the two methods of stacking remains the same.

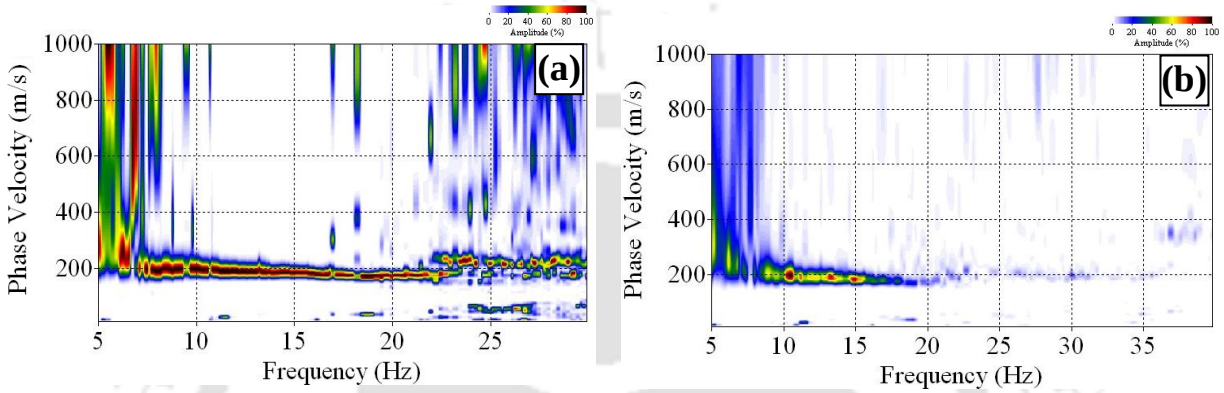

Fig. 7.17 Vertically stacked dispersion images based on wavefield data collected at Site 1 using outer-line source (a) Method II stacking (b) Method I stacking

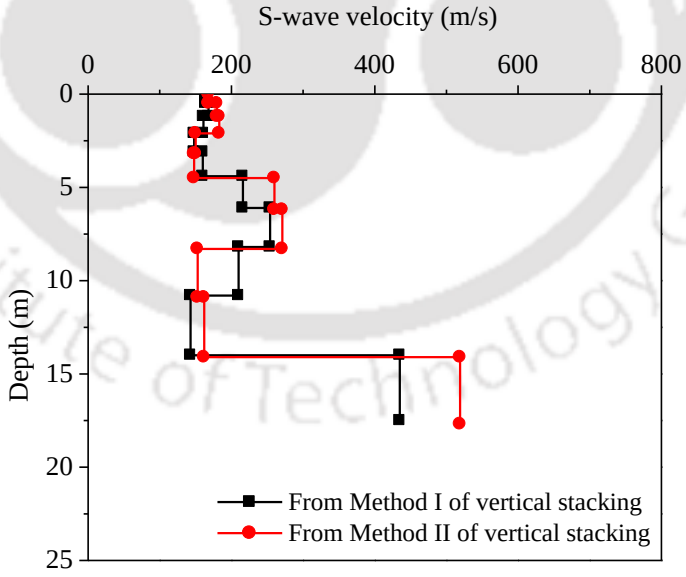

Fig. 7.18 Shear wave velocity profiles obtained from dispersion images produced from an outer-line source and processed through Method I and Method II of vertical stacking

7.5.3 Combined Application of Method I and Method II Stacking of Dispersion Images

In the previous section, the effectiveness of both methods of vertical stacking (Method I and Method II) applied on two separate set of field records, collected from different positioning of the major surface source (intra-line and outer-line), has been evaluated. Although Method II is identified as the superior of the two methods, the resolution in lower frequency ranges in the vertically stacked dispersion images, obtained from any of the two techniques, is not utilizable enough. In this section, another attempt to improve further the resolution of the dispersion images, by combining both of the two above-mentioned methods of vertical stacking in a sequential and systematic order, has been reported. Figure 7.19 provides a typical illustration of the same. Firstly, 15 field data, collected separately using intra-line and outer line sources, have been categorically subjected to Method I stacking. The final dispersion images generated using intra-line and outer-line sources are portrayed in Fig. 7.19a and 7.19b, respectively. The record obtained using intra-line source position showed a slightly better outcome than that obtained using outer-line source position, especially in the lower frequency regions (between 8-12 Hz). The two overtone images are then further stacked by Method II stacking to generate the final dispersion image, as shown in Fig. 7.19c. Thus, the final dispersion image is the result of the combination of two separate passive sources. It can be clearly noticed that the final dispersion image has a significantly improved resolution over a wide frequency band (5-20 Hz), with substantially better resolution manifested at the lower frequency ranges (5-10 Hz). Similar results are obtained with the vertical stacking applied over several such other datasets; however, each of them are not reported herein. These observations clearly highlights that combination of different passive sources (including both intra-line and outer-line sources) and utilizing a sequential application of two different methods of

stacking will be effective in generating a good resolution wide-band dispersion trends. This technique would effectively serve for the proper extraction of dispersion curve, and further determining the best-suited subsurface profile. Figure 7.20 shows the shear wave velocity profiles obtained from the dispersion images shown in Fig. 7.19. It can be clearly noticed that the depth of investigation improves when the combined stacking is considered on the dispersion images obtained from intra and outer-line sources. This is primarily attributed to the fact that the dispersion image obtained using combined stacking (Fig. 7.19c) exhibits better resolution and recognizable dispersion band even at lower frequencies, which was not exhibited in Figs. 7.19a and 7.19b.

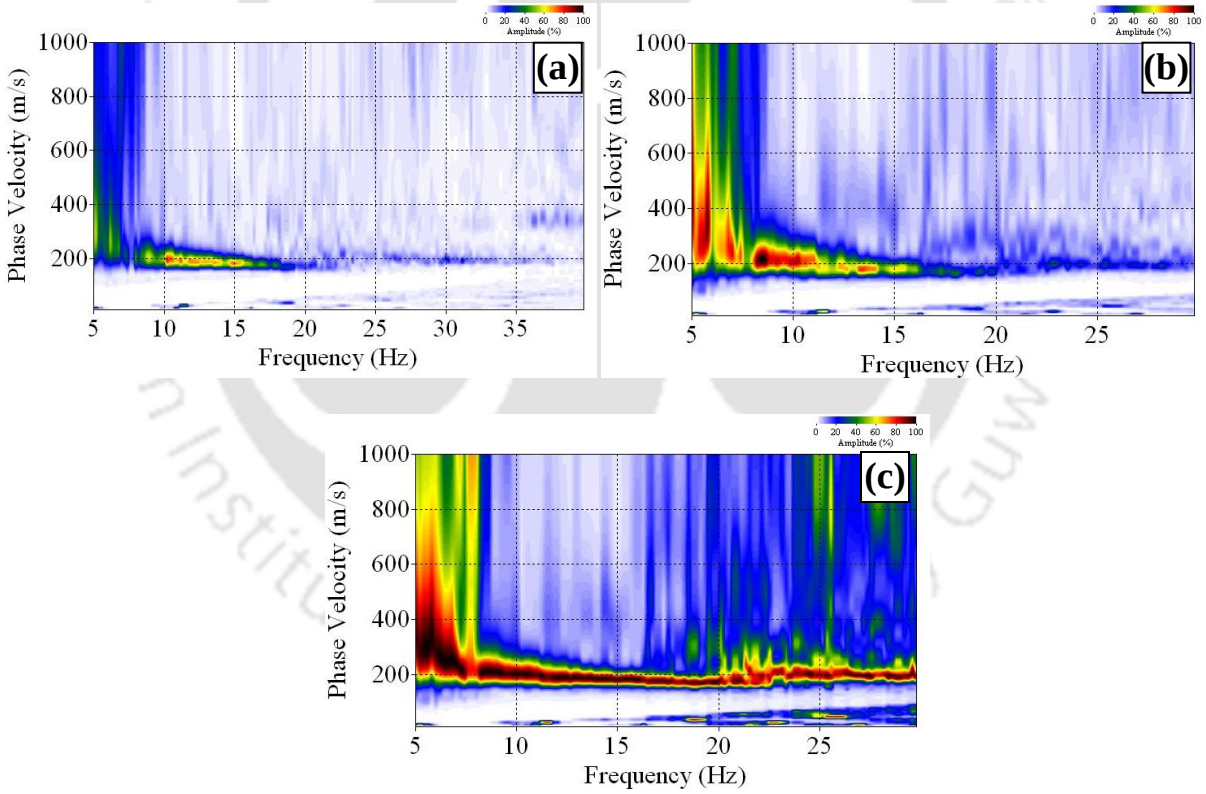

Fig. 7.19 Vertically stacked dispersion images obtained using Method I stacking of (a) 15 field data with outer-line source, and (b) 15 field data with intra-line source (c) Vertically stacked dispersion image obtained by combining (a) and (b) using Method II stacking

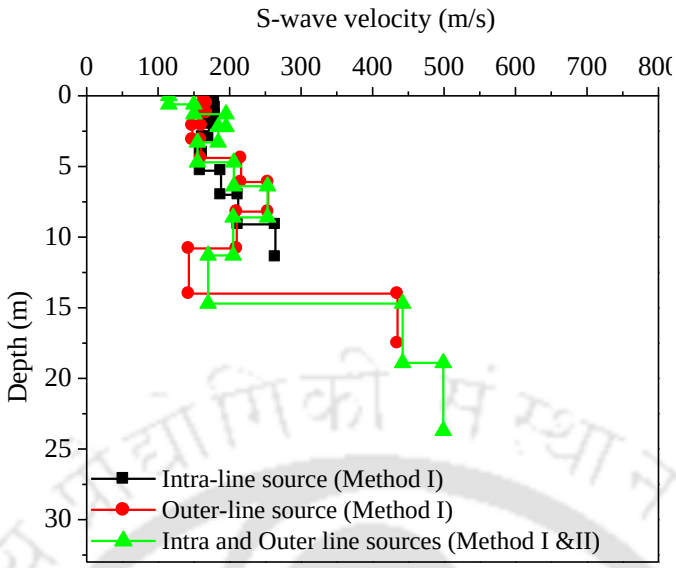

Fig. 7.20 Shear wave velocity profiles obtained from vertically stacked dispersion images produced from individual outer-line and intra-line source through Method I stacking of 15 field datasets, as well as that obtained from the combined dispersion image obtained through vertical stacking by Method II

7.6 Summary

Implementing optimum processing parameters during dispersion analysis is imperative in obtaining dispersion images with high resolution. Setting of the optimum scanning ranges of frequency and phase velocity, during dispersion analysis, helps in enhancing the resolution of dispersion image by discarding contaminating energy bands. In the current study conducted at various locations, the phase velocity range of the subsurface is found to pertain to a range of 50-1500 m/s. An appropriate selection of azimuthal quadrants allow identifying the directions of major wavefield sources, thereby leading to accurate computation of energy along azimuth axis and leading to a resultant dispersion image with substantially better resolution. A wrong selection of quadrant does exactly the otherwise, with no energy peaks being distinct enough. Offline

distance of receiver array is a site parameter, but its use in the dispersion imaging process governs the choice of the processing scheme to be adopted during the dispersion analysis. It is observed that even for a long distance outer-line source with 20 m offset, the two processing schemes namely IP and OC results in dispersion image with different degree of resolution, the latter being the superior. The energy peaks in the dispersion image obtained from IP scheme are relatively indistinct, though there is insignificant difference in the extracted dispersion curve in terms of phase velocity and frequency ranges (which is user dependent). A closely situated intra-line source (with offline distance of 5 m) results in dispersion image with significantly different energy bands when processed with IP and OC schemes. The width of energy band, in case of IP image, is much larger, compared to the OC image. Moreover, the extracted dispersion curve in IP image exhibits a higher range phase velocity as compared to the same obtained using OC scheme. Similar observations are also noticed during the comparison of dispersion images produced using OP and IP scheme. Overall, the study suggests the need of furnishing precise offline distance during dispersion imaging, and choosing an appropriate scheme for the analysis of the result.

Vertical stacking is an advantageous method for the enhancement of dispersion image resolution, especially in passive MASW survey. At sites comprising light and medium traffic volume, 10 numbers of vertical stacking (using Method I) is found to be sufficient, primarily attributed to the acquired non-contaminated field records. However, for the site comprising heavy traffic volume, the required number of vertical stacking is found to be 20 due to the contaminated field records and absence of major surface events. Thus, optimum vertical stacking depends upon raw field records containing major surface event, without which mere increase in number of stacking is not effective. When raw field records acquired from a site is less in numbers, the vertical stacking may

be achieved by Method II, in which individual dispersion images are stacked onto each other. The method holds good particularly when field records are of superior quality. In another study, combined application of Method I and Method II stacking of dispersion images has shown encouraging results. In this part, intra-line and outer-line source originated dispersion images are first stacked with Method I, and the resultant two images are then stacked with Method II to get final image of superior quality.

CHAPTER 8

OPTIMUM SELECTION OF DISPERSION CURVE AND INITIAL MODEL FOR RELIABLE INVERSION ANALYSIS

8.1 Introduction

An important objective of subsurface investigation programmes is to obtain deeper subsoil information with precision. A passive MASW survey is an easier method (in terms of field logistics) that can provide greater investigation depth compared to the conventional borehole and other surface wave techniques. As learned from the literature survey, passive MASW survey, in principle, utilises larger receiver array to record wavefield of long wavelength and, hence, can yield greater investigation depth. However, it was reported in Chapter 6 that in case of passive roadside MASW survey, a mere deployment of longer array may not always be sufficient for the attainment of greater investigation depth, and the same depends upon other factors such as the type of travelling vehicles, presence of major road surface sources and the inherent characteristics of subsoil. In addition, the maximum attainable depth is a function of the resolution of lower frequency band of the dispersion image, which aids in selecting dispersion points in lower frequency region with precision. During the inversion process, the maximum depth that can be evaluated is approximately one-half of the longest wavelength in the recognised dispersion curve. A dispersion curve is nearly independent of the changes in material properties below this depth. However, it should be noted that an accurate and optimum selection of points of the dispersion curve, particularly, in the lower frequency regions, is not easy, attributed to its comparatively larger thickness in most of the obtained dispersion images. A thicker energy band in a dispersion image

raises the probability of selecting an apparent dispersion curve with larger deviation from an actual curve, thereby leading to an erroneous final V_s profile.

8.2 Influence of the Frequency Band of Selected Dispersion Curve

It was observed in Chapter 6 that the first dispersion point selected on the lowest frequency region of the dispersion curve governs the maximum investigation depth. As from the elementary relationship of surface wave, i.e., $\lambda=c/f$, the first point in the lowest frequency region, also being the point of highest phase velocity, is directly related to the longest wavelength of the traversing wave. In this section, the influence of dispersion points, selected from varying lower frequency ranges, on the investigation depth and the stability of the inversion analysis (in terms of RMS error) will be presented.

Figure 8.1 exhibits the dispersion images obtained from field records at Site 1 by using a 46 m receiver array with 24 numbers of receivers and inter-receiver spacing of 2 m. All the raw records were collected based on an acquisition time of 10.8 s, which was sufficient for the occurrence of multiple passive surface events by vehicular movements through the receiver array. The dispersion images, shown in Fig. 8.1, were obtained by stacking 10 dispersion images obtained from 10 individual field records. In the images, the fundamental and first higher order modes are visibly distinct, while the second higher order mode can be barely spotted. In the figure, based on the same dispersion image, four different dispersion curve selections are shown, each beginning at different initial points of phase velocity and frequency. The line connecting the white dots on the dispersion image represents the dispersion curve, while the black dashed line at the top of the figures represent the Signal-to-Noise ratio (SNR) of the selected points. Normally, SNR value close to "1" implies

an appropriate selection of dispersion points, each point having an energy close to the peak of the spectral maxima, which can be visually deduced from the colour map of the image. Dispersion curves, in all the cases, were carefully chosen as per the darkest colour region at every frequency point, so the peak energy points may be captured. Darker side of the colour map represents the energy closer to the peak of the energy band, while the lighter side of the map represents progressively higher deviation from the peak energy spectra. The accuracy of the choice is ascertained by crosschecking the SNR obtained at each of the frequency points. The higher the value of SNR for the selected dispersion curve, the more accurate is the selection. For all the cases of dispersion curve selection from the dispersion image, the overall SNR of the extracted dispersion curve is maintained to be approximately equal to 100% (with meagre tolerances), thereby indicating the superior extraction of the dispersion curve based on visual identification.

In all the cases of dispersion curve selection shown in Fig. 8.1, the highest frequency bound was kept constant at 23 Hz and lower frequency bound was varied from 5.6-12.5 Hz. This strategy was adopted to study the enhancement in the subsurface investigation depth with the lowering of the lower frequency bound, as well as to illustrate its influence on the stability of inversion analysis. In Fig. 8.1a, the selection of dispersion points ranged between 12.5-23 Hz. The energy band, between the adopted frequency ranges, is distinct and thinner compared to other frequency ranges of the image, thereby rendering the extraction of dispersion curve with comparative ease. Accordingly, as shown in Fig. 8.1b, 8.1c and 8.1d, the selection of dispersion curve was initiated from the lower frequencies of 10 Hz, 7.6 Hz and 5.6 Hz, respectively. It can be observed that the energy band in the lower frequency regions has a larger width, as compared to the thin band in the range of 12.5-23 Hz. The dispersion image did not reveal any distinguishable energy peaks in the

frequencies lower than 6.5 Hz and, thus, the selection of dispersion curve between 5.6-6.5 Hz (Fig. 8.1d) was carried out solely based on observed high SNR values. A dispersion image may not show distinguishable energy peak due to several reasons related to the various parameters of the survey conducted, as well as the source and receiver characteristics. However, as already mentioned, the lowest distinguishable frequency is not necessarily restricted by the natural frequency of the geophone. Further, in this study, a 4.5 Hz geophone was used, which, by definition, should have given distinguishable energy peak at least until 4.5 Hz, which was not the case. Such scenarios of indistinguishable dispersion image, recorded from passive roadside survey, can also possibly occur due to the soil profile itself and its influence on the propagating wavefield. Such conditions are beyond the control of the user, and hence, the target of the dispersion analysis should be to extract the dispersion curve as best as possible from the obtained dispersion image. For this reason, it is stated that if the energy peaks are not so easily distinguishable beyond a certain frequency, the extraction of the dispersion points should be solely guided by the SNR of the chosen point (Foti *et al*., 2014) , and the same has been adopted in the present study.

As reported already in Chapter 3, the inversion process in Surfseis is based on the local search algorithm proposed by Xia *et al*. (1999). The process adopts one initial multi layered earth model comprising six parameters, namely: Depth, Thickness, V_s, V_p, Poisson's ratio and Density (Table 8.1). The initial V_s model is approximated from the measured i.e., selected dispersion curve. The initial V_p is then constructed from the approximated V_s model by assuming a constant value of Poisson's ratio of 0.4. In all the layers of the earth model, density is assigned in a constantly increasing value ranging approximately from 1.55 gm/cc at the first layer to 2 gm/cc at the last layer (half space). The maximum investigation depth is obtained from the longest wavelength of

the surface wave from the measured dispersion curve. The thickness of different strata in the model, either in variable or in uniform mode, is constructed based on the maximum investigation depth. The algorithm utilises these set of parameters to search for the most probable solution (i.e., a theoretical dispersion curve) for the most probable input values in an iterative procedure by continuous convergence. Importantly, among all the mentioned parameters, shear wave velocity is the only parameter that significantly influences the sensitivity of fundamental mode dispersion curve (Xia *et al.*, 1999).

For the inversion of the selected dispersion curves, as reported above, initial earth layer models, with varying numbers of layers, were chosen for all the cases. For dispersion curve with frequency ranges of 12.5-23 Hz, 10-23 Hz, 7.6-23 Hz and 5.6-23 Hz, the number of layers in the initial earth models were selected to be 9, 10, 12 and 14, respectively. The selections of the different numbers of layers adopted for the varying frequency range were based on the possible maximum depth of investigation indicated by the selected dispersion curve for each case. The maximum depth of investigation (z) is governed by the maximum wavelength (λ) propagating through the soil medium, which, in turn, depends on the frequency (f) and the phase velocity (φ_v) of the initial point chosen for the selected dispersion curve. Such a strategy was adopted so that the final V_s profiles obtained from the inversion analysis are comprised of layers having equal or comparative thickness, irrespective of the total depth of investigation. The thicknesses of the layers in the model were chosen to be a variable parameter to incorporate maximum tolerance and release the constraint from the iterative inversion scheme. For a dispersion curve selected within the frequency range 12.5-23 Hz, the initial model, with all its layer parameters, is shown in Table 8.1. Similarly, Tables 8.2, 8.3 and 8.4 lists the initial models and its layer characteristics for the dispersion curves

selected in the frequency ranges of 10-23 Hz, 7.6-23 Hz and 5.6-23 Hz, respectively. There are two stopping criteria required to be set during the inversion processing, namely (a) minimum value of RMS error that automatically stops the iterations as soon as the magnitude is reached, and (b) the maximum number of iterations, which stops the iterations in case the minimum RMS error is not attained. In this study, a minimum RMS value of 1.00, and the maximum number of iterations as 40, were set for all the inversion processes. Normally, a low RMS value at the end of the iterations manifests an appropriate selection of the dispersion curve. Moreover, when a logical dispersion curve (i.e., a dispersion curve that is theoretically most feasible for a given subsoil condition; Xia *et al.*, 1999) is processed for inversion, the RMS value drastically reduces during the first few iterations. A prolonged inversion is normally prone to arrive at an impractical V_s profile. Prolonged inversion refers to an unending number of iterations to arrive at a V_s profile. Such occurrence is noticed when the measured dispersion curve is theoretically illogical or erroneous for the given subsoil condition. This type of dispersion curve normally exhibits an abnormal trend, e.g., the phase velocity may increase with frequency for a significant portion, or the dispersion curve may flatten out at low frequencies (Xia *et al*., 1999).

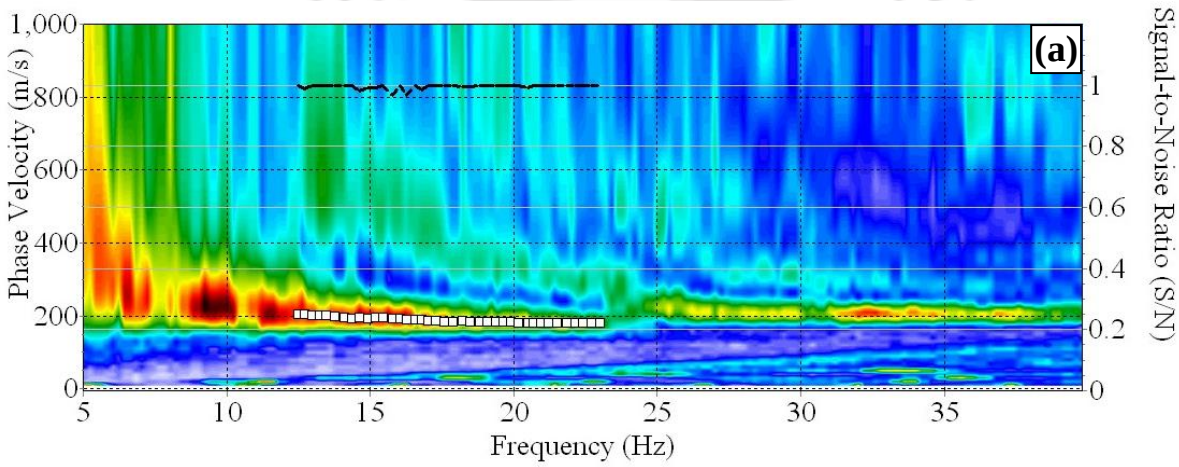

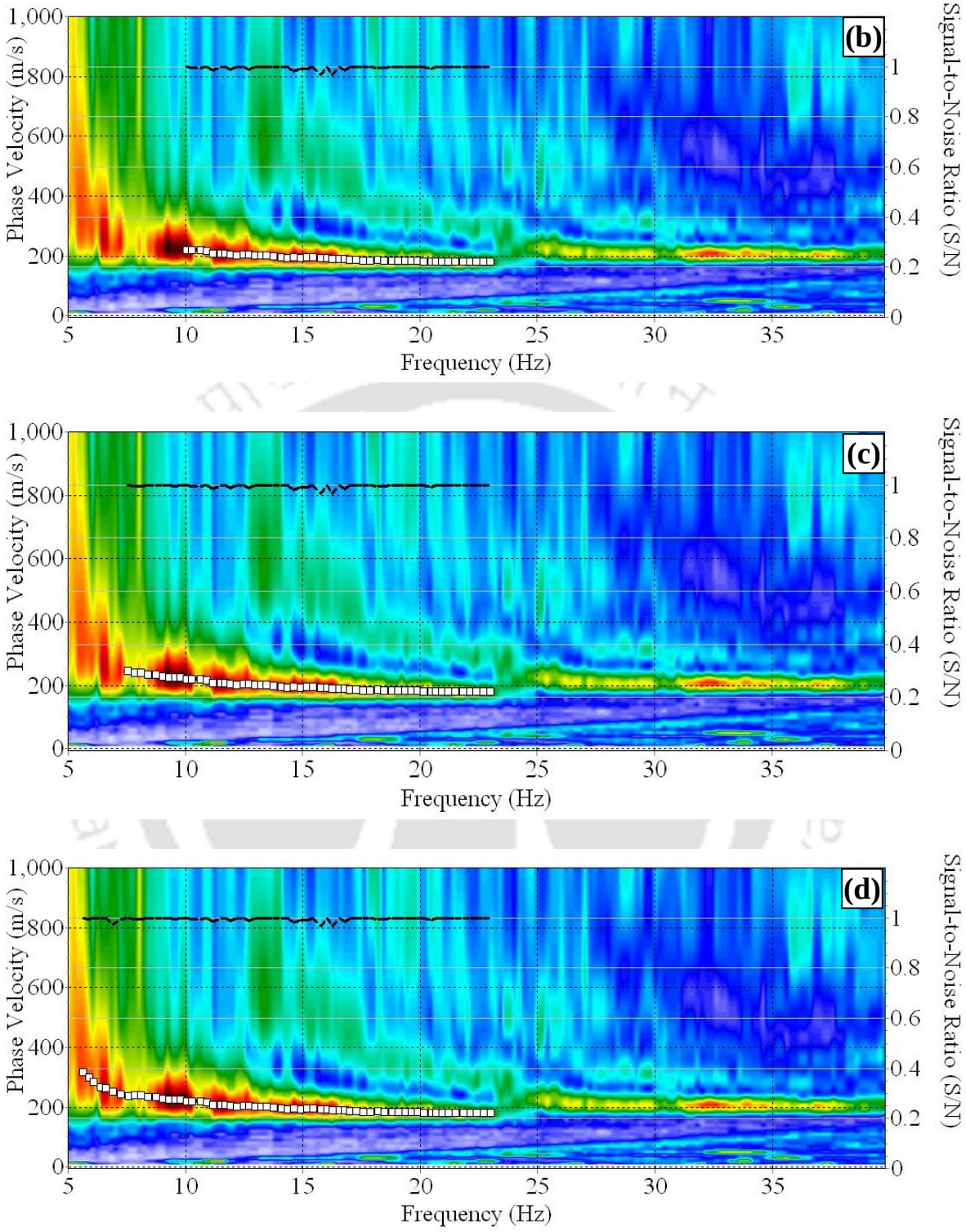

Fig. 8.1 Selection of dispersion curve considering different magnitudes of the lowest frequency (a) 12.5 Hz (b) 10 Hz (c) 7.6 Hz (d) 5.6 Hz

Table 8.1 Initial earth layer model for the dispersion curve selected between 12.5-23 Hz

Initial Model						
Layer	**Depth (m)**	**Thickness (m)**	**V_s (m/s)**	**V_p (m/s)**	**Poisson's ratio**	**Density (gm/cc)**
1	0.3	0.3	198	485	0.4	1.56
2	0.6	0.4	198	485	0.4	1.61
3	1.1	0.5	198	485	0.4	1.67
4	1.7	0.6	198	485	0.4	1.72
5	2.4	0.7	198	485	0.4	1.78
6	3.2	0.9	199	487	0.4	1.83
7	4.3	1.1	206	504	0.4	1.89
8	5.7	1.4	220	538	0.4	1.94
9	Half space	Infinity	335	821	0.4	2

Table 8.2 Initial earth layer model for the dispersion curve selected between 10-23 Hz

Initial Model						
Layer	**Depth (m)**	**Thickness (m)**	**V_s (m/s)**	**V_p (m/s)**	**Poisson's ratio**	**Density (gm/cc)**
1	0.3	0.3	198	485	0.4	1.55
2	0.7	0.4	198	485	0.4	1.6
3	1.2	0.5	198	485	0.4	1.65
4	1.8	0.6	198	485	0.4	1.7
5	2.5	0.7	198	485	0.4	1.75
6	3.4	0.9	199	488	0.4	1.8
7	4.6	1.2	209	512	0.4	1.85
8	6.0	1.5	222	543	0.4	1.9
9	7.9	1.8	238	583	0.4	1.95
10	Half space	infinity	371	910	0.4	2

Table 8.3 Initial earth layer model for the dispersion curve selected between 7.6-23 Hz

Initial Model						
Layer	**Depth (m)**	**Thickness (m)**	**V_s (m/s)**	**V_p (m/s)**	**Poisson's ratio**	**Density (gm/cc)**
1	0.3	0.3	198	485	0.4	1.54
2	0.6	0.3	198	485	0.4	1.58
3	1.0	0.4	198	485	0.4	1.63
4	1.5	0.5	198	485	0.4	1.67
5	2.2	0.6	198	485	0.4	1.71
6	3.0	0.8	198	485	0.4	1.75
7	4.0	1.0	203	497	0.4	1.79
8	5.3	1.3	216	530	0.4	1.83
9	6.9	1.6	228	559	0.4	1.88
10	8.8	2.0	295	601	0.4	1.92
11	11.3	2.5	260	636	0.4	1.96
12	Half space	infinity	463	987	0.4	2.00

Based on different selections of frequency ranges, Table 8.5 lists the shear wave velocity (V_s) profile obtained from the dispersion images shown in Fig. 8.1. It can be observed that with the reduction in lower bound of the frequency range, there is an increase in attained investigation depth. With the selection of 12.5 Hz, 10 Hz, 7.6 Hz and 5.6 Hz as the initial lowermost frequency, the investigation depths achieved are 5.7 m, 7.9 m, 11.3 m and 19.7 m, respectively.

Table 8.4 Initial earth layer model for the dispersion curve selected between 5.6-23 Hz

Initial Model						
Layer	**Depth (m)**	**Thickness (m)**	**V_s (m/s)**	**V_p (m/s)**	**Poisson's ratio**	**Density (gm/cc)**
1	0.3	0.3	198	485	0.4	1.54
2	0.6	0.4	198	485	0.4	1.57
3	1.1	0.4	198	485	0.4	1.61
4	1.7	0.6	198	485	0.4	1.64
5	2.4	0.7	198	485	0.4	1.68
6	3.2	0.9	199	487	0.4	1.71
7	4.3	1.1	206	504	0.4	1.75
8	5.7	1.4	220	538	0.4	1.79
9	7.4	1.7	233	571	0.4	1.82
10	9.5	2.1	249	609	0.4	1.86
11	12.2	2.7	266	651	0.4	1.89
12	15.5	3.3	289	709	0.4	1.93
13	19.7	4.2	328	802	0.4	1.96
14	Half Space	Infinity	524	1283	0.4	2.00

For different lower bound of the selected frequency range, Fig. 8.2 exhibits the progressive convergence of the theoretical (or current iteration dispersion curves) to the measured (or experimental dispersion curves). The variations of RMS error between measured and theoretical dispersion curve, after different iterations, are also presented for various cases. In Fig. 8.2a, the dispersion curves are shown for the frequency band of 12.5-23 Hz. As observed, the initial dispersion curve (DC) profile i.e., DC after Iteration 0, has large difference with the measured dispersion curve, thereby resulting in very high RMS error, as depicted in Fig. 8.2b. With the

progress of the inversion i.e., with increasing number of iterations, the theoretical dispersion curves shifts closer to the measured dispersion curves, exhibiting a gradual decrement in the RMS error.

Table 8.5 Shear wave velocity variation with change in initial frequency range

Dispersion curve selection for frequency range between							
12.5 to 23 Hz		**10 to 23 Hz**		**7.6 to 23 Hz**		**5.6 to 23 Hz**	
Depth (m)	**V_s (m/s)**	**Depth (m)**	**V_s (m/s)**	**Depth (m)**	**V_s (m/s)**	**Depth (m)**	**V_s (m/s)**
0.3	202.0	0.3	201.0	0.3	202.0	0.3	189.0
0.6	195.0	0.7	198.0	0.6	199.0	0.6	184.0
1.1	227.0	1.2	180.0	1.0	212.0	1.1	166.0
1.7	223.0	1.8	161.0	1.5	194.0	1.7	155.0
2.4	202.0	2.5	153.0	2.2	178.0	2.4	162.0
3.2	142.0	3.4	179.0	3.0	172.0	3.2	190.0
4.3	153.0	4.6	212.0	4.0	164.0	4.3	214.0
5.7	253.0	6.0	258.0	5.3	203.0	5.7	210.0
Half Space	235.0	7.9	146.0	6.9	214.0	7.4	180.0
		Half Space	300.0	8.8	248.0	9.5	237.0
				11.3	208.0	12.2	337.0
				Half Space	296.0	15.5	277.0
						19.7	187.0
						Half Space	580.0

The iterative process terminates when the theoretical dispersion curve almost overlaps with the measured dispersion curve, resulting in minimum RMS error. At this stage, the inversion is stated to be complete, and the shear-wave velocity profile corresponding to the final dispersion curve is considered to the best suitable earth-layer model for the investigation. For example, in Fig. 8.2a, the inversion process terminates after iteration 20 when the minimum RMS error is attained. In

each of the case for different frequency band selected, the RMS error drops rapidly in first few iterations and becomes almost asymptotic with higher number of iterations (Fig. 8.2b, d, f, h).

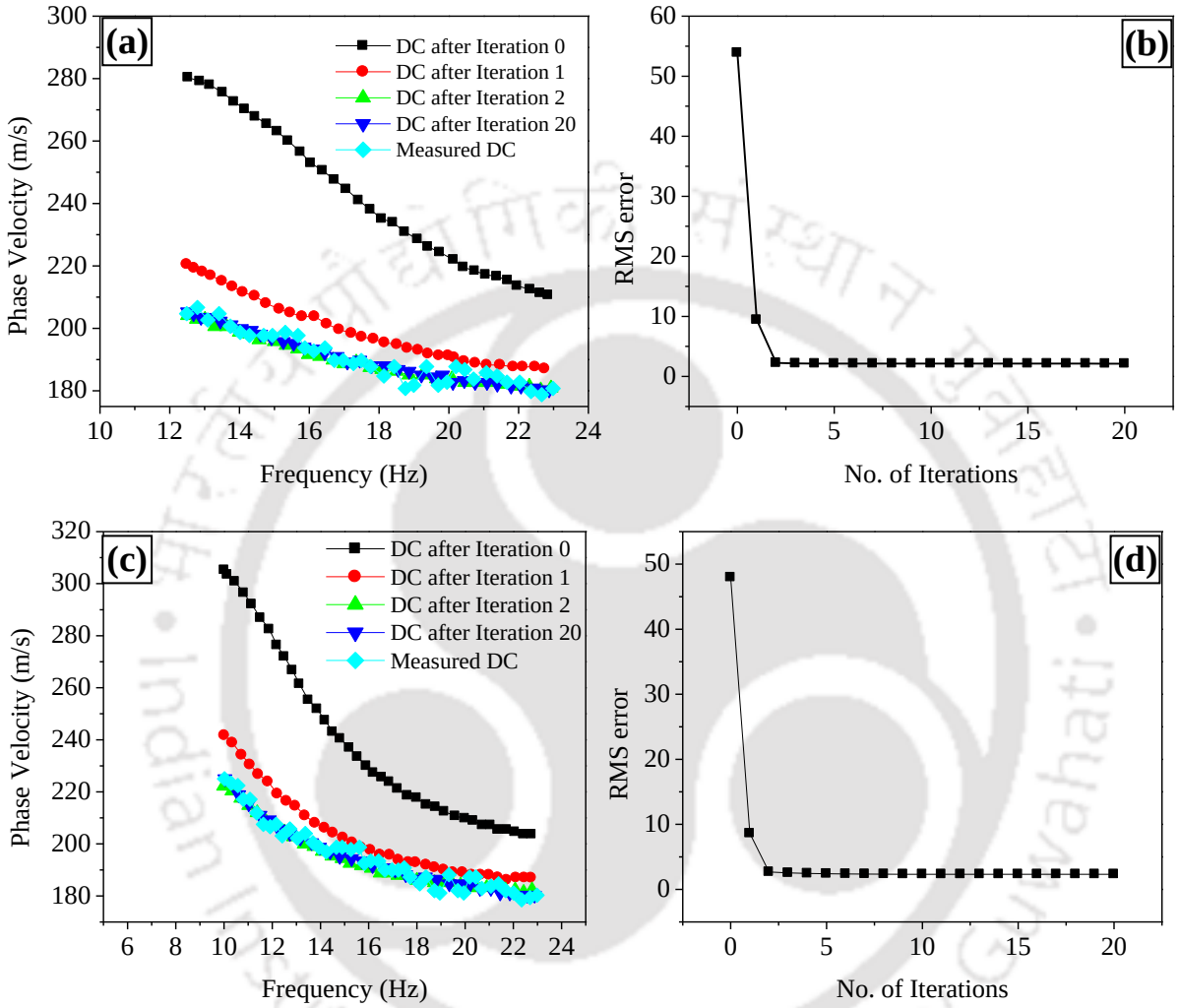

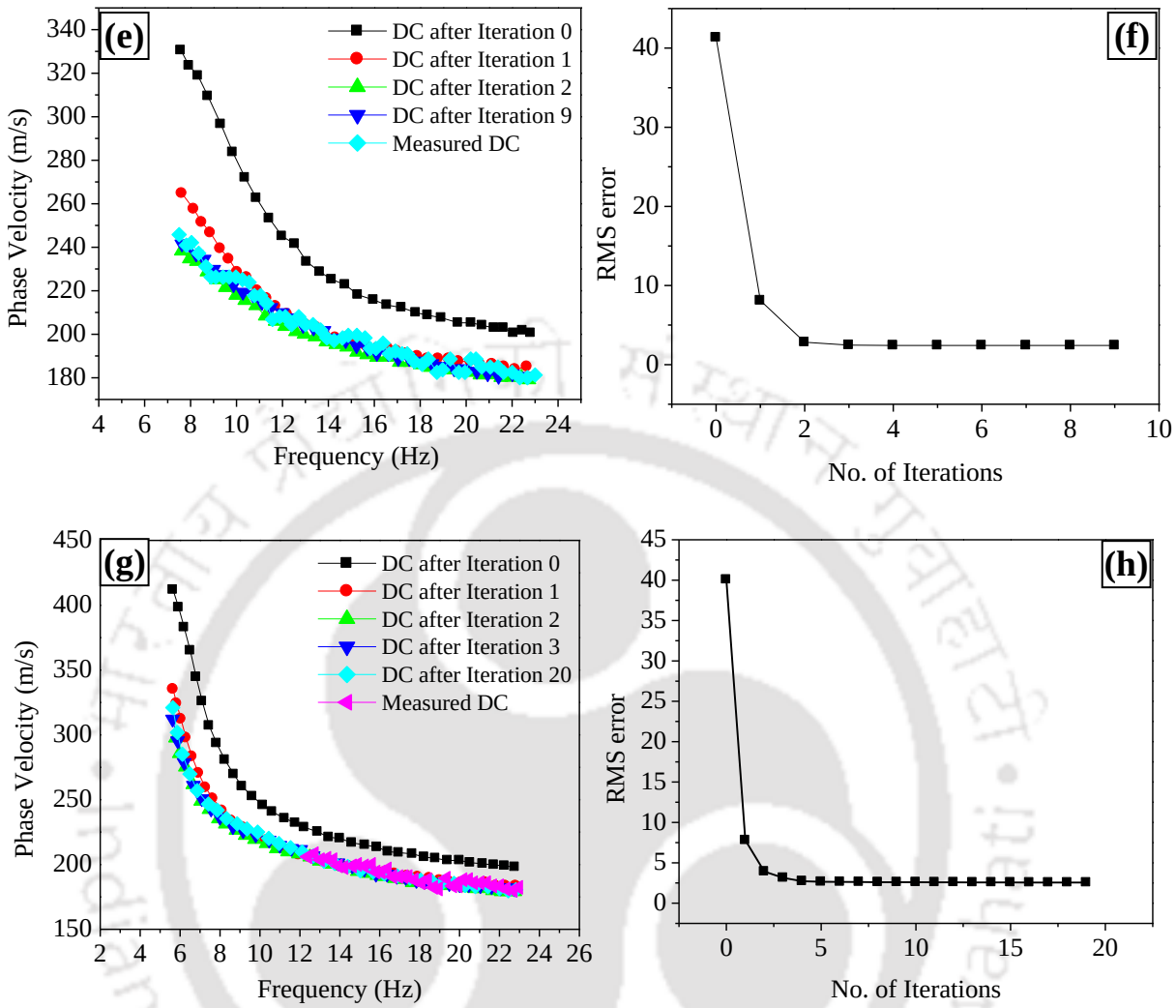

Fig. 8.2 Progressive convergence of the theoretical dispersion curves to the experimentally measured with lowest frequency range as (a) 12.5 Hz (b) 10 Hz (c) 7.6 Hz (d) 5.6 Hz

Figure 8.3 depicts the variation of shear-wave velocity with depth obtained from the inversion analysis of the dispersion curves selected with different frequency bounds. It can be observed that selection of lower frequency bound yields shear-wave velocity profiles of higher depth. Based on the selected frequency bounds, the assigned initial model, for commencing the iterative optimization technique, can be found to have different numbers of layers with unequal thickness (Tables 8.1-8.4). Thus, depending on the initial model and frequency band chosen for analysis, different shear-wave velocity models with varying depth and layer thicknesses are obtained. In spite of the differences, it can be noted that the velocities of the shallower layers are well in coherence to each other, while notable differences are observed at the gradually deeper layers. This observation is attributed to the fact that for the different frequency ranges selected for the analysis, all of them had identical higher frequency range and limits, while the lower bound varied. This resulted in somewhat incoherent and comparatively different velocity profiles at higher depths. In order to check the verity of the obtained profiles, a comparison is also made between the shear-wave velocity profiles obtained from active and passive roadside surveys, both obtained by selecting a frequency range of 7.6-23 Hz (Fig. 8.3b). A good comparison between the two profiles indicate the accuracy of the passive profile obtained from a specific range; similar results are obtained for other frequency ranges as well, however not presented here for the sake of brevity. From Table 8.5 and Fig. 8.3, it can be observed that the velocity profiles normally converges to each other, with meagre exception at some points. For example, at 1.7 m depth of the 2nd and 3rd shear wave profile (12.5-23 Hz and 5.6-23 Hz, respectively), the values of shear wave velocities are 223 m/s and 155 m/s, respectively. These variations are attributed to the differences in the actual thickness of the subsoil layers in the earth layer models chosen for different dispersion curves.

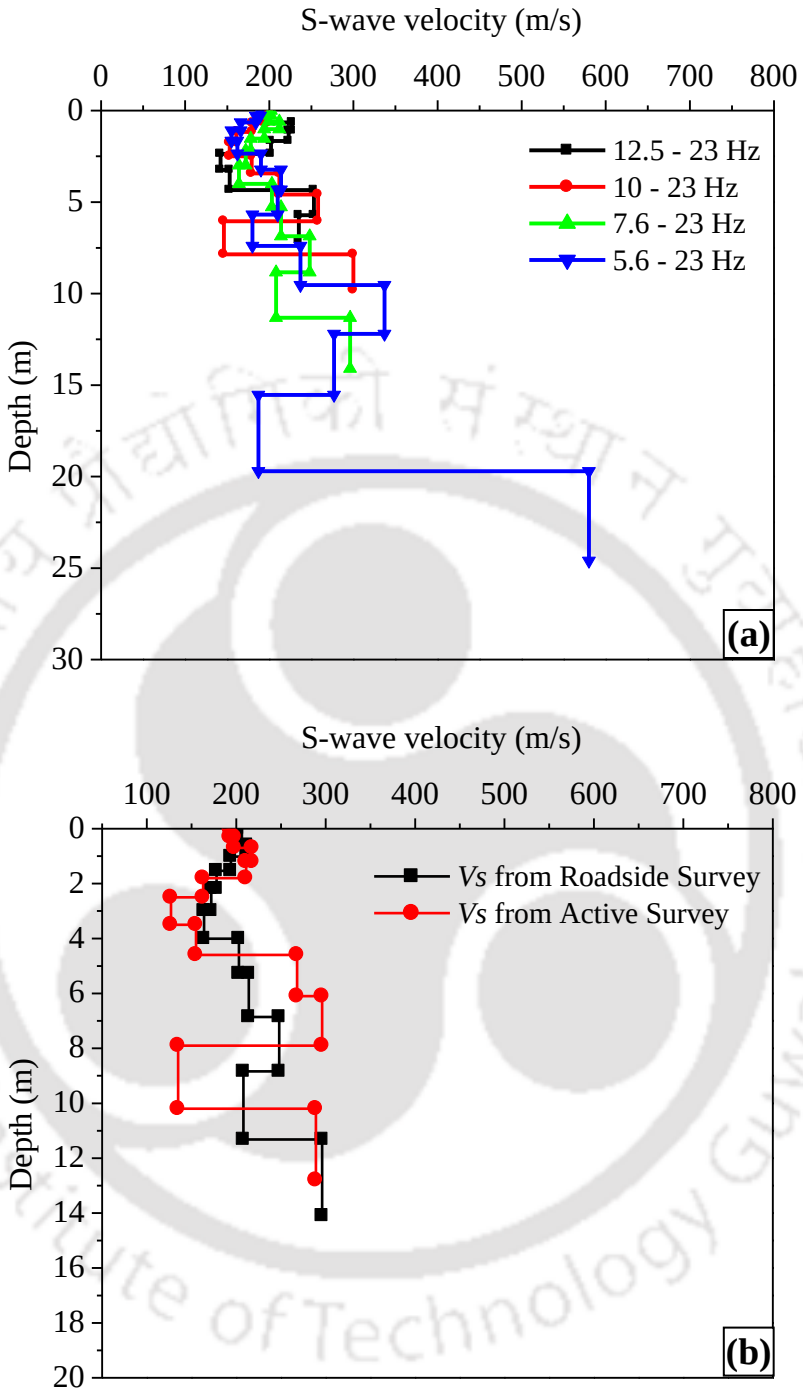

Fig. 8.3 (a) Influence of dispersion curves selected with different frequency bounds on the varying depths of investigation as highlighted by the shear-wave velocity profiles (b) Comparison of the V_s profiles obtained from active and passive roadside MASW surveys in the frequency range of 7.6-23 Hz

The variation in the numbers of iterations and RMS error, due to the changes of the selection in the lower frequency of the dispersion curve, is presented in Table 8.6. The lowest RMS value and the highest number of iterations were fixed at 1.00 m/s and 40, respectively, as the two stopping criteria for the inversion analysis. It can be observed that with the reduction in the lower bound of the frequency range of the selected dispersion curve, the RMS values are marginally increasing, and present almost a constant trend. At the same time, the number of iterations required to achieve the final profile during the inversion analysis vary randomly with change in frequency range of selection, and expectedly does not pertain to any correlation trend. Table 8.6 highlights that the variation in RMS error is only marginal with an apparently increasing trend (2.12 to 2.56) for selecting lower frequency range for dispersion curve extraction. An apparently constant RMS error with increasing depth of exploration can itself be suggestive of choosing the lower frequencies for dispersion curve extraction and inversion analysis.

Table 8.6 Effect of selected frequency range on SNR, number of iterations and RMS values

SL No.	Frequency range of selection (Hz)	Overall SNR (%)	Numbers of iterations required during inversion analysis	RMS value in phase velocity after final iteration (m/s)
1	12.5 to 23	99	33	2.12
2	10 to 23	99	34	2.32
3	6.5 to 23	99	9	2.42
4	5.6 to 23	99	21	2.56

8.3 Influence of the Density of Dispersion Points on V_s Profiling

Another important aspect that influences the shear-wave velocity profile obtained from the inversion analysis is the number of dispersion points selected to represent the dispersion curve,

i.e., the density of dispersion points. In a dispersion image, the dispersion curve can be constituted by selecting any numbers of dispersion points from the energy spectra. In this section, the effect of number of dispersion points on the final V_s profile, and the optimum number of dispersion points required for a stable inversion analysis are reported. For the studies, a dispersion image is selected that was obtained from Site 1 using 69 m receiver array with 24 numbers of receivers, laid at an offline distance of 5 m from the centreline of the road. The basic dispersion image is shown in Fig. 8.4, while the different sub-images highlight the various densities of dispersion points chosen during the selection of dispersion curve. The fundamental mode dispersion band is dominant on the dispersion image and is visibly distinct and clear. The energy band shows clear peaks starting from 5.5 Hz to 20 Hz. Figure 8.4(a-g) shows the selection of dispersion curves using 5, 10, 15, 20, 30, 40 and 50 numbers of dispersion points, respectively. As the objective of this study is to decipher the effect of number of dispersion points on the output V_s profile, all the dispersion curves were selected within the specific range between 5.5-20 Hz, and the varying numbers of intermediate dispersion points were selected within the said range. A high SNR value, almost equal to 1 (or, 100%) was ascertained during the selection of the dispersion curves.

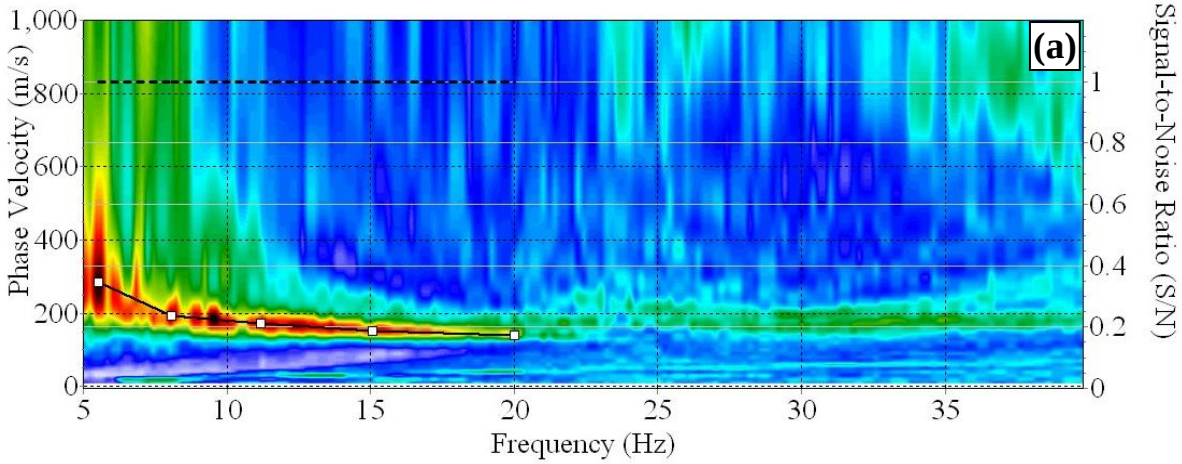

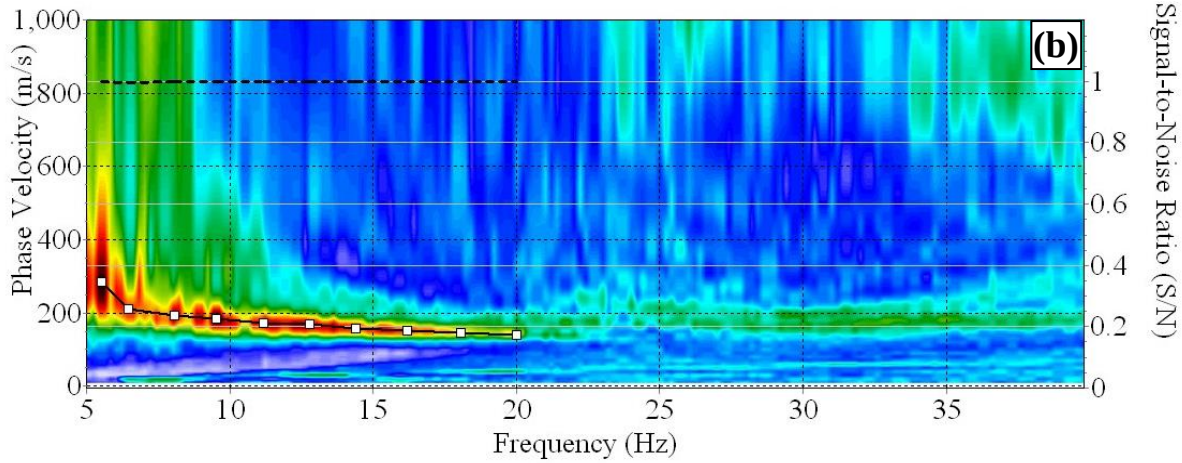

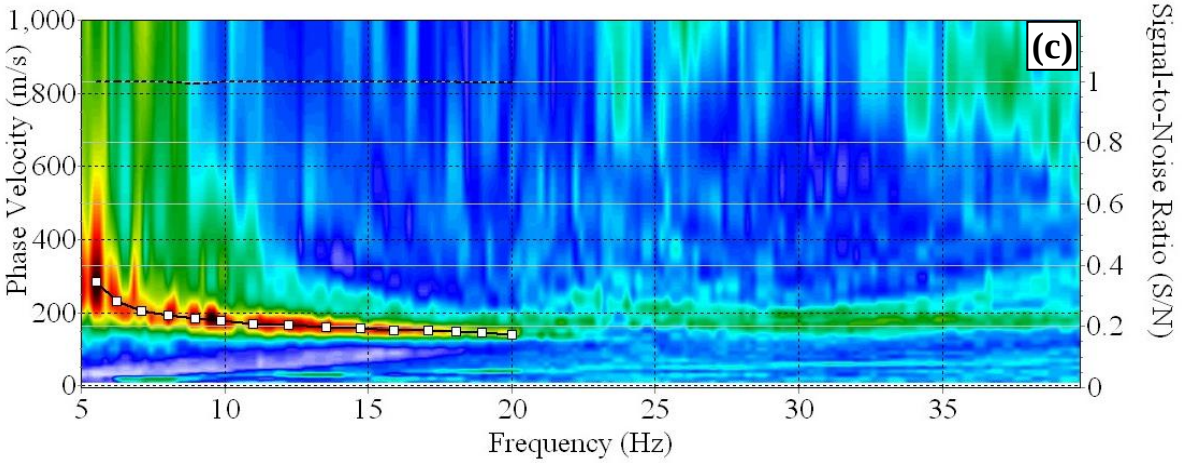

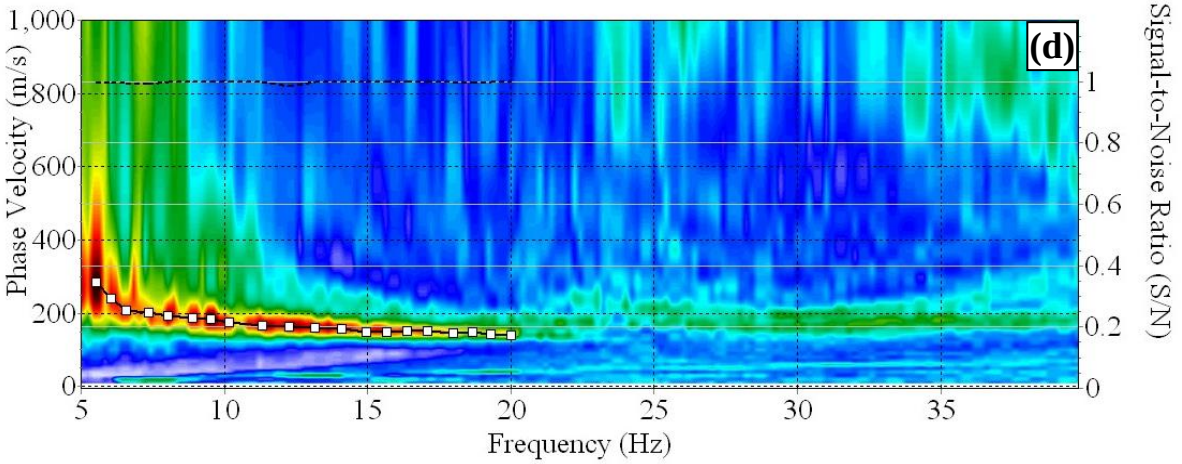

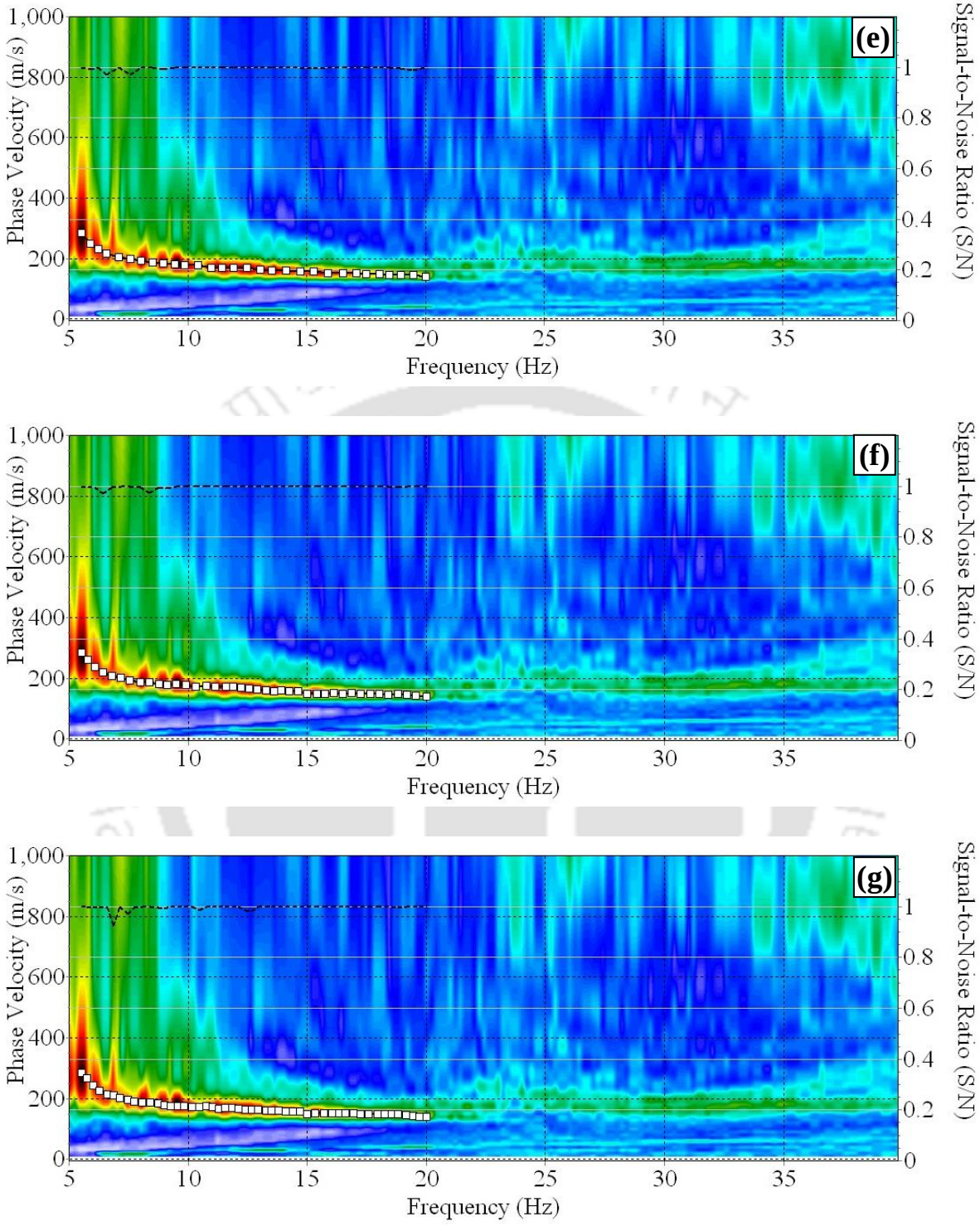

Fig. 8.4 Extraction of dispersion curve from a typical dispersion image using different numbers of dispersion points within a specific frequency range (a) 5 DC points (b) 10 DC points (c) 15 DC points (d) 20 DC points (e) 30 DC points (f) 40 DC points (g) 50 DC points

Table 8.7 lists the shear wave velocity values at different depths obtained from the processing of dispersion curves constituted by different number of dispersion points. For every selection, the attained depth of investigation is 18.04 m, comprising 10 numbers of layers of unequal thickness. On careful scrutiny, it is observed that the fluctuations in V_s values among the first three selections, i.e., 5, 10 and 15 DC points, are much higher than the last three selections, i.e., 30, 40 and 50 DC points. This behaviour is depicted in Fig. 8.5, which shows the graphical representation of the variation of shear-wave velocity with the variation in constituent density of dispersion curve. The convergence of the velocity profiles obtained by inversion of dispersion images constituted 30, 40 and 50 DC points is clearly noticeable, along with the deviation of other profiles with the respect the convergent ones.

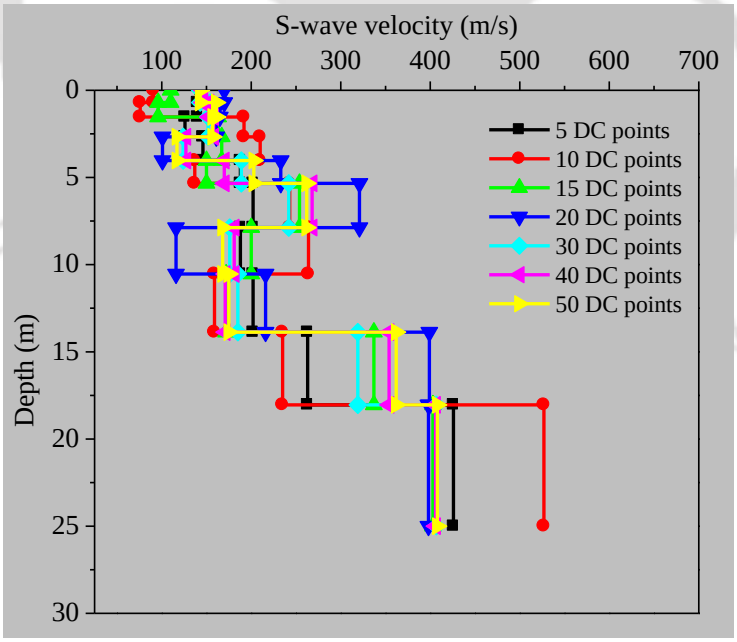

Fig. 8.5 Variation of shear-wave velocity profile with varying density of dispersion points representing the dispersion curve within a selected frequency range

Table 8.7 Shear-wave velocity profile obtained by inversion of dispersion curve comprising varying numbers of dispersion points

Depth (m)	Shear wave velocity (m/s) obtained from						
	5DC pts	10 DC pts	15 DC pts	20 DC pts	30 DC pts	40 DC pts	50 DC pts
0.70	144	91	110	170	143	146	143
1.53	140	76	96	165	154	153	161
2.67	126	192	163	161	152	158	157
4.03	146	210	167	101	124	127	117
5.74	188	137	150	233	189	170	203
7.87	202	243	254	321	242	268	262
10.54	188	264	200	116	176	181	168
13.87	202	159	172	216	185	171	175
18.04	263	235	337	399	319	354	362
Half Space	426	527	403	398	407	406	408

Table 8.8 represents the percentage variation in shear-wave velocity profile obtained by inversion of dispersion curves comprising varying numbers of dispersion points. The comparison is made with respect to the shear-wave velocity profile obtained from the 50-point dispersion curve. It can be observed that the maximum difference in V_s values between 5 and 50, 10 and 50, 15 and 50, 20 and 50, 30 and 50 and 40 and 50-point dispersion curves are 27.3 %, 79.5 %, 42.7 %, 31 %, 11.9 % and 16.3 %, respectively. Therefore, it can be stated that with the increase in the density of dispersion points constituting the dispersion curve, the accuracy of the obtained profile increases, thereby resulting in convergent solutions. Overall, there is a minimal difference in the V_s values obtained from 30, 40 and 50-point dispersion curves.

Table 8.8 Percentage deviation in shear-wave velocity profiles obtained by inversion of dispersion curve comprising varying numbers of dispersion points

Depth (m)	Percentage difference in shear-wave velocity from dispersion curves with					
	5 and 50 DC points	10 and 50 DC points	15 and 50 DC points	20 and 50 DC points	30 and 50 DC points	40 and 50 DC points
0.70	-0.7	36.4	23.1	-18.9	0.0	-2.1
1.53	13.0	52.8	40.4	-2.5	4.3	5.0
2.67	19.7	-22.3	-3.8	-2.5	3.2	-0.6
4.03	-24.8	-79.5	-42.7	13.7	-6.0	-8.5
5.74	7.4	32.5	26.1	-14.8	6.9	16.3
7.87	22.9	7.3	3.1	-22.5	7.6	-2.3
10.54	-11.9	-57.1	-19.0	31.0	-4.8	-7.7
13.87	-15.4	9.1	1.7	-23.4	-5.7	2.3
18.04	27.3	35.1	6.9	-10.2	11.9	2.2
Half Space	-4.4	-29.2	1.2	2.5	0.2	0.5

Figure 8.6 shows the graphical representation of the percentage variation of shear wave velocity with dispersion curves comprising different density of dispersion points. The convergence of V_s profiles obtained from dispersion curves, formed with greater number of dispersion points, can be clearly observed from the figure. Therefore, based on the present study, it can be stated that for a dispersion curve spanning over a frequency range of 14.5 Hz (i.e., 5.5-20 Hz), the minimum numbers of dispersion points required to obtain a reliable V_s profile is 30. Similar exercise was carried out for several other scenarios, which are not repeated here for the sake of brevity. Based on the congregated observations, it can be stated that for a dispersion curve spanning frequency range of **X** Hz, the minimum number of points required to be selected for the representation of the dispersion curve is 2**X** (i.e., twice the magnitude of the frequency range under consideration), so

that a reliable shear-wave velocity profile can be obtained. In other words, it is concluded that the maximum frequency interval between the selections of two points in a dispersion curve should not exceed 0.5 Hz.

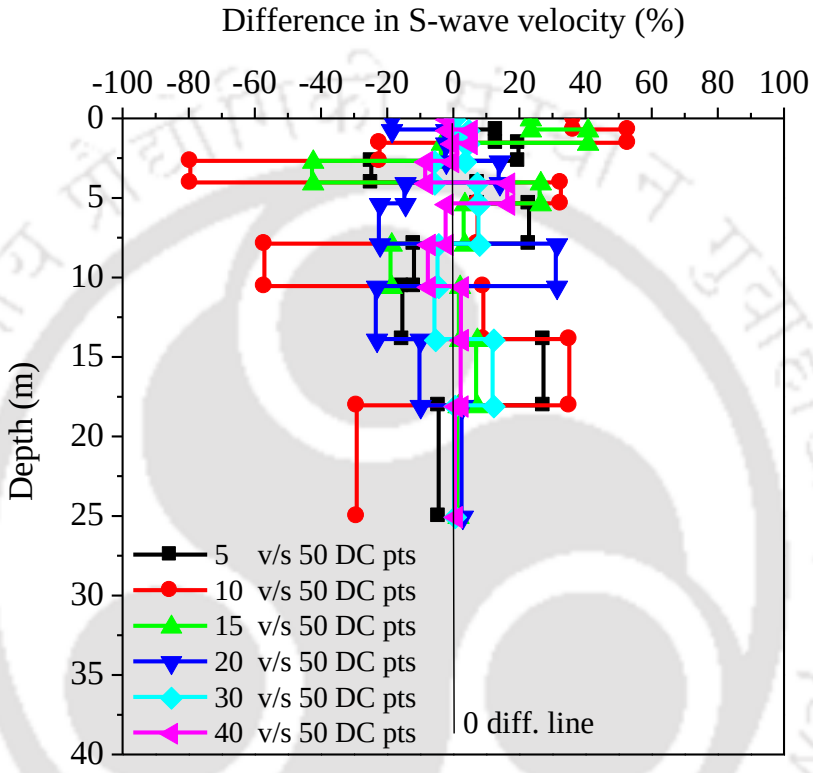

Fig. 8.6 Percentage deviation in the shear-wave velocity profile (compared to the V_s profile from 50 DC points) with the varying density of dispersion points

Table 8.9 shows the effect of number of dispersion points on the number of iterations and the attained RMS value. In the present study, a high SNR value is achieved for every point on the dispersion curve based upon careful selection. In all the above cases of dispersion curve selections, the SNR value is equal to or above 99 %, which indicates an excellent selection for any dispersion curve. It is observed that with the increase in the density of dispersion points up to 20, the number

of iterations required for the inversion process normally increases, beyond which the variation of RMS does not follow any specific pattern. Overall, the RMS values obtained at the end of inversion of the dispersion curves comprising different density of dispersion points do not show a very clear pattern. Importantly, despite having high SNR, less number of iterations and low RMS value in the case of 10-point dispersion curve, the obtained V_s profile is found to be unrealistic, with large deviation from other profiles, as exhibited in Fig. 8.5 and Fig. 8.6. Therefore, it can be stated that simply a high SNR, lesser number of iterations, and low RMS cannot be judged as the governing condition for the accuracy of the final V_s profile. Rather, the density of dispersion points constituting a dispersion curve is the most vital parameter to obtain a reliable and realistic V_s profile.

Table 8.9 Influence of selected dispersion points on the number of iterations and RMS value

SL No.	Number of points selected for the dispersion curve	Overall SNR (%)	Number of iterations required during inversion	RMS value in phase velocity after final iteration (m/s)
1	5	100	4	0.62
2	10	99	9	1.71
3	15	99	8	1.87
4	20	99	19	2.29
5	30	99	14	1.84
5	40	99	30	1.82
6	50	99	16	2.17

8.4 Influence of the Initial Layer Model in V_s Profiling

After selection of an appropriate dispersion curve from the dispersion image, a layered earth model is initially formed with a forward modelling scheme (as reported in Chapter 3) with varying depth, shear-wave velocity, primary-wave velocity, Poisson's ratio and soil density. This model, so

formed, is used as the initial model to initiate the inversion algorithm. The most efficient initial earth model depends upon the selected dispersion curve. In the previous section, the final shear-wave velocity profiles were estimated for a 10-layer earth model with an investigation depth of approximately 18 m. In actual site conditions, there can be any number of soil layers with varying stiffness up to a particular depth. Hence, selecting an earth model with exact number of soil layers for a depth range needs a-priori information of the geology of the site. In this section, a study conducted to understand the effect of varying number of layers in the initial earth model on the final V_s profile and its accuracy (in terms of RMS and number of iterations) is reported.

For the study, a dispersion image is selected from the field test conducted at Site 1 with 69 m receiver array comprising 24 numbers of receivers (Fig. 8.4). A dispersion curve was extracted with the best possible SNR, represented by sufficient density of points as reported in the previous section. The extracted dispersion curve was further subjected to inversion analysis using initial earth models with varying numbers of layers, ranging between 4 and 10. Notably, the maximum number of layers that can be applied in the SurfSeis software platform is 20. The shear-wave velocity profiles from different earth model are presented in Fig. 8.7. It can be observed that the V_s profiles generated using initial earth models with 7, or more, layers converge well to each other. However, with lesser numbers of layers in the initial model, the velocity profiles deviated from the average trend. The deviation of the V_s profile obtained with a 4-layer earth model was found to be the highest. The required numbers of iterations and RMS values for the different initial earth models are presented in Table 8.10. It can be noted that with decrease in numbers of layers in the initial earth model, the approximation during the inversion increases, thereby leading to decreasing number of iterations and increasing value of RMS.

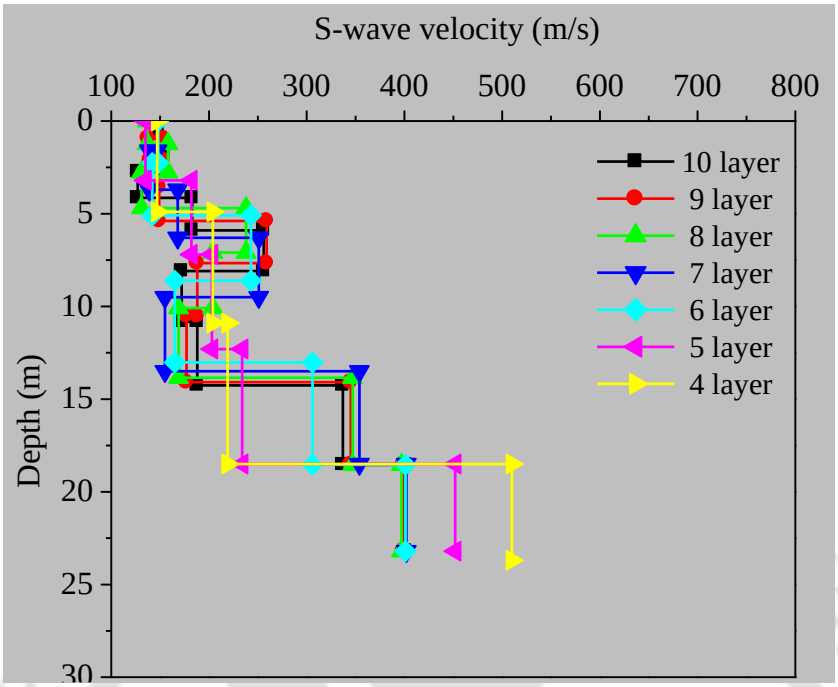

Fig. 8.7 Shear wave velocity profile obtained with varying number of layers in the initial earth model

Table 8.10 Influence of number of layers in the initial model on the number of iterations and RMS values achieved at the end of inversion analysis

SL No.	Number of layers	Number of iterations	RMS value
1	10	20	1.93
2	9	20	1.93
3	8	20	1.93
4	7	20	1.93
5	6	9	1.94
6	5	7	2.14
7	4	4	2.37

8.5 Summary

This chapter presents the influence on the selection of dispersion curve on the reliability and accuracy of shear-wave velocity profile obtained through inversion analysis. Two aspects were highlighted, namely the influence of the density of dispersion points selected to represent the dispersion curve, and the influence of the initial earth model on the resulting V_s profile. It is noted that the lowest frequency component on a selected dispersion curve controls the maximum achievable investigation depth. However, on the other hand, upon extending the selection of dispersion curve in the lower frequency regions, the corresponding RMS value increases, which are indicative of the deviations of the estimated soil profile from its true scenario. Hence, it is recommended that depending on the requirement of depth of investigation, the selection of dispersion curve should be limited in its lower frequency part to avoid the unrealistic deviation between the estimated and actual soil profiles. The density of the dispersion points, representing the selected dispersion curve, within a specific frequency range, affects the stability of inversion and the reliability of obtained shear-wave velocity profile. Based on the conducted studies, in order to achieve a reliable shear-wave velocity profile, the frequency interval of the dispersion points for the selection of the dispersion curve is recommended to be 0.5 Hz or lesser. The adoption of higher number of earth layers in the initial earth model is observed to produce more stable and reliable V_s profile. With decreasing number of earth layers in the initial model, the V_s profile estimated from the inversion procedure results in a higher approximation, leading to significant deviation in V_s values from true earth model. Based on the studies, the number of layers in the initial earth model is recommended to be 7 or more for a depth range of 18 m.

CHAPTER 9

SIGNIFICANCE OF SOURCE AND RECEIVER ARRAY POSITIONS IN DISPERSION IMAGING

9.1 Introduction

Complex source characteristics in passive methods of multichannel analysis of surface wave (MASW) technique leads to the key differences in its analysis and processing techniques from a conventional active MASW survey. As reported in Chapter 5, surface wave signals utilized in passive roadside survey are generated from vehicular movements over various road surface irregularities (i.e., sources) present nearby the test site. Therefore, unlike an active survey, the raw field records in roadside survey are of multi-source and multi-azimuthal characteristics. The current chapter reports the experimental investigations elucidating the effects of positioning of source and receiver array in passive roadside survey on the quality of raw wavefield records, resolution of dispersion imaging and the final V_s profile.

9.2 Effect of Intra-Line and Outer-Line Sources

9.2.1 Influence of Individual Positioning of Intra-line and Outer-line Source

In case of a passive roadside survey, a source position is termed as intra-line when it exists within the length of the array (Park and Miller, 2008). Similarly, in this work, a source is termed as outer-line when it exists outside the length of the array (Fig. 9.1). In passive roadside survey, different types of source positions (intra-line and outer-line) and their existence in multiple numbers are beyond the control of the investigator. Based on the source positions, the characteristics of raw

field record significantly vary. As reported in Chapter 7, a receiver array can record wavefield of different arrival characteristics such as IP, OP and OC type, depending solely upon the source positions. Moreover, it was observed that each of these three types of recorded wavefields require separate and appropriate processing scheme for dispersion imaging so that the respective azimuthal dependency, along with source distance, can be properly taken into account. In this section, the effect of intra-line and outer-line source conditions on the raw field record and dispersion imaging of passive roadside data is reported. The location for all the experimentation was chosen at Site 1 (inside IIT Guwahati campus).

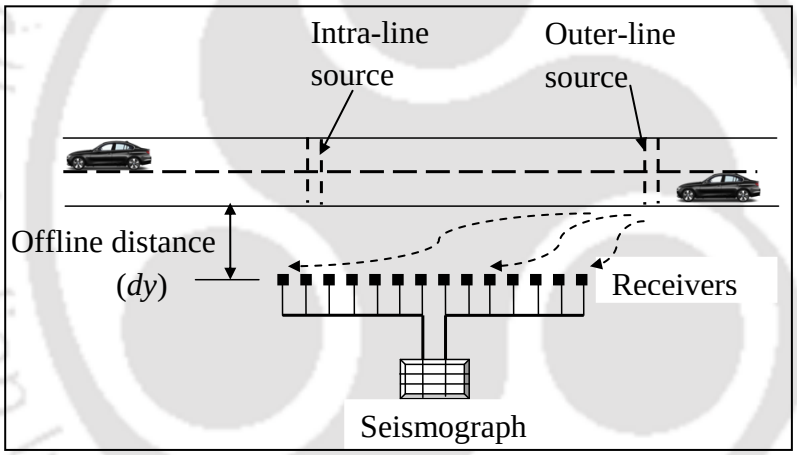

Fig. 9.1 Schematic layout of different types of source positions in Passive roadside MASW survey

The road site chosen for the experimental purpose was sufficiently plane, and no prominent irregularity could be located on its nearby stretch that can possibly produce strong-energy wavefields. In order to investigate the effect of source positioning, a galvanized iron (GI) pipe of 3 cm diameter and 4 m length was laid across the width of the road in desired positions. This user-controlled obstacle served as a source of strong wavefield due to the movement of vehicles over the same. The experimentation site, with the receiver array at the shoulder and the GI pipe on the

road, is shown in Fig. 9.2a. To produce an intra-line situation, the GI rod was placed on the road, at a position between the 8th and 9th receiver; while, to produce an outer-line situation, the same was placed at an offset distance 20 m ahead of the 1st receiver of the array. The schematic diagram of the same is depicted in Fig. 9.2b.

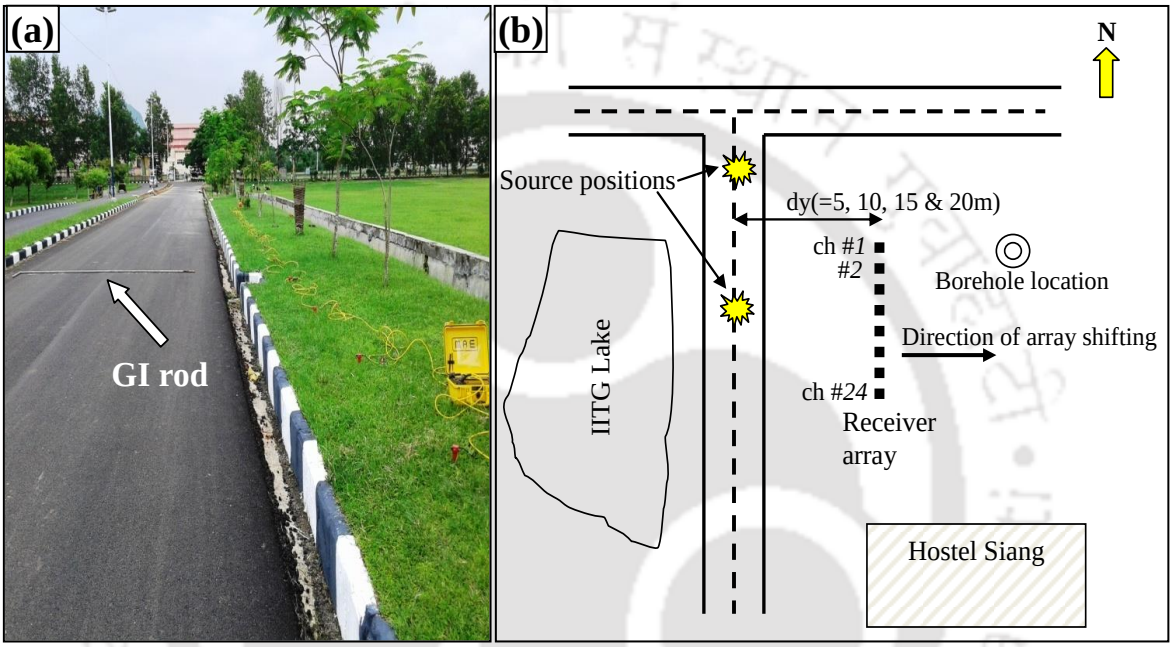

Fig. 9.2 (a) Test site inside IIT Guwahati campus with placed GI rod as source (b) Schematic of field set up for passive roadside MASW survey with the obstacle as intra- and outer-line source

Two typical raw wavefield records with a strong intra-line and outer-line source positions are shown in Fig.9.3a and 9.3b. Both the records were acquired during the passage of a private car (weighing approximately 1000 kg and running at a speed of nearly 30 km/h) by the receiver array. It can be observed from both the figures that there are two prominent wavefields in both the records, manifesting the passage of two vehicles (mentioned as Vehicle A and Vehicle B) over the placed GI rod (source) during the recording of the data. In the intra-line record, the prominent

wavefield starts from a position between 8th and 9th geophone/receiver, exactly where the source was placed on the road, as shown in Fig. 9.3a. As the vehicle passes over the source, the generated wavefield spreads out in both the directions of the receiver array, thereby showing a wave propagation towards the two ends of the array. On the other hand, when the source was placed in front of the receiver array (representing an outer-line source, Fig. 9.3b), the corresponding raw record exhibits a one-directional propagation pattern, much similar to a conventional active survey. In both the records, a significant blurred portion of wavefield can be observed just below the prominent wavefield, marked as "W" and identified by the oval markers on the wavefield signatures (Fig. 9.3a and 9.3b). These wavefields were actually created by the two vehicles while moving through the receiver spread and after passing the source irregularity. These wavefields are primarily the result of traction and drag interaction of vehicle tires with the bituminous pavement while passing over the visually unnoticeable road surface irregularities, and the same is recorded due to their proximity to the receiver array. Careful observations further illustrates that these sources are mostly mini intra-line sources, as manifested from their arrival patterns. For better comprehension of the typical characteristics of the generated wavefields, Fig. 9.3c and 9.3d shows the extracted enlarged view of the two records, particularly on the portions of the strong wavefield signatures (500-1900 ms from Fig. 9.3a, and 600-2000 ms from Fig. 9.3b, respectively). In Fig. 9.3c, some non-planar waves can be observed that were recorded by the near receivers, due to the proximity of the intra-line source to the receiver array. In Fig. 9.3d, the two narrowly spaced wavefields were created by the sequential passage of the front and rear axle wheels over the placed source, the details of which were already discussed in Chapter 5.

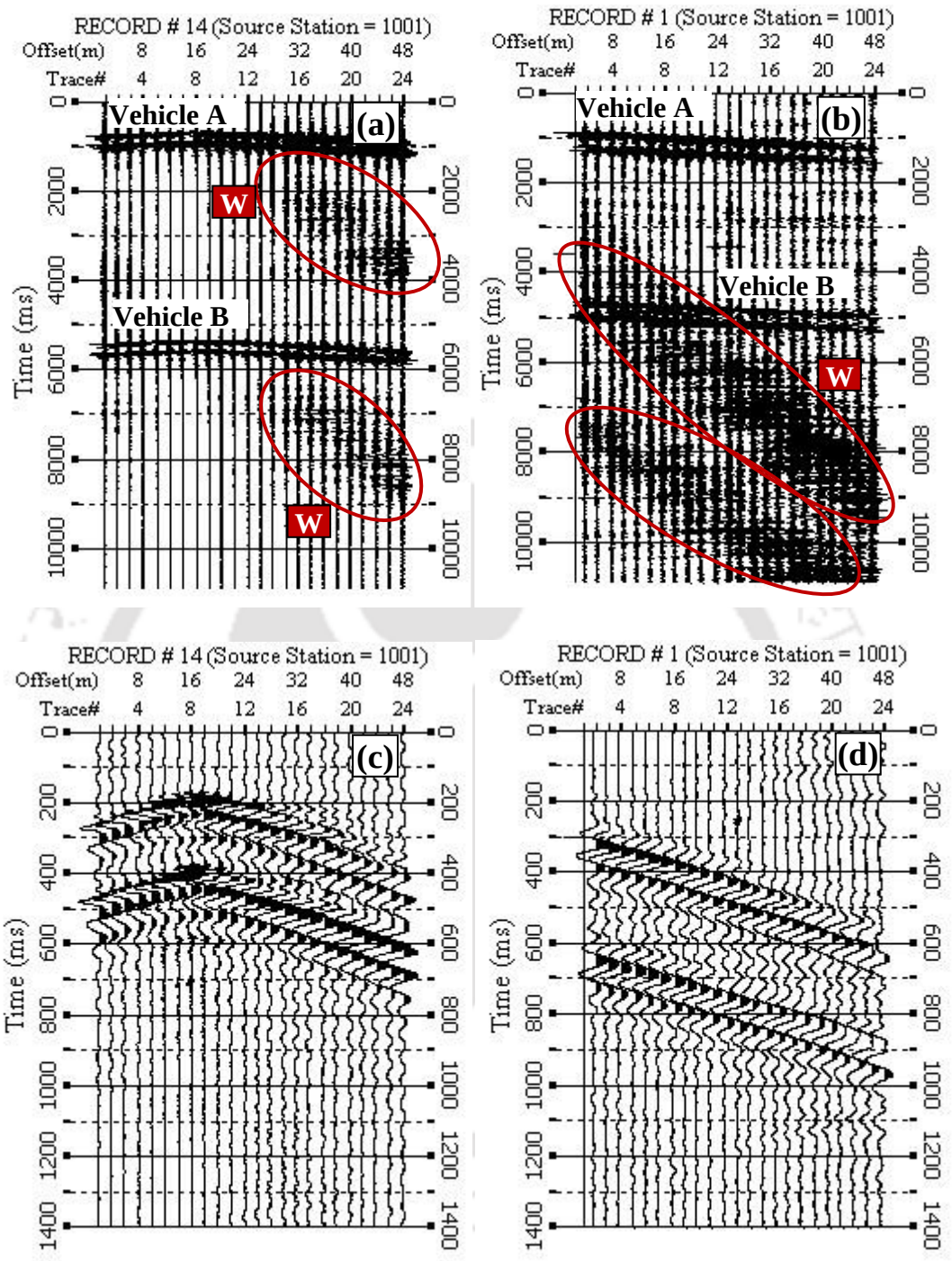

Fig. 9.3 A raw field record (a) with a prominent intra-line source (b) with a prominent outer-line source (c) enlarged view of the intra-line record, 500-1900 ms (d) enlarged view of the outer-line record, 600-2000 ms

Figure 9.4 shows the frequency spectra of the two raw wavefield records depicted in Fig. 9.3. For the intra-line case (Fig. 9.4a), it can be observed that the dominant frequency band for the record is between 6-40 Hz. In particular, there is a peak zone depicting high amplitude in the frequency band of 8-16 Hz. It will be further elaborated in the next section that such high amplitudes yield higher resolution in the dispersion image for the corresponding frequency band. On the other hand, in the outer-line case, as shown in Fig. 9.4b, the dominant frequency band exists between 10-30 Hz. However, in contrary to the previous case, no sharp peak can be observed in the spectra. These variations are attributed to different positions of the sources with respect to both the variations in distance and azimuth.

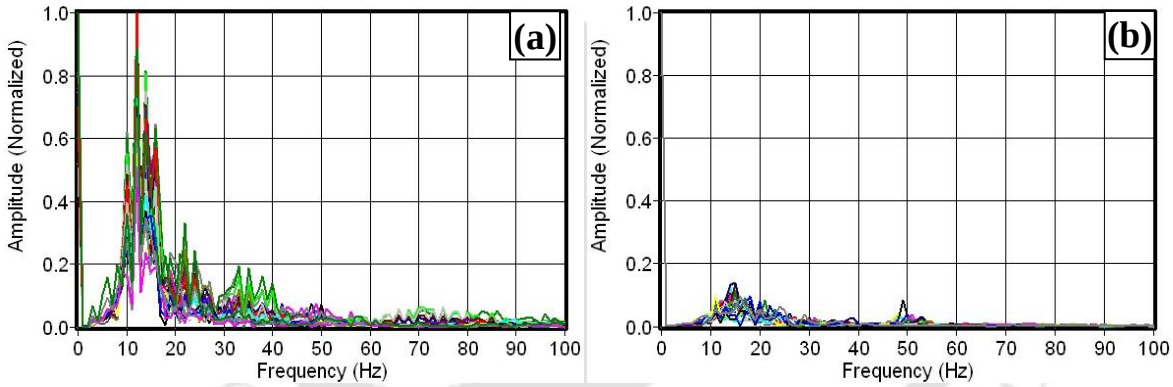

Fig. 9.4 Frequency spectra of a typical (a) intra-line and (b) outer-line source scenario

The dispersion images for the above two descripted situations are displayed in Fig. 9.5. It can be observed that the energy band of the dispersion image is significantly distinct in the presence of an intra-line source (Fig. 9.5a), as was expected from the frequency spectra. On the other hand, the energy trend in outer-line case (Fig. 9.5b) is almost similar to the intra-line case, although the energy peaks in lower frequency region is relatively indistinct. However, the energy band in outer-line case is relatively thinner which helps in subsequent accurate extraction of the dispersion curve.

With thorough numerical modelling, Park and Miller (2008) suggested that a scheme accounting for OC (offline cylindrical) waves gives superior performance, particularly in the presence of strong intra-line sources on the road. The current analysis platform (SurfSeis) can well account for both the distance and azimuthal dependency of passive roadside survey. Further, the intra-line source position performs better for modal identification in dispersion imaging as well. As can be observed from the two figures, the 1st higher order mode (M_1) is relatively more distinct in case of intra-line scenario than the outer-line case.

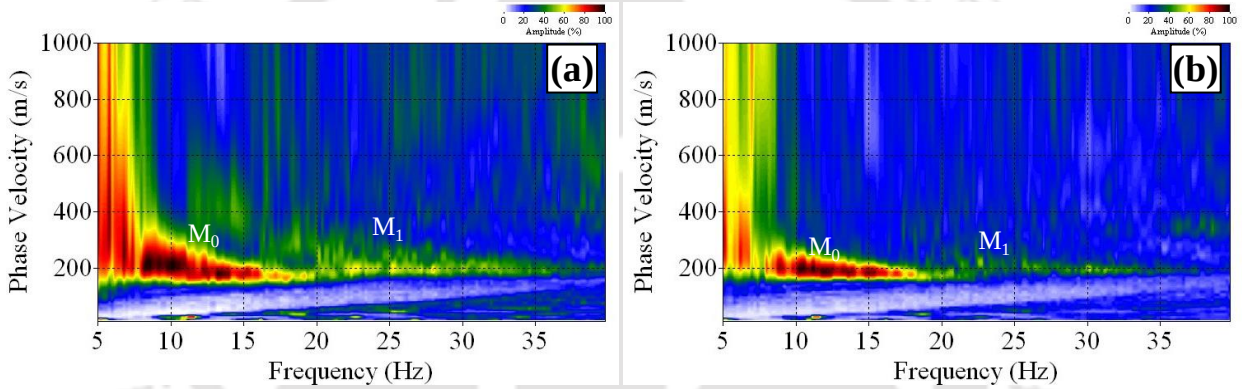

Fig. 9.5 Typical dispersion images with (a) an intra-line scenario (b) an outer-line scenario

9.2.2 Influence of Simultaneous Intra-line and Outer-line Sources

An additional study was conducted to investigate the combined effect of one intra-line and one outer-line source on the dispersion imaging. In this part of the investigation, two sources of identical type and dimension (as mentioned in the earlier section) were placed on the road at suitable locations. Keeping uniformity with the previous source positioning, one source was placed exactly between the 8th and 9th geophone to act as an intra-line source, while the other was placed at an offset distance of 20 m in front of first receiver to act as an outer-line source. Thus, the two obstacles make a combined scenario of the simultaneous presence of both intra-line and outer-line

sources. The corresponding raw record is shown in Fig. 9.6a, where the first wavefield between 0-2000 ms is from the outer-line source, while the second wavefield between 4000-6000 ms is from the intra-line source. Ten such records were collected, using an acquisition time of 10.8 s, and all the individual dispersion images were stacked to form a single final image as shown in Fig. 9.6b. It is observed that in the presence of non-contaminating sources (where the sources are placed well apart each other), the dispersion image has marginal difference with respect to the individual intra-line and outer-line source scenarios (as depicted in Fig. 9.5).

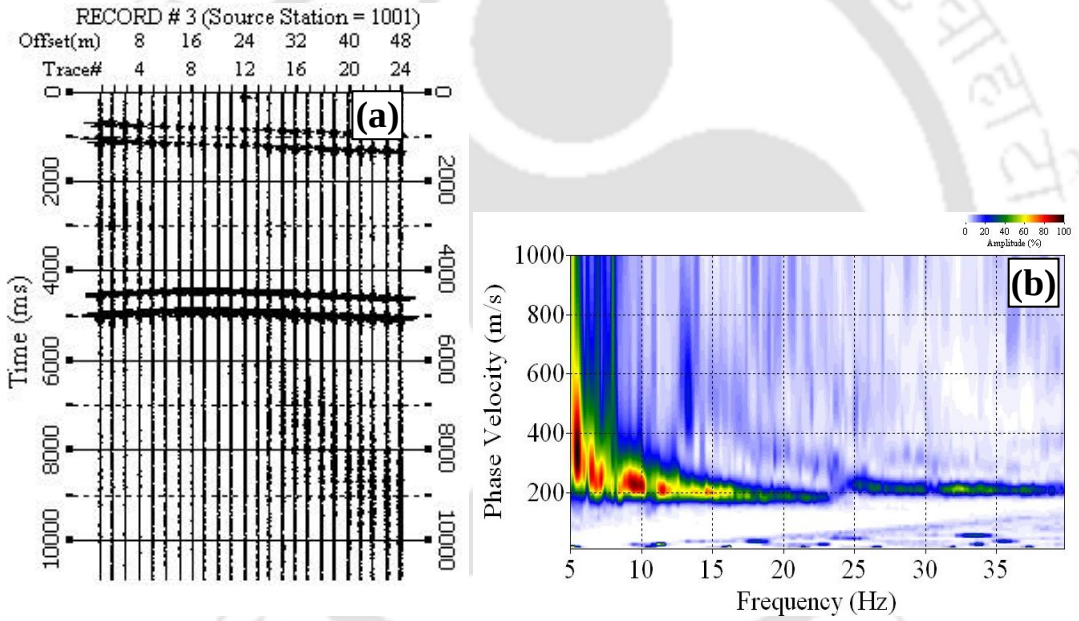

Fig. 9.6 (a) Raw field record obtained from a prominent and non-contaminated but simultaneous intra-line and outer-line source (b) The corresponding dispersion image

In all practical situations of passive roadside survey, there might be existence of multiple strong wavefield generators consisting of a number of intra-line and outer-line sources, which makes this study practically more realistic. Hence, based on the above two studies, it can be summarized that multiple sources have minimal effect on dispersion imaging, provided there is no contamination

or superposition of waves on the raw record obtained from those passive sources. The multiple sources should be sufficiently apart to avoid contamination in raw record. However, it is not always under the control of the user and is guided by the traffic conditions during the test. Hence, proper planning of the passive roadside survey is necessary to ensure the desired source and traffic conditions.

9.2.3 Comparison of V_s Profiles from Individual and Simultaneous Intra-Line and Outer-Line Sources

The pattern of dispersion curve selection, in case of intra-line and outer-line scenarios, was already discussed in Chapter 7. In a similar manner, dispersion curve for the simultaneous intra-line and outer-line source scenario was selected, and all the three dispersion curves from the three source scenarios were processed for inversion to obtain the final V_s profiles. Figure 9.7 shows the comparative representation of the three V_s profiles, which shows nearly identical trend with very marginal differences. Particularly, the outer-line and simultaneous intra-line-outer-line source scenarios exhibits excellent convergence. Some deviation of the V_s profile obtained from the intra-line source generated data can be noticed, which is attributed to approximate selection of dispersion curve from the relatively thicker dispersion energy band. A better resolution in the lower frequency band, in case of simultaneous intra-outer line source scenario, has resulted in a higher depth of investigation than the other scenarios.

9.3 Influence of Offline Distance (*dy*)

In passive roadside MASW survey, it is definitive to lay the receiver array away from the alignment of the road. Therefore, a term ‘offline distance’ is used in passive roadside survey (Park

and Miller, 2008) to denote the distance between centre-line of the road, from where majority of the surface waves generates, to the deployed receiver array, as shown in Fig. 9.1.

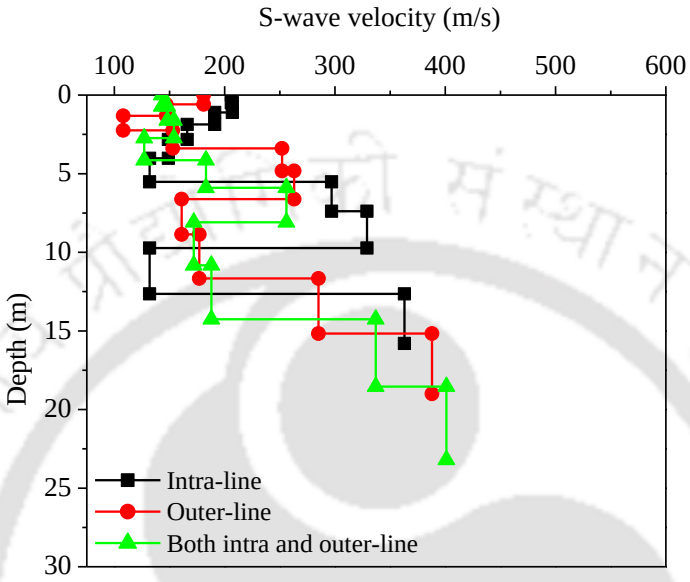

Fig. 9.7 Comparison of shear wave velocity profiles obtained from intra-line, outer-line and simultaneous intra- and outer- line source scenarios

A set of experiments were conducted to study the effect of offline distance (*dy*) on the resolution of dispersion image at the Site 1. The geophone array (with same number of receivers, array length and receiver spacing) was placed at varying offline distance, such as 5 m, 10 m, 15 m and 20 m, from the centre-line of the road/lane, as shown in Fig. 9.2b. Two sources were placed at two desired positions on the road, in a similar way as described in the previous section. Raw field records of all the adopted offline distances are shown in Fig. 9.8. In all the raw records, the wavefield from intra-line source (bottom) is found to be relatively distinct than the wavefield from outer-line source (top), which is attributed to the proximity of the intra-line source to the receiver array. In addition, the wavefield for outer-line position showed progressive reduction in distinctness with

increasing offline distance. Further, for higher offline distance (20 m), as depicted in Fig. 9.8d, a significant noise adulteration is observed in between 0-3000 ms, resulting in a non-utilizable contaminated outer-line source record. This is attributed to the fact that with the increase in the offline distance, wavefields generated from the far placed source on the road surface attenuates, while the wavefields from other stronger natural and/or cultural sources tends to dominate.

The dispersion images for all cases of varying offline distances are shown in Fig. 9.9. It can be observed that the resolution of dispersion image continually degrades with increasing offline distance, the degradation being significant in the lower frequency region. Moreover, in higher frequency zone, the dispersion trend is distinguishable in all the four offline distances, while the sharpness of the energy band (which helps in extraction of the dispersion curve) progressively decreases with increasing offline distance. Moreover, the identification of multimodal characteristics turns out to be difficult with higher offline distances. For dy = 5 m and dy = 10 m (Fig. 9.9a and 9.9b), 2-3 modes are distinctly visible and differentiable from each other. In the dispersion image obtained from 15 m offline distance, only fundamental mode can be distinguished (Fig. 9.9c). With higher offline distance of dy = 20 m (Fig. 9.9d), even the clarity of the fundamental mode gets reduced and the same is recognizable only in some portions of the higher frequencies (> 13 Hz). The poor resolution of the dispersion images obtained from 15 m and 20 m offline distances can be improved to some extent by curtailing frequency band below 10 Hz (Fig. 9.9e and 9.9f), as already described in Section 7.2 (Chapter 7). Observing the overall quality of dispersion images obtained from this study, the largest offline distance, that can be used to obtain usable dispersion image with distinguishable fundamental energy band, is identified and recommended to be 15 m.

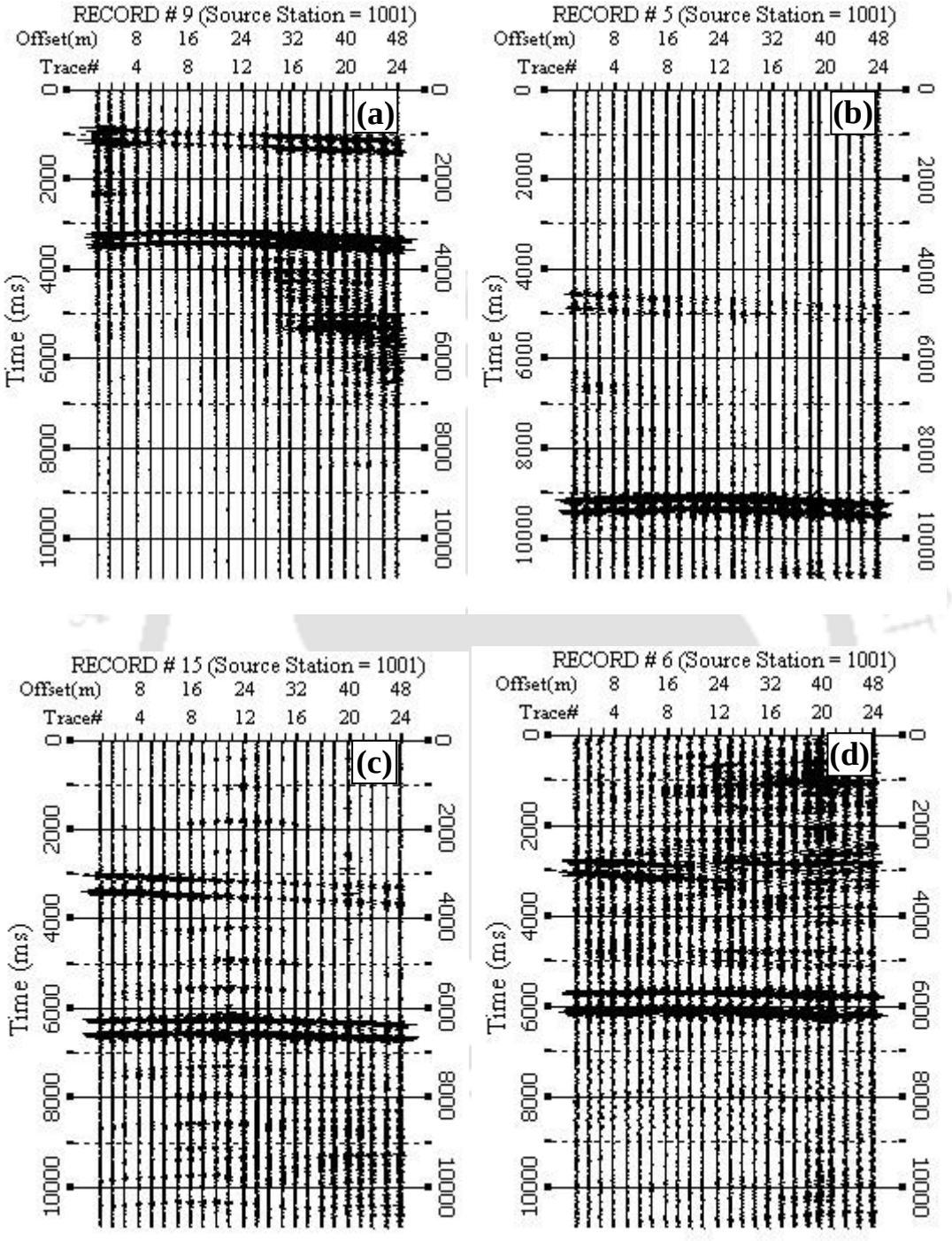

Fig. 9.8 Raw wavefield records for offline distance of (a) 5 m (b) 10 m (c) 15 m (d) 20 m

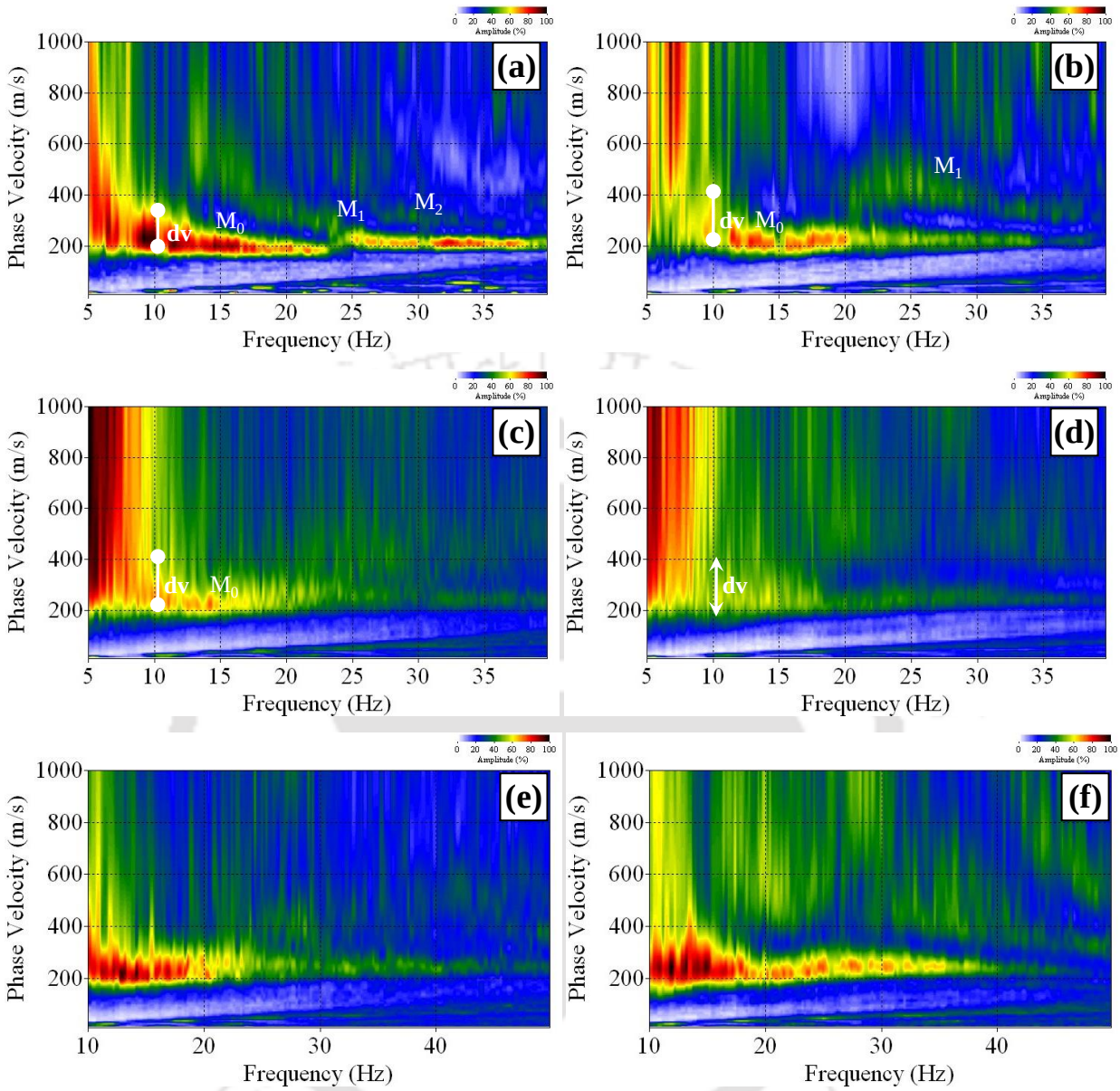

Fig. 9.9 Dispersion image for varying offline distances (a) 5 m (b) 10 m (c) 15 m (d) 20 m. Dispersion images obtained by filtering out frequency band below 10 Hz at offline distance of (e) 15 m (f) 20 m

9.3.1 Evaluation of the Resolution of Dispersion Images

Resolution of the dispersion image can be defined as the capacity to discriminate the phase velocity at a particular frequency from other adjacent phase velocities (Zhang *et al.*, 2004). Therefore,

narrower the width of the dispersion band, easier and accurate will be the extraction of dispersion curve from the dispersion image. On the other hand, in case of wider energy band, it will be difficult to differentiate between the true phase-velocities from the apparent adjacent ones. Hence, the resolution of the dispersion image can be quantified based on the width of the energy band in the velocity-axis or along the frequency axis of the dispersion image. A term, *dv*, is used to measure the thickness of energy band along the velocity axis, at any required frequency. For example, in Fig. 9.9(a-d), at a frequency of 10 Hz, the value of *dv* are approximately 30, 150, 200 and NR (Not recognizable) at offline distances *dy* = 5, 10, 15 and 20 m, respectively. Therefore, in case of a selection of phase velocity at 10 Hz frequency, maximum possible error is only 30 m/s in case of *dy* = 5m, while for other offline distances, the potential error can be of unrealistically higher magnitudes. Such high errors in phase velocity determination directly affects the accuracy of final shear wave velocity (V_s) profile of the site, and will eventually lead to an erroneous survey outcome. For a better comparison, other values of *dv* at various frequencies are listed in Table 9.1.

Table 9.1 Values of *dv* at different frequencies for different offline distances

Offline distance *dy* (m)	**Values of *dv*(m/s)**				**Quality of dispersion image**
	at 7.5 Hz	**at 10Hz**	**at 12.5Hz**	**at 15Hz**	
5	100	30	20	15	Good
10	NR*	150	40	30	Fair
15	NR*	180	40	30	Fair
20	NR*	200	100	100	Poor

*NR – Not recognizable

9.4 Reliability of Passive Roadside MASW Survey

In view of recognizing the reliability and efficacy of the Passive Roadside MASW survey in generating the resultant shear-wave velocity profiles, the more conventional Active MASW and Passive Remote MASW tests were also conducted, and results are compared. As the active and passive remote methods are well established, their comparison with roadside survey results will aid in establishing the latter as a self-sufficient method.

9.4.1 Comparison with Active MASW Survey

For the purpose as mentioned above, a set of active MASW tests were conducted at all the different offline distances, as used in the Passive roadside MASW tests (Fig. 9.2b). The details of various geometrical and acquisition parameters are listed in Table 9.2.

Table 9.2 Details of various parameters tested for active surveys

Inter-receiver spacing(m)	Source offset(m)	No of receivers	Sampling frequency (Hz)	Offline distance (m)
1	1 to 10	24	1000, 2000, 3750	5, 10,15, 20
2	2 to 16	24		
3	3 to 15	12 to 24		

It is to be mentioned here that the comparison of effectiveness of various geometrical and acquisition parameters of active MASW survey are not the in the scope of this study, and is already well documented in the literature (Taipodia *et al.*, 2018a, 2018b). Therefore, in this report, only the best outcomes from the active survey (obtained from optimum geometrical configurations and recording parameters as listed in Table 9.2) are presented. All the active MASW tests were carried

out using a 10 kg sledgehammer as a source of impact, 4.5 Hz geophones as receivers and the same 32-bit seismograph as used in all the other passive experimentations. At least 3 numbers of raw records were collected at every set up of the receiver array. However, only the data of superior quality, with high SNR and without significant contamination from ambient noise, are used for comparison; the data used for the study are shown in Fig. 9.10. Therefore, there were no requirements of conducting vertical stacking during the processing of the active data. The details of extensive active MASW surveys conducted in similar sites can be found in literature (Taipodia and Dey, 2018; Taipodia *et al.,* 2017, 2018a, 2018b, 2018c)

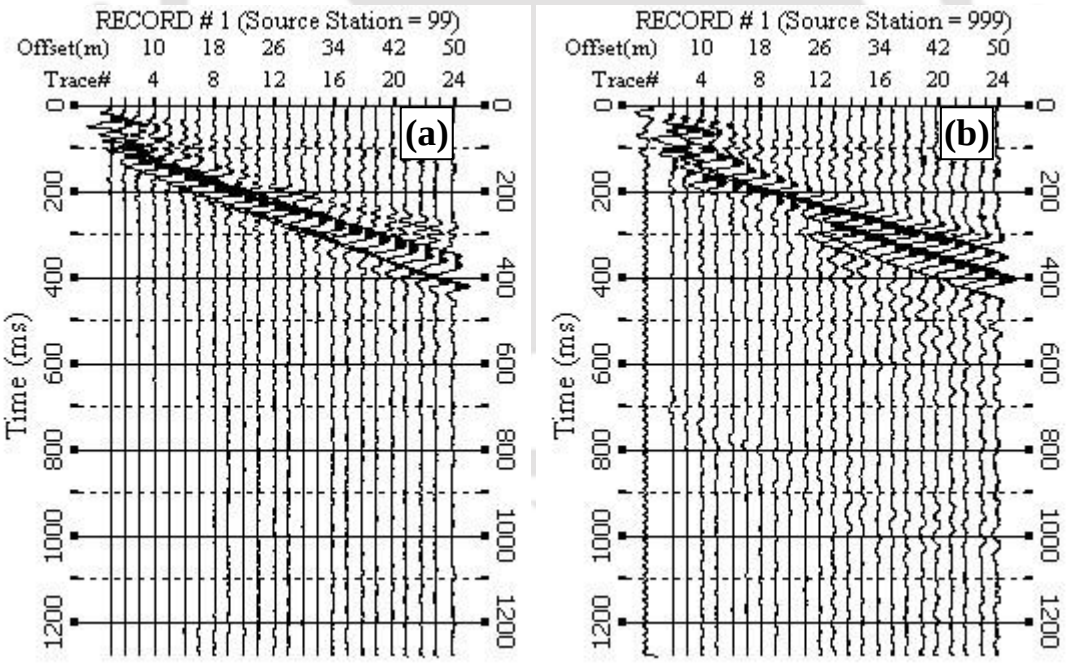

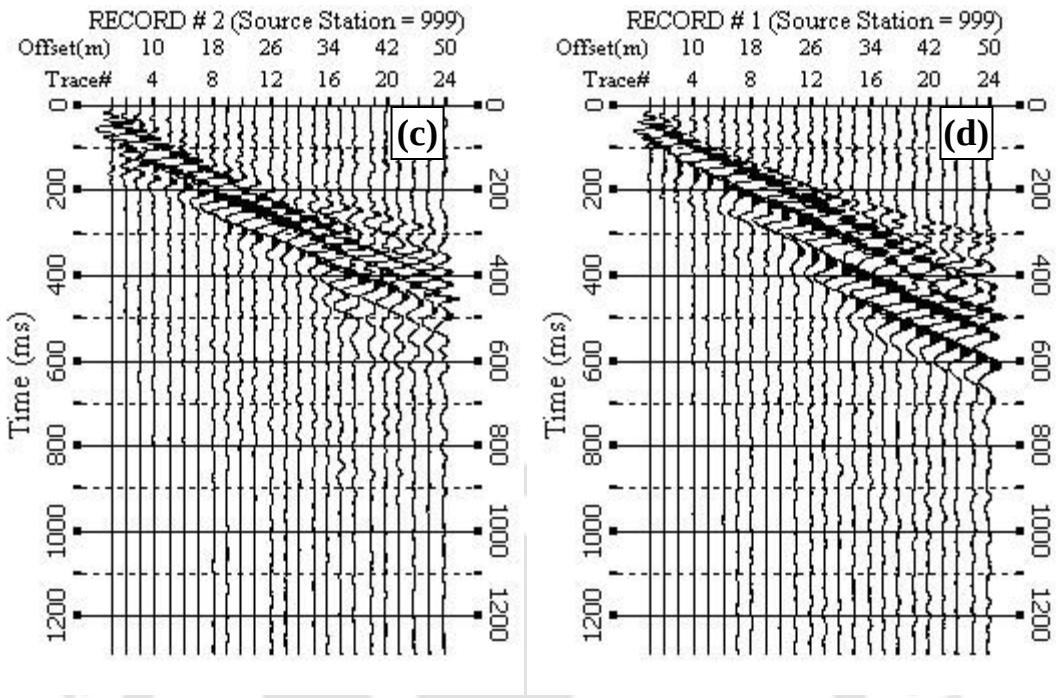

Fig. 9.10 Field record from active tests at offline distance of (a) 5 m (b) 10 m (c) 15 m **(**d) 20 m

Figure 9.11 shows the dispersion images from active MASW survey obtained at different offline distances adopted in the Passive Roadside MASW survey. All the dispersion images are of excellent resolution and have a clear and distinct fundamental mode energy band in a frequency zone of approximately 7-30 Hz. The superior quality dispersion images were attributed to the high quality of raw field data and better control in the pre-processing tools and parameters. Prior to the dispersion imaging, the primary pre-processing tools, namely 'muting' and 'filtering', were utilised on the raw wavefield records. Both of these tools help in enhancing the SNR of the recorded signals by eliminating unnecessary noise from the data, and thereby help improving the resolution of dispersion image (Taipodia *et al*., 2018b). With the aid of the muting tool, all the noises below or above a particular favourable region, in the time domain, can be curtailed to give a cleaner record. In all of the above records, wavefields beyond 600 ms portion were muted, since the primary active surface event exhibits no visible wave component beyond the selected portion,

and, thus, was considered unnecessary for the analysis. With the aid of the filtering tool, unnecessary high frequency component waves (such as body waves, reflected, refracted and backscattered waves which have a frequency greater than 100 Hz), are filtered, and only the utilizable frequency surface wave components are preserved from the field record. There are normally three types of digital filters available in SurfSeis, namely the high-cut, the low-cut and the band-pass filter. A high-cut filter restricts the higher frequency components and allows low frequencies to pass through; a low-cut filter restricts the lower frequency components and allows the higher frequencies to pass through; while a band-pass filter allows only a particular band of frequencies to pass through and restricts the remaining of the spectra. In all the pre-processing editing of the active data, a high-cut filter was used, since the primary objective of all the experimentation is to preserve the highly informative and dispersive low frequency waves. The cutting frequencies *f1* and *f2* were set around 50 Hz and 60 Hz, respectively, wherever necessary. However, in many of the wavefield signature, filtering was not required, attributed to the excellent quality of the recorded data. The comparison of the final V_s profiles obtained from the active surveys with that of roadside and remote surveys, at different offline distances, will be exhibited in the following sections.

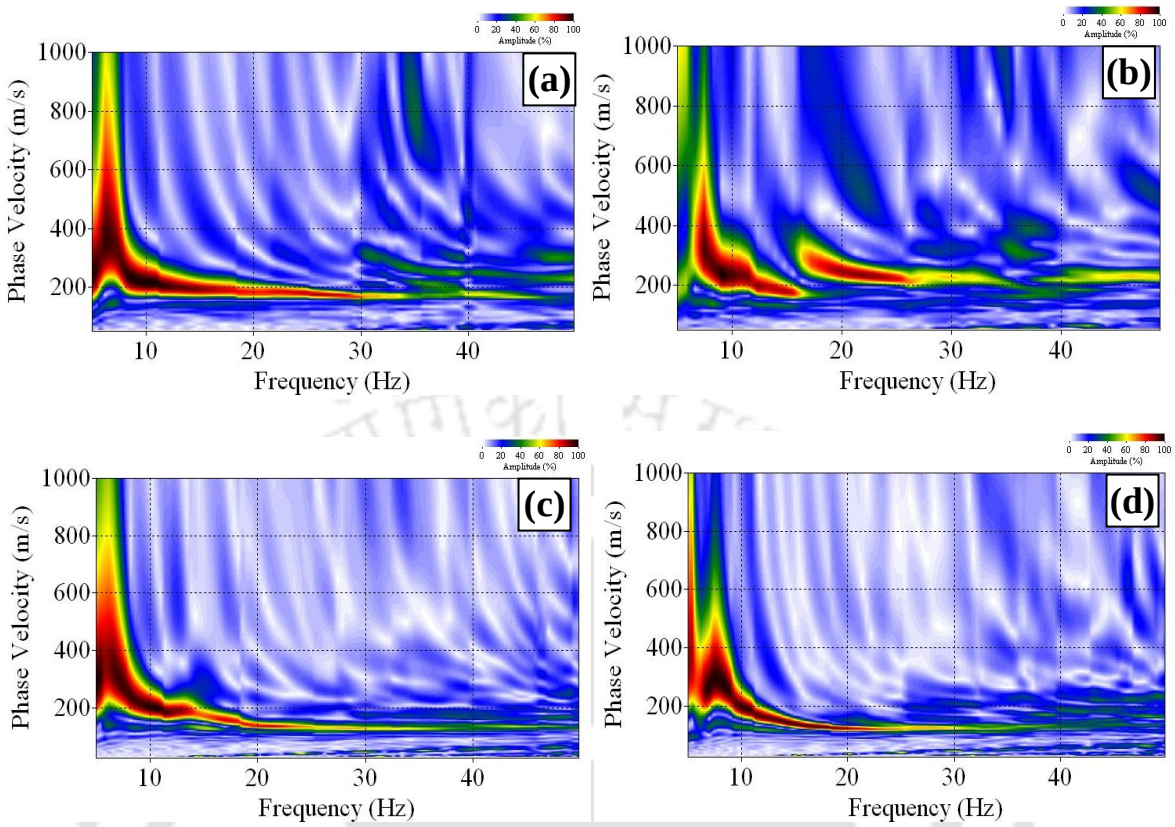

Fig. 9.11 Dispersion images from active MASW tests conducted at Site 1 with inter-receiver spacing of 2 m and with varying offline distances (a) 5 m (b) 10 m (c) 15 m and **(**d) 20 m

9.4.2 Comparison with Passive Remote MASW Survey

It was observed in the previous section that in case of passive roadside survey, with increasing offline distance, the resolution of dispersion image continues to degrade particularly in lower frequency region. This is attributed to the fact that 1-D nature of arrays, in roadside survey, with increasing offline distance, is unable to collect the directional passive surface waves. In such situations, a 2-D array may be adopted and, accordingly, a passive remote survey can be conducted to address the stated complexity.

In this investigation, a passive remote MASW survey was conducted at the mentioned site for checking the possible improvement in dispersion imaging at higher offline distance. The layout of the remote survey is shown in Fig. 9.12, along with a schematic view in Fig. 9.13. A circular array was utilised for the experimentation, having a diameter of 18 m. Twenty-four geophone receivers were placed along the circumference of the measured array, at an inter-receiver peripheral spacing (*dx*) of 2.35 m. While laying a 2-D circular array for passive remote survey, the two parameters to be carefully noted are (a) the angle of the first receiver with respect to a particular reference direction (North-South or East-West), and (b) the installation pattern of the receiver array (clockwise or anticlockwise). These parameters are vital geometrical parameters in passive remote survey and are required during pre-processing of dispersion analysis. Normally, passive remote MASW survey records all the ambient signals and is not limited to only traffic generated surface waves from roadways. However, as the chosen site was mostly silent and no significant cultural activities, other than traffic, were observed during any of the above surveys, a surface source was used on the nearby road as the ambient noise generator, in the similar manner as applied in passive roadside MASW survey. The primary advantages of utilising such a source on the road surface for passive remote survey are the following:

(a) Firstly, it will produce a significant amount of wavefield upon the passage of vehicles over it, and, hence, it will not be necessary to rely on other passive surface waves. It will thus provide a reliable and simplified recording strategy.

(b) It will limit the acquisition time as the recording of the field data will be primarily during movement of vehicles and, thus, will save a significant amount of data acquisition time.

(c) Lastly, and most importantly, it will yield an identical situation to that with roadside survey from the point of view of the position of the source and magnitude of the surface wave

energy produced from it. Hence, the characteristics, outcomes and shortcoming of the roadside survey can be compared directly to those obtained from the remote survey.

Fig. 9.12 Pictorial view of the circular array used for passive remote survey at Site 1

The source for the surface wave generation for the remote survey was the same GI rod that was utilised in the roadside survey. It was placed on the road exactly at par with the 7th receiver geophone of the array, as shown in Fig. 9.13. The acquisition time was chosen to be the same as used in roadside survey, i.e., 10.4 s, which was already found sufficient for the purpose. Twenty numbers of raw field records were collected for taking the benefit of vertical stacking during processing. Each record was collected based on the passage of a single vehicle above the placed source.

A directional or azimuthal study of the experiment was carried out to confirm the effectiveness of the intended source utilized for the purpose. It can be observed from the schematic of the array laid in the field, as shown in Fig. 9.13, that the source was nearly at an angle of 150° with the horizontal line passing through the centre of the circular array. Figure 9.14 represents the azmiuthal

location of surface wave events and respective frequency content indicating the direction of origination of the major incoming waves with their dominating frequency band. In the figure, the strongest energy could be observed starting from approximately 150°, with a dominating frequency band in 5-10 Hz. Thus, the analytical finding of the azimuth of the source agreeably converges with the true situation. The dispersion image obtained from the remote survey is shown in Fig. 9.15. The resolution of the image is superior in lower frequency band (in 5-15 Hz), in spite of high offline distance, contrary to passive roadside image. Finally, it can be observed that the dispersion energy trends from all the three tests complement well with each other. However, the true matching of the results can be ascertained from the comparison of the corresponding V_s profile.

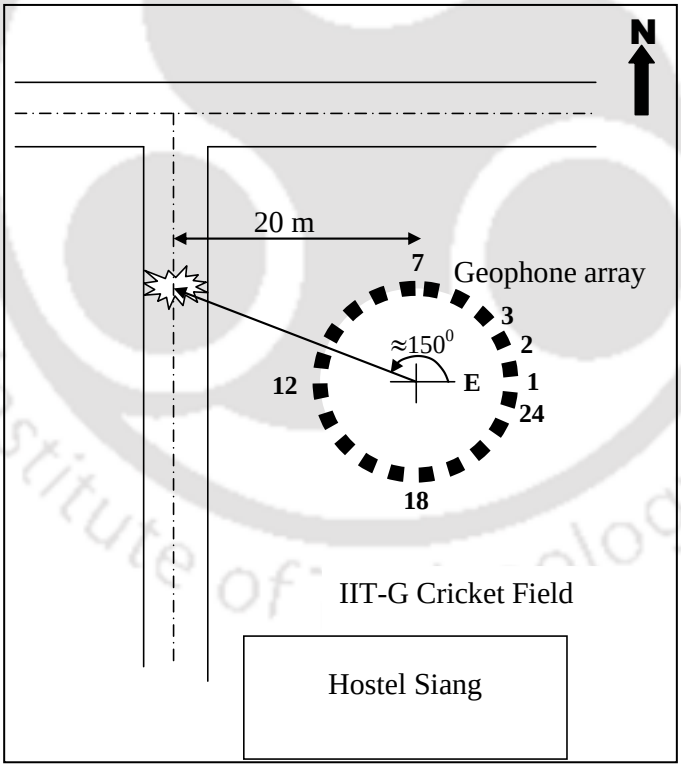

Fig. 9.13 Schematic of passive remote survey conducted at Site 1

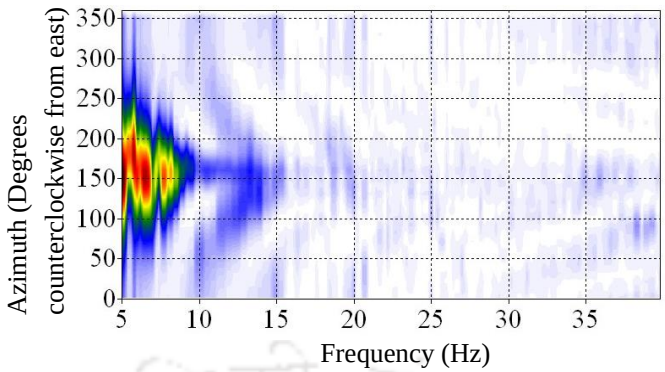

Fig. 9.14 Azmiuthal location of surface wave events and corresponding frequency content

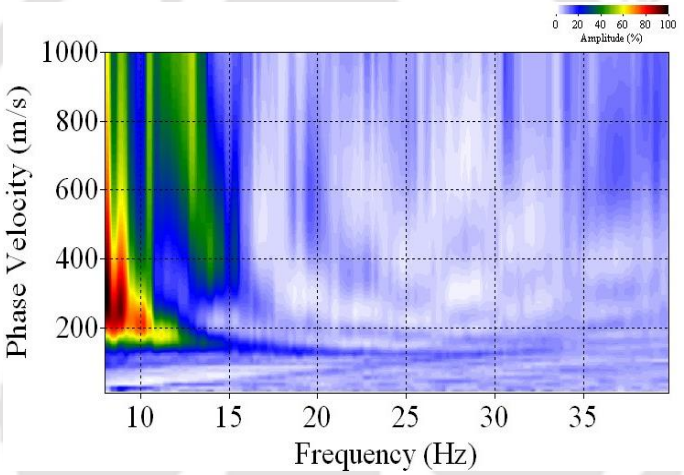

Fig. 9.15 Dispersion image obtained from remote surrvey at 20 m offline distance

After obtaining the dispersion images with desired quality and resolution, dispersion curves were manually extracted while maintaining the highest signal–to-noise ratio (SNR), in the order greater than 90% for all the cases. High SNR values of a dispersion curve is indicative of its probable accuracy and reliability. Hence, shear wave velocity profile obtained from such dispersion curves will be more oriented towards a reasonable and practical profile. The V_s profiles obtained from passive roadside, passive remote and active MASW surveys were systematically compared for different offline distances (Fig. 9.17). All the V_s profiles were obtained with marginal numbers of

iterations (less than 20) and with low Root Mean Square (RMS) error (less than 5 m/s), which further adds to the confidence on the experimental investigation and the subsequent analysis. It can be observed from Fig. 9.17a that at 5 m offline distance, both active and passive roadside method gives identical results with close match between the V_s values, the maximum difference being 15%. For higher offline distances, the velocity profile matches closely except in uppermost 5 m layer, where a recognizable deviation occurs between the V_s values obtained from the two methods. This particular difference in V_s values for 20 m offline distance reaches up to 120%. This difference is mainly due to rapid attenuation property of higher frequency components of passive surface waves. As a result, the waves of higher frequency may not be recorded effectively, leading to missing or misleading information of shallow subsurface layers. It is reported in the earlier studies that such uncertainty in the high frequency range in case of active MASW survey is significantly less (Park *et al.*, 2005; Foti *et al*., 2007; Yoon, 2011). Hence, for better resolution in both shallower and deeper layers, an active MASW test in combination with passive roadside test is recommended. The V_s profile obtained from remote survey matches closely with that obtained from the active survey, as shown in Fig. 9.17d, exhibiting a mutual reliability.

9.4.3 Comparison with SPT Borehole Survey

A borehole test was conducted near the site of the present investigation. It shows a predominantly loose clayey stratum overlying a stiffer sandy stratum. The Standard Penetration Test (SPT) conducted at the site indicates a low stiffness up to 9 m depth, while it increases thereafter. The detailed borehole log is shown in Fig. 9.16. It is worth mentioning that the location of the MASW test and the SPT test are not exactly in the same place; the SPT tests were conducted in front of Hostel Siang and towards the east of the cricket field (as visible in Fig. 9.2b). Moreover, the

borehole survey was conducted in 2002, and thus a significant time lapse exists between the SPT and MASW tests. Therefore, some minor differences in the V_s values obtained from the two tests are expected to exist in the direct comparison made between the results of the two methods, as exhibited later in the corresponding section.

The receiver location at 20 m offline distance is closest to the location of the borehole survey and, hence, the same was used for the comparison of V_s profile on that particular location. The V_s values from SPT-N values were obtained by utilising the correlation, $V_s = 97N^{0.314}$, proposed by Imai and Tonouchi (1982). The trend of V_s profile from SPT-N values matches well with the other profiles from MASW surveys, particularly up to the depth of 14 m. Beyond this depth, there is some deviation between the results from SPT-N and MASW, which can be an actual site characteristic, particularly since the sites for MASW and SPT are not exactly the same. Table 9.3 represents the actual V_s values obtained from different modes of MASW technique and from SPT-N values. As it can be observed, the V_s values from MASW tests (mainly active and passive remote results) match closely with SPT-N values, particularly up to 14 m depth. It is worth mentioning that the sharp increase in V_s values at the bottom-most layers, in most of the profiles from MASW tests, mostly arise from numerical artefacts and are not considered for comparison or analysis.

Type of Boring: Auger /Wash **Date started:** 21/10/2002

Place: Site-1 IIT Guwahati **Date completed:** 23/10/2002

Description of strata	Depth (m)	Strata	Sample collected (m)	Ground water level	SPT	N-Value
Clay soil grey to brown in colour	1		1.5			3
	2					
Black pit soil	3		3			2
	4		4.5			3
	5					
Clay soil grey in colour	6		6			4
	7		7.5			5
	8					
Clay soil ash in colour	9		9			6
	10		10.5			18
	11					
Clay soil brown in colour (hard soil)	12		12			24
	13		13.5			31
	14					
Silty clay grey in colour	15		15	Ground water level at 3 m		20
	16		16.5			22
Sandy clay ash to grey in colour	17					
	18		18			15
Clay soil grey in colour	19		19.5			17
	20					
Sandy clay grey in colour	21		21			22
	22		22.5			26
	23					
Sandy clay grey in colour	24		24			30
	25		25.5			32
Silty clay grey in colour	26					
	27		27			36
Sandy clay ash in colour	28		28.5			39
	29					
Sandy clay black in colour	30		30			42

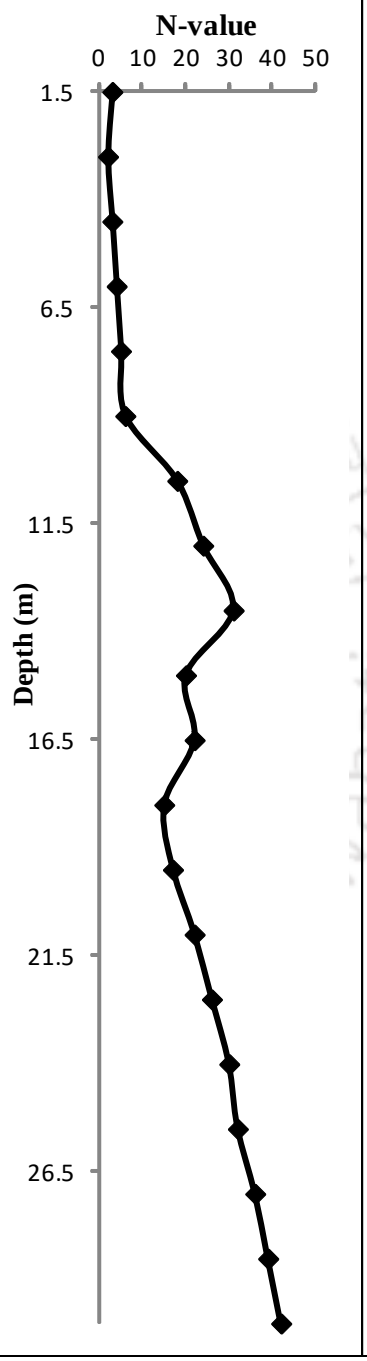

Fig. 9.16 Borehole log report of the hostel site nearby to the MASW test site

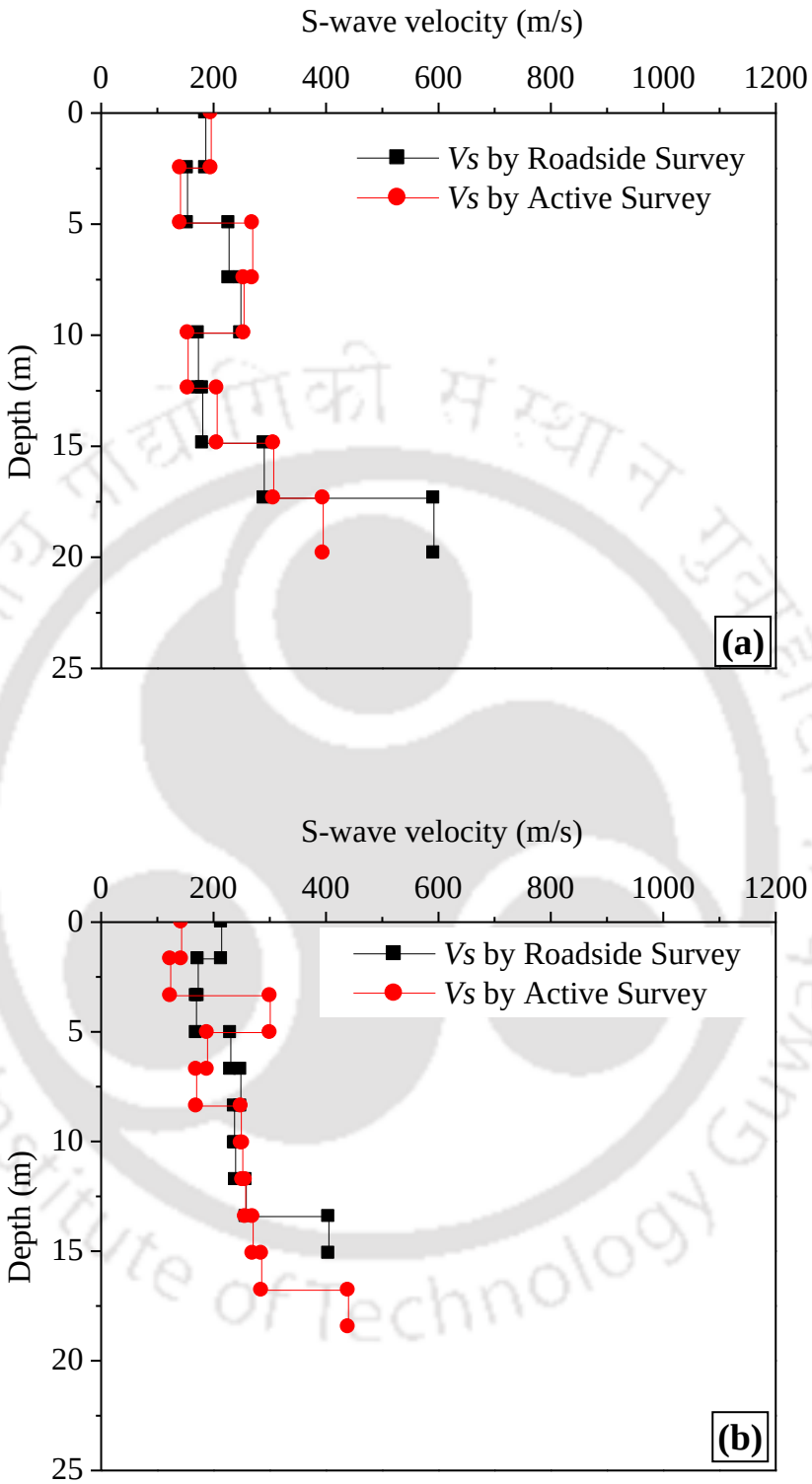

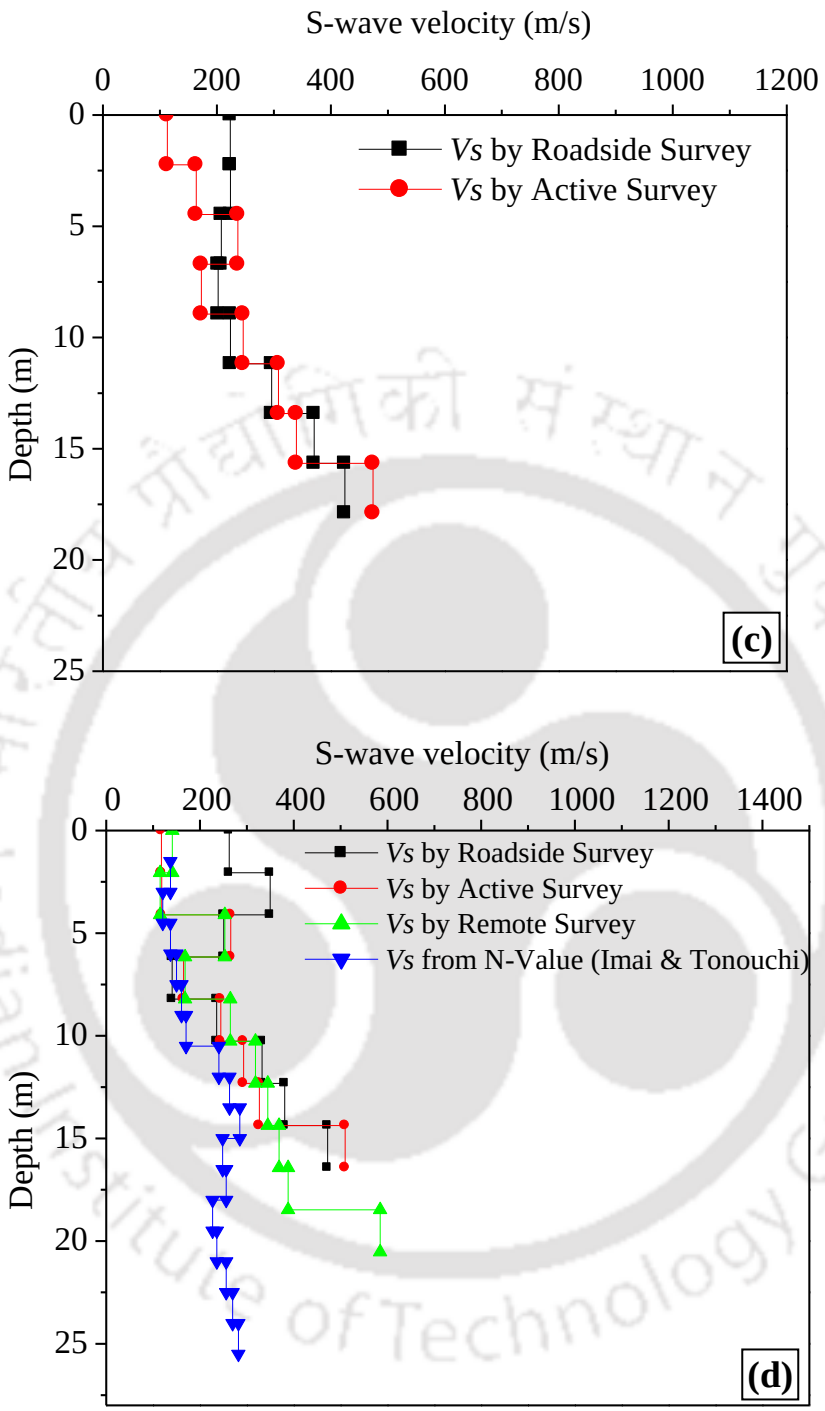

Fig. 9.17 Comparison of shear-wave velocity profiles obtained from various techniques with geophone arrays placed at various offline distances from centreline of the road (a) 5 m (b) 10 m (c) 15 m (d) 20 m

Table 9.3 Comparison of V_s profiles at 20 m offline distance

V_s determination from MASW test				V_s determination from SPT Test	
Depth (m)	**V_s by Roadside survey (m/s)**	**V_s by Active survey (m/s)**	**V_s by Remote survey (m/s)**	**Depth (m)**	**V_s converted from SPT-N value (m/s)**
0	262.24	117.58	140.89	0	136.95
				1.5	137.00
2.05	262.24	117.58	140.89	3	136.96
				4.5	120.59
4.11	349.82	118.34	115.02	6	136.96
				7.5	149.91
6.16	250.78	265.74	253.09	9	160.79
				10.5	170.26
8.2	140.85	165.14	168.38	12	240.40
				13.5	263.12
10.27	235.76	244.41	264.64	15	285.14
				16.5	248.48
12.32	332.2	293.02	318.55	18	256.03
				19.5	227.02
14.37	380.61	326.67	344.88	21	236.12
				22.5	256.03
16.43	472.37	509.67	368.72	24	269.82

Fig. 9.18 represents the percentage variation of shear wave velocity obtained from roadside, remote and active MASW survey, with geophone receiver array being placed at 20 m offline distance from the centreline of the road. Between each pair of methods, the percentage variations of the results were calculated based on the established conventional technique. Therefore, the variation of passive roadside v/s active surveys and passive remote v/s active surveys are calculated on the basis of active results; whereas, the variation of passive roadside v/s passive remote surveys is calculated on the basis of passive remote results. It can be observed that differences in V_s profile between roadside v/s active and between roadside v/s remote surveys are highest at the upper 5 m layer. Moreover, the V_s profile obtained from remote and active survey are almost identical and no

significant deviation between the two results is observed. Table 9.4 represents the exact percentage difference in the V_s values obtained from the three modes of surveys with respect to subsurface depth. It can be observed that at a depth of 4.1 m from the surface, the percentage difference in V_s reaches as high as 195% between passive roadside v/s active surveys, and nearly 204% between passive roadside v/s passive remote V_s profiles. However, with the further increase in depth, the percentage difference in V_s values obtained from the three modes of surveys continually decreases.

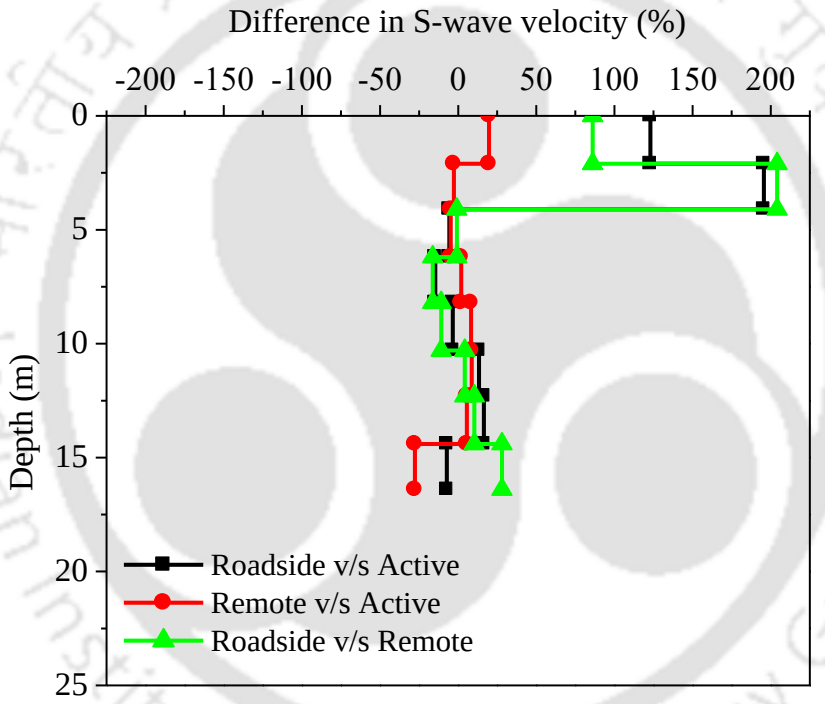

Fig. 9.18 Percentage variation of S-wave velocity of passive roadside v/s active surveys and passive remote v/s active MASW tests

Table 9.4 Comparative of V_s profiles at 20 m offline distance obtained from different methods

Depth (m)	Passive roadside v/s Active (m/s)	Percentage difference Passive roadside v/s Active	Passive remote v/s Active (m/s)	Percentage difference Passive remote v/s Active	Passive roadside v/s Passive remote (m/s)	Percentage difference Passive roadside v/s Passive remote
0	144.66	123.0	23.31	19.8	121.35	86.13
2.05	144.66	123.0	23.31	19.8	121.35	86.13
4.10	231.48	195.6	-3.32	-2.8	234.80	204.14
6.16	-15.02	-5.7	-12.65	-4.7	-2.37	-0.94
8.21	-24.29	-14.7	3.24	1.9	-27.53	-16.35
10.26	-8.66	-3.5	20.23	8.2	-28.88	-10.91
12.32	39.25	13.4	25.53	8.7	13.72	4.31
14.3	53.92	16.5	18.19	5.5	35.73	10.36
16.42	-37.30	-7.3	-140.95	-27.6	103.65	28.11

9.5 Summary

Passive roadside surveys involve complex source characteristics with existence of multiple source having varying azimuthal characteristics. In the current study, the influence of source location in terms of intra-line and outer-line positioning, existence of multiple numbers of strong sources of wavefields, and effect of offline distance of receiver arrays, on the resolution of dispersion image is highlighted, and the resultant V_s profile are illustrated. The primary inferences that are drawn from the study are as follows:

- Both intra-line and outer line scenarios result in identical dispersion images. A slightly better resolution is observed in case of intra-line source, particularly in the lower frequency band, which is attributed to the ability of recording stronger low frequency components of surface waves.

- ❖ Multiple sources have marginal effect on dispersion imaging until there is no contamination of the raw records by mutual interferences.
- ❖ Applicability of roadside survey vastly depends on the accommodated offline distance. Based on the present study, to have recognizable dispersion image, the highest offline distance that can be adopted is found to be 15 m.
- ❖ Increase in offline distance of the receiver array from the centerline of the road yields ambiguous shear-wave velocity profile in the shallower layers (within 5 m form the ground surface). This phenomenon is attributed to the inefficiency of the receiver array, placed at a distance from the centerline of the road, in recording attenuated high frequency Rayleigh waves generated by the passive sources.
- ❖ Based on the close comparison of the results of Passive Roadside MASW survey with those of conventional surveys (Active MASW and Passive remote MASW), the efficacy and applicability of the adopted Passive Roadside MASW technique in identifying subsurface characteristics utilizing the vehicular movement on the roads is suitably established.

CHAPTER 10

CONCLUSIONS AND RECOMMENDATIONS

10.1 Summary and Conclusion

Subsoil exploration with non-destructive surface wave techniques are becoming cheap and effective alternative to the conventional borehole methods. These techniques have been significantly developed over the last few decades by various researchers around the globe. Multichannel analysis of surface wave, or shortly MASW, has been a popular surface wave technique of subsurface exploration ever since its inception, attributed to its swiftness and reliability over the other surface wave techniques. The method utilises the dispersive characteristics of Rayleigh waves in heterogeneous soil medium and yield subsurface information in terms of V_s profile at the surveyed area. Based on the nature of surface wave sources utilised during the survey, MASW survey can be conducted in two modes - Active and Passive survey. Active method utilises an intentional source of wave generation such as a sledgehammer or weight drop, while the latter uses ambient passive sources of natural, cultural or traffic origin. Passive method is again classified into two types based on receiver layout in the field and utilised source of wavefield generation, namely Passive Remote and Passive Roadside. Symmetrical 2-D array shapes are utilised in the remote method to record ambient low frequency signals, while linear 1-D arrays are used in roadside survey aiming mainly to collect signals from traffic sources. Primary steps in MASW survey irrespective of the mode of survey are acquisition of raw field data of wave propagation, dispersion analysis or imaging for characterising frequency dependent phase velocities, and inversion analysis of the result obtained from dispersion analysis to obtain final 1-

D V_s profile of the surveyed area. Dispersion analysis is the most critical stage in MASW as the accuracy of the final V_s profile depends largely on the accuracy of dispersion imaging stage. Under the present research, a detailed study on various aspects and parameters of passive roadside MASW survey affecting its dispersion imaging, and the subsequent subsurface profiling, have been reported.

In the present investigation, three different test sites with different traffic volume have been selected for conducting extensive passive roadside survey inside and nearby IIT Guwahati campus, India. Site 1 is inside IIT Guwahati campus, Site 2 is a road stretch from IIT Guwahati towards Amingaon, and Site 3 is a stretch along national highway NH-31. The three test sites comprise light, medium and heavy volume of traffic, respectively. Passive roadside surveys were conducted in each test site with varying receiver array length from 23-92 m, and acquisition time ranging from 0.7-218 s. Multiple field records have been collected for every testing array during each acquisition time. For comparison of the results obtained from passive roadside survey, active MASW tests have been conducted at every site with varying geometrical and acquisition parameters. The favourable conditions of Site 1 have been utilised to perform a set of passive remote survey. It has been performed using a circular array of diameter 18 m and with 24 numbers of receivers and utilising traffic originated surface waves. The available borehole data of the site further assisted in an extensive comparison.

Based on the various observations and results, the following conclusions can be made on the characteristics of raw field data and resolution of dispersion imaging.

1. Without the presence of major surface sources on the road, traction of any type of vehicle produces significant surface wave energy recordable by the receiver. However, motion of heavier vehicles, such as a bus weighing around 10000 kg, is more effective for creating wavefield of desired energy for passive roadside survey. Presence of a major surface source, i.e., a road surface irregularity, is beneficial for larger impact and generation of surface waves with higher energy. This helps in attaining better resolution dispersion image.
2. Length of receiver array plays significant role in establishing the resolution of dispersion image. The ratio between the longest recordable wavelengths to the receiver array length is obtained in the range of 0.6-1 from the dispersion images. In passive roadside surveys, the highest ratio between the depths of investigation to the longest wavelength recorded is approximately 0.4. At sites with heavy traffic volume, longer array, in the range of 92 m, suffers wavefield contamination, while comparatively shorter array, in the range of 46 m, is effective in sampling higher frequency dispersive components.
3. Acquisition or recording time is a site-specific parameter and depends largely on volume of the traffic and number of existing sources on the road surface nearby the test site. For light, medium and heavy traffic volume conditions, optimum acquisition time of 10.8 s, 5.4 s and 1.4 s, respectively, is beneficial. Smaller recording time is effective for cleaner raw data acquisition at sites comprising heavy traffic flow.
4. Selecting the best-suitable site-specific scanning frequency and velocity range during dispersion analysis, that is achieved by discarding contaminated and/or aliased energy

bands, is important for enhancement of dispersion image resolution. Careful scrutiny of frequency-amplitude spectra is required to decide for the best-suitable ranges.

5. Appropriate site-specific selection of azimuthal quadrants allow identifying the directions of major wavefield sources, thus making energy computation along azimuth axis constructive, thereby yielding dispersion image with better resolution.
6. An inline-processing (IP) scheme for a closely situated intra-line source results in a broader energy band in the dispersion image, and results in a dispersion curve with over-estimated phase velocities, particularly in the low frequency band. On the other hand, the OC scheme, which can be initiated by providing precise offline distance, can take account of such closely situated sources and its cylindrical wavefront, thereby resulting in superior dispersion image resolution and robust extraction of dispersion curve.
7. At least ten to twenty numbers of vertical stacks (by Method I) is required to develop dispersion images of higher resolution for passive roadside MASW surveys. The number of stacks also depends upon the number of raw field records containing major surface event, without which mere increase in number of stacking is not effective. However, with very few numbers (two or three) of good quality raw data, vertical stacking by Method II yields dispersion image with better resolution. Combined application of vertical stacking by Method I and Method II, on intra-line and outer-line source induced images, results in superior dispersion images.
8. The lowest frequency component on a dispersion curve controls the maximum achievable investigation depth, while on the other hand, increases the RMS errors in the subsurface profile. Depending on the requirement of depth of investigation, necessary precision should

be adopted to select the lower frequencies of the dispersion curve to obtain reliable subsurface profile.

9. Density of dispersion curve selection within a frequency range affects the stability of inversion and the reliability of obtained shear-wave velocity profile. A dispersion curve, spanning over a frequency band of **X** Hz, should be represented by at least 2**X** number of dispersion points, for better and reliable subsurface profiling.
10. Higher number of layers, seven or more, in the initial earth layer model provides a stable and reliable V_s profile. Lowering the number of layers in the initial model leads to higher deviations in the final profile.
11. Although the intra-line and outer-line source scenarios result in similar energy trends on the dispersion image, a slightly better resolution in the lower frequency band is obtained in the case of intra-line source. The outer-line source yields a higher resolution dispersion image in the higher frequency bands.
12. Multiple sources have marginal adverse effect on dispersion imaging as long as there is no contamination on the raw records by mutual interferences.
13. The offline distance controls the usability of passive roadside MASW survey. In order to obtain a recognizable dispersion image, the highest offline distance that can be adopted is 15 m from the centerline of the road. Increase in offline distance leads to ambiguous shear-wave velocity profile in the shallower layers within 5 m from the ground surface.

10.2 Recommendations and Guidelines

Based on the understanding developed from the experimental investigations with passive roadside MASW survey using 4.5 Hz geophone and its subsequent dispersion and automated inversion

analysis, the following recommendations and guidelines have been developed. Adopting these guidelines, during data acquisition, subsequent dispersion and inversion analyses, would aid in developing higher resolution dispersion images, leading to reliable estimates of subsurface profile.

- *Guidelines and recommendations for data acquisition*
  - Medium traffic with heavier vehicles (1000 kg or more) with speeds greater than 30 kmph.
  - Simultaneous intra-line and outer-line sources having sufficient temporal spacing to avoid mutual contamination.
  - A receiver array length greater than 46 m.
  - An acquisition time of 1-10 s.
  - An offline distance less than 15 m from the centreline of the road.
  - Adopting minimum 10 numbers of vertical stacks.
- *Guidelines and recommendations for dispersion analysis*
  - Scanning frequency range of 5-50 Hz and scanning velocity range of 10-1500 m/s, with judicious elimination of the low-frequency ranges showing aliasing or banding effects.
  - Appropriate selection of the quadrants, for scanning azimuths, facing the vehicular movements in the road.
  - Selecting OC scheme for wavefield analysis.
- *Guidelines and recommendations for inversion analysis*
  - Lowest frequency for dispersion curve should be judiciously selected to avoid low-frequency aliasing effect.
  - Dispersion point selected should be at every 0.5 Hz frequency.
  - Initial earth model with minimum 7 layers should be chosen, or as guided by a-priori borehole survey.

10.3 Limitations and Future Scopes

Any research will have its own limitation and shortcomings, and the same paves the way for future advancements. The following lists the limitations of the present study and the scope of future research are also mentioned.

- The Passive MASW survey used in this study is conducted using 4.5 Hz geophones, which suffices the target depth of present investigation to 15-30 m achieved through stacking of the dispersion images obtained through multiple repetitions of the test. Other low-frequency geophones (1 Hz or 2 Hz) could not be used or checked due to their unavailability during the conduct of this research. Application of geophones of lower frequency should be tried out in future so that larger depths of soil substrata can be investigated using traffic originated wavefields.
- The present study primarily uses the least-squares based local search algorithms for finding a match between the theoretical and experimental dispersion curves during the inversion analysis. Advanced methods of search algorithms employing Monte-Carlo based random searches or Genetic algorithm and population based searches should be explored to check for possibly better inversion analysis.
- Both velocity and mass of moving vehicles contribute to the generated wavefield. However, the present study only paid attention to the mass of the moving vehicle. Further studies should be conducted in the context of the genres of vehicular traffic, to establish detailed understanding and guidelines correlating the weight, speed and traction of vehicles passing over different depths of surface irregularities.
- In this study, the IP, OP or OC processing schemes were chosen based on the offline and offset distance of the vehicle from the linear receiver array. However, further studies on

the theoretical understanding of processing schemes should be carried out to address the mixed-scheme conditions when the receiver array simultaneously receives various types of waves depending upon the location of multiple vehicles.

- The present study uses manual intervention for the extraction of dispersion curve, which induces user subjectivity in extracting the dispersion curve. Further studies are required to develop automated techniques of dispersion curve extraction to eliminate the subjectivity of the user-based manual extraction.
- The present study considers the inversion of only the fundamental mode dispersion curve. However, depending upon the soil stratification, there can be multiple modes present in the dispersion image that can possess near-comparable energies. Hence, for such cases, further studies on multimodal dispersion analysis should be conducted.

REFERENCES

- Aki, K. (1957) "Space and time spectra of stationary stochastic waves, with special reference to microtremors" *Bulletin of the Earthquake Research Institute*, Vol. 35, pp. 415-457

- Aki, K. (1965) "A note on the use of microseisms in determining the shallow structures of the earth's crust" *Geophysics*, Vol. 30, pp. 665-666.

- Akin M. K., Kramer, S. L. and Topal, T. (2011) "Empirical correlations of shear wave velocity (V_s) and penetration resistance (SPT-N) for different soils in an earthquake-prone area (Erbaa-Turkey)" *Engineering Geology*, Vol. 119, pp. 1-17.

- Anbazhagan, P., and Sitharam, T. G. (2006) "Evaluation of dynamic properties and ground profiles using MASW: correlation between V_s and N_{60}" *Proceedings at 13th Symposium on Earthquake Engineering*, Indian Institute of Technology Roorkee.

- Anbazhagan, P., Bejaj, K., Moustafa, S. R., and Al-Arifi, N. S. N. (2018) "Acquisition and analysis of surface wave data in the Indo-Gangetic basin" *In: Wasowski J., Dijkstra T. (eds) Recent Research on Engineering Geology and Geological Engineering, Sustainable Civil Infrastructures*, Springer, Switzerland, pp. 1-13.

- Anbazhagan, P., Kumar, A and Sitharam, T. G. (2012) "Seismic site classification and correlation between standard penetration test n value and shear wave velocity for Lucknow city in Indo-Gangetic Basin" *Pure and Applied Geophysics*, Vol. 170, pp. 299-318.

- Ariffin, J., Ismail, M. A. M., Tan, C. G. and Murtadza, N. M. (2015) "Site characterization of marine clay deposits in South Seberang Prai, Penang using combined active and passive multichannel analysis of surface wave (MASW)" *IOP Conference Series. In Material Science and Engineering*, 136, pPaper no. 012032, pp. 1-9.

- Asten, M. W. (1977) "Theory and practice of geophone calibration in-situ using a modified step method" *IEEE Transactions on Geoscience Electronics*, Vol. GE-15(4), pp. 208-214.

- Asten, M. W. and Hentridge, J. D. (1984) "Array estimators and the use of microseisms for reconnaissance of sedimentary basins" *Geophysics*, Vol. 40, pp.1828-1837.

- Asten, M. W., Dhu, T. and Lam, N. (2004) "Optimized array design for microtremor array studies applied to site classification; comparison of results with SCPT logs" *Proceedings at 13th World Conference on Earthquake Engineering*, Canada.

- Banab, K. K. and Motazedian, D. (2010) "On the efficiency of the multichannel analysis of surface wave method for shallow and semideep loose soil layers" *International Journal of Geophysics*, vol. 2010, pp. 1-14.

- Beaty, K. S., Schmitt, D. R. And Sacchi, M. (2002) "Simulated annealing inversion of multimode Rayleigh wave dispersion curves for geological structure" *Geophysics Journal International*, Vol. 151, pp. 622-631.

- Boaga, J., Vignoli, G., Deiana, R. and Cassiani, G. (2014) "The influence of subsoil structure and acquisition parameters in MASW mode mis-identification" *Journal of Environmental and Engineering Geophysics*, Vol.19, pp. 87-99.

- Brandes, H. G., Robertson, I. N. and Johnson, G. P. (2011) "Soil and rock properties in a young volcanic deposit on the island of Hawaii" *Journal of Geotechnical and Geoenvironmental Engineering ASCE*, Vol. 137(6), pp. 597-610.

- BSSC (2003) "NEHRP recommended provisions for seismic regulations for new buildings and other structures" FEMA-450 (Part 1: Provisions), *Federal Emergency Management Agency*, Washington.

- Capon, J. (1969) "High-resolution frequency-wavenumber spectrum analysis" *Proceedings of the IEEE*, Vol. 57(8), pp. 1408-1418.

- Cheng, F., Xia, J., Luo, Y., Xu, Z., Wang, L., Shen, C., Liu, R., Pan, Y., Mi, B. and Hu, Y. (2016) "Multichannel analysis of passive surface waves based on cross-correlations" *Geophysics*, Vol. 81(5), pp. 1-10.

- Cheng, F., Xia, J., Shen, C., Hu, Y., Xu, Z. and Mi, B. (2018) "Imposing active sources during high-frequency passive surface-wave measurement" *Engineering*, Vol. 4, pp. 685-693.

- Chevatco, V. (2017) "Calibration of vibration sensors - Evaluation and Effectivization" *Degree Project in Electrical Engineering*, KTH Royal Institute of Technology, Sweden.

- Coccia, S., Del Gaudio, V., Venisti, N. and Wasowski, J. (2011) "Application of Refraction Microtremor (ReMi) technique for determination of 1-D shear wave velocity in a landslide area" *Journal of Applied Geophysics*, Vol.-71, pp.71-89.

- Comina, C., Foti, S., Boiero, D. and Socco, L. V. (2011) "Reliability of $V_{S,30}$ evaluation from surface wave tests" *Journal of Geotechnical and Geoenvironmental Engineering ASCE*, Vol. 137(6), pp. 579-586.

- Cox, B. R. and Beekman, A. N., (2011) "Intra method variability in ReMi dispersion measurements and V_S estimates at shallow bedrock sites" *Journal of Geotechnical and Geoenvironmental Engineering*, ASCE, Vol. 137, 354-362.

- Dal Moro, G., Pipan, M., and Gabrielli, P. (2007) "Rayleigh wave dispersion curve inversion via genetic algorithms and marginal posterior probability density estimation" *Journal of Applied Geophysics*, Vol. 61(1), pp. 39-55.

- Dal Moro, G., Pipan, M., Forte, E., and Finnetti, I. (2003) "Determination of Rayleigh wave dispersion curves for near surface applications in unconsolidated sediments" *Society of Exploration Geophysicists*, Expanded Abstracts, pp. 1247-1250.

- Dikmen, U, Arisoy, M. O. and Akkaya, I. (2010) "Offset and linear spread geometry in the MASW method" *Journal of Geophyics and Engineering*, Vol. 7, pp. 211-222.

- Dikmen, U. (2009). "Statistical correlations of shear wave velocity and penetration resistance for soils" *Journal of Geophysics and Engineering*, Vol. 6(1), pp. 61-72.

- Dorman, J. and Ewing, M., (1962) "Numerical inversion of seismic surface wave dispersion data and crust mantle structure in the New-York-Pennsylvania area" *Journal of Geophysical Research*, Vol. 67(13), pp. 5227-5241.

- Eker, A. M., Akgün, H. and Kockar, M. K. (2012) "Local site characterization and seismic zonation study by utilizing active and passive surface wave methods: A case study for the northern side of Ankara, Turkey" *Engineering Geology*, Vol. 151, pp. 64-81.

- Ezersky, M., Gorstein, M., Kalmanovich, M., and Perelman, N. (2013) "Combining H/V spectral ratio from ambient noise with multichannel analysis of surface waves (MASW) method to map subsurface: Test in the Dead Sea area" *Report No. GII-025-759-13*, Geophysical Institute of Israel.

- Fauzi, A., Irsyam, M. and Fauzi,U. J. (2014) "Empirical correlation of shear wave velocity and N-SPT value for Jakarta" *International Journal of GEOMATE*, Vol. 7(1), pp. 980-984.

- Foti, S., Comina, C., and Boiero, D. (2007). "Reliability of combined active and passive surface wave methods." *Rivista Italiana Geotecnica*, Vol. 41(2), pp. 39-47.

- Foti, S., Lai, C.G., Rix, G. J., and Strobbia, C. (2014) "Surface wave methods for near-surface site characterization" *CRC press*, Taylor and Francis Group.

- Foti, S., Parolai, S., Albarello, D. and Picozzi, M. (2011a) "Application of surface wave methods for seismic site characterization" *Surveys in Geophysics*, Vol. 32, pp. 777-825.

- Foti, S., Parolai, S., Bergamo, P., Di Giulio, G., Maraschini, M., Milana, G., Picozzi, M. and Puglia, R. (2011b) "Surface wave surveys for seismic site characterization of accelerometric stations in ITACA" *Bulletin of Earthquake Engineering*, Vol. 9, pp. 1797-1820.

- Gabriels, P., R. Snieder, and G. Nolet. (1987) "In situ measurement of shear wave velocity in sediments with higher-mode Rayleigh waves" *Geophysical Prospecting*, Vol. 35, pp. 187-196.

- Goh, T. L., Samsudin, A. R. & Rafek, A. G. (2011) "Application of spectral analysis of surface waves (SASW) Method: Rock Mass Characterization" *Sains Malaysiana*, Vol. 40(5) pp. 425-430.

- Gosar A., Stopar R. and Roser, J. (2008) "Comparative test of active and passive multichannel analysis of surface waves (MASW) methods and microtremor HVSR method" *RMZ-Materials and Geoenvironement*, Vol. 55, pp. 41-66.

- Gosniewski, J. P. (2011) "Bedrock mapping using shear wave velocity characterization and H/V analysis" *Masters of Science Thesis*, Ohio State University.

- Gucunski, N. and Wood, R. D. (1992) "Numerical simulation of the SASW test" *Soil Dynamics and Earthquake Engineering*, Vol. 11, pp. 213-227

- Heisey, J. S., Stokoe, K. H., and Meyer, A. H. (1982) "Moduli of pavement systems from spectral analysis of surface waves" *Transportation Research Record* 852, Transportation Research Board, Washington, D.C., pp. 22-31.

- Horike, M. (1985). "Inversion of phase velocity of long-period microtremors to the S-wave-velocity structure down to the basement in urbanized areas" *Journal of Physics of the Earth*, Vol. 33, pp. 59-96.

- Imai, T., and Tonouchi, K. (1982) "Correlation of N-value with S-wave velocity and shear modulus" *Proceedings of the 2nd European Symposium of Penetration Testing*, Amsterdam, pp 67-72.

- Ismail, M. A., Samsudin, A. R., Rafek A. G. and Nayan, K. A. M. (2012) "Road pavement stiffness determination using SASW method" *UNIMAS E-Journal of Civil Engineering*, Vol. 3, pp. 9-16.

- Jones, R. (1958) "In-situ measurement of the dynamic properties of soil by vibration methods" *Geotechnique*, Vol. 8(1), pp. 1-21.

- Jones, R. (1962) "Surface wave technique for measuring the elastic properties and thickness of roads: Theoretical development" *British Journal of Applied Physics*, Vol. 13, pp. 21-29.

- Kanli, A. I., Kang, T. S., Pinar, A., Tildy, P. and Pronay, Z. (2008) "A systematic geophysical approach for site response of the Dinar region, Southwestern Turkey" *Journal of Earthquake Engineering*, Vol. 12(S2), pp. 165-174.

- Kanli, A. I., Tildy, P., Pronay, Z., Pinar, A. and Hermann, L. (2006) "V_{s30} mapping and soil classification for seismic site effect evaluation in Dinar region, SW Turkey" *Geophysics Journal International*, Vol.165, pp. 223-235.

- Karray, M., and Lefebvre, G., (2008) "Techniques for mode separation in Rayleigh wave testing" *Soil Dynamics and Earthquake Engineering*, Vol. 29, pp. 607-619.

- Keceli, A. (2012) "Soil parameters which can be determined with seismic velocities" *Jeofizik*, Vol. 16, pp. 17-29.

- Khalil, A. E. and Hafeiz, E. A. (2012) "Applied MASW Technique for detecting soil condition underneath the packing unit in Helwan Cement factory" *Journal of American Science*, Vol. 8(8), pp. 37-43.

- Kühn, D., Ohrnberger, M. and Dahm, T. (2011) "Imaging a shallow salt diapir using ambient seismic vibrations beneath the densely built-up city area of Hamburg, Northern Germany" *Journal of Seismology*, Vol. 15, pp. 507-531.

- Lacoss, R. T., Kelly, E. J. and Toksoz, M. N. (1969) "Estimation of seismic noise structure using arrays" *Geophysics*, Vol. 34(1), pp. 21-38.

- Lai, C. G. and Rix, G. J. (1998) "Simultaneous inversion of Rayleigh phase velocity and attenuation for near-surface site characterization" *National Science Foundation and U. S. Geological Survey*, Georgia Institute of Technology, Atlanta.

- Leong, E. C. and Aung, A. M. W. (2013) "Global inversion of surface wave dispersion curves based on improved weighted average velocity method" *Journal of Geotechnical and Geoenvironmental Engineering, ASCE*, Vol. 139(12), pp. 2156-2169.

- Lin, C.P., Chang, C.C. and Chang, T.S., (2004) "The use of MASW method in the assessment of soil liquefaction potential" *Soil Dynamics and Earthquake Engineering*, 24, pp. 689-698.

- Liu, Y., Luke, B., Pullammanappallil, S., Louie, J. and Bay, J. (2005) "Combining active and passive source measurements to profile shear wave velocities for seismic microzonation" *Proceedings at Geofrontiers 2005 Congress*, Austin, Texas, Earthquake Engineering and soil dynamics, ASCE Geotechnical special publication (GSP)133, pp.-14.

- Long, M. and Donohue, S. (2007) "In situ shear wave velocity from multi-channel analysis of surface waves (MASW) tests at eight Norwegian research sites" *Canadian Geotechnical Journal*, Vol. 44 (5), pp. 533-544.

- Louie, N.J. (2001) "Faster, Better: Shear wave velocity to 100meters depth from Refraction Microtremor arrays" *Bulletin of the Seismological Society of America*, Vol. 91(2), pp. 347-364.

- Louis, S. J., Chen, Q. and Pullammanappallil, S., (1999) "Seismic velocity inversion with genetic algorithms" *CEC99, 1999 Congress on Evolutionary Computation*, Mayflower Hotel, Washington D.C., July 6-9, 1998, pp. 855-861.

- Luo, Y., J. Xia, R. D. Miller, Y. Xu, J. Liu, and Q. Liu (2008) "Rayleigh-wave dispersive energy imaging by high-resolution linear Radon transform" *Pure and Applied Geophysics*, Vol. 165, pp. 903-922.

- Mahajan, A. K., Galiana-Merino, J.J., Lindholm, C., Arora, B.R., Mundepi, A.K., Rai, N and Chauhan, N (2011) "Characterization of the sedimentary cover at the Himalayan foothills using active and passive seismic techniques" *Journal of Applied Geophysics*, Vol. 73, pp. 196-206.

- McGrath, T., Long, M., O'Connor , P., Trafford, A. and Ward, D. (2016) "Multichannel Analysis of Surface waves (MASW) for offshore Geotechnical Investigations" *Proceedings of the fifth international conference on geotechnical and geophysical site characterisation (ISSMGE TC-102 – ISC'5),* Gold Coast, Queensland, Australia, Australian Geomechanics Society, pp. 911-916.

- McMechan, G. A., and Yedlin, M. J., (1981) "Analysis of dispersive waves by wave field transformation" *Geophysics*, Vol. 46, pp. 869-874.

- Mendecki, M. J., Glazer, M. and Mycka, M. (2014) "Application of passive seismic to shallow geological structures in urban areas" *Studia Quaternaria*, Vol. 31(2), pp. 115-122.

- Mi, B., Xia, J., Shen, C., Wang, L., Hu, Y. and Cheng, F. (2017) "Horizontal resolution of multichannel analysis of surface waves" *Geophysics*, Vol. 82(3), pp. 51-66.

- Miller, R. D., Xia. J., parkPark, C. B. and Ivanov J. (1999) " Multichannel Analysis of surface waves to map bedrock" *The Leading Edge*, pp. 1392-1396.

- Mohamed, A.M.E., Abu El Ata, A.S.A., Abdel Azim, F., Taha, M.A. (2013) "Site-specific shear wave velocity investigation for geotechnical engineering applications using seismic refraction and 2D multichannel analysis of surface waves" *NRIAG Journal of Astronomy and Geophysics*, Vol. 2, pp. 88-101.

- Molisana Apparecchiature Electtroniche (2011) *Frequency characteristics of 4.5Hz geophone: Impostazioni Sismica GS-11D Geophone*, MAE.

- Molnar, S., Cassidy, J.F., Monahan, P.A. and Dosso, S.E. (2007) "Comparison of geophysical shear-wave velocity methods" *Ninth Canadian Conference on Earthquake Engineering Ottawa*, Ontario, Canada, pp. 390-400.

- Moura, R., Umaraliev, R., Almeida, F. and Dal Moro, G. (2012) "V_s measurements through dispersive wave methods in the urban environment of Porto (North Portugal)" *Proceedings at 15th World Conference of Earthquake Engineering*, Lisbon, Portugal.

- Nazarian, S., Stokoe, K. H. and Hudson, W. R., (1983) "Use of Spectral Analysis of Surface Waves Method for Determination of Moduli and Thicknesses of Pavement Systems" *Transportation Research Record 930*, National Research Council, Washington, D.C. pp. 38-45.

- Nolet, G., and G. F. Panza. (1976) "Array analysis of seismic surface waves: Limits and possibilities" *Pure and Applied Geophysics*, Vol. 114, pp. 775-790.

- Noorlandt, R., Kruiver, P. P., Kleine, M. P. E., Karaoulis, M., Lange, G., Matteo, A. D., Ketelhodt, J. V., Ruigrok, E., Edwards, B., Rodriguez-Marek, A., Bommer, J. J., Elk, J. V. and Doornhof, D. (2017) "Characterisation of ground motion recording stations in the Groningen gas field" Journal of Seismology, Vol. 22(3), pp. 605-623.

- Okada, H. (2003) "The microtremor survey method" *Geophysical monograph series, No. 12. Society of Exploration Geophysicists* (SEG), Tulsa, OK.

- Panzera, F. and Lombardo, G., (2013) "Seismic property characterization of lithotypes cropping out in the Siracusa urban area, Italy" *Engineering Geology*, Vol. 153, pp. 12-24.

- Park, C. B. (2005) "MASW-horizontal resolution in 2-D shear-velocity (V_s) mapping" *Kansas Geological Survey*, Open file report, 2005-4.

- Park, C. B. (2008) "Imaging dispersion of passive surface waves with active scheme" *Symposium on the Application of Geophysics to Engineering and Environmental Problems* (SAGEEP 2008), Philadelphia.

- Park, C. B. (2010) "Roadside passive survey- Dynamic detection of source location" *Symposium on the Application of Geophysics to Engineering and Environmental Problems* (SAGEEP 2010), Keystone, Colorado, pp. 528-535.

- Park, C. B. (2013) "MASW for geotechnical site investigation" *The Leading Edge*, pp. 656-662.

- Park, C. B. and Miller, R. D. (2008) "Roadside passive multichannel analysis of surface waves (MASW)" *Journal of Environmental and Engineering Geophysics*, Vol. 13, pp. 1-11.

- Park, C. B., and Miller, R. D. (2005) "Multichannel analysis of passive surface waves-modeling and processing schemes" *In Proceedings: ASCE/GeoInstitute Geo-Frontiers*, pp. 23-26.

- Park, C. B., Cirone, A. and Rodrigues, R. (2019) "Roadside Active-Passive MASW surveys to evaluate soil grouting" *Proceedings of the Geo-Congress, Geotechnical Special Publication*, GSP 311, pp. 354-366.

- Park, C. B., Miller, R. D. and Miura, H. (2002) "Optimum field parameters of an MASW survey" *Expanded Abstracts Society of Exploration Geophysicists*, Extended Abstract, pp. 1-6.

- Park, C. B., Miller, R. D. and Ryden, N. (2006) "Roadside seismic survey utilizing traffic noise" *Proceedings of the NDE Conference Civil Engineering*, St. Louis, MO, pp. 317-324.

- Park, C. B., Miller, R. D. and Xia, J. (1998a) "Imaging dispersion curves of surface waves on multi-channel record" *Proceedings of the 68th Annual International Meeting of the Society of Exploration Geophysicists* (Extended Abstracts), pp. 1377-1380.

- Park, C. B., Miller, R. D. and Xia, J. (1999) "Multichannel analysis of surface waves" *Geophysics*, Vol. 64(3), pp. 800-808.

- Park, C. B., Miller, R. D. and Xia, J. (2001) "Offset and resolution of dispersion curve in multichannel analysis of surface waves (MASW)" *Proceedings of the SAGEEP*, SSM4, pp. 1-6.

- Park, C. B., Miller, R. D., and Xia, J., (1996) "Multi-channel analysis of surface waves using Vibroseis" *66th Annual Meeting,* Society of Exploration Geophysicists, Denver, Expanded Abstracts, pp. 68-71.

- Park, C. B., Miller, R. D., and Xia, J., (1998b) "Ground roll as a tool to image near-surface anomaly" *68th Annual International Meeting,* Society of Exploration Geophysicists, Expanded Abstracts, pp. 874-877.

- Park, C. B., Miller, R. D., Laflen, D., Neb, C., Ivanov, J., Bennett, B., and Huggins, R., (2004) "Imaging dispersion curves of passive surface waves" *79th Annual International Meeting, Society of Exploration Geophysicists*, Expanded Abstracts, pp. 1357-1360.

- Park, C. B., Miller, R. D., Ryden, N., Xia, J. and Ivanov, J. (2005) "Combined use of active and passive surface waves" *Journal of Environmental and Engineering Geophysics*, Vol. 10, pp. 323-334.

- Park, C. B., Miller, R. D., Xia, J. and Ivanov, J. (2007) "Multichannel analysis of surface waves (MASW)- active and passive methods" *The Leading Edge*, pp. 01-06.

- Pezeshk, S. and Zarrabi, M. (2005) "A new inversion procedure for spectral analysis of surface waves using a genetic algorithm" *Bulletin of the Seismological Society of America*, Vol. 95(5), pp. 1801-1808.

- Picozzi, M., Strollo, A., Parolai, S., Durukal, E., Ozel, O., Karabulut, S., Zschau, J. and Erdik, M., (2009) "Site characterization by seismic noise in Istanbul, Turkey" *Soil Dynamics and Earthquake Engineering*, Vol. 29, pp. 469- 482.

- Rix, G. J., Bay J. A. and Stokoe K. H. (1990) "Assessing in situ stiffness of curing Portland cement concrete with seismic tests" *Transportation Research Record 1284*, pp. 8-15.

- Rix, G. J., Hebeler, G. L., and Orozco, M. C. (2002). "Near surface V_s profiling in the New Madrid Seismic Zone using surface wave methods" *Seismological Research Letter*, Vol. 73(3), pp. 380-392.

- Rodriguez-Zuniga, J. L., Ortiz-Aleman, C., Padilla, G. and Gaulon, R. (1997) "Application of genetic algorithms to constrain shallow elastic parameters using in situ ground inclination measurements" *Soil Dynamics and Earthquake Engineering*, Vol. 16, pp. 223-234.

- Roma, V. and Moura, R. M. M. (2009) "The combined MASW and ReMi methods for seismic geotechnical site characterization" *Proceedings of the 13th Conference of ANIDIS*, Bologna, Italy.

- Roma, V., Tononi, C. and Karsli, H. (2011) "Seismic geotechnical site characterization by MASW-ReMi method: Importance of higher modes of Rayleigh waves" *Proceedings of the 6th Congress of Balkan Geophysical Society*, Budapest, Hungary.

- Rosas, R. V., Aguirre, J., Estrella, H. F. and Arellano, H. M. (2011) "Microtremor studies using SPAC method: Experiences and applications to four sites in Mexico" *Geofisica Internacional*, Vol. 50(3), pp. 295-312.

- Ryden, N., Park, C. B., Ulriksen, P. and Miller R. D. (2004) "Multimodal approach to seismic pavement testing" *Journal of Geotechnical and Geoenvironmental Engineering*, ASCE, Vol. 130, pp. 636-645.

- Saez, E., Ledezma, C., de la Maza, G., Cortes, M. and Brunet, S. (2014) "Geophysical survey of two piers affected by liquefaction-induced lateral spreading for the 2010 Maule earthquake"

In: Soil Liquefaction during Recent Large-scale Earthquakes. Taylor and Francis, London, pp. 45-54.

- Sambridge, M. (1999) "Geophysical inversion with a neighbourhood algorithm I. Searching a parameter space" *Geophysical Journal International*, Vol. 103, pp. 4839-4878.

- Sambridge, M. and Mosegaard, K. (2002) "Monte Carlo methods in geophysical inverse problems" *Reviews of Geophysics*, Vol. 40(3), pp. 3.1- 3.29.

- Savvaidis, A., Margaris, B., Theodoulidis, N., Lekidis, V., Karakostas, Ch., Loupasakis, C., Rozos, D., Soupios, P., Mangriotis, M-D., Dikmen, U., Tsangaratos, Par., Kokinou, E., Vafidis, A., Rondoyanni, Th., Kalogeras, I., Koutrakis, S., Sarris, A. and Papadopoulos, N. (2014) "Geo-characterization at selected accelerometric stations in Crete (Greece) and comparison of earthquake data recordings with EC8 elastic spectra" *Central European Journal of Geosciences*, Vol. 6, pp. 88-103.

- Schwab, F. A., and Knopoff, L. (1972) "Fast surface wave and free mode computations, in Bolt, B. A., Ed., Methods in computational physics" *Academic Press*, pp. 87-180.

- Socco, L. V., and Boiero, D. (2008) "Improved Monte Carlo inversion of surface wave data" *Geophysical Prospecting*, Vol. 56(3), pp. 357-371.

- Socco, L. V., Foti, S. and Boiero, D. (2010) "Surface-wave analysis for building near-surface velocity models -Established approaches and new perspectives" *Geophysics*, Vol. 75(5), pp. 75A83-75A102.

- Socco, L.V. and Strobbia, C. (2004) "Surface-wave method for near-surface characterization: a tutorial" *Near Surface Geophysics*, Vol. 2004, pp. 165-185.

- Stoffa, P. L. and Sen, M. K. (1991) "Nonlinear multiparameter optimisation using genetic algorithms: inversion of plane wave seismograms" *Geophysics*, Vol. 56, pp. 1794-1810.

- Stokoe II, K. H., Wright, G. W., James, A. B., and Jose, M. R., (1994) "Characterization of geotechnical sites by SASW method" *In Woods, R. D., Ed., Geophysical Characterization of Sites*, Oxford Publ.

- Strobbia, C. and Foti, S. (2006) "Multi-offset phase analysis of surface wave data (MOPA)" *Journal of Applied Geophysics*, Vol. 59 (4), pp. 300-313.

- Suzuki, H. and Hayashi, K. (2003) "Shallow s-wave velocity sounding using the microtremors array measurements and surface wave method" *Proceedings of the SAGEEP*, San Antonio, Texas, USA.

- Taipodia, J. and Dey, A. (2018) "Impact of Strike Energy on the Resolution of Dispersion Image in Active MASW Survey" *Proceedings of GeoShanghai 2018 International Conference*, Multi-physics Processes in Soil Mechanics and Advances in Geotechnical Testing.

- Taipodia, J., Baglari, D. and Dey, A. (2017) "Resolution of dispersion image obtained from active MASW survey" *Disaster Advances*, Vol. 10(11), pp. 34-45.

- Taipodia, J., Baglari, D. and Dey, A. (2018a) "Effect of Source Characteristics on the Resolution of Dispersion Image from Active MASW Survey" *Indian Geotechnical Journal*, DOI:10.1007/s40098-018-0335-1.

- Taipodia, J., Baglari, D. and Dey, A. (2018b) "Recommendations for generating dispersion images of optimal resolution from Active MASW survey" *Innovative Infrastructure Solutions*, Vol. 3, pp. 1-19.

- Taipodia, J., Dey, A. and Baglari, D. (2018c) "Influence of signal preprocessing parameters on the resolution of dispersion image in active MASW survey" *Journal of Geophysics and Engineering*, DOI: 10.1088/1742-2140/aaaf4c.

- Tokimatsu, K. (1995) "Geotechnical site characterization using surface waves." *Proceedings at 1st International Conference on Earthquake Geotechnical Engineering*, IS-Tokyo, Japanese Geotechnical Society, Balkema, Rotterdam, Netherlands, pp.1333-1368.

- Tokimatsu, K., Kuwayama, S., Tamura, S. and Miyadera, Y. (1991) "V_s determination from steady state Rayleigh wave method" *Soil and Foundations*, Vol. 31 (2), pp. 153-163.

- Tokimatsu, K., Shinzawa, K. and Kuwayama, S. (1992a) "Use of short-period microtremors for V_s profiling" *Journal of Geotechnical Engineering*, Vol. 118 (10), pp. 1544-1558.

- Tokimatsu, S., Tamura, H. and Kojima (1992b), "Effects of multiple modes on Rayleigh wave dispersion characteristics" *Journal of Geotechnical Engineering*, 118(10), pp. 1529-1543.

- Trupti, S., Srinivas, K.N.S.S.S., Pavan Kishore, P. and Seshunarayana, T. (2012) "Site characterization studies along coastal Andhra Pradesh- India using multichannel analysis of surface waves" *Journal of Applied Geophysics*, 79, pp. 82-89.

- Uma Maheswari, R., Boominathan, A. and Dodagoudar, G. R. (2010) "Use of surface waves in statistical correlations of shear wave velocity and penetration resistance of Chennai soils" *Geotechnical and Geology Engineering*, Vol. 28(2), pp. 119-137.

- Uyanik, O, Ekinci, B. and Uyanik, N.A. (2013) "Liquefaction analysis from seismic velocities and determination of lagoon limits Kumluca/Antalya example" *Journal of Applied Geophysics*, Vol. 95, pp. 90-103.

- Wathelet, M., Jongmans, D., and Ohrnberger, M. (2004) "Surface-wave inversion using a direct search algorithm and its application to ambient vibration measurements" *Near Surface Geophysics*, Vol. 2(4), pp. 211-221.

- Weaver, R.L., (1982) "On diffuse waves in solid media" *Journal of the Acoustical Society of America*, Vol. 71, pp. 1608-1623.

- Xia, J. Miller, R.D., Park, C. B. and Tian, G. (2002) "Determining Q of near surface materials from Rayleigh waves" *Journal of Applied Geophysics*, Vol. 51, pp. 121-129.

- Xia, J., Chen, C., Li, P.H. and Lewis, M.J. (2004a) "Delineation of a collapse feature in a noisy environment using MASW" *Geotechnique*, Vol. 54(1), pp. 17-27.

- Xia, J., Chen, C., Tian, G., Miller, R. D. and Ivanov, J. (2005) "Resolution of high frequency Rayleigh wave data" *Journal of Environmental and Engineering Geophysics*, Vol. 10(2), pp. 25-36.

- Xia, J., Miller, R. D. and Park, C. B. (1999) "Estimation of near-surface shear-wave velocity by inversion of Rayleigh waves" *Geophysics*, Vol. 64, pp. 691-700.

- Xia, J., Miller, R. D. and Park, C. B. (2000a) "Advantages of calculating shear wave velocity from surface waves with higher modes" *Society of Exploration Geophysicists*, Expanded Abstracts, pp. 1295-1298.

- Xia, J., Miller, R. D., Park, C. B., Ivanov, J., Tian, G. and Chen, C. (2004b) "Utilization of high-frequency Rayleigh waves in near-surface geophysics" *The Leading Edge*, pp. 753-759.

- Xia, J., Miller, R. D., Park, C.B and Ivanov, J. (2000b) "Construction of 2-D vertical shear wave velocity field by the multichannel analysis of surface wave technique" *Proceedings of the symposium on the Application of Geophysics to engineering and Environmental problems*, Arlington, pp. 1197-1206.

- Yilmaz, O. (1987) "Seismic data processing" *Society of Exploration Geophysicists*.

- Yin, X., Xu, H., Wang, L., Hu, Y., Shen, C. and Sun, S. (2016) " Improving horizontal resolution of high-frequeny surface wave methods using travel time tomography" *Journal of Applied Geophysics*, Vol. 126, pp. 42-51.

- Yoon, S. (2011) "Combined active-passive surface wave measurements at five sites in the western and southern US" *KSCE Journal of Civil Engineering*, Vol. 15(5), pp. 823-830.

- Yoon, S. and Rix, G. J. (2004). "Combined active-passive surface wave measurements for near-surface site characterization" *Proceedings of the symposium on the Application of Geophysics to Engineering and Environmental Problems*, Denver, CO, pp. 1156-1164.

- Zekkos, D. Sahadewa, A, Woods, R. D. and Stokoe, K. H. (2014) "Development of model for shear wave velocity of municipal solid waste" *Journal of Geotechnical and Geoenvironmental Engineering*, ASCE, Vol. 140, pp. 1-14.

- Zhang, S.X., Chan, L.S. and Xia, J. (2004) "The selection of field acquisition parameters for dispersion images from multichannel surface wave data" *Pure and Applied Geophysics*, Vol. 161, pp. 185-201.

- Zywicki, D. J. (1999) "Advanced signal processing methods applied to engineering analysis of seismic surface waves" *PhD Thesis*, Georgia Institute of Technology, USA.

- http://www.mae-srl.it/prodotti/showprodotto/500 (Last accessed: 19 July 2019)
- http://www.mae-srl.it/prodotti/pdfprodotto/23 (Last accessed: 19 July 2019)
- https://web.whoi.edu/obslab/wp-content/uploads/sites/98/2017/10/Geophone_TestingEDIT-1.pdf (Last accessed: 19 July 2019)
- http://www.masw.com (Last accessed: 26 July 2018)

LIST OF PUBLICATIONS

Journals:

1. **Baglari, D.**, Dey, A. and Taipodia, J. "A State-of-the-Art Review of Passive MASW Survey for Subsurface Profiling" *Innovative Infrastructure Solutions*, Vol. 3, Paper No. 66, pp. 1-13 (**DOI: 10.1007/s41062-018-0171-2**)

2. Taipodia, J., Dey, A., Gaj, S. and **Baglari, D**. "Quantification of the resolution of dispersion image in active MASW survey and automated extraction of dispersion curve" *Computers and Geosciences* **(Manuscript Communicated)**

3. **Baglari, D.**, Dey, A. and Taipodia, J. "Influence of Multiple Source Characteristics and Offline Distance of Receiver Array in Passive Roadside MASW Survey" *Geophysical Prospecting*. (**Manuscript communicated**).

4. **Baglari, D.**, Dey, A. and Taipodia, J. "Critical Analysis of Raw Wavefield Records from Passive Roadside MASW Survey" *Journal of Earth System Science* **(Manuscript communicated)**

5. **Baglari, D.**, Dey, A. and Taipodia, J. "Influence of Data Acquisition Parameters on Dispersion Imaging in Passive Roadside Survey" *Geophysical Journal International* **(Manuscript communicated)**

6. **Baglari, D.**, Dey, A. and Taipodia, J. "Influence of Processing Schemes and Stacking on the Resolution of Dispersion Image" *Near Surface Geophysics* **(Manuscript communicated)**

7. **Baglari, D.**, Dey, A. and Taipodia, J. "Optimum Selection of Dispersion Curve and Initial Model for Reliable Inversion Analysis" *Indian Geotechnical Journal* **(Manuscript communicated)**

8. Taipodia, J., Dey, A. and **Baglari, D.** "Influence of receiver layout and substrata characteristics on the resolution of dispersion image from active MASW survey" *Arabian Journal of Geosciences* **(Manuscript Communicated)**

9. Taipodia, J., **Baglari, D.** and Dey, A. (2018) "Effect of Source Characteristics on the Resolution of Dispersion Image from Active MASW Survey" *Indian Geotechnical Journal*. (DOI: 10.1007/s40098-018-0335-1)

10. Taipodia, J., Dey, A. and **Baglari, D.** (2018) "Influence of signal preprocessing parameters on the resolution of dispersion image in active MASW survey" *Journal of Geophysics and Engineering*, Vol. 15, No. 4, pp. 1310-1326. (DOI: 10.1088/1742-2140/aaaf4c).

11. Taipodia, J., **Baglari, D.** and Dey, A. (2018) "Recommendations for generating dispersion images of optimal resolution from Active MASW survey" *Innovative Infrastructure Solutions*, Vol. 3, Article 14, pp. 1-19. (DOI: 10.1007/s41062-017-0120-5).

12. Taipodia, J., **Baglari, D.** and Dey, A. (2017) "Resolution of dispersion image obtained from active MASW survey" *Disaster Advances*, Vol. 10(11), pp 34-45.

Conferences:

1. **Baglari, D.**, Taipodia, J. and Dey, A. (2018) "Critical analysis of traffic origin wavefields for optimum utilisation in passive roadside MASW survey" *International Conference on Advances in Concrete, Structural & Geotechnical Engineering (ACSGE - 2018)*, BITS Pilani, India, pp. 1-6.

2. Dey, A., Mukherjee, M., Taipodia, J., **Baglari, D.** and Biswas, S. (2017) "Non-invasive Geophysical Investigation for Subsurface Profiling in Urbanized Megacities" *Extended Abstract: Proceedings of the 2nd Korea-India Joint Geotechnical Workshop*, Seoul, South Korea, pp. 9-10

3. **Baglari, D.**and Dey, A. (2017) "Effects of Source Characteristics in Passive Roadside MASW Survey" *Geotechnics for Natural and Engineered Sustainable Technologies: Indian Geotechnical Conference (GeoNEst: IGC-2017)*, Guwahati, India, pp. 1-4.

4. **Baglari, D.**, Taipodia, J., Biswas, S. and Dey, A. (2015) "Aspects of dispersion imaging scheme of passive MASW survey for subsurface characterisation" *Indian Geotechnical Conference: IGC 2015*, Pune, India, pp. 1-8.

5. Taipodia, J., **Baglari, D.**, Biswas, S. and Dey, A. (2015) "Dispersion analysis using active MASW survey data" *Indian Geotechnical Conference: IGC 2015*, Pune, India, pp. 1-9.

6. Taipodia, J., Budha Ram, B., **Baglari, D.**, Murali Krishna, Dey, A. (2014) "Geophysical investigations for identification of subsurface stratigraphy at IIT Guwahati" *Indian Geotechnical Conference (IGC-2014)*, Kakinada, India, pp. 219-226.

APPENDIX

This appendix describes working methodology of the software paltform “SurfSeis”, and the various sequential steps involved in the analysis of mainly Passive roadside record, to obatin a shear-wave velocity profle with the depth.

Step 1: The processing by SurfSeis can be started by clicking on “Utilities”, and then importing SG-2 (or SEG-2) format file (shown by the arrows) by clicking on “Open SEG-2 Data File(s)” which cotains recoded raw field data by the seismograph (Fig. A.1).

Step 2: Conversion of SG-2 file to .DAT file by clicking at the “Run Format” button shown in Fig. A.1. The software processes the field record in .DAT file format, and this mandatory conversion is automatically done in this stage. The software thereby makes a separate .DAT file for each of the processed field record. If vertical stacking is to be performed by Method I with mulitple field records, the desired field records can be selected together to form a single .DAT file. Subsequently, the sofware opens a dialog box to save the file name and location. Thereafter, by clicking on “Open Seismic Data File” the saved DAT file can be opened (Fig. A.2).

Step 3: After opening the required DAT file, next task is the selection of survey type e.g., Active or Passive (Remote or roadside) for which a dialog box appears automatically (Fig. A.3).

Step 4: After selecting the type of survey conducted (say Passive roadside as shown below), next operation is to set the geometry of the array laid during the survey. Firstly, first two station numbers

have to be assigned in a consecutive order (e.g., 101, 102 etc.), and, then, the first channel number has to be assigned, depending upon the layout of the receiver array and number of receivers used in the field (e.g., 1 or 24 if 24 number of receivers are used). Other channel numbers will automatically appear if previous geometry is correctly furnished. Further, the inter-receiver spacing, offline distance from the road and the distance unit has to be assigned. On clicking "OK" this dialog box will disappear, and, then, by clicking on the "Apply Geometry", the selected geometry can be registered on the .DAT file (Fig. A.4).

Step 5: The DAT file is now ready for proceeding to the dispersion analysis. The dispersion imaging process is started by selecting the .DAT file from the "Processing Steps" and selecting "Make Dispersion Curve Images" (Fig. A.5).

Step 6: After selecting required .DAT file for dispersion imaging, the Phase velocity-Frequency (overtone [OT]) generator box will appear. Here, the desired range of phase velocity, frequency, searching angle, etc., can be set for the dispersion analysis. Then, by clicking on the "*Start Processing"* button, the dispersion imaging process starts (Fig. A.6).

Step 7: On completion of the dispersion imaging stage, the subsequent operation is to select the dispersion curve from the generated dispersion image. For this, the respective OT.DAT file, comprising the processed dispersion image from the previous stage, has to be opened (Fig. A.7). Then the "Bounds" button helps to select the tentative range and position of dispersion curve points (Fig. A.8). Further, by clicking on "Extract DC", a dispersion curve following the points selected through the "Bounds" button will appear along with a SNR curve showing SNR value of each

dispersion points. The obtained dispersion curve can then be edited with respect SNR value as a reference. The final dispersion curve has to be saved in DC file format for the inversion process (Fig. A.9).

Step 8: Finally, upon clicking "Inversion", the selected dispersion curve is made ready for the analysis (Fig. A.10). In the inversion stage, iteration and layer parameters can be controlled in a variety of ways through the "Control" button that appears in the Inversion page. Particularly, the two important parameters (Stopping parameters for inversion) namely "Maximum number of Iterations" and 'Minimum RMS error (in phase velocity), can be controlled in this stage (Fig. A.11).

Step 9: Finally, clicking on the "Run" button starts the inversion process. During the inversion process, the RMS error at every iterations and total number of iterations performed during the entire inversion stage can be observed. After reaching any of the two stopping criteria, the inversion stage comes to a stop, and final V_s profile is obtained and can be saved (Fig. A.12).

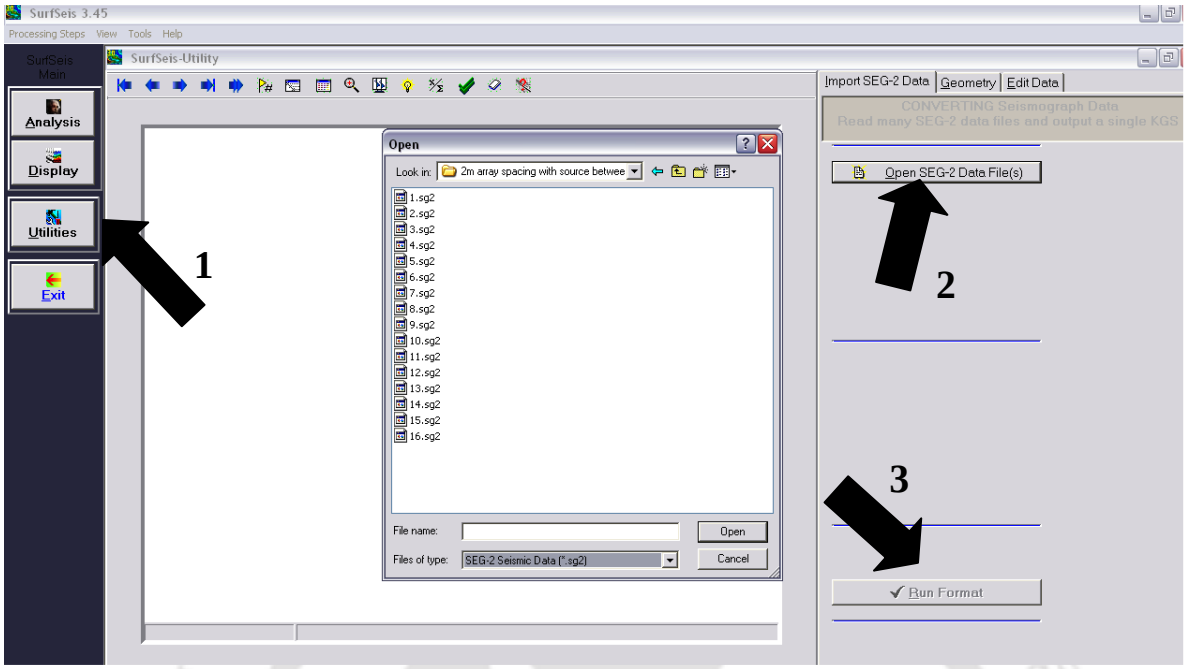

Fig. A.1 Opening SG-2 file format containing raw field data

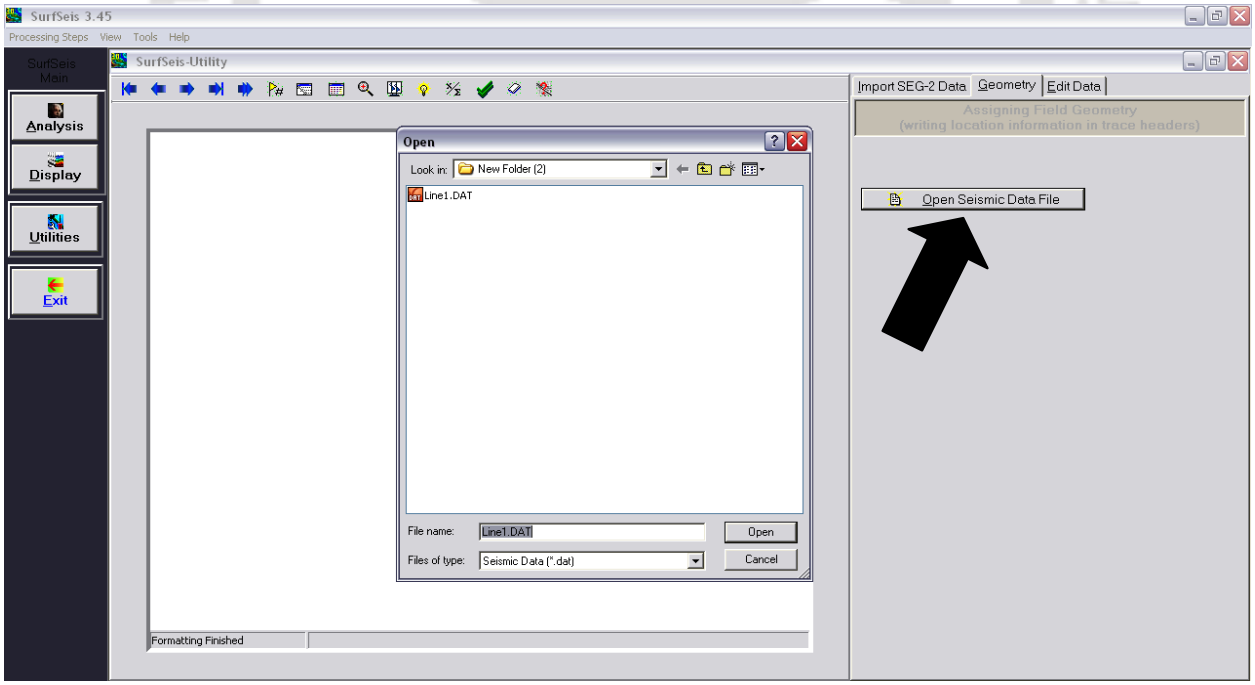

Fig. A.2 Opening .DAT file format

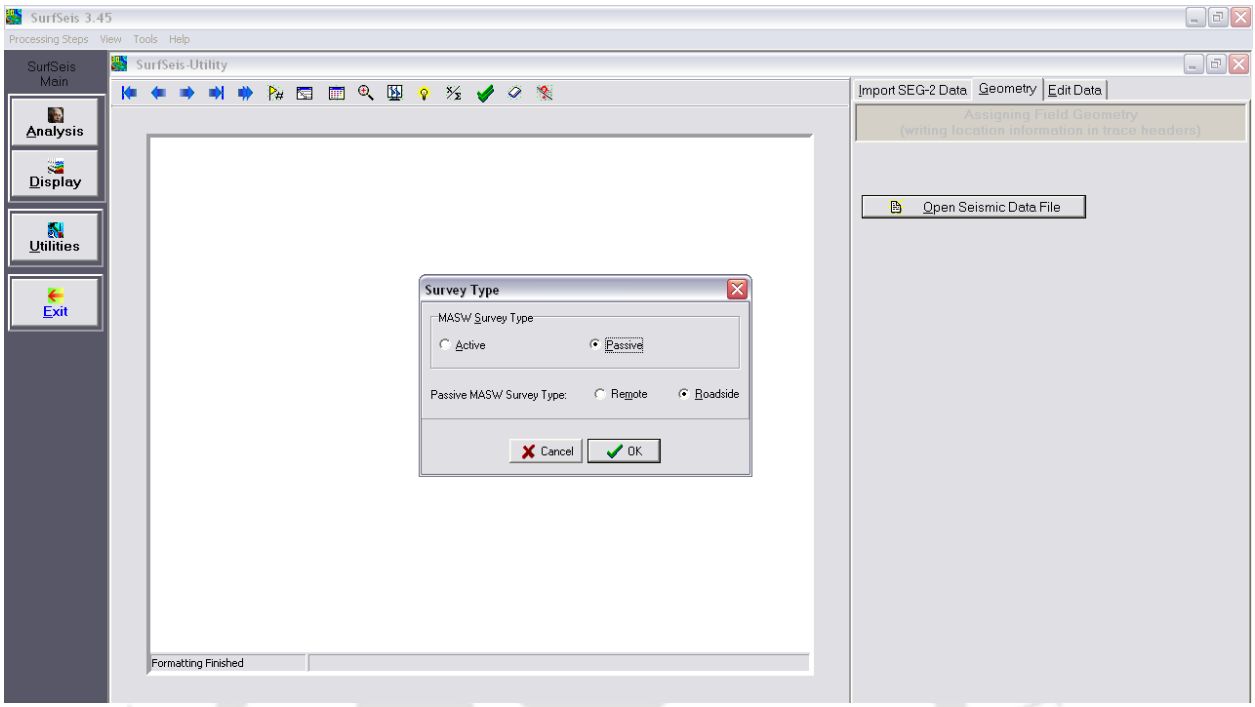

Fig. A.3 Assigning survey type in the .DAT file

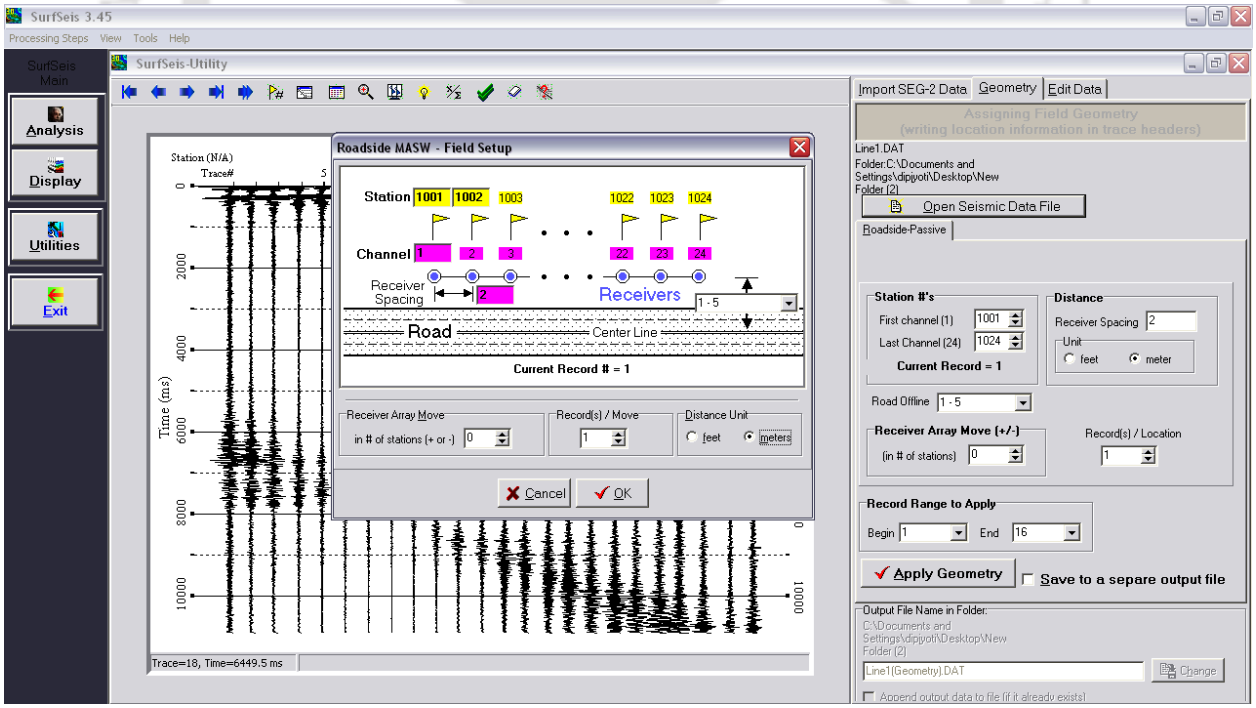

Fig. A.4 Assigning geometry to the .DAT file

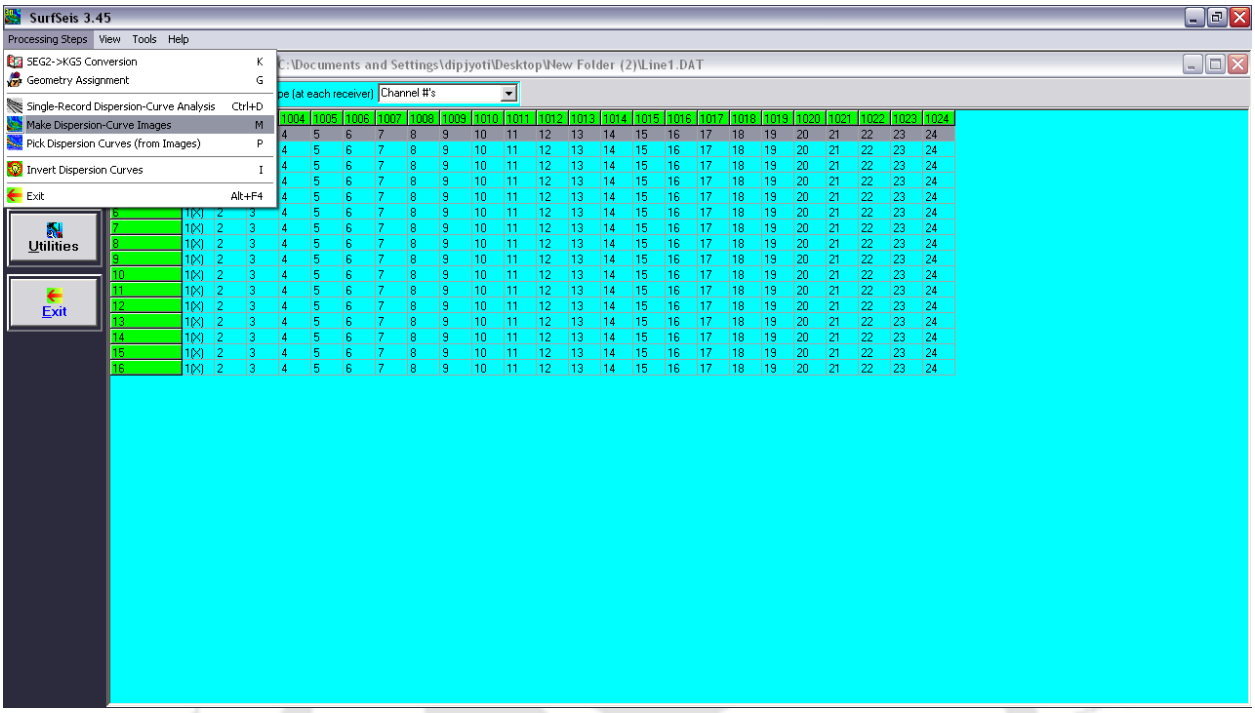

Fig. A.5 Selecting .DAT file for dispersion imaging

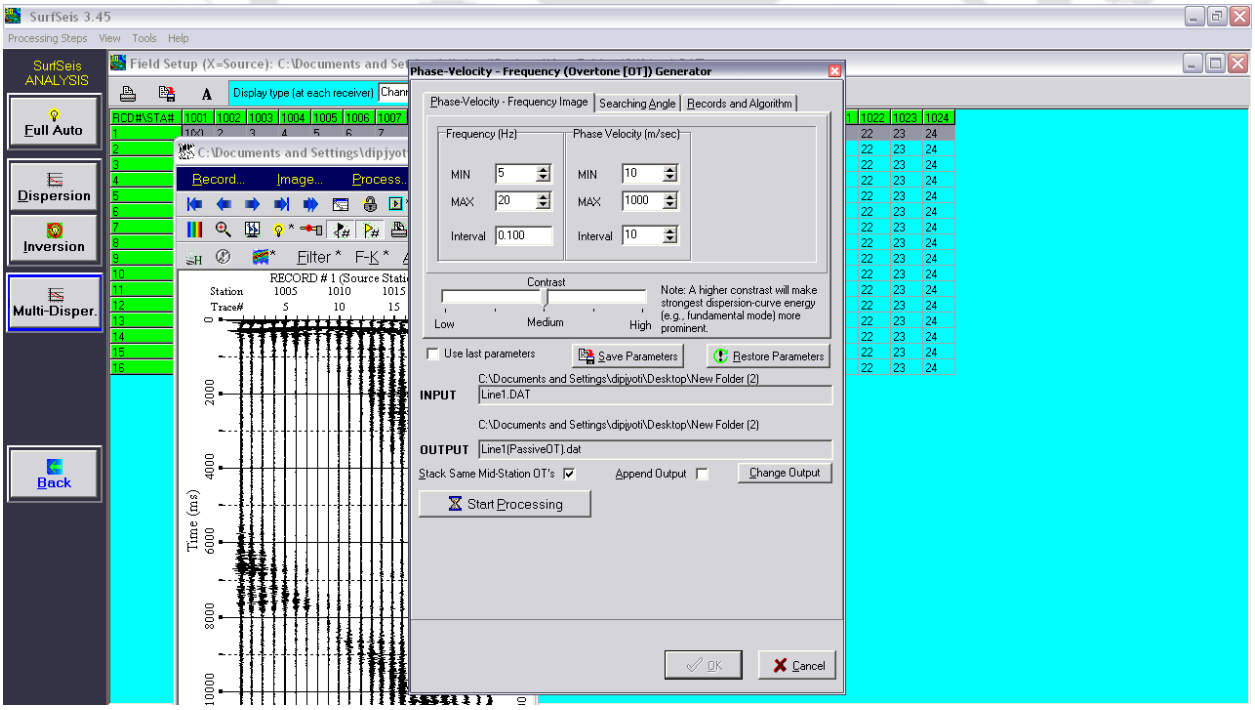

Fig. A.6 Phase velocity-frequency generator dialog box for controlling dispersion imaging

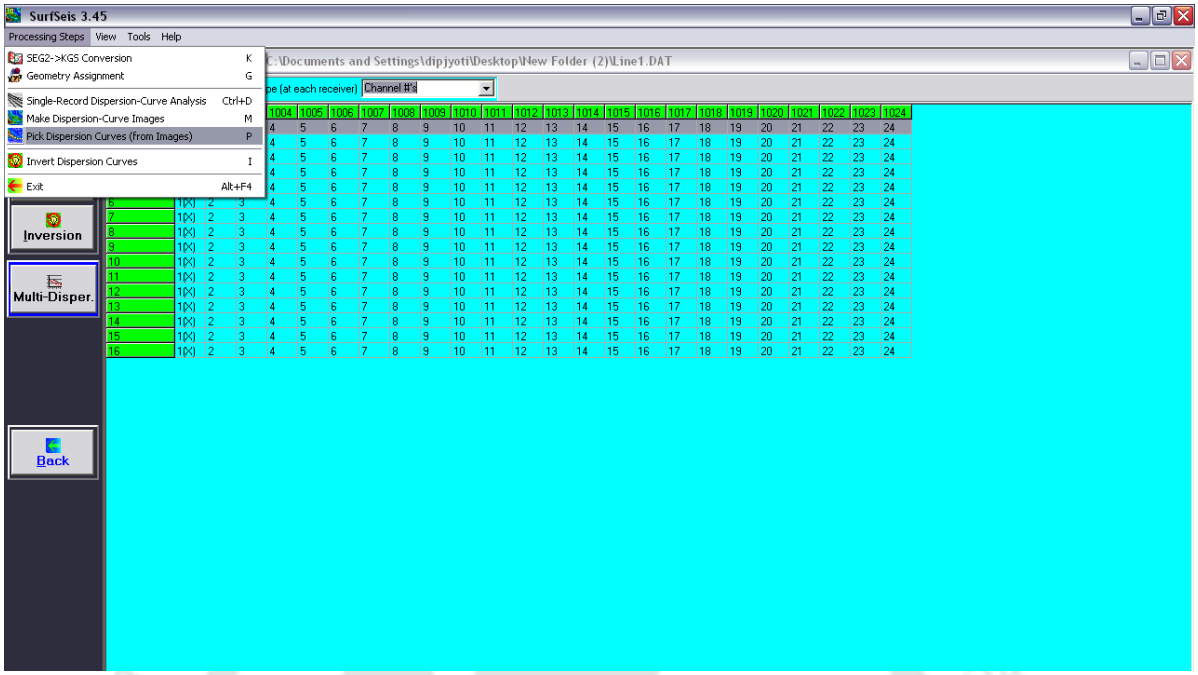

Fig. A.7 Selecting dispersion image from the saved OT.DAT file

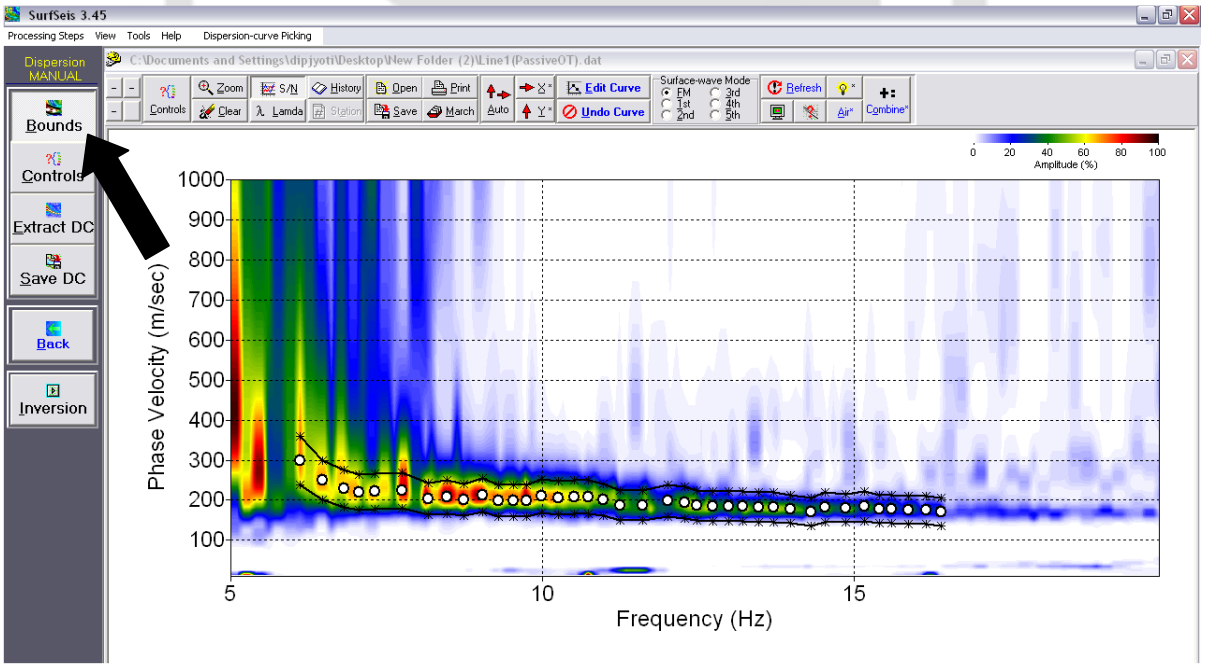

Fig. A.8 Setting bounds for the dispersion curve to be extracted

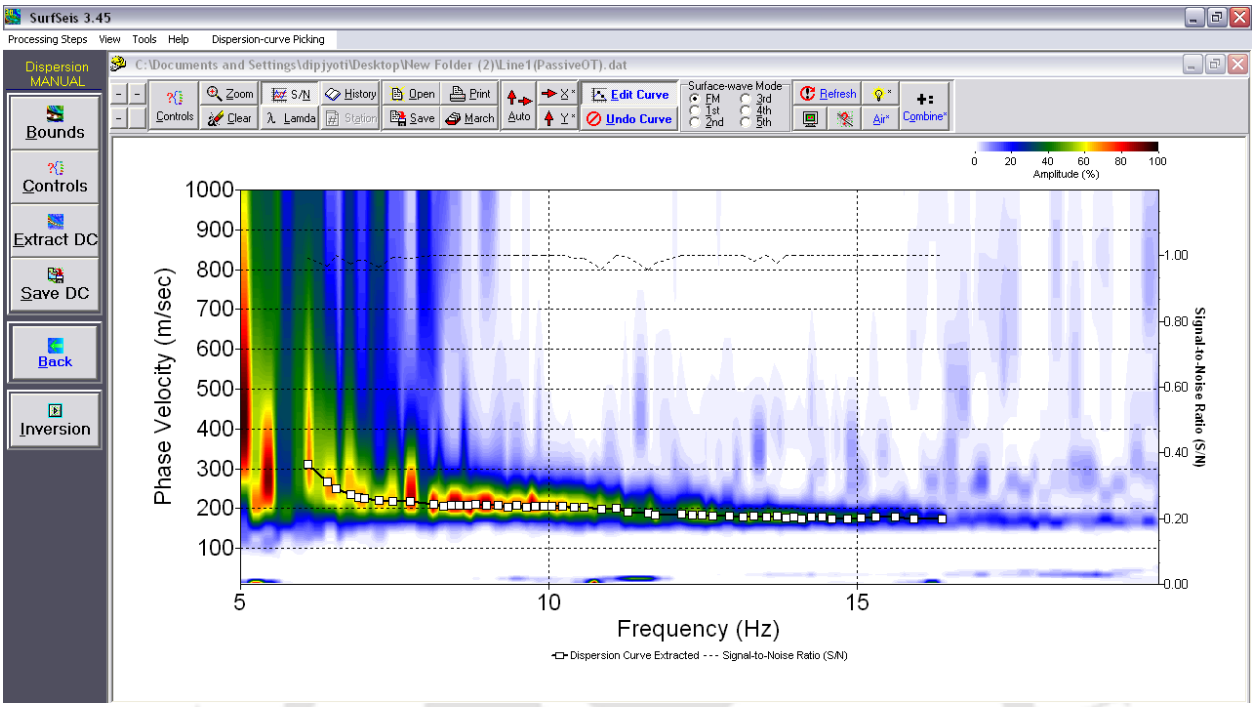

Fig. A.9 Final edited dispersion curve with high SNR value

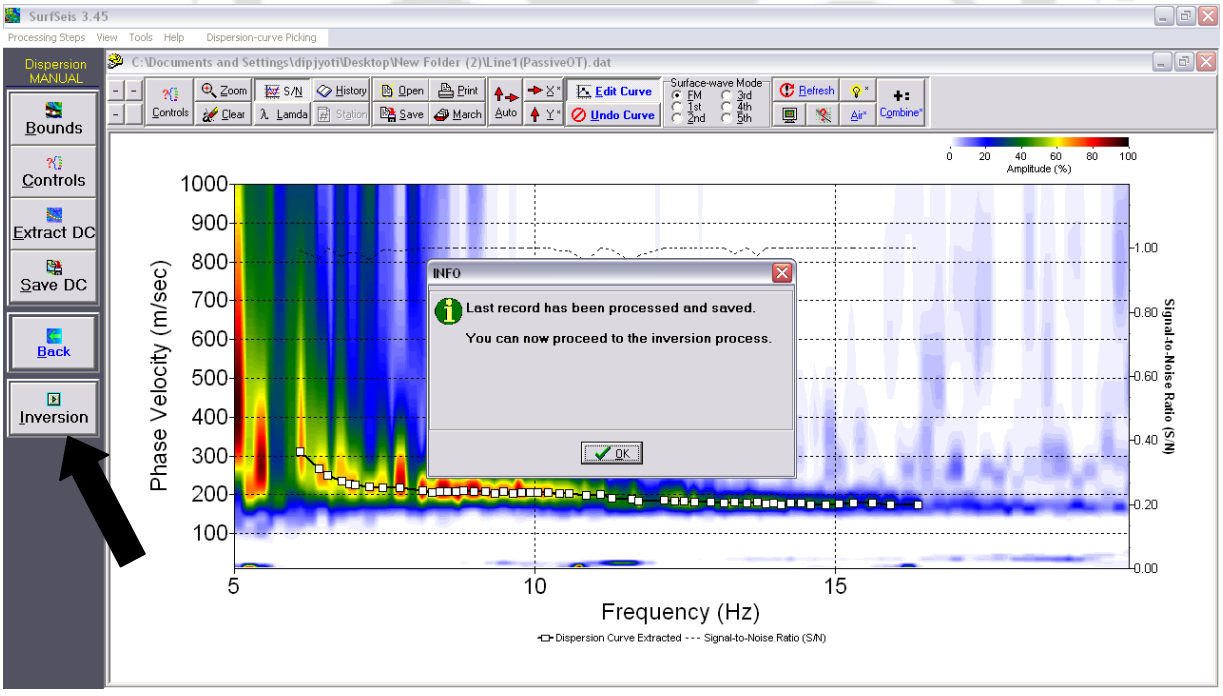

Fig. A.10 Starting the inversion process with the saved dispersion curve

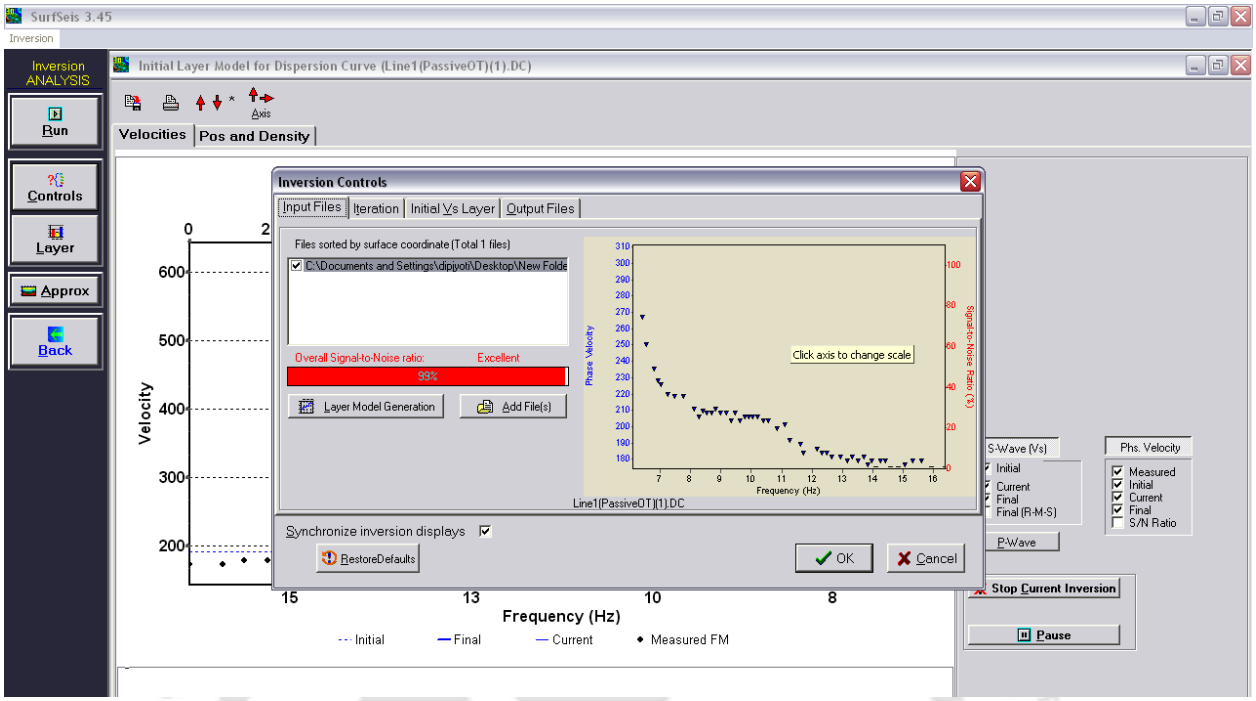

Fig. A.11 Controlling parameters for inversion analysis

.

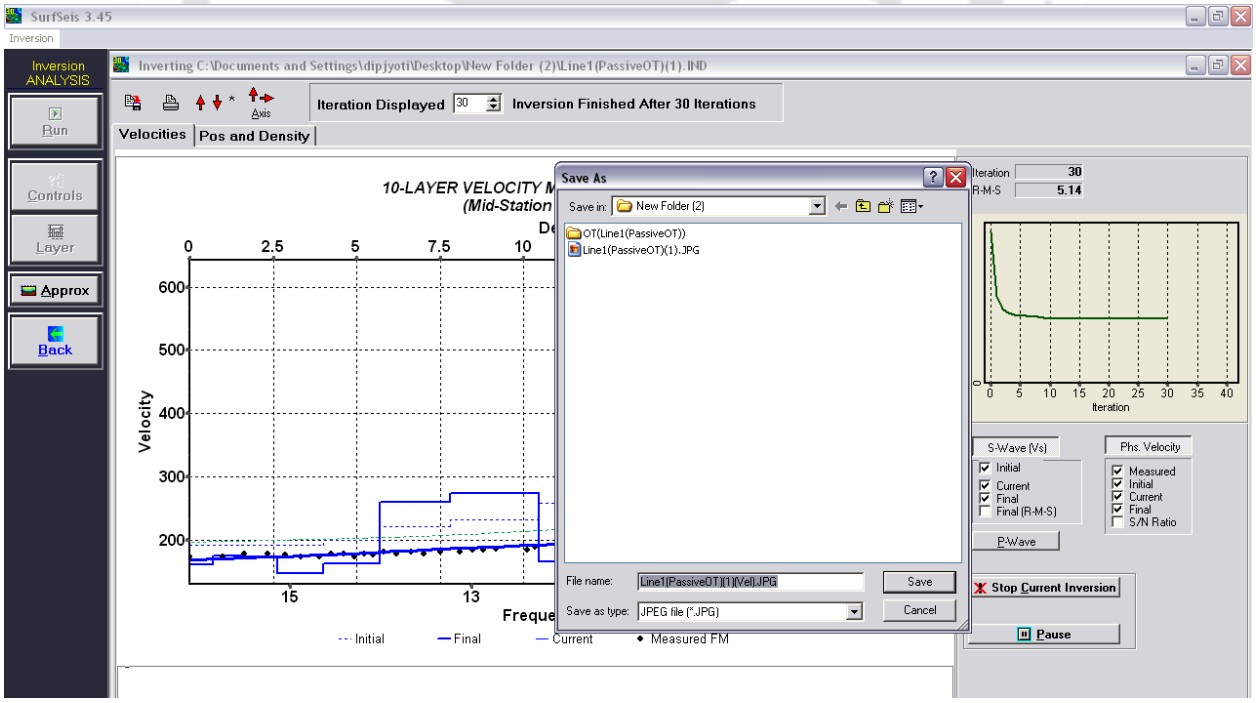

Fig. A.12 Final V_s profile along with the reached values of number of Iterations and RMS error